## Mahinder Ramdin

CO<sub>2</sub> Capture with Ionic Liquids:

Experiments and Molecular Simulations

Delft University of Technology

# CO<sub>2</sub> Capture with Ionic Liquids: Experiments and Molecular Simulations

Proefschrift

ter verkrijging van de graad van doctor aan de Technische Universiteit Delft, op gezag van de Rector Magnificus prof. ir. K.C.A.M. Luyben, voorzitter van het College voor Promoties, in het openbaar te verdedigen op dinsdag 01 december 2015 om 12:30 uur

Door

Mahinder RAMDIN Scheikundig ingenieur geboren te Nickerie, Suriname. This dissertation has been approved by the

promotor: Prof. dr. ir. T.J.H. Vlugt copromotor: Dr. ir. T.W. de Loos

#### Composition of the doctoral committee:

Rector Magnificus Chairman

Prof. dr. ir. T.J.H. Vlugt Promotor, Delft University of Technology Dr. ir. T.W. de Loos Copromotor, Delft University of Technology

#### Independent members:

Prof. dr. H. Zandbergen
Prof. dr. ir. A.B. de Haan
Prof. dr. E.J. Meijer
Prof. dr. J. Snoeijer

Delft University of Technology
University of Amsterdam
University of Twente and

Eindhoven University of Technology
Dr. B.P. Tighe
Delft University of Technology





This work was sponsored by ADEM, A green Deal in Energy Materials, a program of the Dutch Ministry of Economic Affairs, Agriculture and Innovation. In addition, this work was supported by NWO Exacte Wetenschappen (Physical Sciences) for the use of supercomputing facilities, with financial support from the Nederlandse Organisatie voor Wetenschappelijk Onderzoek (Netherlands Organization for Scientific Research, NWO).

Copyright © 2015 by M. Ramdin

ISBN: 978-94-6186-555-7

Printed by: Ipskamp Drukkers



# Contents

1	A E	Brief In	${f CO}_2$ Capture	1
<b>2</b>	CO	2 Capt	cure with Ionic Liquids: A Review	5
	2.1	Introd	luction	5
	2.2	$CO_2$ (	Capture Processes	9
		2.2.1	Post-combustion Capture	9
		2.2.2	Pre-combustion Capture	11
		2.2.3	Oxyfuel Combustion Capture	12
		2.2.4	Natural Gas Sweetening	14
		2.2.5	Conventional Amine Technology	15
	2.3	$CO_2$ (	Capture with Ionic Liquids	18
		2.3.1	Physical Ionic Liquids	21
		2.3.2	Functionalized Ionic Liquids	48
		2.3.3	Reversible Ionic Liquids	57
		2.3.4	CO <sub>2</sub> Capture Performance: ILs vs. Commercial Sol-	
			vents	58
	2.4	Suppo	orted Ionic Liquid Membranes (SILMs)	61
	2.5	Biode	gradability and Toxicity of Ionic Liquids	64
		2.5.1	Biodegradability of Ionic Liquids	65
		2.5.2	Toxicity of Ionic Liquids	69
	2.6	Concl	usions and Future Directions	71

viii CONTENTS

3	$\mathbf{CO}$	<sub>2</sub> /CH <sub>4</sub> Solubility in Ionic Liquids: Ideal Selectivity	<b>75</b>
	3.1	Introduction	75
	3.2	Experiments	77
	3.3	Thermodynamic Modeling	80
	3.4	Results and Discussion	81
	3.5	Conclusions	93
4	CO	<sub>2</sub> /CH <sub>4</sub> Solubility in Ionic Liquids: Real Selectivity	95
	4.1	Introduction	95
	4.2	Experiments	97
	4.3	Thermodynamic Modeling	99
	4.4	Results and Discussion	100
	4.5	Conclusions	114
5	Sol	ubility of Natural Gas Species from Monte Carlo Sim	1-
	lati	ons	115
	5.1	Introduction	115
	5.2	Simulation Details	116
	5.3	Results and Discussion	120
	5.4	Conclusions	124
6	Cor	nputing Bubble Points of Mixtures from Molecular Sin	1-
		tions	125
	6.1	Introduction	125
	6.2	Theory	128
	6.3	Simulation Details	129
	6.4	Results and Discussion	134
	6.5	Conclusion	141
7	Sol	ubility of Pre-combustion Gases from Monte Carlo Sim	1-
		tions	143
	7.1	Introduction	143
	7.2	Simulation Details	145
	7.3	Results and Discussion	

CONTENTS ix

		7.3.1	Solubility	146
		7.3.2	Selectivity	151
	7.4	Conclu	asions	153
8	Mo		rlo Simulations of ${ m CO}_2$ and Monoethanolamine	155
	8.1		uction	155
	8.2	Simula	ating the reactions of $CO_2$ in MEA solution	159
		8.2.1	RxMC/CFC Algorithm	160
		8.2.2	Simulation Details	167
	8.3	Result	s and Discussion	169
		8.3.1	Effect of Electrostatics and intermolecular van der	
			Waals interactions	169
		8.3.2	Chemical Equilibrium of reactions R1+R2+R3+R4	
			and R5	170
	8.4	Conclu	asions	176
9	CO	$_2/\mathbf{CH}_4$	Solubility: ILs versus Conventional Solvents	177
	9.1	Introd	uction	177
	9.2	Result	s and Discussion	178
		9.2.1	$CO_2$ Solubility	178
		9.2.2	CH <sub>4</sub> Solubility	181
		9.2.3	Selectivity	182
	9.3	Conclu	asions	184
Re	efere	nces		185
Su	ımma	ary		245
Sa	men	vatting		251
Cı	ırric	ulum '	Vitae	257
Pι	ıblic	ations	by the Author	259
A	cknov	wledge	ments	261

## Chapter 1

# A Brief Introduction to CO<sub>2</sub> Capture

Carbon dioxide  $(CO_2)$  is considered as one of the major greenhouse gases responsible for climate change [1, 2]. In the process of burning fossil fuels to produce electricity and heat (i.e., the post-combustion process), large amounts of  $CO_2$  are emitted into the atmosphere. In order to prevent irreversible climate change, it is crucial to reduce the CO<sub>2</sub> emissions and one of the options to achieve this is by the carbon capture and storage (CCS) route |3|. In this route,  $CO_2$  is captured from flue gas and subsequently stored in deep underground geological formations. CO<sub>2</sub> capture is not only relevant from an environmental perspective, but it has also industrial significance in the ammonia production process, hydrogen production process, and the natural gas sweetening process [4]. Alternatives for the post-combustion process are the pre-combustion and the oxyfuel combustion process, which is still in the development phase [5]. In the pre-combustion process, a fuel is gasified to produce syngas, which is a mixture of carbon monoxide (CO) and hydrogen  $(H_2)$  [6]. The syngas is shifted in a reactor to produce more hydrogen, but  $CO_2$  is also produced in this step [7]. The  $CO_2$  should be separated from H<sub>2</sub>, which then can be used for several applications. Natural gas is typically contaminated with the sour gases CO<sub>2</sub> and hydrogen sulfide

 $(H_2S)$ , which should be removed to meet customer specifications and to avoid technological problems during transportation of the gas [8].

The choice of technology to capture  $CO_2$  at post-combustion, precombustion or natural sweetening conditions depends on the operating conditions of these processes [9]. Chemical solvents like monoethanolamine (MEA) are preferred for post-combustion  $CO_2$  capture, because the low partial pressure of CO<sub>2</sub> in the flue gas eliminates the use physical solvents [10, 11]. Application of the amine process for  $CO_2$  capture from flue gas at post-combustion (i.e., low pressure) conditions is mainly hindered by the high energy consumption and the immense scale of the problem [12]. To give an impression of the scale of flue gas production relative to the scale of natural gas processing, consider the following example. The global CO<sub>2</sub> emission and the global natural gas production in 2012 was 34.5 billion tonnes ( $\sim 17580$  billion cubic meters (bcm)) and 3364 bcm, respectively [13, 14]. Assuming that the flue gas and the raw natural gas contained 10% CO<sub>2</sub>, one can calculate the actual volume of flue gas or natural gas that had to be processed at the power plant (175800 bcm) or at the well (3738 bcm), respectively. This simple example shows that the global scale of flue gas production is  $\sim 50$  times larger than the global scale of natural gas production. Moreover, the estimated energy penalty of a coal-fired power plant using MEA for CO<sub>2</sub> capture is in the range of 25 to 45% [15]. A huge amount of steam/energy is required in the desorber for solvent regeneration and concurrent liberation of the chemically complexed CO<sub>2</sub> [9].

The main focus of this study is CO<sub>2</sub> capture at pre-combustion and natural gas sweetening conditions. The relatively high operating pressure of these processes allows the use of physical solvents or adsorbents. The physical solvents Selexol, Rectisol, and Purisol are frequently used in the natural gas industry. However, chemical/hybrid solvents (e.g., MEA/Sulfinol) are preferred over physical solvents when a deep removal of the acid gases up to few ppm levels is required. Although the existing solvents/processes are successfully applied, they all suffer from one of the following: a high energy requirement, a high solvent volatility, or a low capacity/selectivity [15]. Recently, ionic liquids (ILs) have gained interest, mainly due to their very low vapor pressure and high acid-gas capacity, as new potential solvents for

natural gas sweetening [9, 16, 17]. However, the performance of ILs with respect to existing solvents (e.g., Selexol, Rectisol, Purisol, etc.) is still under debate [18].

 $\mathrm{CO}_2$  capture at post-combustion conditions requires new solvents which are more energy efficient, less toxic and corrosive, and cheaper than existing solvents. However, designing solvents with these specific characteristics is a challenging task. Moreover, experimentally screening a large number of molecules is a costly and time consuming operation. Here, we develop and apply molecular simulation techniques to screen solvents for  $\mathrm{CO}_2$  capture at post- and pre-combustion conditions.

In this thesis, we investigated the potential of physical ILs for CO<sub>2</sub> capture at pre-combustion and natural gas sweetening conditions. performance of ILs with respect to conventional solvents is assessed in terms of gas solubilities and selectivities. The work discussed in this thesis consists of two parts. The first part deals with experimental determination of gas solubilities in ILs, while in the second part molecular simulations are used to predict gas solubilities in physical solvents. In Chapter 2, a comprehensive review of CO<sub>2</sub> capture with ILs is presented. In Chapter 3, the experimental results of pure CO<sub>2</sub> and CH<sub>4</sub> solubilities in many different kinds of ILs are reported. Ideal CO<sub>2</sub>/CH<sub>4</sub> selectivities are derived from the experimental data and a comparison with conventional solvents is provided. In Chapter 4, the experimental results on the solubility of CO<sub>2</sub>/CH<sub>4</sub> gas mixtures in ILs is discussed. Real CO<sub>2</sub>/CH<sub>4</sub> selectivities are derived from this mixed-gas solubility data. In Chapter 5, Monte Carlo (MC) molecular simulations are used to predict the solubility of natural gas components in ILs and Selexol. In Chapter 6, MC simulations are used to compute the bubble points of CO<sub>2</sub>/CH<sub>4</sub> gas mixtures in ILs. In Chapter 7, MC simulations are used to compute the solubility of the pre-combustion gases CO<sub>2</sub>, CH<sub>4</sub>, CO, H<sub>2</sub>, N<sub>2</sub> and H<sub>2</sub>S in an IL. Separation selectivities relevant for the pre-combustion process are derived from the MC data and a comparison with experimental data is provided. In Chapter 8, a novel Monte Carlo method is developed to study the reactions of CO<sub>2</sub> with aqueous monoethanolamine (MEA). The so-called Reaction Ensemble Monte Carlo method in combination with the Continuous Fractional Component technique (RxMC/CFC) [19] is used to

compute the equilibrium speciation of all relevant species formed during the chemisorption process of  $\mathrm{CO}_2$  with aqueous MEA solutions. The computed speciation results are compared with available experimental data. Finally, Chapter 9 provides a detailed comparison of gas solubilities in ILs with respect to the conventional solvents Selexol, Purisol, Rectisol, propylene carbonate, and sulfolane.

In this work, we demonstrate that, (1) ideal  $CO_2/CH_4$  selectivities are approximately the same as real  $CO_2/CH_4$  selectivities, (2) gas solubilities in IL should be compared on mass or volume basis, (3) MC simulations can be used to quantitatively predict gas solubilities and equilibrium speciation in complex (reacting) solvents, (4) conventional solvents are superior to ILs in terms of gas solubilities.

## Chapter 2

# CO<sub>2</sub> Capture with Ionic Liquids: A Review

This chapter is based on the paper: M. Ramdin, T. W. de Loos and T. J. H. Vlugt. State-of-the-Art of CO<sub>2</sub> Capture with Ionic Liquids. Ind. Eng. Chem. Res., 51 (2012) 8149-8177.

#### 2.1 Introduction

The suspected correlation between the increased CO<sub>2</sub> concentration in the atmosphere and the green-house effect has initiated a worldwide debate aimed at emission reduction of CO<sub>2</sub> and other green-house gases [1, 2]. CO<sub>2</sub> emissions have increased since the dawn of the industrial revolution. This resulted in an increase of CO<sub>2</sub> concentration in the atmosphere from about 280 ppm before the industrialization to 390 ppm nowadays [20]. The global CO<sub>2</sub> emission in 2008 was about 29.4 gigatons (Gt), which is an increase of around 40% relative to the 1990 emission of 20.9 Gt [20]. Currently the power sector is responsible for 41% of all the energy-related CO<sub>2</sub> emissions, followed by the transport sector (23%), industry sector (20%), buildings sector (10%) and others [21]. The high share of the CO<sub>2</sub> emission in the

power sector is related to fuel combustion to generate electricity or heat. The share of coal in the total CO<sub>2</sub> emission from fuel combustion in 2008 was 43%, while the contribution of oil and gas was 37% and 20%, respectively [20]. Under the Baseline Scenario or Reference Scenario [22], the CO<sub>2</sub> emission will continue to increase and will most likely double, relative to the 2007 emission of 28.8 Gt, by 2050 [21]. Under this scenario the anticipated growth in future energy demand will be met using predominantly fossil fuels. This energy path is not consistent with the required deep cuts in global greenhouse-gas emissions by 2050 to limit the long-term global average temperature rise below 2 °C relative to pre-industrial levels [23]. The 2 °C target, which is believed to be the point where dramatic climate change will set in [24], was set during the UN conference on climate change in December 2009 in Copenhagen. In the long-term, a transition in energy path, from fossil fuels to low-carbon-technologies, will be required to meet the 2 °C goal. McKinsey & Company investigated several readily available or developing low-carbon-technologies, which could be used to mitigate CO<sub>2</sub> emissions [25–28]. However, in the foreseeable future, fossil fuel, in particular coal [29, 30], will continue to be a substantial fraction of the energy portfolio [20]. In this regard CO<sub>2</sub> capture and storage (CCS) will be essential [3], although it should be considered as a temporary solution to the problem. Both, the capture of CO<sub>2</sub> and the storage are technical challenging and many hurdles have to be overcome to commercialize these processes [3, 31, 32].

The major barrier to commercialize the CO<sub>2</sub> capture and storage process at large scale is the energy/cost associated with the separation method. Currently available technology for CO<sub>2</sub> capture is based on amine-solvents, for example monoethanolamine (MEA) [33]. The capture of CO<sub>2</sub> with amines involves a chemical reaction with a large enthalpy of reaction [34]. Consequently, a large amount of heat is required to release the captured CO<sub>2</sub> in the regeneration step. Retrofitting a CCS unit to an existing power plant, using conventional-amine solvents for CO<sub>2</sub> scrubbing, would lower the energy output of the plant by 25-40% [3]. Accordingly, the price of electricity would rise by 0.01-0.07 \$/kWh relative to a plant without a CCS system [1, 35]. The energy consumption for removing one ton of CO<sub>2</sub>, by employing a 30 wt% MEA (aqueous) solution and assuming 90%

2.1 Introduction 7

CO<sub>2</sub> removal, is estimated to be in the range of 2.5-3.6 Gigajoule (GJ). The theoretical minimum work for CO<sub>2</sub> separation and compression to the required pressure of 150 bar is 0.42 GJ/ton CO<sub>2</sub>, indicating the potential for process improvements [33, 36]. About half of this energy is required in the stripper to regenerate the  $CO_2$  and the other half is used to compress the  $CO_2$  to about 150 bar for subsequent sequestration [33]. Currently, not a single large scale plant with CCS is known to be operational. The primary reason for this is the high CO<sub>2</sub> removal cost ranging from 50 to 150 \$/ton  $CO_2$  removed, although recently much lower costs (30-35 \$/ton  $CO_2$ ) were reported [37]. Even a lower and debatable cost of 15 \$/ton CO<sub>2</sub> was reported by Inventys [38], but their technology is based on an adsorbent material instead of amines. However, the existing methodologies for CO<sub>2</sub> capture are energy intensive and far from cost effective, hence unattractive for large scale applications [1]. Therefore, much research has been devoted to find or design new solvents/materials for CO<sub>2</sub> capture. This includes CO<sub>2</sub> separation by chemical/physical absorption, chemical/physical adsorption, membranes, solid adsorbents and biomimetic approaches [5, 12, 15, 39, 40]. Recently D'Alessandro et al. [15] reviewed new and emerging materials for CO<sub>2</sub> capture, with particular attention for Metal-Organic Frameworks (MOFs). A special class of absorption materials, namely ionic liquids (ILs), have been proposed as an alternative to the volatile, corrosive and degradation sensitive amine-solvents [41, 42].

Ionic liquids are salts, which consist exclusively of ions, with a melting point lower than 100 °C [43]. The use of ionic liquids, although discovered a long time ago, was very limited until the late 1990s to few examples in electrochemistry and organic chemistry. This changed unexpectedly as a result of an article published by Freemantle [44] in 1998, describing the potential applications of ionic liquids as novel solvents for green chemistry [45–47]. Since then, ionic liquids have been the interest of many researchers, resulting in an expansion of the application field. So far, (potential) applications of ionic liquids have been reported in analytical chemistry [48], biochemistry [43], catalysis [49–51], electrochemistry [52, 53], separation technology [54–57], fluid engineering [58] and others [59, 60]. ILs are nowadays applied at industrial scale in the BASIL™process of BASF for pro-

ducing alkoxyphenylphosphines and the Degussa process for pigment paste production [61]. We note that the IL in the BASIL process does not serve as a solvent, but it is produced during the reaction step. ILs owe their unexpected popularity to their remarkable properties, such as: (nearly) negligible volatility, high thermal stability, non-flammability, tunability, solvation properties and high CO<sub>2</sub> solubility. The major driving force for research on ILs is their potential to replace traditional industrial solvents, which are often volatile organic compounds (VOCs). Substitution of the conventional volatile solvents by the relatively non-volatile ionic liquids would prevent environmental pollution due to emission of VOCs into the atmosphere. Furthermore, the tunability property of ILs provide an extra degree of freedom for designing solvents with certain specific characteristics [62].

This introduction provides an indication of the scale of the problem and the urgency to take action in order to prevent irreversible climate change. CCS is one of the remedies to the problem and in the following we will focus on the special application interest of ionic liquids as a CO<sub>2</sub> capture medium. Blanchard et al. [41] were the first to observe that significant amounts of CO<sub>2</sub> could be dissolved in imidazolium-based ionic liquids to facilitate an extraction of a dissolved product, without contaminating that product with the ionic liquid, since the ionic liquid was insoluble in CO<sub>2</sub>. This study initiated an explosion of scientific research on CO<sub>2</sub> absorption with ionic liquids, leading to a rapid growth of the literature on this specific topic [63]. Therefore, the aim of the present chapter is to give an extensive review of the achievements and recent developments in the search for a suitable ionic liquid for CO<sub>2</sub> capture from flue-gas streams and other point-sources. This review provides a different perspective on CO<sub>2</sub> capture with ILs than those published in other recent reviews [17, 55, 64–68]. That is, we focus on the potential application of ILs for CO<sub>2</sub> capture at the post-, pre-combustion and natural gas sweetening process. More importantly, a comparison of the CO<sub>2</sub> capture performance (i.e. solubility, selectivity, viscosity, price, etc.) of ILs with the commercially available solvents is presented. The review is started with an analysis of the relevant CO<sub>2</sub> capture processes (i.e. post-combustion, pre-combustion, oxyfuel combustion and natural gas

sweetening) and the conventional amine technology. Subsequently, a comprehensive overview of the main literature on  $\mathrm{CO}_2$  capture with ionic liquids is given. More specifically, attention is paid to the trends observed regarding  $\mathrm{CO}_2$  solubilities and selectivities in different ionic liquids, effect of anions, cations and functional groups on physical properties, biodegradability and toxicity of ionic liquids. The  $\mathrm{CO}_2$  capture performance of ILs is then compared with existing solvents (e.g. Selexol, Purisol, Sulfinol, etc.). The trends highlighted here may eventually help solvent designers to navigate through the massive number (about  $10^{18}$ ) of theoretically possible ternary IL systems [62, 69]. Recent developments on task specific or functionalized ionic liquids and supported ionic liquid membranes are also discussed. Finally, the remaining challenges and future research possibilities are outlined.

### 2.2 CO<sub>2</sub> Capture Processes

The conditions for  $CO_2$  capture, hence also the economics, are determined by the technology used for the production of electricity (or heat) from fossil fuels [70]. Today, a power company planning to build a new power station utilizing fossil fuels, can choose from two technologies, and a third one, which is in the development phase [71]. The characteristics of all the three processes (i.e. post-combustion, pre-combustion and oxyfuel combustion) are different, yielding different conditions for  $CO_2$  capture.

### 2.2.1 Post-combustion Capture

The first option is the post-combustion process [72], which is widely used at traditional fossil-fuel-fired power stations to produce electricity. Under post-combustion conditions the fuel is burned fully in one step in air, see Figure 2.1. The released heat is used to produce high-pressure steam, which drives a steam turbine to generate electricity. The flue-gas leaving the boiler contains substantial amounts of particulate matter, which is filtered out in the soot removal step. Subsequently, the sulphur in the flue-gas is scrubbed by a limestone slurry to produce gypsum. The cleaned flue-gas, which now contains 10-16% CO<sub>2</sub>, would be released into the atmosphere in the absence

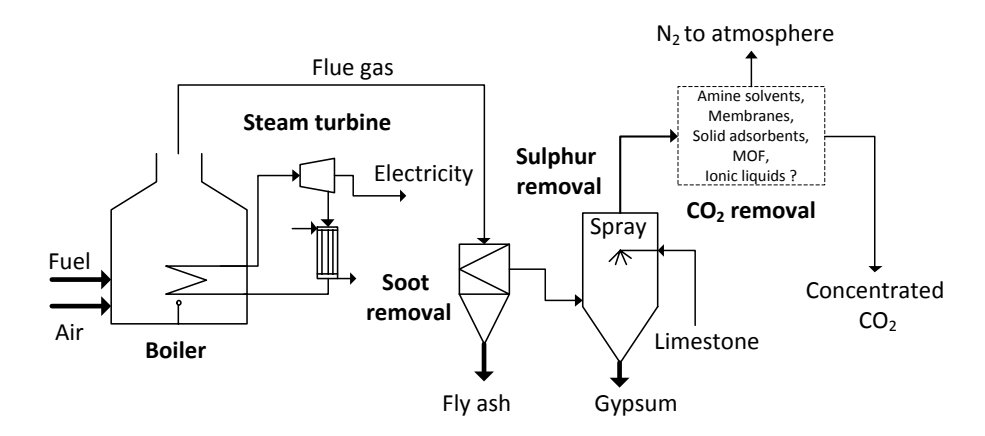


Figure 2.1: Schematic representation of a simplified post-combustion  $CO_2$  capture system [72]. In this process, the fuel is directly burned in air to produce large volumes of fluegas with low partial pressures of  $CO_2$ . The  $CO_2$  can in principle be captured with amines, but this process turns out to be expensive [15].

of a  $CO_2$  capture system. However, as explained in the introduction, the role of  $CO_2$  in the global warming requires it to be captured and stored safely underground for some time. The following can be stated by analyzing the data shown in Table 2.1 for the post-combustion process; (1) the relevant separation is  $CO_2/N_2$ , hence any separation process should be  $CO_2$  selective and (2) the process outputs large volumes of flue-gas with low  $CO_2$  partial pressures, accordingly the separation process should be able to cope with these conditions. We will see later that a low  $CO_2$  partial pressure, which is typical for post-combustion processes, is not very advantageous for (physical)  $CO_2$  capture. However, the advantage of the post-combustion process is that the CCS unit can be retrofitted without major modifications to an existing power plant.

Table 2.1: Typical conditions for post-combustion [15, 66] capture, pre-combustion [15, 73] capture and the natural gas sweetening [6, 17, 74] process.

	Dogt	Pre-	Notunal mag
	Post-		Natural gas
	combustion	$combustion^a$	sweetening
Gas composition	by mole	by mole	by mole
$CO_2$	10-15%	37.7%	0.1  8%
$_{\mathrm{H_2O}}$	5-10%	0.14%	
$\mathrm{H}_2$		55.5%	
$O_2$	3-4%		
CO	20  ppm	1.7%	
$N_2$	70 - 75%	3.9%	0 - 0.2%
$\mathrm{NO}_x$	< 800  ppm		
$\mathrm{SO}_x$	<500 ppm		
$H_2S$		0.4%	0 - 15%
$\mathrm{CH}_4$			70- $95%$
C2+			0 - 15%
Conditions			
Temperature (°C)	40-75	40	30-40
Pressure (bar)	1	30	5-120

<sup>&</sup>lt;sup>a</sup> After the water-gas-shift reaction

### 2.2.2 Pre-combustion Capture

The second option is the pre-combustion process [75], which is associated with the integrated gasification combined cycle (IGCC) and is more complex as shown in Figure 2.2. In this approach the fuel (coal, oil, etc.) is gasified, rather than burning it completely like in the post-combustion process, in presence of pure oxygen and steam to produce syngas. The syngas, which is a mixture of carbon monoxide (CO) and hydrogen (H<sub>2</sub>), is purified and fed to the water-gas-shift (WGS) reactor. In this reactor, steam is added to convert the CO, according to the water-gas-shift reaction, to H<sub>2</sub> and CO<sub>2</sub>. The gas can be desulphurized either before or after the WGS reactor, but preferentially before since any sulphur may be poisonous to the catalyst

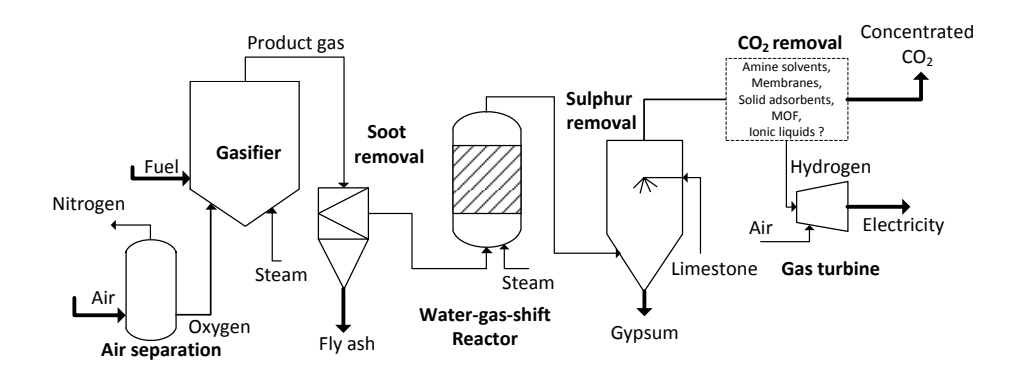


Figure 2.2: Schematic representation of a simplified pre-combustion  $CO_2$  capture system [75]. In this process, the fuel is first gasified to produce syngas, which is converted to  $CO_2$  and  $H_2$  in the WGS reactor. Since this process operates at high pressures, the  $CO_2$  can in principle be captured by several techniques.

used in the WGS reactor [6]. At this stage the gas consist primarily of  $CO_2$  and  $H_2$ . Subsequently, the  $CO_2$  is captured and the  $H_2$  is combusted in a gas turbine to produce electricity and heat. The heat produced during the combustion can be recovered by a heat recovery system (not shown in Figure 2.2) to generate more electricity. The typical conditions, after the WGS reactor, for pre-combustion  $CO_2$  capture are given in Table 2.1, from which we can deduce that the relevant separation is  $CO_2/H_2$ . Furthermore, the pre-combustion process yields a gas mixture with high  $CO_2$  partial pressures, which is favorable for  $CO_2$  separation.

### 2.2.3 Oxyfuel Combustion Capture

The third option is the oxyfuel combustion [76] process, which is a promising concept but still under development. A simplified schematic representation of this process is given in Figure 2.3. In this approach concentrated oxygen, instead of air, is used to burn the fuel. The released heat is used to produce high-pressure steam, which turns a steam turbine to generate electricity. The flue-gas, which mainly consists of  $H_2O$  and  $CO_2$ , is stripped of the soot

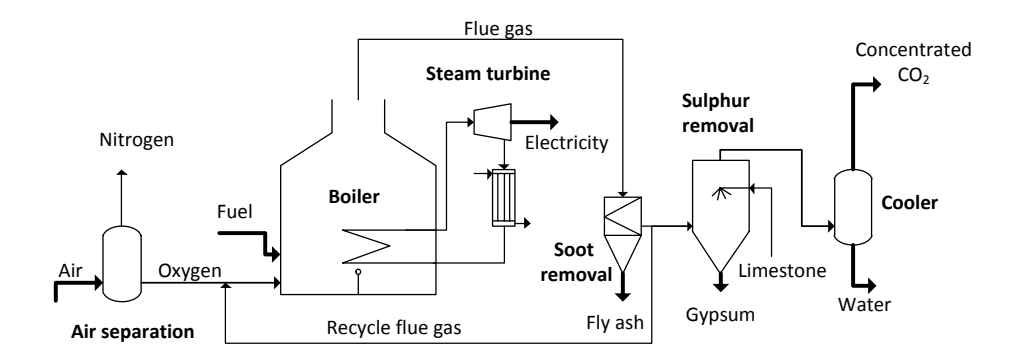


Figure 2.3: Schematic representation of a simplified oxyfuel-combustion  $CO_2$  capture system [76]. In this process, pure oxygen instead of air is used to burn the fuel, thereby eliminating nitrogen in the downstream separation.

particles and partly recycled to the boiler to control the temperature. The remaining flue-gas stream is desulphurized and cooled down to condense the water. The result is a concentrated stream of  $CO_2$ , which is ready to be stored underground. The fundamental difference between this process and the other two processes is that no  $CO_2$  capture is involved; instead  $N_2/O_2$  is the relevant separation in this process. The concentrated  $CO_2$  stream is a result of excluding nitrogen in the burning step.

Detailed economic evaluation of the three processes is provided by the US Department of Energy [77–84]. These cost estimation studies suggest that pre-combustion CO<sub>2</sub> capture is the least expensive option for CO<sub>2</sub> capture, but the investment for this process is higher than for the post-combustion and oxyfuel combustion process. In fact, pre-combustion and oxyfuel combustion technology can only be applied at new power plants, since existing power plants operate and will continue to operate at least a decade according to the post-combustion scheme [77]. Currently, no commercial power plant (either post- or pre-combustion) with CCS is in operation, hence cost estimates are highly uncertain [28]. Nevertheless, the factors determining the cost for the different CO<sub>2</sub> capture processes can

readily be identified. The most expensive component at post-combustion conditions in the CCS chain process is the CO<sub>2</sub> absorption/desorption, in particular the solvent regeneration step. In addition, the post-combustion capture process produces CO<sub>2</sub> at low pressures compared to sequestration requirements, adding significant expenses for pressurization. On the other hand, the advantage of the post-combustion process is that the CCS unit can be retrofitted directly, without major modifications, to an existing power plant. The pre-combustion process benefit from the high operating pressures, since (1) CO<sub>2</sub> is produced at high pressures reducing cost for pressurization, and (2) the higher pressures allows application of less energy intensive separation technologies. However, these cost savings may be offset as the capital cost might be higher due to the complexity of the process. The utilization of an expensive high-pressure WGS reactor and a costly air separation unit may bring extra cost. The major disadvantage of the pre-combustion capture process is that it can be applied only at new power plants, since the majority of the existing power plants operate according to the post-combustion method. The oxyfuel combustion process eliminates the expensive  $CO_2$  capture step, but on the other hand the process requires a costly air separation step. The boiler of the oxyfuel combustion process requires special construction materials to withstand the high temperatures, which is a consequence of using pure oxygen [5]. Other concern of the oxyfuel combustion process is the high  $SO_2$  concentration in the flue gas causing tube corrosion [85]. It is evident that CCS will bring extra cost and that the cost will be governed by the process type utilized for power generation.

### 2.2.4 Natural Gas Sweetening

CO<sub>2</sub> capture is not only important from an environmental perspective, but is also of industrial relevance in the natural gas sweetening process. The global natural gas demand is expected to increase with 1.4% per year the coming two to three decades [86]. Hence it would be beneficial to find an efficient and cost effective method for CO<sub>2</sub> removal from natural gas. Natural gas contains large amounts of methane (CH<sub>4</sub>), but also all kind

of impurities resulting in a classification as 'sour' for high content of sour gases (e.g. H<sub>2</sub>S and CO<sub>2</sub>) or 'sweet' for low content of H<sub>2</sub>S and CO<sub>2</sub>. The composition of natural gas is highly dependent on the location of the gas field, which is reflected in the large variation of the natural gas components shown in Table 2.1. The relevant separation in this process is  $CO_2/CH_4$ , but an additional separation may be required if other (e.g. H<sub>2</sub>S) sour gases are involved. However, the acid gases in the natural gas should be removed at the well to avoid technological problems during gas transportation and to comply with environmental regulations [17]. Accordingly, the  $CO_2$  should be removed to prevent dry ice or gas hydrate formation, which can clog the system during liquefaction of the natural gas. Furthermore, the corrosiveness of H<sub>2</sub>S and CO<sub>2</sub> in the presence of water, the toxicity of H<sub>2</sub>S and the lack of heating value of CO<sub>2</sub> requires sweetening of the sour natural gas [87]. The most popular technology, comprising for over 95\% of the units in the field in the United States [17], to capture H<sub>2</sub>S and CO<sub>2</sub> is amine-based, although the high pressure at the gas well (see Table 2.1) allows the use of physical absorbents, solid adsorbents and membranes [15]. In fact, physical solvents like Rectisol, Purisol and Selexol are preferred over chemical solvents for high pressure gas purification processes [10].

### 2.2.5 Conventional Amine Technology

Many CO<sub>2</sub> capture technologies are under investigation, but presently amine scrubbing is probably the only feasible technology to capture CO<sub>2</sub> from a large scale fossil-fuel-fired power plant [33]. Amine scrubbing for CO<sub>2</sub> removal is a mature technology used in the ammonia process, steam reforming process and the natural gas sweetening process [34]. Many alkanolamines, like primary amines monoethanolamine (MEA) and digly-colamine (DEA), secondary amines like diethanolamine (DEA) and disopropanolamine (DIPA) and tertiary amines like methyldiethanolamine (MDEA) and triethanolamine (TEA) and sterically hindered amines have been considered for CO<sub>2</sub> capture [34]. However, due to its high reactivity with CO<sub>2</sub>, MEA is predominantly used for CO<sub>2</sub> capture. A typical process configuration for post-combustion CO<sub>2</sub> capture from flue-gas streams

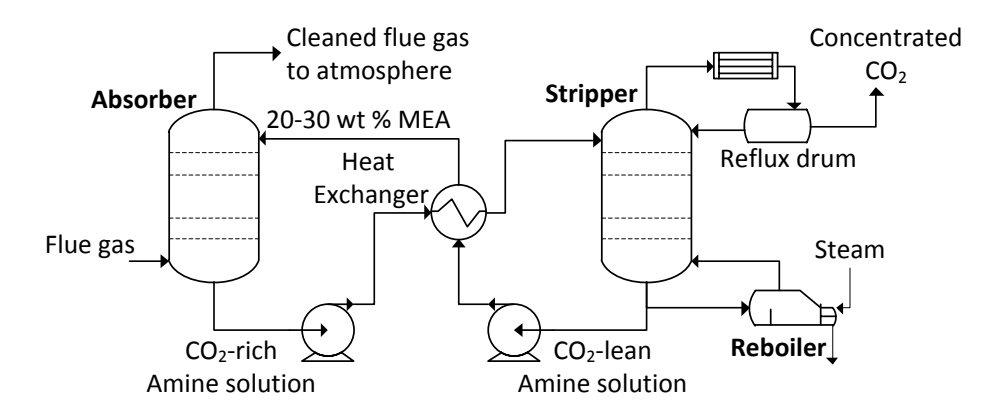


Figure 2.4: Schematic representation of a simplified process for  $CO_2$  absorption with amines [33].  $CO_2$  is captured in the absorber by a reaction with monoethanolamine (MEA) and subsequently released in the stripper by heating.

$$\begin{bmatrix} O & & & & \\ C & + & 2 & HN & & & & \\ O & & & & R^1 & & & \\ O & & & & & R^1 \end{bmatrix} + H_2N^+$$

Figure 2.5: Absorption of  $CO_2$  with primary amines.  $CO_2$  reacts in a 1:2 stoichiometry with a primary amine forming a carbamate salt.

is shown in Figure 2.4. The flue-gas, which is typically at 40-60  $^{\circ}$ C, is introduced at the bottom of an absorption tower, while a 20-30 wt% MEA solution is continuously added at the top. The CO<sub>2</sub> in the flue gas is selectively and chemically absorbed by a primary amine (e.g. MEA) through a zwitterion mechanism [34] to form carbamates, see Figure 2.5. Subsequently, the CO<sub>2</sub>-rich amine solution is drained off from the bottom of the absorber and introduced at the top of the stripper where the bounded CO<sub>2</sub> is released upon heating with steam. The regeneration of the amine solvent

and concurrently liberation of the  $\rm CO_2$  takes place at elevated temperatures, typically at 100-140 °C, and at near atmospheric (1-2 bar) pressures. The regenerated amine solvent is recycled back to the absorption tower for continuing the cycle. The concentrated  $\rm CO_2$  stream leaving the stripper is ready to be stored underground after pressurization.

The major drawback of this process is the high energy requirement for solvent regeneration, which is a consequence of the high reactivity of MEA leading to a large enthalpy of reaction associated with the carbamate production. Beside this energy penalty, MEA suffer a number of other drawbacks making it unattractive for large scale applications. These include the corrosiveness of MEA, this in fact is the reason for using dilute solutions, degradation of the solvent in the presence of oxygen, and the volatility of the solvent, which causes environmental pollution [15]. Furthermore, the theoretical maximum CO<sub>2</sub> loading of MEA for the carbamate formation scheme is approximately  $0.5 \text{ mol CO}_2$  per mol of MEA, as can be deduced from Figure 2.5 [34]. Clearly, MEA is not a very energy efficient and environment friendly solvent for CO<sub>2</sub> capture. Hence, much research focused on developing solvents with improved characteristics with respect to the following: energy requirements for solvent regeneration, CO<sub>2</sub> loading, kinetics, volatility, chemical degradation and corrosivity [88]. Improved amines, such as the secondary amines (e.g. DEA) and tertiary amines (e.g. MDEA) have been considered as an alternative for MEA. The reaction of CO<sub>2</sub> with secondary amines is also described by the zwitterion mechanism, but the enthalpy of reaction is lower due to the lower stability of the carbamate formed during the reaction [15]. Since tertiary amines do not have any hydrogen atom attached to the nitrogen atom, the carbamation reaction cannot take place. Instead, bicarbonate formation takes place according to a base-catalyzed hydration mechanism [34]. The enthalpy of reaction for the bicarbonate formation is lower than for the carbamate formation, resulting in a lower energy penalty for solvent regeneration. In addition, tertiary amines have a theoretical CO<sub>2</sub> loading capacity of 1 mole of CO<sub>2</sub> per mole of amine, although the reactivity of tertiary amines with respect to CO<sub>2</sub> is lower [34]. This is inherent to the thermodynamics of the reaction, since the enthalpy of reaction is related to the CO<sub>2</sub> capacity as  $K = -\Delta_r G^0/RT$ , with K the equilibrium constant of the reaction,  $\Delta_r G^0 = \Delta_r H^0 - T \Delta_r S^0$  the standard Gibbs reaction energy,  $\Delta_r H^0$  the standard enthalpy of reaction and  $\Delta_r S^0$  the standard entropy of the reaction. Clearly, there is a trade-off between aiming a high CO<sub>2</sub> capacity at a certain temperature and wanting to keep the enthalpy of reaction low at the same time [66].

Given the many disadvantages of the amine-process, it is highly desirable to develop solvents that perform substantially better than conventional amines with respect to energy requirement for solvent regeneration, corrosivity, chemical degradation, thermal stability and volatility. The last decade, ionic liquids (ILs) have emerged as a promising alternative to the amines due to their remarkable properties, such as negligible volatility, high chemical/thermal stability and tunability. The latter is probably the most important property of ionic liquids, since it allows design of task-specific ionic liquids (TSILs). In the following we analyze the data reported in the literature on CO<sub>2</sub> capture with ionic liquids.

### 2.3 CO<sub>2</sub> Capture with Ionic Liquids

The number of possible ILs is very large. Few examples of commonly used cations and anions of ILs are shown in Figure 2.6, where the  $R_i$  groups are often alkyl groups. Among these ILs, the imidazolium class is most widely investigated and reported in the literature. Initial research on  $CO_2$  capture with ILs focused primarily on the phase behavior of  $CO_2$  with different physical (non-functionalized) ionic liquids. As shown in Figure 2.7, the phase behavior of IL- $CO_2$  systems is remarkable compared to conventional organic solvents (e.g. n-hexane, toluene). Firstly, a relatively large amount of  $CO_2$  can be dissolved in a typical ionic liquid, like [emim][Tf<sub>2</sub>N]. Secondly, conventional molecular solvent- $CO_2$  systems show a simple two-phase envelope with a mixture critical point at moderate pressures [89]. Clearly, this is not the case for a  $CO_2$ -IL system, instead  $CO_2$  dissolves well at low pressures, but at higher mole fractions of  $CO_2$  the bubble-point pressure sharply increases to very high pressures, without showing a critical point at moderate pressures. This unusual behavior is common for  $CO_2$ -IL systems

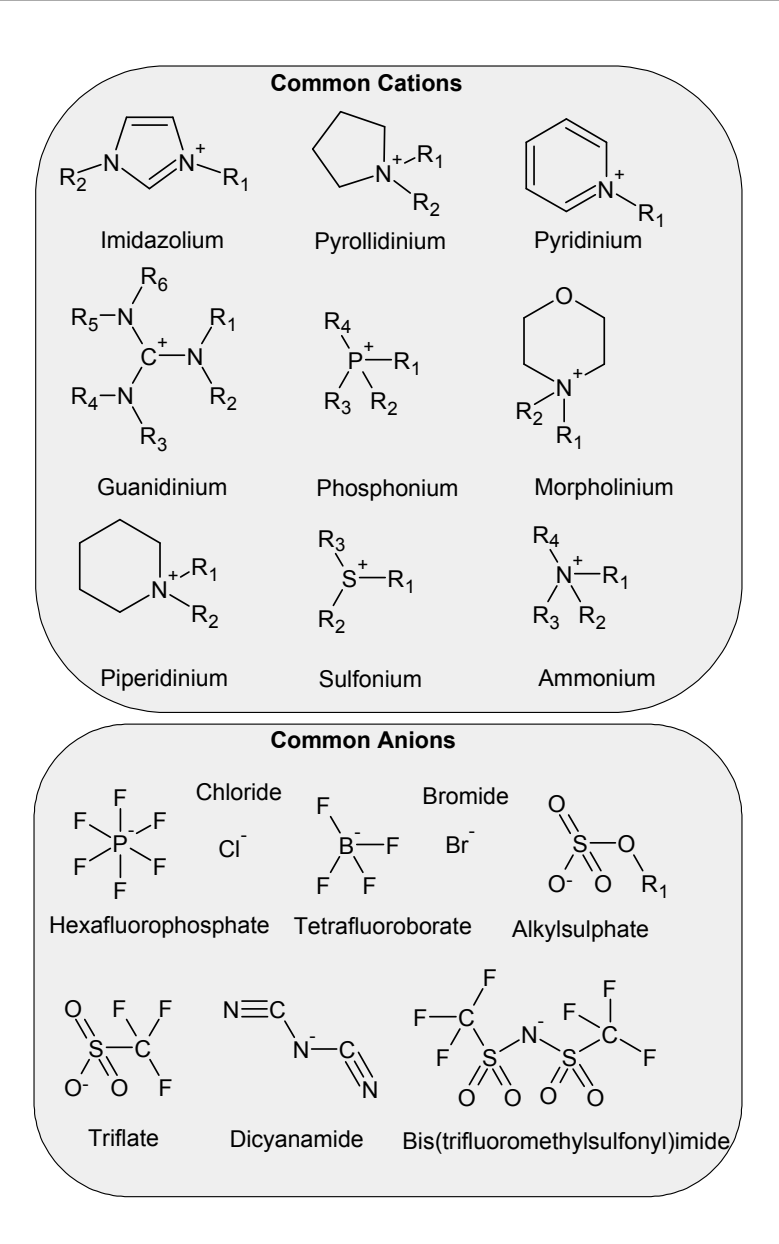


Figure 2.6: Commonly used anions and cations of ionic liquids.

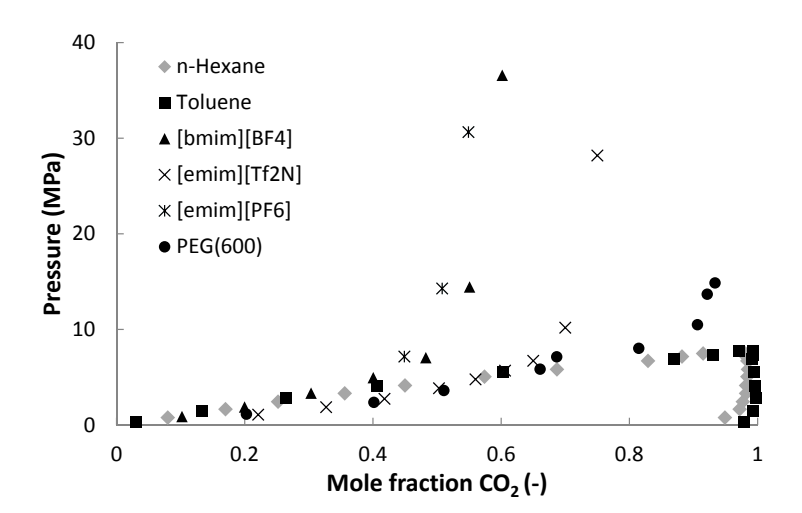


Figure 2.7: Comparison of the VLE phase behavior of  $CO_2$ -conventional solvents systems with  $CO_2$ -ILs systems. Conventional solvents show a critical point at moderate pressures, whereas ILs systems do not show this behavior. The behavior of  $CO_2$ -IL systems is comparable with high molecular weight liquid polymers, for example PEG(600)- $CO_2$  system. Data at 313 K taken from Refs [90–95].

and can be classified as type III fluid-phase behavior according the classification of van Konynenburg and Scott [92, 96]. We note, however, that it is not fair to compare high molecular weight and almost nonvolatile ILs with low molecular weight volatile compounds. A more justifiable comparison of  $\rm CO_2$ -IL systems would be that with high molecular weight liquid polymers. As shown in Figure 2.7, the PEG(600)-CO<sub>2</sub> system shows a behavior comparable to that of  $\rm CO_2$ -IL systems. In the following a more systematic approach is used to show trends regarding  $\rm CO_2$  capture with ILs.

#### 2.3.1 Physical Ionic Liquids

In this section we will only concentrate on  $CO_2$  absorption by conventional ILs based on a physical mechanism (i.e. upon absorption of  $CO_2$ , no chemical reaction takes place).  $CO_2$  solubility, selectivity, ionic liquid viscosity and volatility are considered.

#### CO<sub>2</sub> Solubility

The anion is believed to play a key role in the dissolution of  $CO_2$ , whereas the cation is supposed to have a secondary role [97]. This finding is supported by molecular simulation studies and experimental data [98, 99]. To help understanding the high solubility in imidazolium ILs, Cadena et al. [99] used molecular simulations. These authors found that the CO<sub>2</sub> primarily associates with the [PF<sub>6</sub>] anion, regardless of the cation. The in situ ATR-IR spectroscopy data of Kazarian et al. [100] again reveals the favorable interaction between the anions ( $[BF_4]$  and  $[PF_6]$ ) and  $CO_2$ . The spectroscopic data suggested that the interaction is a Lewis acid-base type where the anion serve as a Lewis base, while  $CO_2$  act as a Lewis acid. Furthermore, the spectroscopic data provide strong evidence that the interaction between CO<sub>2</sub> and [BF<sub>4</sub>] anion should be stronger than for the [PF<sub>6</sub>] anion, since [BF<sub>4</sub>] is a stronger base. However, experimental solubility data show a higher  $CO_2$  solubility in  $|bmim||PF_6|$  rather than  $|bmim||BF_4|$ . Thus, the solubility cannot solely be explained by anion-CO<sub>2</sub> interactions and a free volume mechanism is also expected to play a significant role in dissolving CO<sub>2</sub> [100]. A free volume mechanism where CO<sub>2</sub> molecules are hosted in the free spaces (cavities) of the liquid is not unlikely, since the liquid volume of ILs do not change significantly upon dissolution of large amounts of CO<sub>2</sub> [89, 97, 99]. In addition, Kanakubo et al. [101] performed X-Ray diffraction measurements on the [bmim][PF<sub>6</sub>]-CO<sub>2</sub> system and showed that CO<sub>2</sub> preferentially organizes around the [PF<sub>6</sub>] anion. The effect of the anion has been studied experimentally by pairing the [bmim] cation with several anions as shown in Figure 2.8. This figure show data at 333 K with CO<sub>2</sub> solubilities increasing in order of the anions:  $[NO_3] < [SCN] < [MeSO_4] < [BF_4] < [DCA]$ 

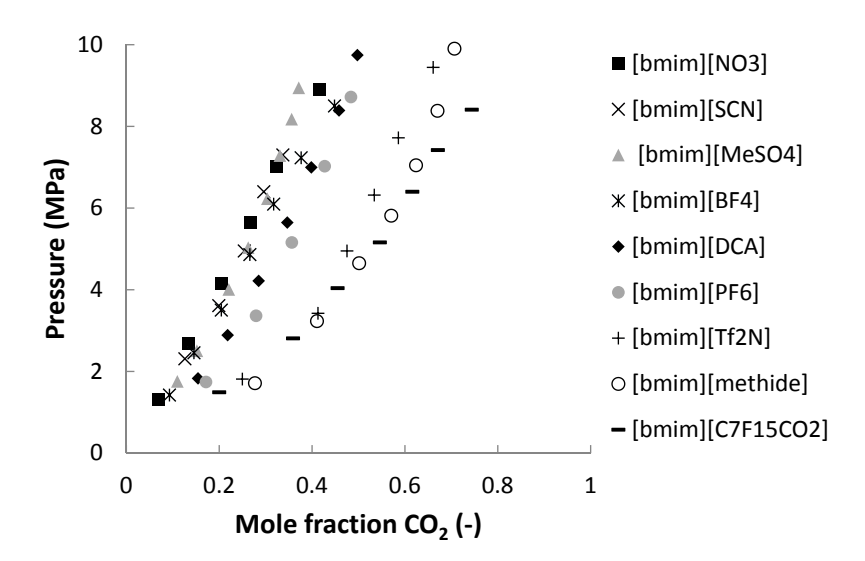


Figure 2.8: Effect of anion on  $CO_2$  solubility. Fluorinated anions show higher  $CO_2$  solubilities than unfluorinated ones. Data at 333 K taken from Refs [97, 102, 103].

< [PF<sub>6</sub>] < [Tf<sub>2</sub>N] < [Methide] < [C<sub>7</sub>F<sub>15</sub>CO<sub>2</sub>]. This trend was successfully reproduced by Maiti [104] and Sistla [105] using the COSMO-RS model (Conductor-like Screening Model for Real Solvent) where guanidinium and phosphonium based ILs were supposed to be promising for higher CO<sub>2</sub> solubility than the corresponding imidazolium-ILs. Generally, fluor containing ILs have higher CO<sub>2</sub> solubilities compared to ILs without a fluor group. The effect of anion-fluorination is shown in Figure 2.9 for ILs with a common [bmim] cation. CO<sub>2</sub> solubility increases as the number of fluor groups in the anion increases. The solubility increases in the following anion order: [BF<sub>4</sub>] < [TfO] < [TfA] < [PF<sub>6</sub>] < [Tf<sub>2</sub>N] < [methide] < [C<sub>7</sub>F<sub>15</sub>CO<sub>2</sub>] < [eFAP] < [bFAP]. Consistently, in a screening study Zhang et al. [106] used COSMO-RS to demonstrate that using a longer fluoroalkyl chain in the anion (e.g. [FAP] anion) corresponds to higher CO<sub>2</sub> solubilities. Recently, Palomar et al. [107] used the COSMO-RS methodology to achieve deeper

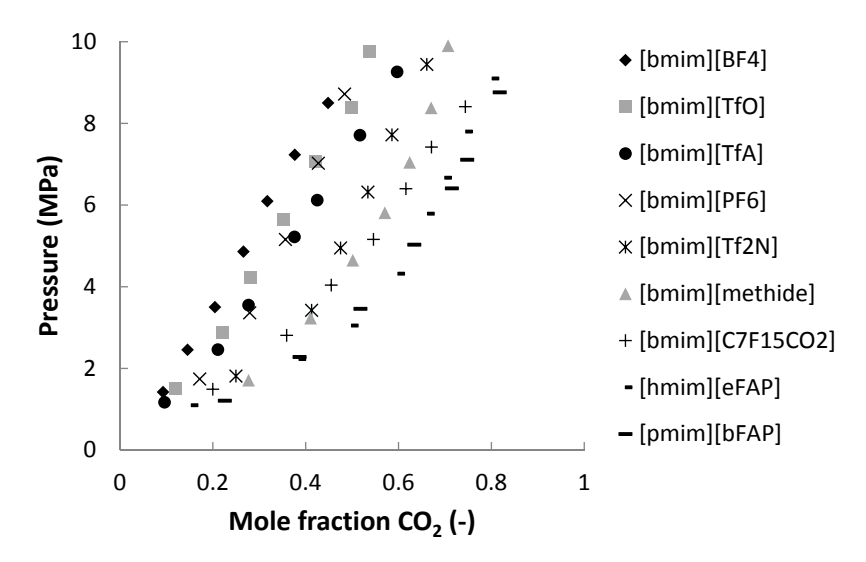


Figure 2.9: Effect of anion fluorination on  $CO_2$  solubility.  $CO_2$  solubility increases as the number of fluor groups increases in the anion. Data at 333 K taken from Refs [97, 102].

insight into the dissolution behavior of CO<sub>2</sub> in ionic liquids. To this end, a wide number of ILs liquids were screened and the Henry's constants of CO<sub>2</sub> were successfully related to the excess enthalpy of dissolution of CO<sub>2</sub> in ILs. This indicated that higher solubilities are associated with a higher exothermicity of the mixture. Further, the intermolecular interactions (electrostatic, hydrogen bonding, and van der Waals) between the species in the fluid phase were computed. The contribution of each of these interactions to the solubility of CO<sub>2</sub> in ILs was determined and the results indicate that the attractive van der Waals forces dominate the behavior of CO<sub>2</sub> dissolution in ILs. The electrostatic interactions had a secondary contribution to the excess enthalpy of dissolution, whereas the contribution of hydrogen bonds were found insignificant [107]. On the basis of this finding, Palomar *et al.* [107] carried out a guided COSMO-RS screening to find ILs, which have increased van der Waals interactions with the CO<sub>2</sub>. The screening resulted

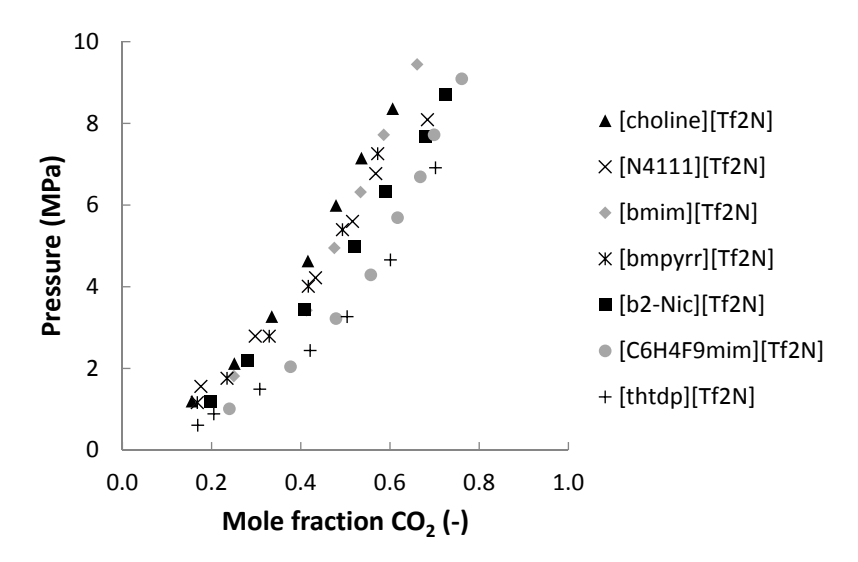


Figure 2.10: Effect of cation on  $CO_2$  solubility. The cation seems to have a minor influence on the solubility of  $CO_2$ . Data at 333 K taken from Refs [97, 102, 108, 109].

in new potential ILs with highly brominated anions (e.g.  $[emim][PBr_6]$ ) with high  $CO_2$  solubilities.

It is widely accepted that the anion dominates the dissolution of  $CO_2$ , although the cation is believed to play a secondary role. The small effect of the cation on the  $CO_2$  solubility is clearly shown in Figure 2.10. Cholinium, ammonium, imidazolium, pyridinium, pyrrolidinium and phosphonium cations were paired with the  $[Tf_2N]$  anion. Nevertheless, fluorination of the cation (e.g.  $[C_6H_4F_9mim]$ ) can significantly improve the solubility, although to a lesser extent than anion-fluorination [111]. Moreover, using long alkyl chains on the phosphonium cation [P66614] can also improve the solubility. Generally, the  $CO_2$  solubility increases slightly by increasing the alkyl chain length as shown in Figure 2.11. All the ionic liquids were paired with a common bis(trifluoromethylsulfonyl)amide  $[Tf_2N]$  anion, while the alkyl chain length on the imidazolium cation was varied. Clearly, as the alkyl

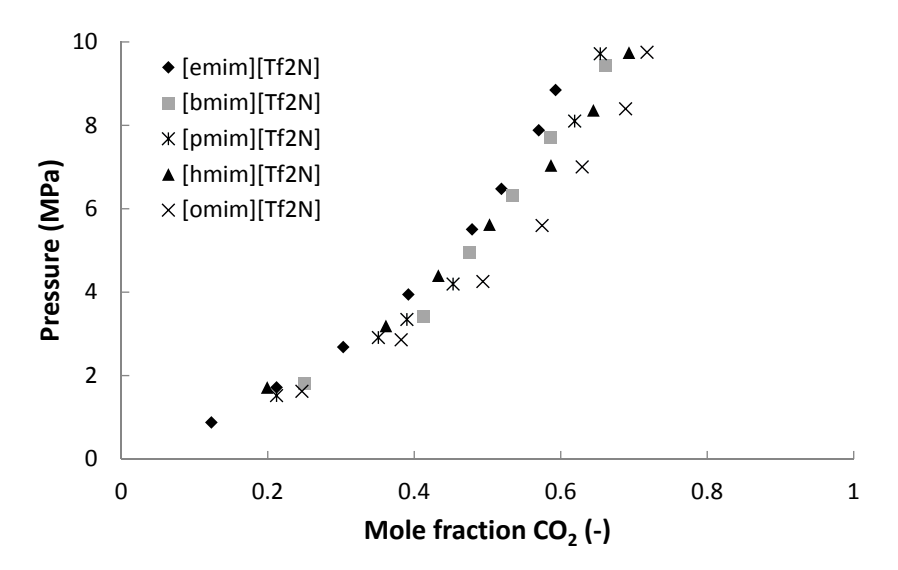


Figure 2.11: Effect of alkyl chain length on  $CO_2$  solubility.  $CO_2$  solubility increases as the alkyl chain length becomes longer. Data at 333 K taken from Refs [94, 97, 110].

chain becomes longer the solubility increases in the following order: [omim] > [hmim] > [pmim] > [bmim] > [emim]. These trends have also been predicted using the COSMO approach [104, 105, 107, 112]. It is known that the hydrogen attached to the  $C_2$  position ( $C_2$ -H) on the imidazolium ring is acidic (i.e. it has a relatively large positive charge). Therefore, additional  $CO_2$  may be dissolved at this  $C_2$  site via hydrogen bonds. The effect of this acidic site has been investigated by means of molecular simulations and experiments [97, 99]. Molecular simulation shows that replacing the proton in the  $C_2$  position with a methyl group ( $C_2$ -methyl) slightly decreases the  $CO_2$  solubility [99]. Experiments support this finding, as the Henry's constant at 298 K for  $CO_2$  in [bmim][PF<sub>6</sub>] and [bmmim][PF<sub>6</sub>] are 53.4 bar and 61.8 bar, indicating a lower solubility in the methyl-substituted [bmmim] IL [99].

Although molecular simulations have been used extensively to study the

solvation behavior of CO<sub>2</sub> in ILs, computed solubility isotherms of CO<sub>2</sub> in ILs have been reported scarcely due to the increased computational effort [7, 18, 113, 114]. For choosing an optimal IL for CO<sub>2</sub> capture from flue-gases, from a tremendous amount (around  $10^{18}$ ) of possible ILs, fast screening methods like COSMO are beneficial. However, several other methods using surface tension or viscosity as an input have been reported in the literature to predict gas solubilities in ILs [115, 115–117]. A review of the different approaches that have been used to model the phase behavior of IL-gas systems is provided by Vega et al. [118]. Camper et al. [117, 119– 123 demonstrated that regular solution theory (RST) is also able to predict solubility trends of various gases in ILs at low pressures. This is an interesting finding, since RST without taking into account the intermolecular interactions between the gas and the anion was used for describing solubility trends. Indeed, this contradict the conventional wisdom that CO<sub>2</sub> solubility is dominated by CO<sub>2</sub>-anion interactions. In RST, Equation (2.1), the activity coefficient of a solute,  $\gamma_1$ , is related to its liquid molar volume,  $V_1$ , and the difference in solubility parameters  $\delta_1$  and  $\delta_2$  of solute and solvent, respectively.

$$RT \ln \gamma_1 = V_1 \Phi_2^2 [\delta_1 - \delta_2]^2 \tag{2.1}$$

Shi and Maginn [124] showed that when the RST parameters are known one can calculate the complete solubility isotherm for a gas. However, until recently the solubility parameter of ILs,  $\delta_2$ , was unknown and was adjusted to fit experimental isotherms [113]. Recently, enthalpies of vaporization for many ILs were determined experimentally allowing to calculate directly the solubility parameter by  $\delta_2 = (\Delta_{\text{vap}}U_2/V_2)$ . Using experimentally obtained solubility parameters, RST was found to significantly underpredict the solubility of  $\text{CO}_2$  in [hmim][Tf<sub>2</sub>N]. The poor performance of the RST when using actual, instead of correlated, solubility parameters to describe  $\text{CO}_2$  solubility is not surprising. As shown in Figure 2.12,  $\text{CO}_2$  solutions in ILs at low pressure show negative deviations from ideality as represented by Raoult's law:

$$y_1 P = x_1 P_1^{\text{sat}} \tag{2.2}$$

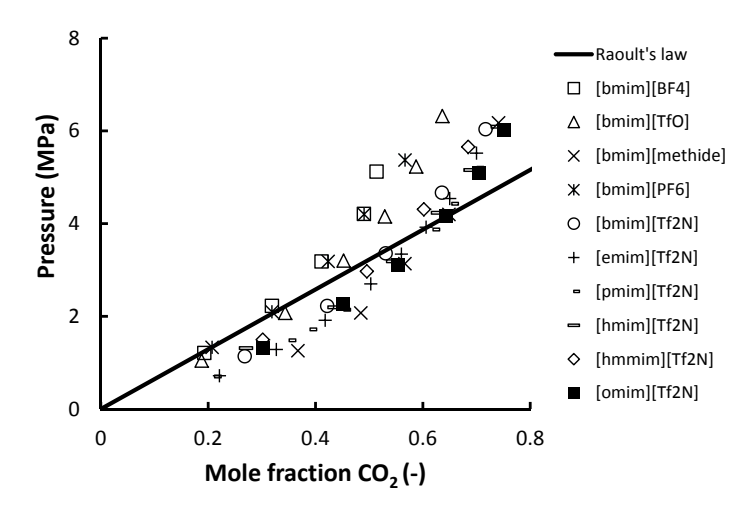


Figure 2.12: Comparison of the behavior of  $CO_2$ -ILs systems with Raoult's law predictions. Typically,  $CO_2$ -ILs systems show negative deviations to the ideality as represented by Raoult's law. Data at 298 K taken from Refs [94, 97].

where P is the pressure,  $P_1^{\rm sat}$  the vapor pressure of  ${\rm CO}_2$ ,  $x_1$  the mole fraction of  ${\rm CO}_2$  in the liquid phase and  $y_1$  the mole fraction of  ${\rm CO}_2$  in the gas phase, which is equal to 1 assuming nonvolatility of ILs. As a consequence, the activity coefficient of  ${\rm CO}_2$  in ILs is lower than 1, while RST can only describe solutions with positive deviations from ideality. The performance of RST to predict solubilities should further be tested in the future using experimentally solubility parameters.

So far, CO<sub>2</sub> solubilities on mole fraction basis were considered. Recently, Carvalho and Coutinho [125] claimed that physical CO<sub>2</sub> absorption in ILs is dominated by entropic effects, hence CO<sub>2</sub> solubilities when plotted as molality (e.g mole/kg) versus pressure are solvent independent and fall on a common universal curve. Subsequently, they developed a universal correlation for the solubility of CO<sub>2</sub> in nonvolatile solvents with a validity for pressures up to 5 MPa, molalities up to 3 mole/kg and temperatures

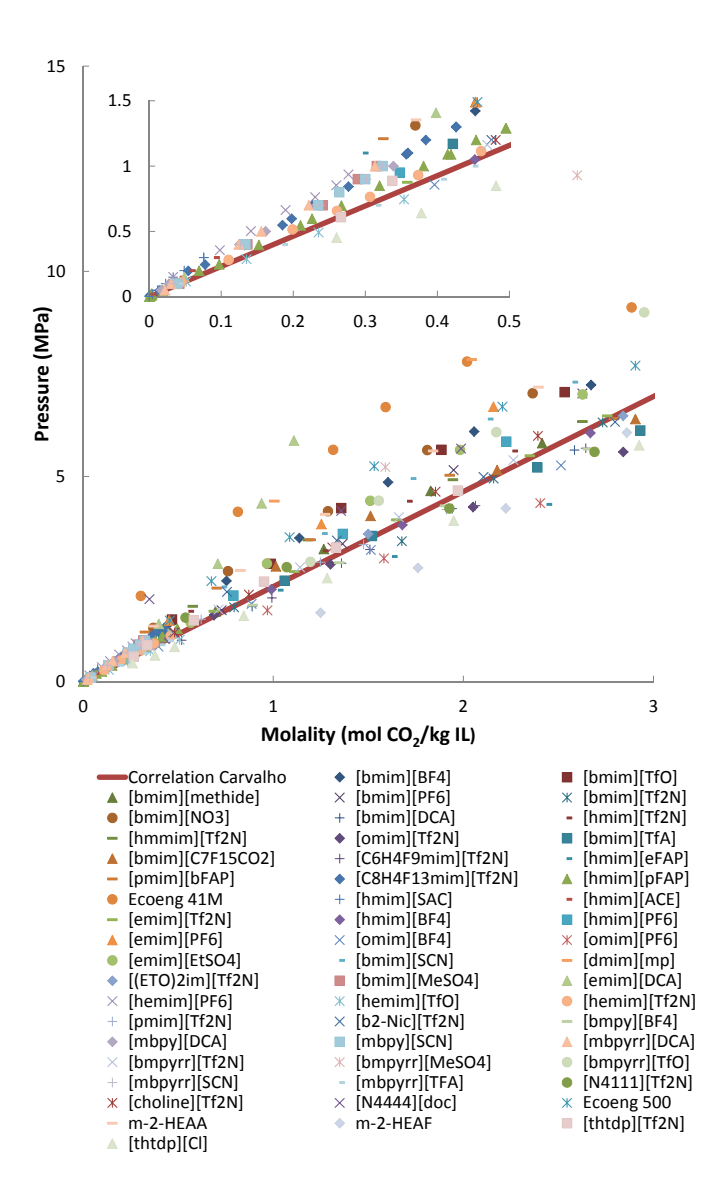


Figure 2.13: Solubility of carbon dioxide expressed as molality in different ionic liquids. Data show that many ILs do not fall on the universal curve proposed by Carvalho and Coutinho [125]. Data at 333 K taken from Refs [89, 93, 97, 102, 103, 108–110, 126–136].

ranging from room temperature to 363 K. This universal correlation is given by the following equation, where p is the pressure in MPa,  $m_i^0$  the molality in mole/kg and T the temperature in Kelvin:

$$p = m_i^0 e^{6.8591 - \frac{2004.3}{T}} \tag{2.3}$$

Unfortunately, many ILs that do not obey the trend were excluded in the analysis [66, 125]. The validity of the model, Equation (2.3), proposed by Carvalho and Coutinho is explored by plotting a large number of ILs in the pressure-molality diagram shown in Figure 2.13. Indeed, the differences in CO<sub>2</sub> solubilities among many of the ILs are minimized. However, there are many ILs that significantly deviate from the curve proposed by Carvalho and Coutinho [66, 125]. In the case of acetates (m-2-HEAA) and formates (m-2HEAF) the solubility is dominated by the formation of electron donoracceptor (EDA) complexes and do not follow the universal curve, which was also noted by Carvalho and Coutinho. Furthermore, ILs with the following anions, regardless of the cation, also do not obey the curve: [SO<sub>4</sub>], [SCN], [mp], [doc] and [NO<sub>3</sub>]. Even the simple IL [bmim][BF<sub>4</sub>] and many of the [PF<sub>6</sub>], [DCA] and [TfO] ILs do not follow the trend. It is likely that the model suggested by Carvalho and Coutinho [125] is a severe oversimplication. Nevertheless, these authors correctly noticed that there is a strong influence of the IL molecular weight on the CO<sub>2</sub> solubility as can be seen in Figure 2.13. In the following, we will show that the  $CO_2$  solubility increases with increasing IL molecular weight, but first we consider the CO<sub>2</sub> solubility as given in molarity (mol/m<sup>3</sup>). The solubility data of CO<sub>2</sub>, which are the same as in Figure 2.13, but now expressed in molarity is shown in Figure 2.14. We can see in Figure 2.14 that a pressure-molarity plot for many ILs yield nearly straight lines up to  $\sim 60$  bar. The slope of these lines gives a first-order approximation of the (molarity based) Henry constants. This Henry constants are plotted against the molecular weight of the IL in Figure 2.15. Clearly, the Henry constant (CO<sub>2</sub> solubility) show a decreasing (increasing) trend with an increasing IL molecular weight. The Henry constants of CO<sub>2</sub> in the imidazolium-based ILs when plotted against the IL molecular weight seems to fall on a common curve, while this is apparently

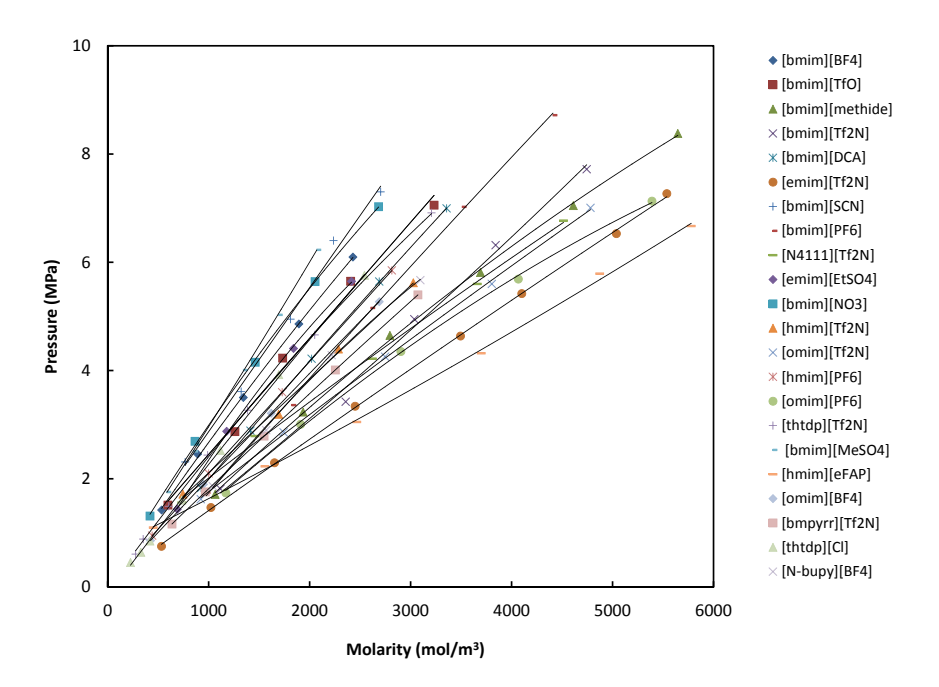


Figure 2.14: Solubility of carbon dioxide expressed as molarity (mol  $CO_2/m^3$  solvent) in different ionic liquids. Solubility data at 333 K as used in Figure 2.13. Density data at 333 K taken from Refs [137–146].

different for phosphonium-based ILs. However, considering the free-space mechanism it would be more interesting to analyze the  $\rm CO_2$  solubility with respect to the IL molar volume or IL free volume. In Figure 2.16 the Henry constants are plotted as a function of the molar volume of the IL. The trend is similar as for molecular weight effects, i.e., the Henry constant ( $\rm CO_2$  solubility) shows a decreasing (increasing) trend with an increasing IL molar volume. The free volumes of the ILs listed in the legend of Figure 2.14 have been estimated by:

$$V_{\rm f} = V_{\rm m} - 1.3 V_{\rm vdW}$$
 (2.4)

where  $V_{\rm f}$  is the free volume of the IL,  $V_{\rm m}$  the IL molar volume and  $V_{\rm vdW}$  the

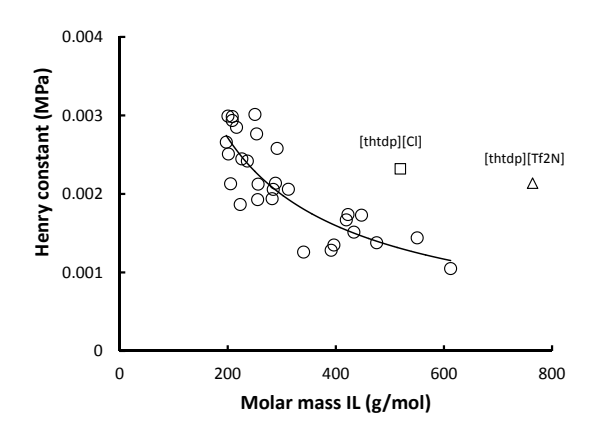


Figure 2.15: Henry constants (molarity based) at 333 K plotted as a function of the molecular weight of the IL show that the Henry constant ( $CO_2$  solubility) is decreasing (increasing) with an increasing molecular weight. Imidazolium-based ILs (circles), phosphonium-based ILs (square and triangle) and the lines are fit through the imidazolium-based data to guide the eye.

van der Waals molar volume. Zhao et al. [147] provide a correlation based on Bondi principles [148] to estimate  $V_{\text{vdW}}$  (Å<sup>3</sup>/molecule) rapidly with very good accuracy using only atomic and bond contributions:

$$V_{\text{vdW}} = \sum AAC - 5.92N_{\text{B}} - 14.7R_{\text{A}} - 3.8N_{\text{NR}}$$
 (2.5)

where AAC is the atomic contribution of all atoms  $V_{\rm vdW}$  (as given by Bondi [148]),  $N_{\rm B}$  is the number of total bonds,  $R_{\rm A}$  is the number of aromatic rings and  $N_{\rm NR}$  is the number of nonaromatic rings. Zhao et al. [147] used Equation (2.5) to calculate  $V_{\rm vdW}$  of 677 organic compounds and compared their values with the values computed using the TSAR program (Oxford Molecular) having a regression coefficient value of 0.992 and a standard error of 8.6 Å<sup>3</sup>/molecule. Using Equation (2.4) and Equation (2.5) we have estimated the free volume of all ILs listed in the legend of Figure 2.14. Subsequently, we have correlated the Henry constants (molarity based) with the free volume of the IL as shown in Figure 2.17. Again, the Henry constant (CO<sub>2</sub> solubility) shows a decreasing (increasing) trend with an increasing

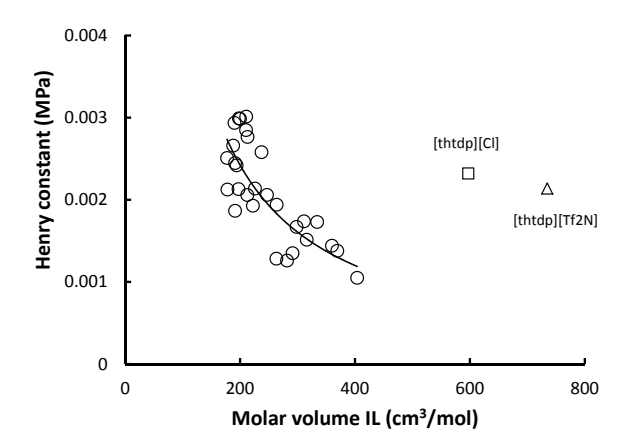


Figure 2.16: Henry constants (molarity based) at 333 K plotted as a function of the molar volume of the IL show that the Henry constant ( $CO_2$  solubility) is decreasing (increasing) with an increasing molar volume. Imidazolium-based ILs (circles), phosphonium-based ILs (square and triangle) and the lines are fit through the imidazolium-based data to guide the eye.

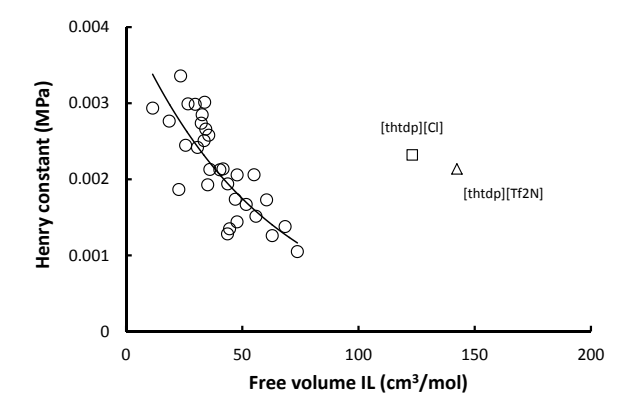


Figure 2.17: Henry constants (molarity based) at 333 K plotted as a function of the free volume of the IL show that the Henry constant ( $CO_2$  solubility) is decreasing (increasing) with an increasing free volume. Imidazolium-based ILs (circles), phosphonium-based ILs (square and triangle) and the lines are fit through the imidazolium-based data to guide the eye.

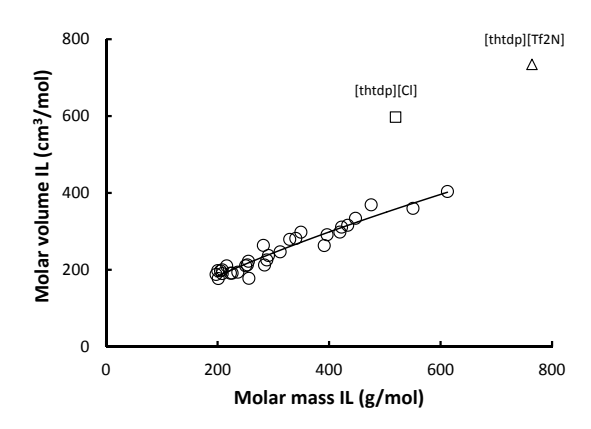


Figure 2.18: Molecular weight plotted as a function of the IL molar volume at 333 K show that the molar volume almost linearly increases with increasing IL molecular weight. Imidazolium-based ILs (circles), phosphonium-based ILs (square and triangle) and the lines are fit through the imidazolium-based data to guide the eye.

IL free volume. We note that in the calculation of the free volume based on Equation (2.5), the imidazolium and the pyridine rings have been considered as aromatic, while the pyrrolidine ring has been taken as nonaromatic. Furthermore, the molar volume of ILs seems to be correlated with their molecular weight, see Figure 2.18. The molar volume increases with an increasing IL molecular weight, although the trends seems to be different for imidazolium and phosphonium-based ILs.

Recently, Shannon et al. [149] also showed that  $CO_2$  solubility and selectivity in ILs are governed by the free volume of the IL. These authors used the COSMOtherm program to calculate the free volume of 165 existing and theoretical imidazolium-based ILs. Subsequently, they showed that the volume-normalized solubility of  $CO_2$  is proportional to the free volume to the power -0.5, while the solubility of  $CH_4$  and  $N_2$  exhibited a linear dependence on the IL free volume.

In summary, CO<sub>2</sub> solubility increases with increasing IL molecular weight, molar volume and free volume. All these results support the claim by Carvalho and Coutinho [125] that CO<sub>2</sub> solubility in ILs is dominated by

entropic effects rather than solute-solvent interactions as claimed by many authors. It is clear that the solubility trends as a function of molality or molarity will be different than the trends established on mole fraction basis at the beginning of this chapter. The only trend that seems to survive (see Figure 2.14) is that the  $CO_2$  solubility in fluor-containing ILs is higher than in nonfluorinated ILs. This suggest that in addition to the dominating free-space mechanism also solute-solvent interactions are important. The most important message here is that  $CO_2$  solubility should not be evaluated on mole fraction basis due to the strong molecular weight (molar volume) effect. In fact, from an application point of view it is more interesting to analyze the solubility per volume solvent (molarity) or on a molality basis [17].

## CO<sub>2</sub> Selectivity

In practice, separation processes involve mixtures of two or more components that have to be purified or separated, hence solubility data only is not enough to judge the separation performance of a solvent, but also selectivity is essential. Although dozens of CO<sub>2</sub> solubility data are avaible in the literature, selectivity data of CO<sub>2</sub> in ionic liquids are scarcely reported. Nevertheless, for CO<sub>2</sub> capture from flue-gas and natural gas the following selectivities are mainly relevant:  $CO_2/N_2$ ,  $CO_2/H_2$  and  $CO_2/CH_4$ . Flue-gas or natural gas can contain a large number of impurities and selectivities like CO<sub>2</sub>/H<sub>2</sub>S, CO<sub>2</sub>/SO<sub>x</sub>, H<sub>2</sub>S/CH<sub>4</sub> and CO<sub>2</sub>/CO might also become important. Anderson et al. [150] measured the solubility of various gases in the IL  $[hmpy][Tf_2N]$ , see Figure 2.19. The solubility of the gases in  $[hmpy][Tf_2N]$ at 298 K decreases by the following order:  $SO_2 > CO_2 > C_2H_4 > C_2H_6$  $> CH_4 > O_2 > N_2$ . Similar gas solubility trends (i.e.  $CO_2 > C_2H_4 >$  $C_2H_6 > CH_4 > O_2$ ) were observed in the ILs [hmim][Tf<sub>2</sub>N], [bmim][PF<sub>6</sub>] and  $[bmim][Tf_2N]$  [42, 98, 150]. In general,  $N_2$  and  $O_2$  solubilities are much lower compared to CO<sub>2</sub> leading to a high CO<sub>2</sub>/N<sub>2</sub> or CO<sub>2</sub>/O<sub>2</sub> selectivity. The hydrocarbons show moderate solubilities, thereby reducing the  $CO_2$ /hydrocarbon selectivity.  $SO_2$  is by far the most soluble component in [hmpy][Tf<sub>2</sub>N], suggesting that it could compete with CO<sub>2</sub> in an absorption

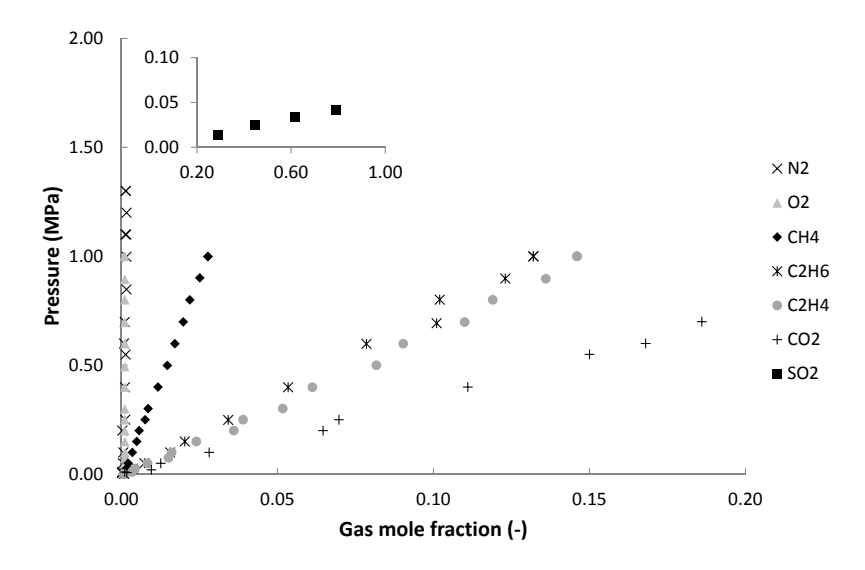


Figure 2.19: Solubility of gases in the ionic liquid [hmpy][Tf<sub>2</sub>N]. Solubility of the gases show the following trend:  $N_2 < O_2 < CH_4 < C_2H_6 < C_2H_4 < CO_2 < SO_2$ . The inset shows the solubility behavior of  $SO_2$  in [hmpy][Tf<sub>2</sub>N] (axis the same as in the main figure). Data at 298 K taken from Refs [150, 151].

process. As usual, the solubility of  $CO_2$ ,  $C_2H_4$ , and  $C_2H_6$  decreases as the temperature increases, however the solubilities of  $CH_4$  and  $O_2$  were nearly temperature independent. Kumelan *et al.* [152] also observed the temperature independence of  $O_2$  solubilities in [bmim][PF<sub>6</sub>].

Recently, Carvalho and Coutinho [153] measured  $\mathrm{CH_4}$  solubilities in imidazolium, phosphonium and ammonium ILs. They also noticed that an increase in temperature had a small or even negligible impact on  $\mathrm{CH_4}$  solubility. The peculiarities of  $\mathrm{CH_4} + \mathrm{IL}$  systems do not end here, Carvalho and Coutinho also observed a crossover in the P-x diagram above which the temperature dependency is reversed such that the  $\mathrm{CH_4}$  solubility increases with increasing temperature. Furthermore, the solubility of  $\mathrm{CH_4}$  was shown to relate to the polarity of the IL and  $\mathrm{CO_2/CH_4}$  or  $\mathrm{H_2S/CH_4}$  selectivities

were correlated using the Kamlet-Taft  $\beta$  parameter. The Kamlet-Taft parameters,  $\alpha$  the hydrogen bond donor,  $\beta$  the hydrogen bond acceptor and  $\pi$  the polarizability properties, are measures for the overall solvent polarity. The selectivities of sour gases/CH<sub>4</sub> were shown to increase with the  $\beta$  parameter, hence it could be used as a basis for designing ILs which maximize sour gases/CH<sub>4</sub> selectivities.

Hydrogen and carbon monoxide (CO) solubility was measured, respectively in  $[hmim][Tf_2N]$  and  $[bmim][PF_6]$  by Kumelan *et al.* Solubility of both gases in the ILs was remarkably low compared to CO<sub>2</sub>, which is indicative for high CO<sub>2</sub>/H<sub>2</sub> and CO<sub>2</sub>/CO selectivities in the corresponding ILs. The solubility of H<sub>2</sub> in [hmim][Tf<sub>2</sub>N] and [bmpy][Tf<sub>2</sub>N] was shown to increase with temperature [108]. This is in contrast with  $CO_2$  + IL systems where the solubility decreases with temperature. CO solubility in [bmim] [PF<sub>6</sub>] was not influenced upon increasing the temperature, while the CO solubility increased in [bmim][CH<sub>3</sub>SO<sub>4</sub>] with increasing temperature [156]. Jacquemin et al. [157, 158] measured low pressure solubilities of several gases in [bmim][BF<sub>4</sub>] and [bmim][PF<sub>6</sub>]. The solubility of CO<sub>2</sub> was the highest in both ILs, whereas the solubility of  $H_2$  was the lowest. In addition, the hydrogen solubility was shown to increase with temperature at lower temperatures, but it started to decrease with increasing temperatures at higher temperatures. The solubility of the gases in [bmim][BF<sub>4</sub>] and  $[bmim][PF_6]$  increases in the order:  $H_2 < CO < N_2 < O_2 < Ar < CH_4 < O_2$  $C_2H_6 < CO_2$ . The effect of the cation on the solubility of hydrogen was investigated by Jacquemin et al. [159]. The [bmim], [emim] and [N4111] cation was paired with the [Tf<sub>2</sub>N] anion and the subsequent solubility results show that the cation had a small effect on the H<sub>2</sub> solubility, although the solubility was higher in the ammonium [N4111] IL. For all the three systems, the hydrogen solubility decreased with temperature, this is opposite to what was found for [bmim][PF<sub>6</sub>], [hmim][Tf<sub>2</sub>N] and [bmpy][Tf<sub>2</sub>N] systems. Shiflett and Yokozeki [160] showed that much higher CO<sub>2</sub>/H<sub>2</sub> selectivities (about 30-300) could be obtained with [bmim][PF<sub>6</sub>] compared to novel polymeric membranes which had selectivities ranging from 10 to 30 under typical operating conditions. The same authors developed an equation of state (EOS) for the  $CO_2/H_2S/[bmim][PF_6]$  and  $CO_2/H_2S/[bmim][MeSO_4]$ 

systems [161, 162]. Subsequently they showed that competition between the two solutes exists, leading to a low (about 3.2 to 4) CO<sub>2</sub>/H<sub>2</sub>S selectivity in the  $[bmim][PF_6]$  system. For the  $[bmim][MeSO_4]$  system the selectivity was dependent on the  $CO_2/H_2S$  feed ratios, for large and intermediate feed ratios the selectivity was 10 to 13 [162]. In particular, solubilities of diatomic gases (e.g. H<sub>2</sub>, O<sub>2</sub>, CO, N<sub>2</sub>) measured in the same IL but by different authors show large discrepancies [42, 152, 155, 157, 158, 163]. For example, the Henry constant for  $O_2$  in  $|bmim||PF_6|$  at 283 K was reported by Anthony et al. [42] to be  $650 \pm 425$  MPa, while Kumelan et al. [152] reported a value of  $51.5 \pm 0.6$  MPa at 283 K. Nevertheless, the solubility trends of several gases observed in ILs are more or less similar. Simple gases often interact weakly with the IL ions, hence the polarizability of the gases is reflected in the solubility behavior, leading to the series  $H_2$  $CO < N_2 < O_2 < Ar < CH_4 < C_2H_6 < CO_2$ . Molecules that possess an electric quadrupole moment (e.g. CO<sub>2</sub> and C<sub>2</sub>H<sub>4</sub>) show higher solubilities [164]. Accordingly, polar gases like SO<sub>2</sub>, H<sub>2</sub>S and water vapor show very high solubilities.

Applying regular solution theory, Camper et al. [117, 119–123] showed that the physical solubility of gases in ILs was well correlated with the liquid molar volume of the IL and that ideal selectivities for CO<sub>2</sub>/N<sub>2</sub> and  $CO_2/CH_4$  should increase as the molar volume of the IL decrease. Finotello et al. [123] measured CO<sub>2</sub>, N<sub>2</sub> and CH<sub>4</sub> solubilities in pure [bmim][BF<sub>4</sub>] and  $|\text{bmim}||\text{Tf}_2\text{N}|$  and in mixtures of these ILs. They showed that  $\text{CO}_2/\text{N}_2$ and  $CO_2/CH_4$  ideal selectivity in [bmim][BF<sub>4</sub>] could be enhanced by adding 5 mole %  $[bmim][Tf_2N]$ , which is consistent with RST as this IL mixture represented the lowest liquid molar volume. Bara et al. [165] measured the solubility and ideal selectivities of the gas pairs CO<sub>2</sub>/N<sub>2</sub> and CO<sub>2</sub>/CH<sub>4</sub> in imidazolium-based ILs functionalized with oligo(ethylene glycol). They showed that the CO<sub>2</sub> solubility in these oligo(ethylene glycol) functionalized ILs were similar to their corresponding alkyl analogues, but  $N_2$  and  $CH_4$ solubilities were lower corresponding to a higher ideal selectivity for the two gas pairs. Similar results were reported by Carlisle et al. [166] for nitrilefunctionalized ILs. The nitrile-functionalized ILs exhibited lower CO<sub>2</sub>, N<sub>2</sub> and CH<sub>4</sub> solubilities, but showed improved CO<sub>2</sub>/N<sub>2</sub> and CO<sub>2</sub>/CH<sub>4</sub> selectivities compared to alkyl-substituted analogues. Mahurin et al. [167] measured  $CO_2/N_2$  ideal selectivities in imidazolium, pyridinium and pyrrolidinium ILs functionalized with a benzyl group. Improved CO<sub>2</sub>/N<sub>2</sub> ideal selectivities, ranging from 22 to 33, were reported for these benzyl-functionalized ILs. It should be stressed here that mainly ideal selectivities (i.e. the ratio of pure gas solubilities) are reported in de literature. Unfortunately, real or actual selectivities in mixtures of gases can not always be determined from pure gas solubilities with the assumption of ideal mixing. In general, measuring mixed-gas solubilities is significantly more difficult, therefore almost no mixture data can be found in the literature [113]. One of the first mixed gas solubilities was reported by Hert et al. [168]. In this study, the authors reported an enhancement of the sparingly soluble gases O<sub>2</sub> and CH<sub>4</sub> in the IL [hmim][Tf<sub>2</sub>N] in the presence of CO<sub>2</sub>. However, using molecular simulations Shi and Maginn [124] showed that there is no or very little enhancement of O<sub>2</sub> solubility in the presence of CO<sub>2</sub>. Revised experiments on  $CO_2/O_2$  support this finding, hence  $CO_2/O_2$  selectivities can be expected to have near-ideal selectivities [113]. The literature on mixed gas solubilities has mostly focused on the gas pairs CO<sub>2</sub>/H<sub>2</sub>S, CO<sub>2</sub>/SO<sub>2</sub> and  $CO_2/H_2$ . The  $CO_2/H_2S$  and  $CO_2/SO_2$  selectivities are extremely important in desulfurization processes and the natural gas sweetening process as natural gas can contain large amounts of sulfur compounds. CO<sub>2</sub>/H<sub>2</sub>S solubilities in ILs were investigated by Shiflett et al. [161, 162] in the ILs [bmim][MeSO<sub>4</sub>] and [bmim][PF<sub>6</sub>], while Jalili et al. measured CO<sub>2</sub>/H<sub>2</sub>S solubilities in [omim][Tf<sub>2</sub>N]. CO<sub>2</sub>/H<sub>2</sub>S (gas phase) selectivity in [bmim][MeSO<sub>4</sub>] and [bmim][PF<sub>6</sub>] is somewhat dependent on the CO<sub>2</sub>/H<sub>2</sub>S feed ratio, but at 298.15 K it was  $\sim 10$  and 1-4, respectively. Jalili et al. [135] reported a (gas phase) selectivity of  $\sim 3$  at 303.15 K in the [omim][Tf<sub>2</sub>N] IL. Yokozeki and Shiflett [169, 170] investigated experimentally the CO<sub>2</sub>/SO<sub>2</sub> (gas phase) selectivity in the ILs [hmim][Tf<sub>2</sub>N] and [bmim][MeSO<sub>4</sub>], while Shi and Maginn [124] used molecular simulation for the  $CO_2/SO_2/[hmim][Tf_2N]$ system. The  $CO_2/SO_2$  (gas phase) selectivity in the ILs  $[hmim][Tf_2N]$  and  $[bmim][SO_4]$  was highly dependent on the gas feed ratio and IL addition, but for a  $CO_2/SO_2$  ratio of 9/1 the selectivity was  $\sim 30$  and 226-348, respectively. We note that H<sub>2</sub>S and SO<sub>2</sub> are much more soluble than CO<sub>2</sub> and

the selectivities reported here are gas phase selectivities (i.e. a high H<sub>2</sub>S or SO<sub>2</sub> solubility in the liquid phase result in a high gas phase CO<sub>2</sub>/sulfuric gas selectivity.) Beside CO<sub>2</sub>/H<sub>2</sub>S, also CO<sub>2</sub>/CH<sub>4</sub> selectivities are important in the natural gas sweetening process, however, no data could be found for real CO<sub>2</sub>/CH<sub>4</sub> selectivities. Nevertheless, the natural gas process operates at high pressures and ideal selectivity should not be expected for CO<sub>2</sub>/CH<sub>4</sub> separation. As previously noted, in the pre-combustion process the relevant separation/selectivity is CO<sub>2</sub>/H<sub>2</sub>. Mixed gas solubility of CO<sub>2</sub>/H<sub>2</sub> mixtures has been investigated by Yokozeki and Shiflett [160], Kumelan et al. [171] and Shi et al. [172]. Yokozeki and Shiflett reported a CO<sub>2</sub>/H<sub>2</sub> selectivity of 30-300 in the IL [bmim][PF<sub>6</sub>], but the selectivity was shown to decrease with increasing temperature. Kumelan et al. investigated a mixture of  $CO_2/H_2/[hmim][Tf_2N]$  and found that  $CO_2$  act as a cosolvent for hydrogen, thereby enhancing the solubility of the sparsely soluble hydrogen gas. Shi et al. found a  $CO_2/H_2$  selectivity of  $\sim 30$  in the IL [hmim][Tf<sub>2</sub>N] at 313 K, but this number decreased to about 3 at 573 K. The CO<sub>2</sub> solubility decreases with increasing temperature, while this is the opposite for hydrogen resulting in a lower  $CO_2/H_2$  selectivity at higher temperatures. The most relevant separation in the post-combustion process is the  $CO_2/N_2$ separation, hence CO<sub>2</sub>/N<sub>2</sub> selectivities are important in this process. Kim et al. [173] measured the mixed gas solubility of  $CO_2/N_2$  mixtures in the IL  $[hmim][Tf_2N]$ . Their results show that negligible amounts of  $N_2$  were absorbed in the IL suggesting a high and ideal selectivity for this gas pair.

In summary, the most important separation in the post-combustion process is  $\rm CO_2/N_2$ . Ideal  $\rm CO_2/N_2$  selectivity in ILs is expected to be high and close to real selectivity, since  $\rm N_2$  solubility in ILs is not influenced by the presence of the  $\rm CO_2$ . In the pre-combustion process, assuming that the  $\rm CO_2$  is captured after the WGS reaction, the relevant separation is  $\rm CO_2/H_2$ . Although ideal  $\rm CO_2/H_2$  selectivity in ILs are relatively high, real selectivity is expected to be lower than ideal selectivity especially at higher temperatures, since  $\rm H_2$  solubility in ILs shows a increasing trend with increasing temperature while this is the opposite for  $\rm CO_2$ . In the natural gas sweetening process many impurities can be present, but the relevant separations considered here are  $\rm CO_2/CH_4$  and  $\rm CO_2/H_2S$ . Ideal selectivity

of  $\mathrm{CO_2/CH_4}$  in ILs is comparable to that in conventional physical solvents, however real  $\mathrm{CO_2/CH_4}$  selectivity in ILs is also expected to be lower than the ideal selectivity, since  $\mathrm{CH_4}$  solubility in many ILs also increases for increasing temperature while this is the opposite for  $\mathrm{CO_2}$ . Ideal selectivity should not be expected for the gas pair  $\mathrm{CO_2/H_2S}$ , since  $\mathrm{CO_2}$  solubility is significantly inhibited by the presence of  $\mathrm{H_2S}$ . In fact,  $\mathrm{H_2S}$  is much more soluble in ILs and both gases will compete in an absorption column. It is possible to remove both gases simultaneously, but this is not necessarily an advantage as an additional step may be required for separating  $\mathrm{CO_2}$  from  $\mathrm{H_2S}$ .

## Viscosity of Ionic Liquids

The shear viscosity,  $\eta$ , of an IL is one of the key material properties in process design, because high viscosities often form barriers for many applications and may lead to mass transfer limitations in chemical reactions [164]. Many ILs form highly viscous gel-like materials. Nevertheless, the tunability property of ILs can be invoked to design ILs with a broad range of viscosities. Figure 2.20 shows a plot of the shear viscosity  $\eta$  versus 1/T of some commonly used ILs. Simple liquids obey Arrhenius law, according to which the  $\eta$  versus 1/T plot yields a straight line. However, the data given in Figure 2.20 significantly deviates from Arrhenius law and are usually described by the Vogel-Fulcher-Tammann (VFT) equation:

$$\eta = A \cdot \exp(B/(T - T_0)) \tag{2.6}$$

where A, B and  $T_0$  are specific adjustable parameters [164]. Also the pressure dependence of the viscosity of ILs shows notable differences from the typical behavior of molecular solvents [174, 175]. It can readily be seen in Figure 2.20 that the IL viscosities are much higher than for conventional solvents like water, alcohols or acetonnitrile. Therefore designing ILs with low viscosities by manipulating the nature of cations and anions has been the objective of many researchers. An analysis of the effect of the cation on the viscosity is given in Figure 2.21. In this figure the viscosity of imidazolium, pyridinium, pyrrolidinum, phosphonium and ammonium ILs

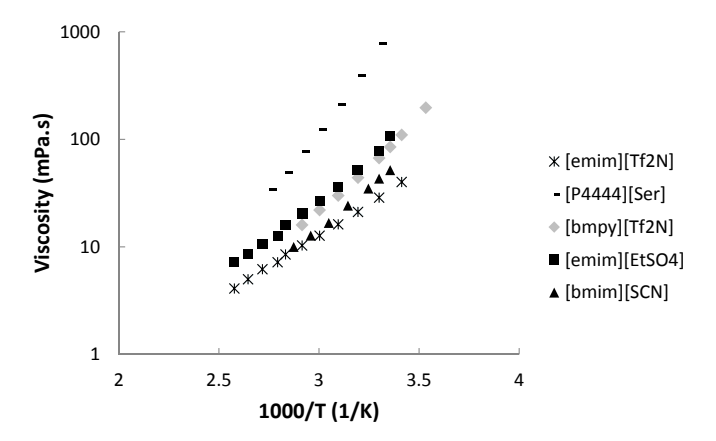


Figure 2.20: Temperature dependence of the viscosity. The data significantly deviates from Arrhenius law and is usually described by the Vogel-Fulcher-Tammann [138, 139, 176, 177].

with a common [Tf<sub>2</sub>N] anion at 298 K is given. The viscosity increases with the cation series: imidazolium [hmim] < pyridinium [hmpy] < pyrrolidinum [hmpyrr] < phosphonium [P2228] < ammonium [N2228]. mentioned here that physical properties of ILs like density and viscosity are influenced by the amount of water and other impurities present in the IL [139]. To make a fair comparison in this section only viscosity data of dried ILs (i.e. water content lower than 1000 ppm) are considered. The effect of the anion on the viscosity at 303 K for ILs with a common [bmim] cation is given in Figure 2.22. The viscosity increases with the anion order:  $|DCA| < |Tf_2N| < |SCN| < |TfA| < |TfO| < |BF_4| < |BETI| < |NO_3| < |TfO| <$  $[MeSO_4] < [PF_6] < [Ac]$ . The dicyanamide anion [DCA] possess the lowest viscosity for the [bmim] cation. The relatively high viscosity of [bmim][PF<sub>6</sub>] is remarkable, since fluorinated ILs (e.g. [Tf<sub>2</sub>N], [TfO] and [BF<sub>4</sub>]) generally show lower viscosities. The effect of the alkyl-chain length for several ILs is given in Figure 2.23. The viscosity increases almost linearly with alkylchain length for all ILs. Gardas and Coutinho [186, 187] developed a group contribution method to estimate thermophysical and transport properties

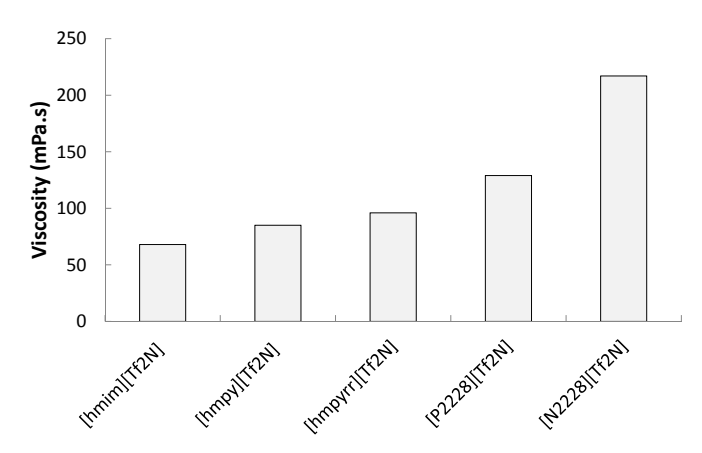


Figure 2.21: Effect of cation on viscosity for a common  $[Tf_2N]$  anion. Viscosity shows the following trend: [imidazolium] < [pyridinium] < [pyrrolidinium] < [phosphonium] < [ammonium]. Data at 298 K taken from Refs <math>[177-179].

(i.e. viscosity, electrical conductivity, thermal conductivity, refractive index, isobaric expansivity and isothermal compressibility) of ILs. The group contribution approach estimated the viscosity of 29 ILs with a mean percent deviation of 7.7% and a maximum deviation of 28%. Molecular simulations have also been used for studying the dynamics of ILs. Recently, Maginn [113] gave an excellent state-of-the-art review on the dynamics of ILs and in general about molecular simulations of ILs. Although simulations generally capture the slow dynamics of IL systems the simulations in the past were performed on too short timescales to calculate reliable viscosities [113, 188]. In chemical reactions, viscosity plays an important role, since in diffusioncontrolled reactions the rate constant should be inversely proportional to the viscosity of the solvent [164]. For this reason, many reactions are slower in ILs than in conventional solvents due to the high viscosity of ILs. The self-diffusion coefficients (D) of cations and anions at 298 K are of the order  $D = 10^{-11} - 10^{-10} \text{ m}^2/\text{s}$ , compared to  $D = 10^{-10} - 10^{-9} \text{ m}^2/\text{s}$  for simple molecular liquids [113, 164]. The self-diffusion of a spherical particle with a radius r is often related to the viscosity,  $\eta$ , through the Stokes-Einstein

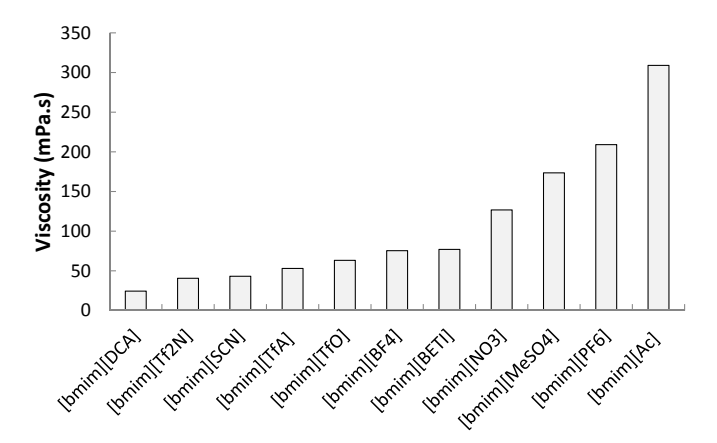


Figure 2.22: Effect of anion on viscosity for a common [bmim] cation. Data at 303 K taken from Refs [138–140, 143, 177, 180–182].

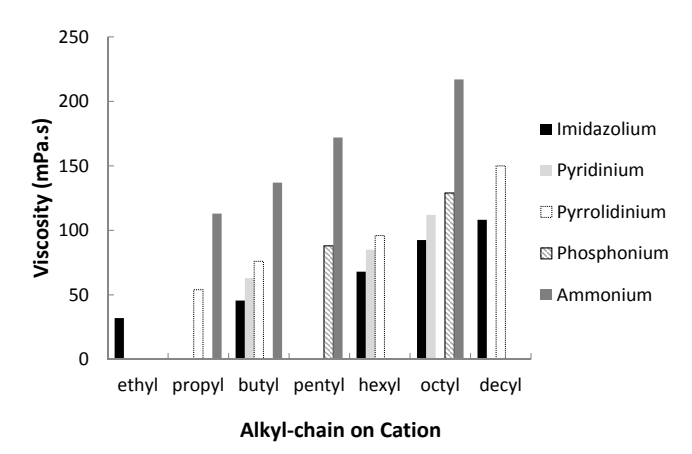


Figure 2.23: Effect of alkyl-chain length on viscosity for different ionic liquids with a common  $Tf_2N$  anion. Viscosity increases with increasing alkyl chain length for all IL classes. Data at 298 K taken from Refs [177–179, 183–185].

relation, where  $k_B$  is the Boltzman constant:

$$D = \frac{k_B T}{6\pi \eta r} \tag{2.7}$$

The relation of CO<sub>2</sub> diffusivity normalized with temperature and solvent viscosity is shown in Figure 2.24. The figure contains data of several imidazolium, ammonium, phosphonium and pyridinium ILs as well as alcoholic and hydrocarbonous solvents. Despite the complex structure of ILs the CO<sub>2</sub> diffusivity dependency on solvent viscosity appears to be universal, with self-diffusivities proportional to solvents viscosity to the power -0.43. Similarly, Moganty and Baltus [183] found a power of -0.45 by taking fewer data points of ILs into account. It is surprising to note that a power of around -0.45 was found for CO<sub>2</sub> diffusion in organic solvents and dilute liquids [189–191]. The data for diffusion of gases in ILs reported so far indicate a fractional Stokes-Einstein behavior having the form given by:

$$D \propto (T/\eta)^m \tag{2.8}$$

The exponent m in Equation (2.8) is generally lower than 1 (m < 1) and has been determined for imidazolium, ammonium and phosphonium ILs. Morgan et al. [182] used a Lag-Time technique to measure gas diffusivities in imdazolium based ILs. They found m=0.6 for imidazolium ILs. Furthermore, they provided a correlation based on IL viscosity and solute molar volume for the diffusivity of gases in imidazolium ILs. However, Hou and Baltus [193] used a different correlation for CO<sub>2</sub> diffusivity in imidazolium ILs taking IL viscosity, molar mass, density and temperature into account. Diffusion of gases in phosphonium ILs was investigated by Ferguson and Scovazzo [194]. They found that the diffusivity was inversely related to the phosphonium IL viscosity with a power of 0.35 (m = 0.35). The diffusivity of gases in phosphonium ILs was correlated with the solvent viscosity, solvent and solute molar volumes. Diffusivities of gases in ammonium ILs were measured by Condemarin and Scovazzo [195] and they found a viscosity dependence with a power of 0.5 (m = 0.5). In this study the authors correlated the diffusion of gases in ammonium ILs with IL viscosity, molar

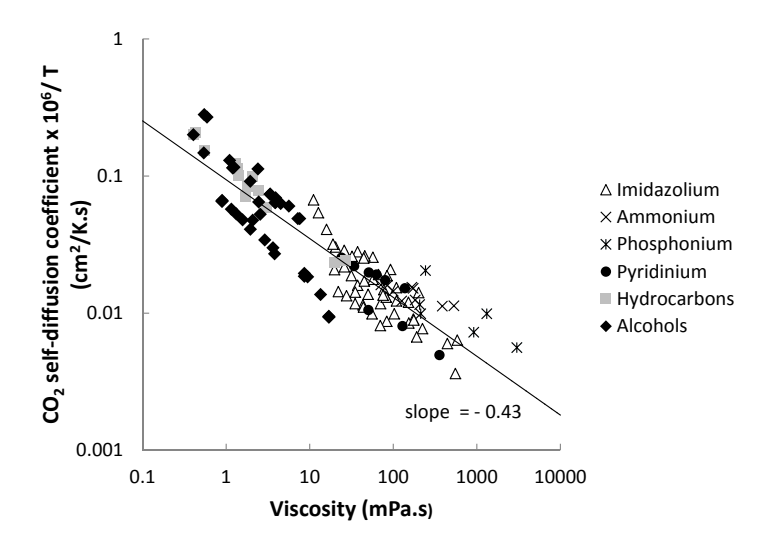


Figure 2.24: Viscosity/diffusivity relationship for ionic liquids and conventional solvents. Self-diffusivities of  $CO_2$  in different solvents appears to be proportional to solvents viscosity to the power -0.43. Ionic liquids data taken from Refs [182, 183, 192–195]. Data of alcohols and hydrocarbonous solvents taken from Refs [189, 191, 196–198].

volume of solvent and solute. Clearly, the power dependency of diffusivity is different for different classes of ionic liquids. The diffusivity of gases in ILs are less dependent on the viscosity (0.3 < m < 0.7) than predicted by Stokes-Einstein equation (m = 1). This is probably not very surprising, since the Stokes-Einstein equation generally represents the case where a large solute molecule is diffusing in a solvent of relatively small molecules [182]. Nevertheless, the self-diffusion coefficients of CO<sub>2</sub> at room temperature in all the ILs are  $\sim 1 \times 10^{-10}$  m<sup>2</sup>/s, which is an order of magnitude lower than for conventional solvents. Molecular simulations have also been used to calculate diffusivities, however the simulation runs in many of these computational studies in the past were too short (i.e. ps scale) to calculate reasonably transport properties [113, 164, 188, 199]. More recent studies

with much longer simulation times (i.e. several to hundreds of ns) have overcome this problem and reliable transport properties could be calculated [113, 188, 200].

## Volatility of Ionic Liquids

The discussion here will be limited to aprotic ionic liquids, since protic ILs contain an acidic proton on the cation, which can be abstracted by the basic anion. This acid-base reaction leads to the formation of neutral molecular species that can readily evaporate, hence protic ILs are volatile by their nature [201]. Since its origins ionic liquids were considered substances with zero vapor pressure, but this general belief changed abruptly after the publication by Earle et al. [202] In this study the authors showed that several commonly used aprotic ionic liquids, pure and mixed, could be distilled at 300 °C and high vacuum without significant decomposition. For example the IL [hmim][Tf<sub>2</sub>N] could be distilled at 170 °C and 0.07 mbar. Since the breakthrough publication by Earle et al. several studies have been reported concerning the nature of the vapor phase, vapor pressure  $(P^{\text{sat}})$ , enthalpy of vaporization  $(\Delta_{\text{vap}}H)$ , boiling point  $(P_b)$  and boiling temperature  $(T_b)$ of ILs. Review on these topics are provided by Ludwig and Kragl [203] and Esperanca et al. [201] Both reviews address the difficulty in experimentally determining the liquid-vapor equilibrium (VLE) properties (e.g.  $\Delta_{\text{vap}}H$ ,  $P^{\text{sat}}$ ) for ILs. This is mainly due to the competition between evaporation and decomposition mechanisms at sufficiently high temperatures complicating the experimental interpretation. A detailed study on the nature of the vapor phase and enthalpy of vaporization was first given by Armstrong et al. [204] The ionic liquid was evaporated under ultra-high vacuum and the vapor phase was analyzed by line of sight mass spectroscopy (LOSMS). The vapor phase was shown to consist of neutral ion pairs, where the enthalpy of vaporization was primarily dependent on the Coulombic interactions between the gas-phase and the liquid-phase ion pair [204]. Similar results on the nature of the vapor phase were found by Leal et al. [205] using Fourier Transform Ion Cyclotron Resonance Mass Spectrometry (FTICR-MS) at reduced-pressure distillation conditions. The FTICR-MS results indicated

that at low pressures and at temperatures above 474 K the vapor phase consist of neutral ion pairs, without free ions, and larger clusters. By contrast, the vapor phase of protic ILs was shown to consist of isolated neutral molecules, supporting the proton transfer mechanism. Much recently, Rai and Maginn [206] investigated the nature of the vapor phase by means of molecular simulations. Their simulation results support the experimental finding that the vapor phase predominantly consist of isolated ion pairs. However, the molecular simulations also indicate that a substantial fraction of the ions is present in larger aggregates, and this fraction increases as the temperature and pressure increases. The enthalpy of vaporization,  $\Delta_{\text{vap}}H$ , has been measured by several techniques: the Knudsen method, surface tension, microcalorimetry, temperature-programmed-desorption, transpiration and Molecular Dynamics (MD) simulation [201, 207]. Unfortunately, the different techniques do not yield uniform enthalpies of vaporizations for a given IL, for example the measured values of  $\Delta_{\text{vap}}H$  for [omim][Tf<sub>2</sub>N] range from 150 to 192 kJ/mol [203]. Nonetheless, reliable  $\Delta_{\rm vap}H$  values range from 120 to 200 kJ/mol rather than the very high values up to 300 kJ/mol reported by Rebelo et al. [208] Recently, Fumino et al. [209] used Far-Infrared measurements to measure the enthalpy of vaporization of several imidazolium ILs. The values reported were in the range of 128-165 kJ/mol. Devko et al. [210] used LOSMS for the measurement of twelve ILs and provided a simple theory for estimating the enthalpy of vaporization as a sum of a Coulombic contribution and two van der Waals contributions resulting from the anion and the cation. Verevkin [211] developed a simple group contribution approach to accurately estimate the enthalpy of vaporization of several imidazolium and pyrrolidinium based ILs. Furthermore, the experimental data compiled by Esperanca et al. [201] indicate that Trouton's rule  $(\Delta_{\text{vap}} H_{T_b}/T_b = \text{constant})$  is not obeyed by  $[C_n \text{mim}][\text{Tf}_2 N]$ IL family. The  $\Delta_{\text{vap}}H_{T_b}$  values showed an increasing and decreasing trend with maximum at n = 4. This is opposite to what is found by molecular simulation for  $[C_n mim][BF_4]$  series where it was shown that  $\Delta_{vap} H_{T_h}$ decreases with increasing chain length showing a Trouton-like correlation with a Trouton's constant of approximately 65 kJ/mol [206]. The vapor pressure of ILs in the homologues series of  $[C_n mim][Tf_2N]$  was measured

by Zaitsau et al. using a Knudsen effusion method [212]. They obtained vapor pressures between  $10^{-1}$  and  $10^{-3}$  Pa for temperatures ranging from 450 to 550 K. Recently, Rocha et al. [213] presented high-accuracy vapor pressure data of nine imidazolium based ILs. These authors provided for the first time a quantitative evidence for the structural percolation phenomenon in ILs and its relation with the thermodynamic properties of ILs. Furthermore, the high-accuracy vapor pressure data of all the ILs at 450 K were  $\sim 0.02$  Pa. Since these pressures are so low and even lower at standard experimental conditions, it is not very surprising that it took some time to notice the volatility of ionic liquids. However, the proven (negligible) volatility of ionic liquids will not damage the reputation, which is largely built on their nonvolatility property, as green solvents [214].

## 2.3.2 Functionalized Ionic Liquids

Large scale application of physical ILs for  $\mathrm{CO}_2$  capture from flue-gas is mainly hindered by the low  $\mathrm{CO}_2$  absorption capacity at post-combustion conditions. The partial pressure of  $\mathrm{CO}_2$  at post-combustion conditions (see Table 2.1) is rather low, hence  $\mathrm{CO}_2$  solubility is lower than 5 mol-% even for the best physical ILs. To overcome this problem researchers appealed to the amine chemistry by arguing that including an amine moiety to conventional ILs (amine-functionalized ILs) could greatly improve  $\mathrm{CO}_2$  absorption capacity. The progress in this branch of research is reported in this section.

#### Cation Functionalization

The concept of ionic liquid functionalization or task-specific ionic liquid (TSIL) was first introduced by Bates et~al.~[215,~216]. In this study the authors functionalized the imidazolium cation with a primary amine moiety. This new TSIL was shown to react in a 2:1 stoichiometry with CO<sub>2</sub> according to Figure 2.25. We note that this stoichiometry is similar to the theoretical maximum molar uptake of CO<sub>2</sub> by conventional amines under the carbamate formation scheme.

Figure 2.25: Reaction between cation functionalized ionic liquid and  $CO_2$ . The IL react in a 2:1 stoichiometry with  $CO_2$  forming a carbamate salt [215].

Evidence for carbamate formation as proposed in Figure 2.25 was given by FT-IR and NMR spectra analysis of the CO<sub>2</sub> treated and CO<sub>2</sub> untreated ionic liquids. Furthermore, the authors reported that the reaction was reversible and the CO<sub>2</sub> could be released upon heating (80-100 °C) for several hours under vacuum. Although the authors observed a relatively high viscosity of the synthesized ionic liquid, they did not notice the dramatic viscosity increase after reacting the CO<sub>2</sub> with the TSIL. Galán Sánchez et al. [128, 217] further verified this concept by functionalizing the [bmim] cation by a primary and tertiary amine. These functionalized cations were paired with [BF<sub>4</sub>] and [DCA] anions. The CO<sub>2</sub> solubility in the physical non-functionalized ILs, [bmim][BF<sub>4</sub>] and [bmim][DCA], does not vary significantly. Functionalization of the [bmim] cation with an amino group [Ambim] improved the CO<sub>2</sub> absorption, relative to the non-functionalized counterparts, by a factor 13 and 4, respectively for [Ambim][BF<sub>4</sub>] and [Ambim][DCA] at 0.1 MPa and 303 K. Clearly, the CO<sub>2</sub> solubility can be enhanced by including amine groups in the cation and by choosing a proper anion. Furthermore, the isotherms of CO<sub>2</sub>-functionalized ILs show a trend which is typical for chemical absorption. At low pressures the solubility increases sharply, while a steady increase in solubility is observed at higher pressures due to contribution of the physical mechanism. Although a similar trend was observed for the tertiary-amine-functionalized

IL [3Amim][BF<sub>4</sub>]-CO<sub>2</sub> system the solubility was significantly lower compared to the primary-amine-functionalized ILs. This is likely due to the lower reactivity of tertiary amines towards CO<sub>2</sub> [34]. The ILs did not show reduced absorption capacity after regenerating it at 353 K in vacuum. However, the viscosity problem after reaction with CO<sub>2</sub> was again noted. To overcome the viscosity problem of the amine-functionalized ILs to some extent, Camper et al. [218] proposed the use of (nonfunctionalized) RTIL-amine solutions. They showed that a RTIL solution containing 50 mol % MEA is capable of rapidly and reversibly capture CO<sub>2</sub> approaching a stoichiometry of 1 mol of CO<sub>2</sub> per 2 moles of MEA. Since the viscosity of the used IL was much lower than the amine-functionalized IL by Bates et al., the absorption rate in the IL-MEA solution was much faster. Nevertheless, the lowest viscosity of an IL measured up to now is  $\sim$ 20 mPa.s, which is still much higher than for aqueous MEA solutions (e.g. the viscosity of 30 wt% MEA solution at 25 °C is 2.2 mPa.s).

To help understanding the high viscosities in neat cation-amine-functionalized IL Yu et al. [219] used molecular simulations. They found that amino addition does not significantly affect the organization of the anions around the imidazolium ring, instead the anions strongly organize around the -NH<sub>2</sub> forming strong hydrogen bonds. The calculated ionic self-diffusion coefficients of the functionalized ILs were roughly 2 orders of magnitude lower than of the nonfunctionalized counterparts, consistent with the observed high viscosities in the experiments. A mechanistic explanation for the dramatic viscosity increase upon reaction of  $\rm CO_2$  with the amine-functionalized ionic liquid was given by Gutowski and Maginn [220] using molecular simulations. They performed a detailed hydrogen bond analysis and found evidence for the formation of strong, dense hydrogen-bonded networks, primarily between the zwitterion and dication species formed during the reaction.

### **Anion Functionalization**

It is obvious that CO<sub>2</sub> uptake by ILs with amine-functionalized cations is much greater (at pre-combustion conditions) than by physical absorption. However, the 1:2 reaction stoichiometry for cation-functionalized ILs is atom inefficient and the question remains whether a more favorable stoichiometry can be achieved. To answer this question Gurkan et al. [221] used ab initio calculations to investigate the relationship between the position of amine functional group and the reaction stoichiometry. They showed that tethering the amine to the cation favored the formation of the carbamate leading to 1:2 stoichiometry, while tethering the amine to the anion favored 1:1 reaction stoichiometry. Accordingly, they synthesized two amino acidbased ILs, trihexyl(tetradecyl)phosphonium prolinate [P66614][Pro] and trihexyl(tetradecyl)phosphonium methionate [P66614][Met], which were experimentally shown to react with CO<sub>2</sub> in a 1:1 stoichiometry. Figure 2.26 shows clearly a CO<sub>2</sub> uptake greater than one mole CO<sub>2</sub> per two mole IL which approaches the 1:1 stoichiometry. The isotherms can be subdivided in two distinct parts: a sharp increase at low pressures due to chemical absorption and a marginal increase in capacity at higher pressures which is typical for physical absorption. Nonetheless, it was shown that the vast majority of the uptake was due to chemical absorption. Furthermore, the 1:1 stoichiometry was confirmed by FTIR spectroscopy [221]. Inherent to these amine-functionalized ILs is the increase in the enthalpy of reaction and the increase in the viscosity. The enthalpy of reaction of CO<sub>2</sub> with [P66614][Pro] and [P66614][Met] was measured at 25 °C with calorimetry to be -80 kJ/mol and -64 kJ/mol, respectively. These values are intermediate compared to physical absorption (-10 to -20 kJ/mol) and chemical absorption with conventional amines (-85 to -100 kJ/mol). Of course the increased reaction enthalpy will bring extra expenses in the regeneration step. Similar to the case of cation-functionalized ILs, the viscosity increases further upon reaction with  $CO_2$ . The occurrence of the latter phenomena was recently demonstrated for amino-acid based ionic liquids [222]. In this study the trihexyl(tetradecyl)phosphonium [P66614] cation was paired with several deprotonated amino acid anions, like glycinate, isoleucinate, etc.

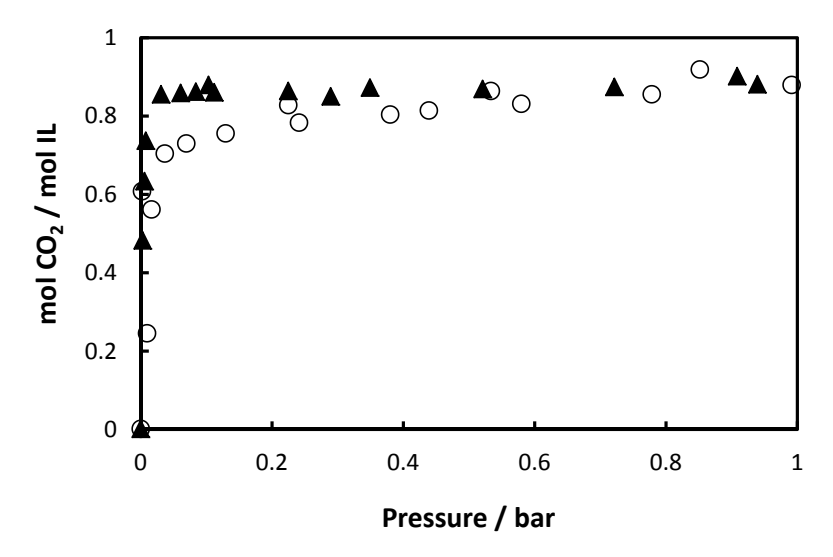


Figure 2.26: Experimental  $CO_2$  absorption isotherm by anion-functionalized ILs [P66614][Pro] (triangles) and [P66614][Met] (circles) at 22 °C [221]. Note that the reaction stoichiometry of these ILs with  $CO_2$  approaches 1:1, which is better than the 2:1 stoichiometry for conventional amines and  $CO_2$ .

The viscosity of the isoleucinate IL was shown to increase 240-fold, relative to the neat IL. Such high viscosities will preclude the application of these viscous, gel like, ionic liquids in an industrial absorber-stripper configuration. The energy requirement for pumping the viscous IL will increase, but also the absorption kinetics will deteriorate as diffusion might be slow in these viscous ILs. The slow diffusion will cause mass transfer limitations, requiring more (equivalent) trays in a typical absorption column, thereby increasing the capital cost.

Carboxylate functionalized anions, such as acetate, also deserve special attention. Chinn et al. [223] investigated the [bmim][acetate] IL diluted in a 14 wt% water solution and showed that CO<sub>2</sub> absorption in this IL exhibit an absorption behavior, which is typical for a chemical complexation process. The volumetric absorption capacity of this acetate-based

IL ( $\sim 25 \text{ m}^3/\text{m}^3$ ) is intermediate between amines ( $\sim 65 \text{ m}^3/\text{m}^3$  for 30 wt% aqueous MEA solution) and physical ILs ( $\sim 3 \text{ m}^3/\text{m}^3$ ). The enthalpy of reaction of CO<sub>2</sub> in the acetate IL is -40 kJ/mol, which is also intermediate compared to MEA (-85 kJ/mol) and physical ILs (-15 kJ/mol). Therefore, the regeneration step requires a much lower energy input than the MEA process. Chinn et al. [223] put forward a mechanism where the acetate group interacts with the water and the CO<sub>2</sub> is captured as a bicarbonate group. The  $CO_2+[bmim][acetate]$  system has also been studied experimentally by Maginn et al. [224], but they offered a different mechanism involving a proton extraction by the acetate anion from the C<sub>2</sub>-position of the imidazolium ring leading to acetic acid in the process. In a next step, the  $CO_2$  reacts with the carbene to form a bicarbonate. Shiflett et al. [225] performed a detailed experimental study on the CO<sub>2</sub>+[bmim][acetate] system in presence or absence of water. These authors used spectrocsopic analyses to show that the acetic acid formation mechanism put forward by Maginn et al. is not very likely. However, the authors did smell some acetic acid during the experiments, which suggests that at least a limited amount of acetic acid is produced. They classified the phase behavior of CO<sub>2</sub>+[bmim][acetate] system as an extremely rare case with strong intermolecular interactions and complex formation. An economic avaluation of the process using [bmim][acetate] for CO<sub>2</sub> capture carried out by Shiflett et al. [226] showed that the IL-process could reduce the energy losses by 16% compared to a the MEA process. Furthermore, they estimated a 11% lower investment for the IL-process and 12% reduction in equipment footprint relative to the MEA process. Shiflett and Yokozeki [227] investigated CO<sub>2</sub> solubility in the ILs [emim][acetate], [emim][trifluoroacetate] and mixtures of both ILs. The [emim][acetate] IL absorbed the CO<sub>2</sub> chemically, while the [emim][trifluoroacetate] IL showed physical absorption behavior. The mixture of both ILs showed a combination of a physical and a chemical absorption behavior. Carvalho et al. [228] studied the specific interactions of CO<sub>2</sub> with imidazolium-based [bmim] ILs containing the [acetate] and [trifluoroacetate] anion. Their experimental data showed that CO<sub>2</sub> solubility in [bmim][acetate] unlike in [bmim][trifluoroacetate] is spontaneous due to the differences in enthalpies of solvation. Furthermore, these

authors used ab initio calculations and high resolution spectroscopy to provide evidence for an acid/base type of solvation mechanism in the acetate IL. Recently, Gurau et al. [229] demonstrated the chemisorption of CO<sub>2</sub> in 1,3-dialkylimidazolium acetate ILs using NMR spectroscopy and X-ray diffraction analysis. These authors explored the reactivity of CO<sub>2</sub> with [emim] [acetate] by bubbling CO<sub>2</sub> through the acetate IL at atmospheric and ambient temperature conditions. Using NMR spectroscopy after 24 h bubbling, the formation of 1-ethyl-3-methylimidazolium-2-carboxylate was observed. In addition, X-ray diffraction analysis of single crystals clearly showed that imidazolium carboxylate and acetic acid are formed in the absence of water. Water was shown to inhibit the interaction of acetate with the proton at the  $C_2$  position of the imidazolium ring, thereby inhibiting the CO<sub>2</sub> reaction. Almost simultaneously, Besnard et al. [230] also studied the [bmim][acetate]+CO<sub>2</sub> system using Raman, infrared spectroscopy, DFT calculations and NMR spectroscopy. They also showed that CO<sub>2</sub> reacts with [bmim][acetate] to form an imidazolium carboxylate and acetic acid originating from the deprotonation of the  $C_2$  of the imidazolium ring.

Much recently, Gurkan et al. [231] used a computational approach to design a new class of ILs, namely aprotic heterocyclic anions (AHAs). The authors computed the structure and energetics of pyrrolide, an AHA, and CO<sub>2</sub> reaction product using molecular electronic structure calculations at the G3 level. The pyrrolide was computed to directly combine with  $CO_2$ to form a carbamate product with a computed enthalpy of reaction of -109 kJ/mol. Subsequently, they showed that the reaction enthalpy could be tuned depending on the position of substitution on the pyrrolide ring. Further, MD simulations were used to probe the viscosity of the pyrrolide-based IL with CO<sub>2</sub>. For this purpose 2-cyanopyrrolide anions (AHA) were paired with tetrabutylphosphonium [tbp] cations. The MD simulations suggest that the viscosity will not suffer the large viscosity increase upon reaction with CO<sub>2</sub>. This result stands in stark contrast with previously reported results for amine-functionalized TSILs where the viscosity increases dramatically upon complexation with CO<sub>2</sub>. In addition, experiments with trihexyl(tetradecyl)phosphonium 2-cyanopyrrolide [thtdp][2-CNpyr] confirmed the findings of the simulations. The [thtdp][2-CNpyr] IL was shown to react

in a 1:1 stoichiometry with CO<sub>2</sub> forming carbamate, which was identified using in situ infrared spectrometry. The viscosity was also measured and indeed the viscosity of the reacted and unreacted IL remained nearly the same. Differential calorimetry was used to measure the enthalpy of reaction with a value of -53 kJ/mol, which was in good agreement with the G3-computed value of -49 kJ/mol. Furthermore, these authors state that the approach is not limited to pyrrolides only but imidazolides and pyrazolides may also show similar chemistry. For proving this they synthesized a 3-(trifluoromethyl)pyrazolide [3-CF<sub>3</sub>pyra] IL containing the [thtdp] cation. Indeed, CO<sub>2</sub> uptake of this IL was similar to the [2-CNpyr]-IL showing a stoichiometry close to 1:1. Again the viscosity increase was not significant, while the calorimetrically measured enthalpy of reaction for [3-CF<sub>3</sub>pyra] was -46 kJ/mol. Hence, AHA-ILs provide a platform with the possibility to tune the reaction enthalpy, to enhance reaction stoichiometry relative to conventional amines and to circumvent the viscosity increase when reacting with  $CO_2$ . Unfortunately the viscosity problem remains also for AHA-ILs, since the neat or CO<sub>2</sub> reacted AHA-ILs given by Gurkan et al. [231] had viscosities at room temperature higher than 100 cP. Such a high viscosity may be still a barrier for using AHAs in industrial CO<sub>2</sub> capture processes. Nonetheless, there is still some room to improve the viscosity and enthalpy of reaction of AHAs by including proper functional groups.

Wang et al. [232–235] also reported equimolar CO<sub>2</sub> absorption in IL-superbase mixtures. Superbases are neutral organic bases, which possess very high proton affinities enabling their protonated conjugate acids to withstand deprotonation by the hydroxide ion [233]. Hence, superbases play an important role as proton acceptors, thereby providing the opportunity to capture CO<sub>2</sub>. Wang et al. [233] investigated the CO<sub>2</sub> absorption performance of the IL-superbase system containing two ILs 1-(2-hydroxyethyl)-3-methylimidazolium bis-(trifluoromethylsulfonyl)imide [Im21OH][Tf<sub>2</sub>N] and 2-hydroxyethyl(dimethyl)-isopropylammonium bis-(trifluoromethylsulfonyl)-imide [Nip,211OH][Tf<sub>2</sub>N] and four superbases 1,8-diazabicyclo-[5.4.0]undec-7-ene (DBU), 1,3,4,6,7,8-hexahydro-1-methyl-2H-pyrimido[1,2-a]pyrimidine (MTBD), 2-tert-butylamino-2-diethylamino-1,3-dimethylperhydro-1,3,2-diazaphosphorine (BEMP) and 1-ethyl-2,2,4,4,4-pentakis(di-methylamino)-

 $2\lambda^5, 4\lambda^5$ 5-catenadi(phosphazene) (EtP2(dma)). The performance of the  $[Im21OH][Tf_2N]-DBU$  system was the best achieving a molar ratio of  $CO_2$ to DBU slightly more than one, indicating a combination of physical and chemical absorption. NMR results showed that CO<sub>2</sub> reacted with DBU forming a amidinium alkylcarbonate salt. Furthermore, the absorbed CO<sub>2</sub> could be released easily by heating and minor loss of activity was observed during several absorption-desorption cycles. The authors reported similar results using imidazolium-based ILs containing different type of anions and the bases DBU, MTBD, EtP2 and tetramethyl guanidine (TMG). Recently, Wang et al. [232] synthesized superbase-derived protic ionic liquids (PILs) for CO<sub>2</sub> capture. They combined the superbases MTBD or P2Et with six weak proton donors (i.e. partially fluorinated alcohols (TFE, TFPA, HFPD), imidazole, pyrrolidone and phenol) to obtain the superbase-derived PILs. These superbase-derived PILs showed excellent CO<sub>2</sub> capture properties, for example the [MTBDH<sup>+</sup>][TFE<sup>-</sup>] PIL absorbed 1.13 mol of CO<sub>2</sub> per mol of PIL. Since the viscosity of [MTBDH<sup>+</sup>][TFE<sup>-</sup>] was relatively low (8.63 cP at 23 °C), the absorption of CO<sub>2</sub> in [MTBDH<sup>+</sup>][TFE<sup>-</sup>] was very fast. Furthermore, the CO<sub>2</sub> could be released completely by bubbling nitrogen at 80°C and the PILs showed only a slight capacity loss after several absorption-desorption cycles. The same group reported equimolar CO<sub>2</sub> capture by tuning the basicity of ILs. These basic ILs were synthesized by deprotonating several weak proton donors (i.e. trizole, tetrazole, imidazole, pyrazole, oxazolidinone, phenol, indole and bentrizole) with trihexyltetradecylphosphonium hydroxide [thtdp] [OH]. ILs containing the [thtdp] cation and the [pyrazole], [imidazole], [indole] [trizole] or [oxazolidinone] cation showed an absorption capacity close to 1 mol CO<sub>2</sub> per mol of basic IL. Moreover, the absorption capacity and the enthalpy of reaction was shown to increase with an increasing  $pK_a$  value of the ILs. Although the  $CO_2$ could be released easily, the viscosity of the basic ILs after reacting with  $CO_2$  was very high (> 550 cP), which will cause serious problems in a typical absorption-desorption process.

## 2.3.3 Reversible Ionic Liquids

The relatively new approach to capture  $CO_2$  with reversible ionic liquids (RILs) was introduced by Jessop et al. [236, 237]. Jessop et al. showed that RILs could be formed from a non-ionic liquid (an alcohol and an amine base) by exposing it to CO<sub>2</sub> forming a salt (ionic liquid), which can revert back to its non-ionic initial state by exposing it to nitrogen or other inert gas [236]. These kind of solvents are also referred to as switchable solvents, since the polarity of the solvent can be tuned upon reaction with CO<sub>2</sub> [238]. Heldebrant et al. [237] investigated the reaction of 1,8-diazabicyclo[5.4.0]undec-7-ene (DBU) with carbon dioxide in the absence and presence of water. Their spectroscopic data showed that an IL  $[DBUH^+][HCO_3^-]$  is formed when DBU (amidine) is exposed to  $CO_2$  in the presence of water, while there is no reaction in the absence of water. Phan et al. [239] showed that a guanidine/alcohol mixture also exhibit a similar chemistry as an amidine/water or amidine/alcohol mixture when exposing it to CO<sub>2</sub>, thereby forming a carbonate salt. The solution could be reversed to its non-ionic state by bubbling nitrogen or mild heating. Heldebrant et al. [240] performed a detailed study on organic liquid CO<sub>2</sub> capture using DBU, TMG, Barton's base and Hunig's base mixed with water or an alcohol. These authors showed that CO<sub>2</sub> reversibly and chemically bind in a mixture of alcohols and amidine/guanidine bases to form a liquid alkylcarbonate. The  $CO_2$  capacity of these RILs was up to 19% by weight, which is comparable to that of MEA.  $CO_2$  was shown to absorb selectively in the presence of  $N_2$  and the RILs did not show any loss of activity or selectivity after five cycles. The enthalpy of reaction of CO<sub>2</sub> in the Barton's base is comparable with MEA, while it was significantly higher for the TMG/alcohol and DBU/alcohol mixtures. However, the authors estimated that 50% less energy would be required in the regeneration step for the RILs compared to the MEA process, since the anticipated specific heat of RILs is three times lower than water. Unfortunately, in the presence of water undesired bicarbonates were formed, which will cause problems when considering that fluegas can contain substantional amounts of water. Blasucci et al. [241] developed an onecomponent RIL derived from siloxylated amines, which formed a carbamate

salt upon reaction with CO<sub>2</sub>. Blasucci *et al.* [242] investigated four silylated amines and their corresponding RILs in combination with CO<sub>2</sub> absorption. They showed that the silyl amines were stable also in presence of water, while the siloxylated amines were susceptible to degradation. Furthermore, they showed these RILs obeyed both physical and chemical absorption mechanism to have a absorption capacity of 13-20 mole CO<sub>2</sub>/kg amine at 35 °C and 62.5 bar. For more information on this topic, the reader is referred to the reviews by Blasucci [241], Jessop [243] and Shannon [244].

# 2.3.4 CO<sub>2</sub> Capture Performance: ILs vs. Commercial Solvents

The application potential of ILs for  $CO_2$  capture depends on their performance with respect to already commercialized solvents. The measures that can be used to gauge a solvents' performance are for example: absorption capacity, gas selectivity, viscosity, stability, solvents' cost and most importantly the overall process cost. Table 2.2 provides an overview of the performance of ILs for CO<sub>2</sub> capture with respect to six commercially applied solvents. The Selexol, Fluor Solvent, Purisol and Rectisol processes utilize a physical solvent, while the Sulfinol process uses a mixed solvent, either DIPA or MDEA with Sulfolane. The standard Econamine process of Fluor uses 30 wt% MEA, which runs on a chemical reaction [245]. However, Fluor has recently improved the Econamine process allowing a higher MEA concentration [245]. All these physical or chemical solvents are applied industrially in the natural gas sweetening process. Tennyson and Schaaf [10] provide useful guidelines for solvent selection depending on acid gas conditions (e.g. partial pressure of acid gas, impurities and product specification). Ionic liquids exhibiting only physical absorption have been considered in Table 2.2. Upon comparison of the data presented in Table 2.2 it becomes clear that ILs are much more expensive than conventional solvents. Current (labscale) prices of ILs are  $\sim 1000$  \$/kg, but economy of scale should apply and according to BASF the price for a large scale process will drop to <40 \$\frac{10}{2}\$ kg. The cost of ILs, even at this price level, would still be a factor of 10 to 20 higher than conventional solvents.

Table 2.2: Comparison of the properties<sup>a</sup> of commercially used solvents and ionic liquids for CO<sub>2</sub> capture. Many other commercial solvents exist, only the ones commonly used are listed.\*

Process name	Selexol	Fluor Solvent	Purisol	Rectisol	Sulfinol	Econamine FG	Ionic liquids
chemical	DMPEG	PC	NMP	MeOH	DIPA+Sulfolane	$MEA^j$	Salts
licensor	100	Fluor	Lurgi	Linde+Lurgi	Shell	Fluor	n/a
type absorption	physical	physical	physical	physical	$^{e}/\mathrm{phys.}^{f}$	chemical	physical
solvent cost $(\$/kg)^b$	2.5	1.5-2	4	0.7	2.5/4	1.5-2	$<\!40^{m}$
viscosity (mPa.s)	5.8	က	1.65	9.0	$186^{g}/10$	$18.98^{k}$	20-1000
density $(kg/m^3)$	1030	1195	1027	785	1004/1261	1017	800 - 1500
molar mass (g/mol)	280	102	66	32	133.19/120.17	61.09	200 - 750
vapor pressure (mmHg)	0.00073	0.085	0.4	125	0.035/0.02	0.36	0.000001
freezing point (°C)	-28	-48	-24	-92	44/26	10.5	-140 to 180
boiling point (°C)	275	240	202	65	249/285	171	> 250
max. operating Temp. (°C)	175	65	202	65	150	150	> 200
operating pressure	high	high	high	high	low	low	high
$\Delta_{abs}H$ (kJ/mol CO <sub>2</sub> )	-14.3	-15.9	-16.4	-13	$-73.7^{h}$	-85	-10  to  -20
$CO_2$ solubility $(m^3/m^3)$	3.63	3.4	3.57	$14.4^{d}$	$30-40^{i}$	$50-85^{l}$	> 2.51
$CO_2/CH_4$ selectivity <sup>c</sup>	15	26	14	$20^d$	n/a	n/a	8-35
$H_2S/CO_2$ selectivity <sup>c</sup>	& &.	3.3	10.2	pL	$1-2^i$	$1-2^l$	2-10
$CO_2/H_2$ selectivity <sup>c</sup>	22	126	178	$185^d$	n/a	n/a	50 - 150
$CO_2/N_2$ selectivity <sup>c</sup>	20	117	20	$83^{d}$	n/a	n/a	30 - 100
$\Delta_{vap}H$ (kJ/mol)	$76.16^{n}$	60.2	$54.5^{o}$	35.27	57.4/66.8	49.8	>120
H <sub>2</sub> O miscibility	yes	partial	yes	yes	yes	yes	$variable^p$

<sup>a</sup> Properties at 25 °C and 1 bar, unless otherwise stated. <sup>b</sup> Indicative prices (\$/2007) taken from www.icis.com or from supplier info. e Pure compound property of DIPA / f pure compound property of Sulfolane. g Property at 45.5 °C taken from Henni et al. [246]. <sup>c</sup> Ideal selectivity, real H<sub>2</sub>S/CO<sub>2</sub> selectivity will differ significantly from ideal selectivity. <sup>d</sup> Solubility, selectivity data at -25 °C.

 $^{h}$  Enthalpy of reaction of CO<sub>2</sub> in dissopropanolamine.  $^{i}$  Property in a mixture of 40 wt% DIPA + 40 wt% Sulfolane + 20 wt% water. <sup>j</sup> Properties of pure MEA is reported, unless otherwise stated. <sup>k</sup> Viscosity of 30 wt% aqueous MEA solution is 2.2 mPa.s at 25 °C.

\* Majority of the data taken from Refs [11, 247–250]. Other data taken from Refs [108, 122, 123, 160–162, 171, 251–263]

Solubility, selectivity in a solution of 30 wt% MEA. " Estimation of BASF (30 euro/kg) for ton scale production of ionic liquids.  $^{n}$  Property of tetra-ethylene glycol dimethyl ether.  $^{o}$  Property at 20  $^{\circ}$ C.  $^{p}$  Ranging from completely miscible to immiscible.

This means that a successful application of ILs would rely on other properties of ILs. This property is certainly not the viscosity, since the viscosity of ILs is also significantly higher than of conventional solvents. We note that the viscosity of pure DIPA and MEA are also very high, but these solvents are always used in diluted form with viscosities not much higher than that of water. A property, which is inherently related to and in favor of ILs is the vapor pressure. Indeed, the vapor pressure of ILs is much lower than of the currently used solvents. However, the Selexol process also uses a solvent with a very low vapor pressure, but with a much lower viscosity compared to ILs. The volatility of a number of amines, including MEA, has been reported by Nguyen et al. [264, 265]. However, volatility is not the only cause for the solvent losses in a CO<sub>2</sub> capture process, but also losses due to thermal and chemical degradation should be considered. Rochelle et al. [266, 267] estimated the total MEA loss at stripper conditions to be 80-540 g/ton CO<sub>2</sub> captured, where the lower and upper limit correspond to a stripper operating temperature of  $\sim 110$  °C and  $\sim 130$  °C, respectively. In terms of process cost, this loss would result in a solvent replacement cost of \$0.19-\$1.31/ton CO<sub>2</sub> removed assuming a price of \$1.10/lb of MEA. Reddy et al. [268] estimated the solvent replacement cost of Fluor's Econamine FG Plus $^{SM}$  process to be \$2.30/ton CO<sub>2</sub> removed. A property not considered in Table 2.2 is the corrosivity and degradation sensitivity of the solvents. Although MEA is known to be corrosive and sensitive to chemical degradation, these properties have been scarcely investigated and reported for ILs. However, some of the commonly used ILs are also known to be corrosive especially at higher temperatures and for copper alloys, but carbon steel show very low corrosion rates [269–277]. Surprising to note is that some ILs have been considered as anti-corrosion agents [278, 279]. Nonetheless, a systematic analysis of the corrosion and degradation behavior of ILs is still lacking, but these issues should be considered in future research. Considering the price/performance ratio of ILs and conventional solvents for CO<sub>2</sub> capture it seems that we will not gain much utilizing physical ILs. We could take advantage of the tunability property of ILs, which can be used to design ILs with an improved selectivity of a gas pair over conventional solvents. Furthermore, ILs can

be designed to operate in a range where conventional (physical) solvents can not be applied. For example, at post-combustion conditions where the CO<sub>2</sub> partial pressure is very low, none of the physical solvents including ILs can be applied. Nevertheless, in this case an amine functionalized IL with a better energy efficiency and reaction stiochiometry than the Sulfinol or MEA process could be used. In this regard, it is very promising and challenging to design ILs with a lower enthalpy of reaction than conventional amines. At pre-combustion and natural gas sweetening conditions where the CO<sub>2</sub> partial pressure can be quite high (see Table 2.1), one can optionally choose for a physical IL solvent. However, the price/performance ratio of existing ILs is still insufficient to compete with existing commercial solvents (e.g. Selexol).

In the following we will discuss an another approach for gas separation, namely supported ionic liquid membranes (SILMs), which is a promising alternative for low pressure applications.

## 2.4 Supported Ionic Liquid Membranes (SILMs)

A relatively new research field is the application of ILs as a solvent in supported liquid membranes (SLMs) technology. Usually, SLMs consist of two phases, a supporting porous (or nonporous) membrane and a liquid solvent phase, which resides in the pores (or are being held between two non porous membrane sheets). Solute molecules diffuse/dissolve into the membrane facilitating a reaction or separation in the liquid phase and finally desorb at the opposite side of the membrane [280]. One of the disadvantages of conventional SLMs is the loss of solvent due to evaporation of the stabilized liquid phase [281–283]. This problem can be circumvented by using ILs as the liquid phase and taking advantage of their unique properties such as, relatively low volatility, high chemical and thermal stability [284]. The potential of supported ionic liquid membranes (SILMs) for gas separation has been studied by several researchers [281, 285–290]. Reviews of SILMs for gas separation are given by Bara et al. [291] and by Noble and Gin [284]. The performance of SILMs is generally evaluated through a 'Robeson plot'

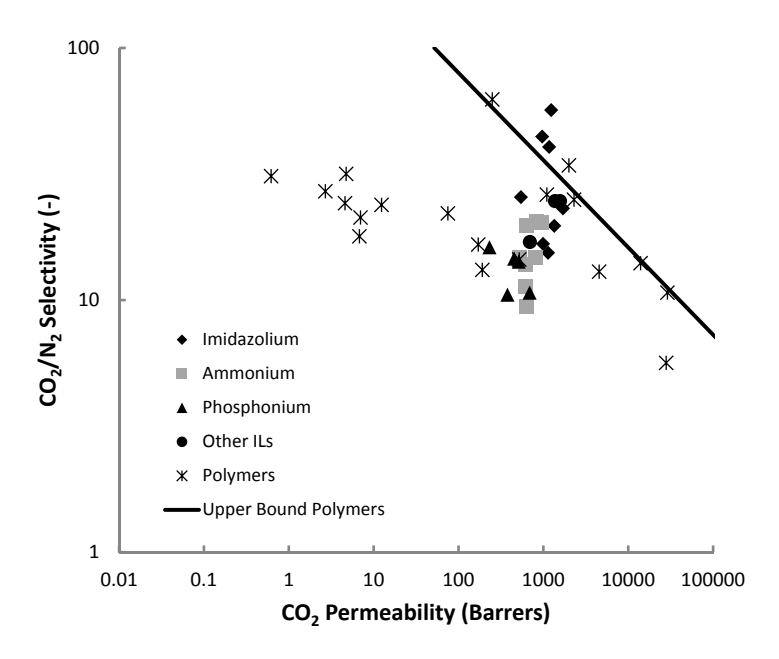


Figure 2.27: Robeson plot showing the performance of polymeric membranes and supported IL membranes (SILMs) for  $CO_2/N_2$  separation. Some of the SILMs cross the 'upper bound' [292] limit of polymeric membranes. SILMs data at 303 K taken from Scovazzo [293] and data of polymers taken from Robeson [292] and Stern [294].

together with polymeric membranes data. An example of a Robeson plot, which shows a tradeoff between permeability and selectivity for  $\rm CO_2/N_2$  separation by polymers, is given in Figure 2.27. Interesting to see in Figure 2.27 is that some SILMs crosses the upper bound limit set for polymeric membranes. This means that SILMs can be designed with a permeability and selectivity superior to traditional polymeric membranes.

The transport mechanism of gases through membranes is extremely important and for SILM it is assumed that a solution-diffusion mechanism governs this transport [293]. Therefore, the ideal permeability  $(P_i)$  of a gas through a SILM can be expressed as a product of the solubility coefficient

(in moles per volume per partial pressure) and the diffusion coefficient:

$$P_i = S_i \cdot D_i \tag{2.9}$$

The ideal selectivity  $(\alpha_{ij})$  is then calculated by taking the ratio of the ideal gas permeabilities for a given gas pair:

$$\alpha_{ij} = \frac{P_i}{P_j} = \frac{S_i}{S_j} \cdot \frac{D_i}{D_j} \tag{2.10}$$

Several correlations for predicting gas solubilities [115, 121, 295] and diffusivities [182, 194, 195] in ILs have been proposed. Recently, Scovazzo [293] reviewed the progress in the SILM field and presented upper limits and benchmarks for guiding future research. Scovazzo provide a correlation, depending only on the molar volume of the IL, for the selectivity of the gas pairs  $CO_2/N_2$  and  $CO_2/CH_4$ . A correlation, only depending on the IL viscosity, for CO<sub>2</sub> permeability through SILMs is also provided by Scovazzo. The (ideal) selectivity correlation by Camper [120] and the universal correlation by Scovazzo [293] both predict an increasing selectivity with decreasing IL molar volume for the gas pairs CO<sub>2</sub>/N<sub>2</sub> and CO<sub>2</sub>/CH<sub>4</sub>. Ideal  $CO_2/N_2$  selectivity in SILMs has been reported by Scovazzo et al. [280], Bara et al. [296], Neves et al. [289] and Cserjesi et al. [297]. Scovazzo investigated SILMs based on [emim][Tf<sub>2</sub>N], [emim][CF3SO3], [emim][dca] and [thtdp][C1] reporting CO<sub>2</sub> permeabilities in the range of 350-1000 barrers (1 barrer =  $10^{-10}$  cm<sup>3</sup> (STP) cm/cm<sup>2</sup> s cmHg) and ideal CO<sub>2</sub>/N<sub>2</sub> selectivities of 15-61. Bara et al. measured the solubility of CO<sub>2</sub>, N<sub>2</sub>, O<sub>2</sub> and CH<sub>4</sub> in fluoroalkyl-functionalized imidazolium-based SILMs. They reported  $CO_2$  permeabilities of 210-320, while the ideal selectivity of  $CO_2/N_2$  and  $CO_2/CH_4$  was 16-27 and 13-19, respectively. Neves et al. studied the ideal and mixed gas solubility of several gases in imidazolium-based ILs using two membrane supports with different hydrophobicity. They reported mixedgas CO<sub>2</sub>/N<sub>2</sub> and CO<sub>2</sub>/CH<sub>4</sub> selectivities, which was not much different than the ideal selectivities, ranging from 20-32 and 98-200, respectively. Furthermore, they showed that the hydrophobic supports were more stable than the hydrophilic ones. Cserjesi et al. investigated the solubility of several

gases in SILMs using different type of ILs. Ideal selectivities of the gas pairs  $CO_2/N_2$ ,  $CO_2/H_2$  and  $CO_2/CH_4$  ranged from 10-52, 5-13 and 5-23, respectively. Mixed gas solubilities of the gas pairs CO<sub>2</sub>/N<sub>2</sub> and CO<sub>2</sub>/CH<sub>4</sub> in several SILMs were reported by Scovazzo et al. [281] The highest mixedgas selectivity for  $CO_2/N_2$  and  $CO_2/CH_4$  was 21.2 and 27 for [emim][Tf<sub>2</sub>N] and [emim][BF<sub>4</sub>] based SILMs, respectively. Furthermore, the mixed-gas selectivities were approximately equal to the ideal selectivities for the corresponding gas pairs. Mixed gas solubility of the gas pair  $CO_2/H_2$  was measured by Myers et al. [287] using an amine-functionalized IL in a crosslinked Nylon 66 support. They reported selectivities greater than 15 and CO<sub>2</sub> permeabilities ranging from 100-1000 barrers. Ideal CO<sub>2</sub>/CH<sub>4</sub> selectivity has also been studied by Iarikov et al. [290] and Yoo et al. [288], while Hanioka et al. [286] measured mixed-gas solubilities. Iarikov et al. studied SILMs based on ammonium, imidazolium, pyridinium and pyrrolidinium an phosphonium ILs obtaining a ideal selectivity of 5-30. You et al. obtained an ideal CO<sub>2</sub>/CH<sub>4</sub> selectivity of 26 using imidazolium-based ILs in a Nafion membrane. Hanioka et al. used an amine-functionalized IL membrane obtaining high CO<sub>2</sub>/CH<sub>4</sub> selectivity and a high membrane stability. On the basis of limited amount of data, Scovazzo [293] concluded that solubility selectivity dominate the selectivity in SILMs, whereas diffusion determines the selectivity in polymers. Since, diffusion selectivity plays a minor role, mixed gas solubilities in SILMs are expected to be approximately equal to ideal selectivities [281]. For more information on SILMs, the reader is referred to the excellent reviews by Scovazzo [293] and Lazano [298].

## 2.5 Biodegradability and Toxicity of Ionic Liquids

Ionic liquids are often referred to as 'green' and environment benign. This classification was initially justified on the ground of their low vapor pressure, nonflammability and reusability. However, important issues within the context of green chemistry [299, 300] (e.g. biodegradability and toxicity) were initially neglected [301]. The importance of biodegradability and toxicity should not be underestimated, since these parameters are relevant

in the authorization process of any substance [302]. Persistent and toxic ionic liquids, due to their potential hazard to environment and humans, may fail the authorization process or their use will be restricted to only a few applications [303]. Anticipating on the large scale application of ionic liquids, disposal of exhausted non-biodegradable ionic liquids may also become an issue [304]. Therefore, a thoroughly assessment of the potential risks of ILs is essential before commercializing IL processes. Since recently much more attention has been paid to these issues, as a result the IL literature for biodegradability and toxicity has grown considerably. Here, we analyze data from existing literature and aim to provide rules of thumbs or generalizations, which might be relevant for designing inherently safer ionic liquids.

In the next section we will discuss the biodegradability and toxicity of ILs. As the research field is expanding and IL processes are close to reaching the market, it is important to analyze the environmental fate of IL. An IL may come in contact with several streams, in which they might be soluble (for example water) thereby having a chance to end in the environment via the effluent streams of a process. Environmental issues of ILs have been characterized as a major barrier to commercialize IL processes, therefore these topics will be discussed next [305].

#### 2.5.1 Biodegradability of Ionic Liquids

It is well known that biodegradability is affected not only by a compounds structure, but also by the environmental conditions. However, safe design of a product should start at the earliest phase in the long process of commercializing a new chemical. The earliest phase in product/process design is often the design of the molecule itself, hence the principles of safe design should preferentially be applied at molecular level [306]. The emphasis, here, is the effect of molecular structure (i.e. anion, cation, functional groups) on the biodegradability of ionic liquids. Before starting with the analysis of the reported data, it is informative to mention the rules of thumbs given by Boethling et al. [306] for the biodegradability of small molecules.

#### Rules of Thumb

These rules of thumb are not specifically for ionic liquids, but originate from decades of research mainly in the detergent and pesticide industry. However, initial research suggest that designing ILs according to some of these rules of thumbs may also improve the biodegradability of ionic liquids [304, 307]. According to Boethling et al. the following molecular features generally result in poor biodegradation and should be avoided when possible: halogens (e.g. chlorine and fluorine), extensive chain branching (e.g. quaternary C), tertiary amine, nitro, nitroso, azo, arylamino groups, polycyclic residues (e.g. polycyclic aromatic hydrocarbons), heterocyclic residues (e.g. imidazole) and aliphatic ether bonds.

The following molecular features generally improve biodegradation: esters, amides, hydroxyl, aldehyde, carboxylic acid groups, probably ketone, unsubstituted linear alkyl chains ( $\geq 4$  carbons) and phenyl rings. The rules of thumb given here should not be used as universal generalizations, since exceptions exist for these rules of thumb [306]. Nevertheless, it can serve as a good starting point in the design of biodegradable ILs.

#### Biodegradation Studies of Ionic Liquids

Biodegradability of substances are generally assessed according to the guidelines laid down by the Organization for Economic Co-operation and Development (OECD) [308]. Several standard methods compliant with the OECD guidelines exist: Die-Away test (OECD 301 A), Modified Sturm test (OECD 301 B), Closed Bottle test (OECD 301 D), CO<sub>2</sub> Headspace test (ISO 14593), OECD 309 and ASTM D 5988 test. Each method employs a different principle, whereby depending on the chosen method one of the following is monitored as a measure for biodegradability: the dissolved organic carbon (DOC), CO<sub>2</sub> production and O<sub>2</sub> uptake. However, care should be taken in the selection, since the suitability of each method for assessing biodegradation depends on several physical properties of the compound in question (i.e. water solubility, volatility and the tendency to adsorb on solid phases). Detailed information on the measuring principle of each method, a selection criterion and a review on the biodegradation of ILs is given by Coleman and Gathergood [308]. The group of Scammells [304, 307, 309] was the first to report the poor biodegradability of commonly used imidazolium ILs. Garcia et al. [309] used the Closed Bottle test to evaluate the biodegradability of [bmim][X] ILs, where X =Br, BF<sub>4</sub>, PF<sub>6</sub>, TF<sub>2</sub>N, DCA and octylsulphate. All the ILs, except for the octylsulphate IL, underwent a biodegradation less than 5 % while the octylsulphate IL had a modest biodegradability of 25 %. Clearly, these ILs cannot be classified as "readily biodegradable", which is an arbitrary classification for substances that undergo more than 60 % biodegradation within a specified test period (normally 28 days) [309]. In a subsequent study, Gathergood et al. [304] applied some of the rules of thumbs given by Boethling et al. [306] to improve biodegradation of the above mentioned ILs. Accordingly, they incorporated an ester or an amide group in the alkyl side chain of the imidazolium cation. The ester-functionalized ILs were shown to significantly improve biodegradation, while the effect of the amide-functionalization was negligible. Furthermore, biodegradability was shown to increase with alkyl-chain length of the ester-functionalized cation. Introduction of a methyl group at the C<sub>2</sub>-position of the imidazolium ring was shown to have negligible effect on biodegradability compared to the C<sub>2</sub>-unsubstituted ILs. Although biodegradability of the ester-functionalized ILs was higher than of the nonfunctionalized ILs, only a combination of [mim-ester] cation and [octylsulphate] anion resulted in biodegradabilities higher than 60 %. These ester-functionalized imidazolium cations with the [octylsulphate] anion formed the first readily biodegradable ILs [310]. Morrissey et al. [311] measured the biodegradability of a large number of imidazolium-based ILs containing an ester and/or ether group in the alkyl side chain, using the "CO<sub>2</sub> Headspace" test. Ester-functionalized ILs were shown to have a higher degree of degradation, while including ether groups into the side chain did not have a detrimental effect on the biodegradation of the ILs. Morrissey et al. paired the ester/ether-functionalized cations with several commonly used anions (i.e. Br, BF<sub>4</sub>, PF<sub>6</sub>, Tf<sub>2</sub>N, DCA and octylsulphate), however, only ILs containing the [octylsulphate] anion passed the readily biodegradable test. Clearly, the [octylsulphate] anion has a important role in determining the high biodegradation of ILs [311, 312]. Moreover, the data reported by Morrissey *et al.* [311] and Docherty *et al.* [313] show close agreement with Boethling's rules of thumb where biodegradability increases as the alkyl chain length ( $\geq 4$  carbons) increases.

Biodegradability of pyridinium-based ILs has been measured by several authors [313–317]. Docherty et al. [313] used the "Die-Away" test to investigate the biodegradability of six imidazolium and pyridinium ILs ([bmim], [hmim], [omim], [bmpy], [hmpy] and [ompy]), all containing the [bromide] anion as the counter ion. None of the imidazolium ILs could be classified readily biodegradable, while the pyridinium IL with the longest alkyl chain [ompy] passed the test. The data showed further that the pyridinium ILs had higher biodegradabilities than the imidazolium analogues and that the biodegradability improved with increasing alkyl length. Harjani et al. [315] evaluated the biodegradability of several (ester-functionalized) pyridinium ILs using the "CO<sub>2</sub> Headspace" test. The (ester-functionalized) pyridinium cations were paired with a range of anions (i.e. Br, PF<sub>6</sub>, octylsulphate, bis(trifluoromethylsulfonyl)imide and iodide). Pyridinium ILs bearing an ester side chain moiety was shown to have high levels of biodegradation and could be classified as 'readily biodegradable'. In contrast, pyridinium ILs with alkyl side chains without an ester functionality did not pass the biodegradability test. In this case, the biodegradability did also not improve as the alkyl chain length was increased, contradicting Boethling's rules of thumb. Further, the effect of the anion on the biodegradability was shown to be insignificant [314, 315]. Ford et al. [316] studied the biodegradability (CO<sub>2</sub> Headspace test) of pyridinium and thiazolium ILs containing one of the following functionalities: hydroxyethyl side chain, methyl or ethyl ether side chain, acetal and carbamate. Pyridinium ILs, regardless of the anion, containing the hydroxyethyl functionality showed higher levels of biodegradation and passed the readily biodegradable test. In contrast, thiazolium ILs containing the hydroxyethyl functionality showed surprisingly low biodegradation. Pyridinium ILs bearing an ether, acetal or carbamate functionality showed significantly lower biodegradation. Biodegradation studies of ammonium and phosphonium ILs are relatively scarce so far. Yu et al. [318] and Pavlovica et al. [319] reported that cholinium (i.e. 2-hydroxyethylammonium) ILs containing napthenic acid or lactate anion were highly biodegradable. Atefi  $et\ al.\ [320]$  used the 'CO<sub>2</sub> Headspace' test to evaluate biodegradation of phosphonium-based ILs. The phosphonium cation was functionalized with an ester, ether, alcohol or alkane moiety and paired with halide, triflimide or octylsulphate anions. As expected, ILs containing the octylsulphate anion showed an increased biodegradation, but in all cases the biodegradability was lower than 30 %. It is surprising to note that ester-functionalization of phosphonium, in contrast to imidazolium and pyridinium, ILs failed to promote biodegradation.

In summary, pyridinium and cholinium ILs are more biodegradable than imidazolium and phosphonium ILs. Biodegradation can be improved by including ester-functionalities in the imidazolium and pyridinium cations, while the phosphonium cation is an exception to this rule of thumb. A longer alkyl chain seems to promote biodegradation in many cases, however exceptions exist also for this rule of thumb. The anion seems to play a minor role in biodegradation, although the octylsulphate anion generally yields higher biodegradation. Overall, the rules of thumbs given by Boethling et al. [306] should not be used as universal generalizations, but can serve as guidelines for designing biodegradable ILs.

#### 2.5.2 Toxicity of Ionic Liquids

Toxicological studies are essential in determining the impact of ILs on the environment and humans. Generally, toxicity of ILs is evaluated according to standard methods (i.e. OECD, ISO or ASTM), where a test model (e.g. microorganisms) is exposed to the IL and the response of it is a measure of toxicity, often expressed as a LC<sub>50</sub>, EC<sub>50</sub> or IC<sub>50</sub> value. Many studies appeared in the last few years addressing the toxic nature of some commonly used ILs. Compilation of raw data on the toxicity of ILs can be found in several recent reviews and the references cited therein [321–325]. However, the emphasis here is to show toxicity trends with respect to anions, cations and functional groups of ILs.

The cation is believed to play a key role in determining the toxicity of an IL, while the anion has a minor influence [303, 326]. Wells and Coombe [317]

studied the ecotoxicity of quaternary-ammonium, imidazolium, quaternaryphosphonium and pyridinium ILs towards two aquatic test models. All the investigated ILs were shown to have EC<sub>50</sub> based toxicities much greater  $(\sim 10^4 - 10^6)$  for the worse cases) than conventional solvents like methanol and acetonitrile. Further, toxicity was shown to increase as the alkyl chain length on the imidazolium cation was increased for an IL containing the [chloride] anion [317, 327]. This trend has consistently been reported for ammonium [328], morpholinium [328], phosphonium [317], pyridinium [329, 330] and pyrrolidinium [330] ILs. Stolte et al. [331] studied the aquatic toxicity of a large number of ILs with a different head group. These authors found a correlation between the lipophilicity of ILs and (eco)toxicity, where the toxicity increases as the lipophilicity (i.e hydrophobicity) becomes higher [332]. This may explain the increased toxicity of ILs containing a large alkyl chain (i.e. increased lipophilicity). Furthermore, the toxicity not only increases with an increasing alkyl chain length also the number of alkyl chains on the cation increases the toxicity [324]. The latter explains the higher toxicity of quaternary-ammonium and quaternary-phosphonium ILs compared to imidazolium and pyridinium analogues. Couling et al. [326] developed a quantitative structure-property relationship (QSPR) for assessing and predicting the toxicity of a range of ILs. The QSPR-model predicted the following toxicity trend with cation: ammonium < pyridinium < imidazolium < triazolium < tetrazolium. Unfortunately, this trend is not universal since many ammonium and pyridinium ILs are shown to be more toxic than imidazolium ones [328, 331, 333].

Although the anion is believed to play a secondary role in the toxicity of ILs, it can significantly increase or reduce toxicities. Toxicity data for aquatic organisms compiled by Frade *et al.* [324] show the following anion trend:  $[Br] < [DCA] < [Cl] < [BF_4] < [PF_6] < [Tf_2N]$ . Especially the fluorinated anions (e.g.  $BF_4$  and  $Tf_2N$ ) are highly toxic and forms a serious risk for the environment [303, 332, 334].

In summary, the toxicity data reported in the literature should be treated with some caution. Different test models have been used in the separate studies to evaluate toxicity, which complicate data interpretation since different test models can respond differently to the same IL. This is also the

reason why data extrapolation from one test model to another should be avoided [325]. So far, the only consistently reported trend is that toxicity increases with alkyl chain length and with the number of alkyl chains on the cation. Further, the [morpholinium] cation and the [DCA] anion seems to be good candidates for reducing toxic effects [324, 333]. In the future more unified and systematic approaches should be used to evaluate toxicity of ILs.

#### 2.6 Conclusions and Future Directions

Efficient removal of the greenhouse gas carbon dioxide (CO<sub>2</sub>) from fluegas turns out to be extremely challenging from an economic and technical point of view. The energy penalty, hence also the cost, for CO<sub>2</sub> removal from fluegas/natural gas is extremely high, thus, unattractive for large scale applications. Many new processes/materials, in particular ionic liquids (ILs) due to their unique properties, have been proposed to overcome this problem. In this review we have analyzed the literature data of the last decade on CO<sub>2</sub> capture with ILs and aimed to present trends regarding: CO<sub>2</sub> solubilities and selectivities in different ILs, effect of anions, cations and functional groups on physical properties, volatility, biodegradability and toxicity of ionic liquids. In addition, recent developments on functionalized ILs and supported IL membranes have also been addressed. Among the many solubility trends reported here, the main finding is that the CO<sub>2</sub> solubility in conventional ILs based on a physical mechanism is still too low at post-combustion capture conditions to compete with the amine process. Furthermore, the Henry constant (CO<sub>2</sub> solubility) tends to decrease (increase) with an increasing IL molecular weight, molar volume and free volume. Therefore, the CO<sub>2</sub> solubility in ILs should be compared on molality (mol/kg) or molarity (mol/m<sup>3</sup>) basis, instead of mole fraction basis. CO<sub>2</sub> absorption capacity have successfully been improved by functionalizing conventional ILs with an amine moiety, thereby allowing the CO<sub>2</sub> to react chemically with the amine. In this way even a better (1:1) reaction stoichiometry, compared to conventional CO<sub>2</sub>-amine chemistry, could be

achieved when the amine was functionalized to the anion of the IL. Not only solubility, but also selectivity is of great importance in industrial separation processes. Selectivity analysis show that CO<sub>2</sub> is generally much more soluble than other simple gases (e.g. H<sub>2</sub>, N<sub>2</sub>, O<sub>2</sub>), however SO<sub>2</sub> and H<sub>2</sub>S are by far the most soluble gases in ILs. This means that the selectivity will be high for CO<sub>2</sub>/simple-gas systems, while the selectivity will likely drop for  $CO_2$ /sour-gas systems. Regular solution theory predict that  $CO_2/N_2$ and CO<sub>2</sub>/CH<sub>4</sub> selectivity can be improved by using ILs with a low molar volume. A common problem to all functionalized or nonfunctionalized ILs is their high viscosity, which forms a great barrier for industrial application. Trends are shown in this review, which can be used to design low viscosity ILs. Biodegradability and toxicity data analysis show that many commonly used ILs are nonbiodegradable and highly toxic. Rules of thumbs from the detergent industry have been used to improve biodegradation, however only some of the rules of thumbs applies also to ILs. Within the limited amount of toxicity data some trends are apparent, which could be used to design inherently safer ILs. As a final note, we want to address the following issues [305], which should be resolved in the future to commercialize IL processes: (1) Lack of physicochemical and thermodynamic data. Although some physical properties of ILs have been reported recently, there is need for more data on density, viscosity, surface tension, diffusion coefficients, specific heat, chemical/thermal stability, heat of fusion, water solubility, corrosivity, etc. These properties of ILs have scarcely been reported in the literature and accurate property predicting tools are still lacking. (2) Lack of lifetime and recyclability studies. Analysis of long term chemical and thermal stability of ILs is required under severe conditions to prevent degradation during absorption/desorption cycles. (3) Lack of scale-up studies. Lab-scale processes need to be scaled up to a pilot plant scale to assess the feasibility of ILs on industrial scale. Industry almost always demand demonstration on pilot scale before commercialization. (4) Lack of engineering studies. Manufacturing and process cost of ILs can only be reduced/optimized by systematic process engineering studies. These studies are lacking, mostly due to the absence of physicochemical properties of ionic liquids. (5) Lack of safety, health and environmental studies. Biodegradability and toxicity

of candidate ILs should be assessed thoroughly to prevent environmental pollution. (6) High price of ILs. The current lab-scale price of ILs is extremely high ( $\sim 1000 \ \text{s/kg}$ ), which is 100-1000 times more expensive than conventional solvents. The price will drop for a large scale production of ILs, but a price level typical for conventional solvents should not be expected since ILs are complex molecules, requiring advanced synthesis and purification steps. To conclude, a lot of research is going on to improve  $CO_2$  absorption capacities by taking advantage of the tunability property of ILs. Nevertheless, many barriers need to be overcome before ILs can be applied at a commercial scale.

## Chapter 3

# CO<sub>2</sub>/CH<sub>4</sub> Solubility in Ionic Liquids: Ideal Selectivity

This chapter is based on the paper: M. Ramdin, A. Amplianitis, S. Bazhenov, A. Volkov, V. Volkov, T. J. H. Vlugt and T. W. de Loos. Solubility of CO<sub>2</sub> and CH<sub>4</sub> in Ionic Liquids: Ideal CO<sub>2</sub>/CH<sub>4</sub> Selectivity. Ind. Eng. Chem. Res., 53 (2014) 15427-15435.

#### 3.1 Introduction

Natural gas contains a variety of impurities including the sour gases carbon dioxide (CO<sub>2</sub>) and hydrogen sulfide (H<sub>2</sub>S) [10, 11]. These sour gases have to be removed in order to meet customer specifications and to avoid technical problems during gas transportation. CO<sub>2</sub> should be eliminated, because of its low caloric value and due to the risk of dry ice formation during the liquefaction of natural gas. H<sub>2</sub>S concentrations should be reduced drastically to avoid pipeline corrosion [17]. The sweetening of the natural gas is typically performed in an absorber-stripper configuration using either a physical solvent, a chemical solvent or a mixture of both depending on the type and concentration of the impurities [10]. Despite

the inherent high pressure of the sweetening process, which is favorable for physical absorption purposes, the majority of the units in the field utilizes chemical solvents (e.g., monoethanolamine (MEA)) [9]. The use of physical solvents (e.g., Purisol, Rectisol, Selexol etc.) is not uncommon in the natural gas industry and is in fact preferred over chemical solvents at high acid gas partial pressures [10]. The selection of the proper solvent for natural gas sweetening is not trivial, since it depends on many factors (e.g., composition, temperature and partial pressures of the acid gases, and product specifications). For guidelines the reader is referred to the work of Tennyson and Schaaf [10] and Kohl and Nielsen [11]. Although the aqueous amine process is effective at removing acid gas components from natural gas for a wide range of conditions, it suffers a number of serious drawbacks. These include the high energy requirement for solvent regeneration, the low CO<sub>2</sub>/H<sub>2</sub>S selectivity, the corrosivity, and the volatility of the used amines [15]. Therefore, many researchers have posed alternatives to overcome some of the problems associated with the amine process. In the last few years, ionic liquids (ILs), which are salts with melting points lower than 100 °C and characterized by very low vapor pressures, have emerged as a promising solvent for acid gas removal [16, 17]. In the past decade, a large number of studies reported the solubility of CO<sub>2</sub> and to a lesser extent of other acid gas components in many different kinds of ionic liquids [9, 335]. In practice, however, not the solubility, but the selectivity of one component towards the another is more important for judging the separation performance of an absorption process [9]. This implies that a potential IL for natural gas sweetening should not only have a high individual CO<sub>2</sub> and H<sub>2</sub>S solubility, but at the same time also a low CH<sub>4</sub> solubility. In other words, the IL should have a high CO<sub>2</sub>/CH<sub>4</sub> and CO<sub>2</sub>/H<sub>2</sub>S selectivity. Lei et al. [335] provide an excellent review of the solubility of different gases in ILs, whereas Karadas et al. [17], Ramdin et al. [9] and Kumar et al. [16] review the application potential of ILs for natural gas sweetening. Recently, Mortazavi-Manesh et al. [336] used the COSMO-RS model to screen more than 400 ILs for the separation of acid gases. Unfortunately, the amount of experimental data on CO<sub>2</sub>/CH<sub>4</sub> and CO<sub>2</sub>/H<sub>2</sub>S selectivities in ILs are extremely scarce, which is mainly due to the high toxicity of H<sub>2</sub>S for the latter system, but this

3.2 Experiments 77

reason is less obvious for the  $CO_2/CH_4$  system.

This motivated us to study CO<sub>2</sub> and CH<sub>4</sub> solubilities and CO<sub>2</sub>/CH<sub>4</sub> (ideal) selectivities in a total of 10 ILs composed of 8 different classes of cations and 4 different types of anions. A synthetic method has been used to measure the bubble-point pressures of CO<sub>2</sub> and CH<sub>4</sub>, for a temperature range of 303.15 - 363.15 K and for pressures up to 14 MPa, in the ionic liquids: 1-ethyl-3-methylimidazolium diethylphosphate [emim][dep], trihexyltetradecylphosphonium bis(2,4,4-trimethylpentyl)phosphinate [thtdp][phos], trihexyltetradecylphosphonium dicyanamide [thtdp][dca], 1-allyl-3-methylimidazolium dicyanamide [amim][dca], 1-butyl-1-methylpyrrolidinium dicyanamide [bmpyrr][dca], 1,2,3-tris(diethylamino)cyclopropenylium dicyanamide [cprop][dca], 1,2,3-tris(diethylamino)cyclopropenylium bis(trifluoromethylsulfonyl)imide [cprop][Tf<sub>2</sub>N], 1-butyl-1-methylpiperidinium bis(trifluoromethylsulfonyl)imide [bmpip][Tf<sub>2</sub>N], triethylsulfonium bis(trifluoromethylsulfonyl)imide [tes][Tf<sub>2</sub>N] and methyl-trioctylammonium bis(trifluoromethylsulfonyl)imide [toa][ $Tf_2N$ ]. The experimental data has been reduced by calculating the Henry constants from which the ideal CO<sub>2</sub>/CH<sub>4</sub> selectivities are obtained. The ideal CO<sub>2</sub>/CH<sub>4</sub> selectivities of the investigated ILs are compared with those of conventional solvents used in the natural gas industry. Furthermore, the experimental data has been modeled with the Peng-Robinson equation of state in combination with van der Waals mixing-rules.

## 3.2 Experiments

The gases CO<sub>2</sub> and CH<sub>4</sub> used in the experiments had a purity of 99.995 mole % and were purchased from the Linde Group. The ILs, purchased from Sigma-Aldrich, were always dried in vacuo at a temperature of 80 °C for several days before usage. The molecular structures of the investigated ILs are shown in Figure 3.1. The water content of the ILs after drying was determined by Karl Fischer titration and the results together with other properties are shown in Table 3.1. Note that the purity of the ILs reported in Table 3.1 is prior to drying, while the water content is only measured

	36.1.1.	D 1: 0	
Name IL	Molecular weight	Purity <sup><math>a</math></sup>	Water content <sup><math>b</math></sup>
(Abbreviation)	(g/mol)	(mole %)	(ppm)
[emim][dep]	264.26	$\geq 98.0$	< 250
[thtdp][phos]	773.27	$\geq 95.0$	< 350
[thtdp][dca]	549.90	$\geq 95.0$	< 350
[amim][dca]	189.22	$\geq 98.5$	< 200
[bmpyrr][dca]	208.30	$\geq 97.0$	< 200
[cprop][dca]	318.46	$\geq 96.5$	< 200
$[cprop][Tf_2N]$	532.56	$\geq 96.5$	< 150
$[bmpip][Tf_2N]$	436.43	$\geq 96.5$	< 150
$[\mathrm{tes}][\mathrm{Tf_2N}]$	399.39	$\geq 99.0$	< 150
$[toa][Tf_2N]$	648.85	$\geq 99.0$	< 150
$[bmim][Tf_2N]$	419.36	$\geq 98.0$	< 150

Table 3.1: Properties of the used ILs. The water content was measured with Karl Fischer titration, whereas the purities were reported by the supplier (Sigma-Aldrich) [339].

and reported after the drying step. The ILs contained typically 1-2% water, therefore the actual purity of the ILs will always be higher than the reported values. The VLE experiments start with filling a Pyrex glass-tube with a known amount of IL. This tube is then connected to a gas-dosing system, which is used to degas the IL and to dose a known amount of gas into the tube using mercury as a displacement fluid. The exact amount of gas is calculated through the virial equation of state truncated after the second term [337]. Subsequently, the tube with a known composition is disconnected from the gas-dosing system and placed in the Cailletet apparatus. Here only a brief description of the Cailletet apparatus will be presented, since a detailed explanation of the experimental procedure can be found elsewhere [338]. The Cailletet apparatus allows phase equilibria measurements in a temperature and pressure range of 255-470 K and 0.1-15 MPa, respectively. For a binary system at bubble point conditions, the Gibbs phase-rule unequivocally requires two independant variables to be fixed. Therefore, the composition and the temperature were fixed in the experiments, while the

<sup>&</sup>lt;sup>a</sup> Purity of ILs before drying

<sup>&</sup>lt;sup>b</sup> Water content of ILs after drying

3.2 Experiments 79

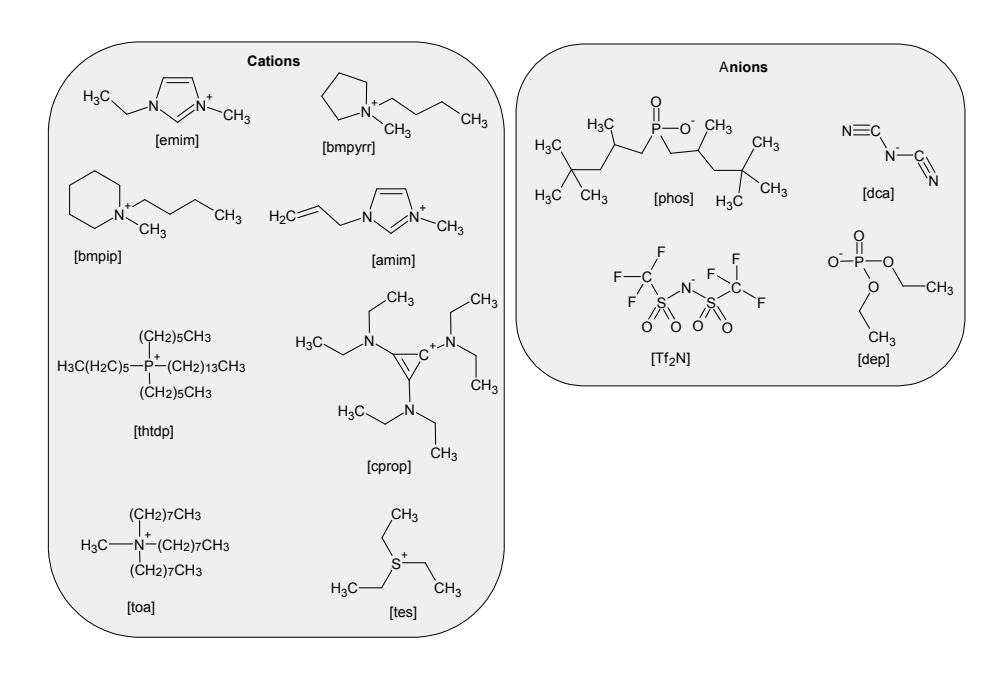


Figure 3.1: Cations and anions of the investigated ILs. Abbreviation cations: 1-allyl-3-methylimidazolium [amim], 1-ethyl-3-methylimidazolium [emim], 1,2,3-tris(diethylamino)cyclopropenylium [cprop], 1-butyl-1-methylpiperidinium [bmpip], 1-butyl-1-methylpyrrolidinium [bmpyrr], methyl-trioctylammonium [toa], trihexyltetradecylphosphonium [thtdp] and triethylsulfonium [tes]. Abbreviation anions: bis(trifluoromethylsulfonyl)imide [Tf $_2$ N], dicyanamide [dca], bis(2,4,4-trimethylpentyl)phosphinate [phos] and diethylphosphate [dep].

pressure was gradually increased until the disappearance of the last bubble in the liquid (i.e., the bubble-point pressure). The VLE measurements then involve the determination of bubble-point pressures at different, but fixed compositions and temperatures. The pressure is obtained by a dead weight gauge, while the temperature is controlled by a thermostatic bath equiped with a Pt-100 (ASL F250) thermometer. The standard uncertainty in the experimental pressure, temperature and composition is  $\pm$  0.005 MPa,  $\pm$  0.01 K (i.e., the fluctuations in temperature were within the accuracy of

the thermometer) and  $\pm 0.003$  in the mole fraction, respectively.

### 3.3 Thermodynamic Modeling

The Peng-Robinson (PR) equation of state [340] (EoS) has been applied to model the experimental data,

$$P = \frac{RT}{v - b_m} - \frac{a_m}{v(v + b_m) + b_m(v - b_m)}$$
(3.1)

where v is the molar volume,  $a_m$  and  $b_m$  are constants for the mixture accounting for the molecular interaction and covolume, respectively. The PR EoS is used in combination with the quadratic van der Waals (vdW) mixing rules [337]:

$$a_m = \sum_{i} \sum_{j} x_i x_j a_{ij}, \quad a_{ij} = \sqrt{a_i a_j} (1 - k_{ij}), \qquad k_{ii} = k_{jj} = 0 \quad (3.2)$$

$$b_m = \sum_{i} \sum_{j} x_i x_j b_{ij}, \quad b_{ij} = \frac{1}{2} (b_i + b_j) (1 - l_{ij}), \quad l_{ii} = l_{jj} = 0 \quad (3.3)$$

where  $k_{ij}$  and  $l_{ij}$  represent the binary interaction parameters,  $a_i$  and  $b_i$  the pure component parameters accounting for molecular interaction and covolume, respectively. Calculation of the pure component parameters requires the critical properties and acentric factors of all the components participating in the mixture. These properties are not known (i.e., not experimentally available) for ILs, since many ILs start to decompose before reaching the critical point. Therefore, one has to rely on group-contribution methods [341], molecular simulations [206, 342] or suitable correlations [208]. Here, the modified Lydersen-Joback-Reid group-contribution method proposed by Valderrama et al. [341] is used to obtain the critical properties of all the investigated ILs. The critical parameters and acentric factors of all the ILs are listed in Table 3.2. Once these properties have been obtained, the PR EoS can readily be applied to calculate the bubble point of the gas-IL

Component	$T_c$ / K	$P_c$ / MPa	$\omega$
$\overline{[\text{emim}][\text{dep}]^a}$	877.2	2.147	0.722
$[\mathrm{thtdp}][\mathrm{phos}]^a$	1878.8	0.551	-0.139
$[{\rm thtdp}][{\rm dca}]^a$	1525.5	0.765	0.582
$[amim][dca]^a$	1019.2	2.799	0.788
$[bmpyrr][dca]^a$	887.2	2.061	0.855
$[\text{cprop}][\text{dca}]^a$	1073.7	1.615	1.073
$[\text{cprop}][\text{Tf}_2N]^a$	1255.7	1.803	0.588
$[bmpip][Tf_2N]^a$	1108.0	2.264	0.392
$[\mathrm{tes}][\mathrm{Tf_2N}]^a$	1189.9	2.190	0.160
$[toa][Tf_2N]^a$	1376.1	1.064	0.996
$[\text{bmim}][\text{Tf}_2\text{N}]^a$	1269.9	2.765	0.3004
$CH_4{}^b$	190.6	4.599	0.012
$CO_2^b$	304.12	7.374	0.225

Table 3.2: Critical temperature  $(T_c)$ , pressure  $(P_c)$  and acentric factor  $(\omega)$  of the components used in the modeling.

systems. The binary interaction parameters  $k_{ij}$  and  $l_{ij}$  are simultaneously optimized using a simplex algorithm in MATLAB [343] minimizing the objective function:

$$OF = \frac{1}{N} \sum_{i=1}^{N} \left| \frac{P_i^{\text{exp}} - P_i^{\text{pred}}}{P_i^{\text{exp}}} \right|$$
(3.4)

where N is the number of experimental points,  $P_i^{\text{exp}}$  and  $P_i^{\text{pred}}$  the experimental and predicted bubble-point pressure, respectively.

#### 3.4 Results and Discussion

Due to space constraints, only a selection of the data will be presented here. The raw experimental data, extensive p-T and p-x diagrams of all the

<sup>&</sup>lt;sup>a</sup> Calculated using the method of Valderrama *et al.* [341].

<sup>&</sup>lt;sup>b</sup> Taken from Poling et al. [344].

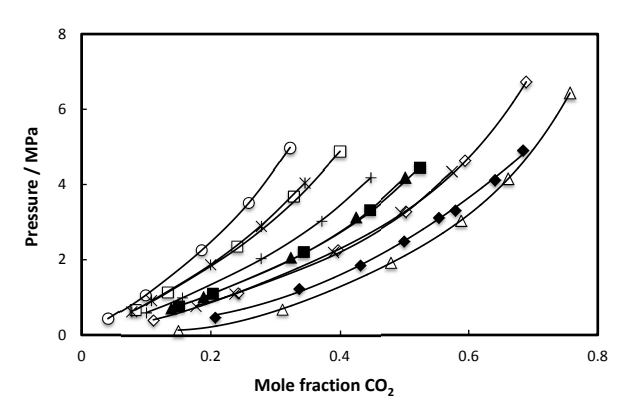


Figure 3.2: Comparison of  $CO_2$  solubility at 313.15 K in the investigated ILs: [emim][dep] (open squares), [thtdp][phos] (open triangles) [346], [thtdp][dca] (open diamonds) [346], [amim][dca] (open circles), [bmpyrr][dca] (stars), [cprop][dca] (plusses), [cprop][Tf<sub>2</sub>N] (crosses), [bmpip][Tf<sub>2</sub>N] (closed squares), [tes][Tf<sub>2</sub>N] (closed triangles) and [toa][Tf<sub>2</sub>N] (closed diamonds) [347]. The lines are PR EoS modeling results using the parameters of Table 3.2.

systems can be found in the Supporting Information of Ref. [345]. A comparison of the CO<sub>2</sub> solubility in the investigated ILs is shown in Figure 3.2. The  $CO_2$  + IL systems show a typical behavior: the solubility increases with increasing pressure and decreases with increasing temperature. The solubility trend, on mole fraction basis, observed for CO<sub>2</sub> obeys the following order: [thtdp][phos] > [toa][Tf2N] > [thtdp][dca] > [cprop][Tf2N] > [bmpip][Tf2N] > [tes][Tf2N] > [cprop][dca] > [emim][dep] > [bmpyrr][dca]> [amim][dca]. However, this trend completely vanishes if the solubility is compared on molality basis indicating a strong molecular weight effect. The data more or less collapse on the universal solubility curve proposed by Carvalho and Coutinho [125] as can be seen in Figure 3.3. The behavior of CH<sub>4</sub> is similar to that of CO<sub>2</sub>, but the solubility of CH<sub>4</sub> is an order of magnitude lower compared to  $CO_2$  at similar conditions, see Figure 3.4. It is surprising to see that the data for CH<sub>4</sub> do not collapse on an universal absorption curve as in the case of CO<sub>2</sub>, see Figure 3.5. The CH<sub>4</sub> solubility is higher in ILs containing large nonpolar alkyl-chains, which obviously inter-

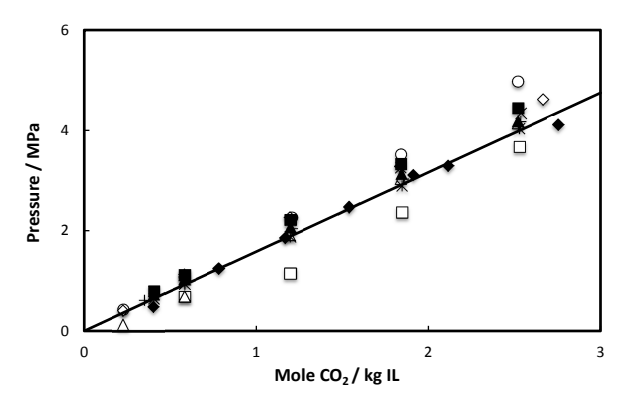


Figure 3.3: Comparison of  $CO_2$  solubility on molality scale at 313.15 K in the investigated ILs: [emim][dep] (open squares), [thtdp][phos] (open triangles) [346], [thtdp][dca] (open diamonds) [346], [amim][dca] (open circles), [bmpyrr][dca] (stars), [cprop][dca] (plusses), [cprop][Tf<sub>2</sub>N] (crosses), [bmpip][Tf<sub>2</sub>N] (closed squares), [tes][Tf<sub>2</sub>N] (closed triangles) and [toa][Tf<sub>2</sub>N] (closed diamonds) [347]. The line is correlation by Carvalho and Coutinho [125].

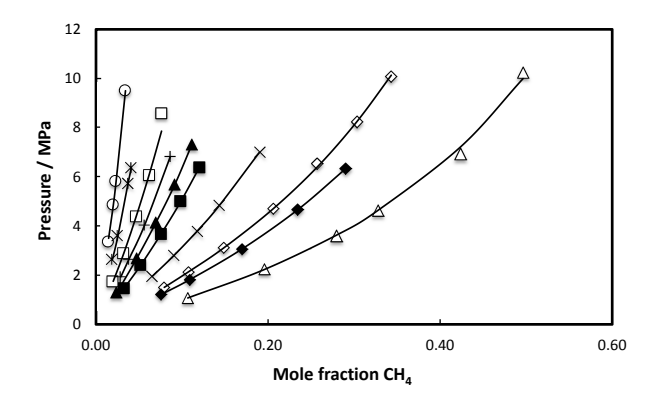


Figure 3.4: Comparison of CH $_4$  solubility at 313.15 K in the investigated ILs: [emim][dep] (open squares), [thtdp][phos] (open triangles) [346], [thtdp][dca] (open diamonds) [346], [amim][dca] (open circles), [bmpyrr][dca] (stars), [cprop][dca] (plusses), [cprop][Tf $_2$ N] (crosses), [bmpip][Tf $_2$ N] (closed squares), [tes][Tf $_2$ N] (closed triangles) and [toa][Tf $_2$ N] (closed diamonds) [347]. The lines are PR EoS modeling results using the parameters of Table 3.2.

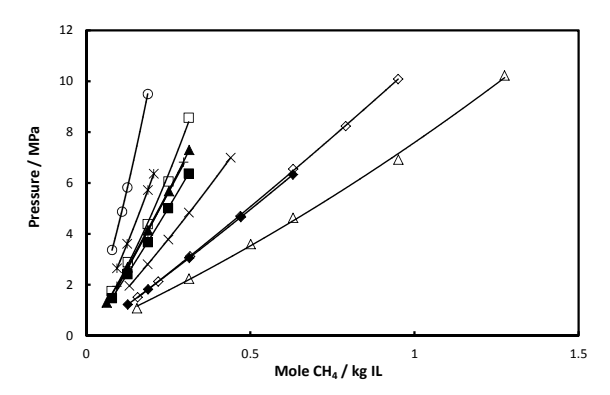


Figure 3.5: Comparison of CH<sub>4</sub> solubility on molality scale at 313.15 K in the investigated ILs: [emim][dep] (open squares), [thtdp][phos] (open triangles) [346], [thtdp][dca] (open diamonds) [346], [amim][dca] (open circles), [bmpyrr][dca] (stars), [cprop][dca] (plusses), [cprop][Tf<sub>2</sub>N] (crosses), [bmpip][Tf<sub>2</sub>N] (closed squares), [tes][Tf<sub>2</sub>N] (closed triangles) and [toa][Tf<sub>2</sub>N] (closed diamonds) [347]. The lines are polynomial fits to guide the eye.

acts with the nonpolar CH<sub>4</sub> molecule (i.e., 'like dissolve like' principle). As explained earlier, in practice not the solubility, but the selectivity is the key parameter for judging the separation performance. There are several ways to obtain the ideal selectivity,  $(S_{i/j}^{\rm I})$ , from VLE data. The first approach to calculate the selectivity is to use the liquid-phase mole fractions of the individual gases at a constant temperature and pressure:

$$S_{\text{CO}_2/\text{CH}_4}^{\text{I}} = \left(\frac{x_{\text{CO}_2}}{x_{\text{CH}_4}}\right)_{p,T} \tag{3.5}$$

The second approach is to use the the ratio of the bubble-point pressures at a constant temperature and composition:

$$S_{\text{CO}_2/\text{CH}_4}^{\text{I}} = \left(\frac{p_{\text{CH}_4}}{p_{\text{CO}_2}}\right)_{T,x} \tag{3.6}$$

The third approach is to use the ratio of the Henry constants of  $CH_4$  over that of  $CO_2$ :

$$S_{\mathrm{CO}_2/\mathrm{CH}_4}^{\mathrm{I}} = \left(\frac{H_{\mathrm{CH}_4}}{H_{\mathrm{CO}_2}}\right) \tag{3.7}$$

In principle, the ideal selectivity will be different depending on which of the above equations are used for the calculations. For convenience, we will use Equation (3.7) for all the ideal selectivity calculations, since Equation (3.5) and Equation (3.6) will require interpolations or extrapolations, because the data of  $CO_2$  and  $CH_4$  are generally not measured at the same mole fraction or pressure. The Henry constants,  $H_{12}$ , are calculated as [337]:

$$H_{12} = \lim_{x_1 \to 0} \frac{f_1^L}{x_1} \tag{3.8}$$

The fugacity of the solute '1', either  $CO_2$  or  $CH_4$ , in the solvent '2',  $f_1^L$ , is calculated using a suitable equation of state for CO<sub>2</sub> [348] and CH<sub>4</sub> [349] assuming pure CO<sub>2</sub> or CH<sub>4</sub> in the gas phase and applying the equilibrium condition  $f_1^L = f_1^V$ . The calculated Henry constants for CO<sub>2</sub> and CH<sub>4</sub> in all the ILs are listed in Table 3.3 and Table 3.4, respectively. The Henry constants (solubility) increases (decreases) with increasing temperature for both, CO<sub>2</sub> and CH<sub>4</sub>, systems. Henry contants for the systems  $CO_2$ -[emim][dep] and  $CO_2$ -[tes][Tf<sub>2</sub>N] have been reported by Palgunadi et al. [350] and Nonthanasin et al. [351], respectively. The values for Henry constants reported in Table 3.3 agree within 10% of the literature data (e.g., the Henry constant of CO<sub>2</sub> in [tes][Tf<sub>2</sub>N] reported by Nonthanasin et al. is 4.5 MPa at 313 K, which is slightly lower than the 5.0 MPa reported here). The deviation in the Henry constants is likely due to errors using Equation (3.8) as the extrapolation  $x_1 \to 0$  is performed. Information on the dissolution behavior at the molecular level can be obtained by calculating the enthalpy and entropy of absorption of the solute in the solvent. These properties are closely related to the strength of the interaction between the solute and the solvent and the degree of ordering of the solvent molecules around a solute molecule, respectively.

Table 3.3: Henry constants  $(H_{12}/\text{MPa})$  of  $\text{CO}_2$  (1) in the investigated ILs (2) obtained by plotting the fugacity versus the mole fraction and taking the limit of  $x_1 \to 0$ .

ILs	Temperature / K						
Abbreviation	303.15	313.15	323.15	333.15	343.15	353.15	363.15
[emim][dep]	6.53	7.91	9.38	10.95	12.60	14.35	16.19
$[thtdp][phos]^a$		0.71	0.86	1.08	1.37	1.73	2.16
$[thtdp][dca]^a$	3.00	3.58	4.14	4.67	5.18	5.68	6.15
[amim][dca]	8.19	10.04	11.99	14.02	16.16	18.39	20.71
[bmpyrr][dca]	6.62	7.96	9.44	11.07	12.84	14.77	16.85
[cprop][dca]	4.98	5.88	6.82	7.82	8.88	9.99	11.15
[cprop][Tf2N]	3.61	4.26	4.94	5.65	6.40	7.19	8.01
[bmpip][Tf2N]	4.19	5.01	5.88	6.81	7.79	8.83	9.92
[tes][Tf2N]	4.20	5.03	5.93	6.89	7.93	9.02	10.19
$[toa][Tf2N]^b$	1.67	2.28	2.89	3.49	4.05		

<sup>&</sup>lt;sup>a</sup> Data taken from Ramdin et al. [346].

Table 3.4: Henry constants  $(H_{12}/\text{MPa})$  of CH<sub>4</sub> (1) in the investigated ILs (2) obtained by plotting the fugacity versus the mole fraction and taking the limit of  $x_1 \to 0$ .

ILs	Temperature / K						
Abbreviation	303.15	313.15	323.15	333.15	343.15	353.15	363.15
[emim][dep]	82.02	85.79	89.26	92.42	95.26	97.77	99.96
[thtdp][phos]	9.38	9.92	10.42	10.89	11.32	11.72	12.09
[thtdp][dca]	18.02	18.95	19.83	20.66	21.42	22.12	22.76
[amim][dca]	216.3	218.94	220.97	222.4	223.23	223.46	223.1
[bmpyrr][dca]	128.36	133.25	137.65	141.55	144.95	147.82	150.18
[cprop][dca]	63.56	65.35	66.92	68.27	69.40	70.30	70.97
$[cprop][Tf_2N]$	27.87	29.03	30.12	31.13	32.07	32.94	33.73
$[bmpip][Tf_2N]$	41.77	43.93	45.94	47.80	49.50	51.04	52.42
$[\mathrm{tes}][\mathrm{Tf_2N}]$	50.22	52.34	54.33	56.20	57.94	59.55	61.03
$[toa][Tf_2N]$	15.06	15.84	16.60	17.32	18.01	18.66	19.28

<sup>&</sup>lt;sup>b</sup> Calculated from Nam and Lee. [347].

The calculation of the Gibbs energy, the enthalpy and entropy of absorption requires an appropriate correlation of the Henry constants as a function of temperature. Therefore, the temperature dependency of the Henry constant was fitted to the Benson-Krause (BK) equation [352]:

$$\ln[H_{12}/\text{MPa}] = \sum_{i=0}^{m} a_i (T/K)^{-i}$$
(3.9)

Using the BK equation, the Gibbs energy, the enthalpy and entropy of absorption of the solute in the IL can be calculated using the thermodynamic relations [157]:

$$\Delta_{\text{abs}}G^{\infty} = RT[\ln\left(H_{12}\right)] \tag{3.10}$$

$$\Delta_{\text{abs}} H^{\infty} = -T^2 \left[ \frac{\partial}{\partial T} \left( \frac{\Delta_{\text{abs}} G^{\infty}}{T} \right) \right] = -RT^2 \left[ \frac{\partial \ln (H_{12})}{\partial T} \right]$$
(3.11)

$$\Delta_{\text{abs}} S^{\infty} = \frac{\left(\Delta_{\text{abs}} H^{\infty} - \Delta_{\text{abs}} G^{\infty}\right)}{T} = -RT \left[\frac{\partial \ln\left(H_{12}\right)}{\partial T}\right] - R\ln\left(H_{12}\right) (3.12)$$

The calculated properties of CO<sub>2</sub> and CH<sub>4</sub> are listed in Table 3.5 and Table 3.6, respectively. The negative value of the enthalpy of absorption of CO<sub>2</sub> and CH<sub>4</sub> indicates that the dissolution process is exothermic and the higher values of CO<sub>2</sub> compared to CH<sub>4</sub> is consistent with the higher solubilities of CO<sub>2</sub>. However, the solubility trend of CO<sub>2</sub> observed in the ILs can not solely be explained by solute-solvent interactions. For example, the enthalpy of absorption of CO<sub>2</sub> in [amim][dca] is higher (*i.e.*, stronger interaction) than in [thtdp][phos], while the solubility of CO<sub>2</sub> is much lower in the former IL. The solubility trend can be explained by the entropic effects, which dominate the dissolution behavior of CO<sub>2</sub> in the ILs. This is completely opposite for CH<sub>4</sub>, as can be seen in Table 3.6.

Table 3.5: The Gibbs energy  $(\Delta_{abs}G)$ , the enthalpy  $(\Delta_{abs}H)$  and entropy of absorption  $(\Delta_{abs}S)$  of CO<sub>2</sub> in the ILs. The values of  $\Delta_{abs}G$ ,  $\Delta_{abs}H$  and  $\Delta_{abs}S$  are consistent with a reference state of 0.1 MPa and 313.15 K.

$CO_2 + IL$	$\Delta_{\rm abs}G/{\rm kJ~mol^{-1}}$	$\Delta_{\rm abs}H/{\rm kJ~mol^{-1}}$	$\Delta_{\rm abs} S/{ m J~mol^{-1}~K^{-1}}$
[emim][dep]	11.4	-14.7	-83.2
$[thtdp][phos]^a$	5.1	-12.5	-56.1
$[thtdp][dca]^a$	9.3	-13.1	-71.5
[amim][dca]	12.0	-15.4	-87.4
[bmpyrr][dca]	11.4	-14.4	-82.4
[cprop][dca]	10.6	-12.7	-74.5
$[cpop][Tf_2N]$	9.8	-12.7	-71.7
$[bmpip][Tf_2N]$	10.2	-13.7	-76.3
$[tes][Tf_2N]$	10.2	-14.0	-77.2
$[toa][Tf_2N]^b$	8.1	-22.3	-97.1

<sup>&</sup>lt;sup>a</sup> Calculated from Ramdin *et al.* [346].

Table 3.6: The Gibbs energy  $(\Delta_{\rm abs}G)$ , the enthalpy  $(\Delta_{\rm abs}H)$  and entropy of absorption  $(\Delta_{\rm abs}S)$  of CH<sub>4</sub> in the ILs. The values of  $\Delta_{\rm abs}G$ ,  $\Delta_{\rm abs}H$  and  $\Delta_{\rm abs}S$  are consistent with a reference state of 0.1 MPa and 313.15 K.

$\mathrm{CH_4} + \mathrm{IL}$	$\Delta_{\rm abs}G/{\rm kJ~mol^{-1}}$	$\Delta_{\rm abs}H/{\rm kJ~mol^{-1}}$	$\Delta_{\rm abs} S/{ m J~mol^{-1}~K^{-1}}$
[emim][dep]	17.6	-3.5	-67.2
[thtdp][phos]	12.0	-4.3	-51.9
[thtdp][dca]	13.7	-3.9	-56.1
[amim][dca]	20.0	-0.9	-66.8
[bmpyrr][dca]	18.7	-2.9	-69.0
[cprop][dca]	16.9	-2.1	-60.7
$[cpop][Tf_2N]$	14.8	-3.2	-57.3
$[bmpip][Tf_2N]$	15.8	-3.9	-63.0
$[tes][Tf_2N]$	16.3	-3.2	-62.3
$[toa][Tf_2N]$	13.2	-4.0	-54.8

<sup>&</sup>lt;sup>b</sup> Calculated from Nam and Lee. [347].

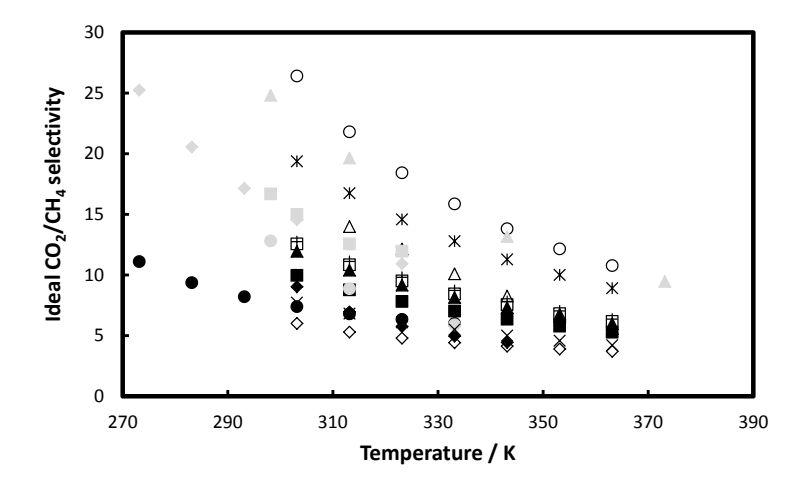


Figure 3.6: Comparison of the ideal  $CO_2/CH_4$  selectivity in the investigated ILs and in conventional solvents at 313.15 K: [emim][dep] (open squares), [thtdp][phos] (open triangles), [thtdp][dca] (open diamonds), [amim][dca] (open circles), [bmpyrr][dca] (stars), [cprop][dca] (plusses), [cprop][Tf<sub>2</sub>N] (crosses), [bmpip][Tf<sub>2</sub>N] (black squares), [tes][Tf<sub>2</sub>N] (black triangles), [toa][Tf<sub>2</sub>N] (black diamonds), Rectisol (black circles), Fluor solvent (gray squares), Sulfolane (gray triangles), Purisol (gray diamonds) and Selexol (gray circles). Data of conventional solvents taken from Refs [260, 263, 353–362].

The CH<sub>4</sub> solubility trend observed in the ILs is consistent with the enthalpy of absorption values reported in Table 3.6. The enthalpy of absorption of CH<sub>4</sub> is higher for ILs containing long nonpolar alkyl-chains, which is due to nonpolar-nonpolar interactions. This suggests that the solute-solvent interactions dominate the dissolution of CH<sub>4</sub>, while entropic effects are much more important for CO<sub>2</sub>. Subsequently, the ideal CO<sub>2</sub>/CH<sub>4</sub> selectivities are calculated using Equation (3.7) and the results are presented in Table 3.7. Interestingly, the ideal selectivity decreases rapidly with increasing temperature for all the investigated systems. However, Figure 3.6 shows that this trend is not unique for IL-systems, but also holds for conventional solvents like Selexol, Purisol, Rectisol, Fluor solvent and Sulfolane. The reason for this dramatic reduction of selectivity at higher temperatures

ILs Temperature / K Abbreviation 303.15 313.15 323.15 333.15343.15 353.15 363.15[emim][dep] 12.6 10.8 9.5 8.4 7.6 6.8 6.2 [thtdp][phos] 12.1 10.1 6.8 5.6 14.0 8.3 [thtdp][dca] 6.0 5.3 4.8 4.4 4.1 3.9 3.7 [amim][dca] 26.4 21.8 18.4 15.9 12.2 10.8 13.8 [bmpyrr][dca] 14.6 12.8 11.3 10.0 8.9 19.4 16.7[cprop][dca] 12.8 7.0 11.1 9.8 8.7 7.8 6.4  $[cprop][Tf_2N]$ 7.7 6.8 4.6 4.2 6.15.5 5.0  $[bmpip][Tf_2N]$ 10.0 8.8 7.8 7.0 6.4 5.8 5.3  $[tes][Tf_2N]$ 12.0 10.4 9.2 8.2 7.3 6.6 6.0  $[toa][Tf_2N]$ 9.0 7.0 5.8 5.0 4.4

Table 3.7: Ideal  $CO_2/CH_4$  selectivity obtained by calculating the ratio of the Henry constants of  $CH_4$  over  $CO_2$ .

is that the methane solubility is only slightly influenced by the temperature, while the effect for  $CO_2$  is much larger. The consequence of this is that the Henry constant of CH<sub>4</sub> is nearly independent of temperature, while the Henry constant of CO<sub>2</sub> increases rapidly with temperature. Nevertheless, some of the ILs (e.g., [amim][dca] and [bmpyrr][dca]) perform better in terms of ideal selectivities than most of the conventional solvents. Moreover, the ideal selectivity decreases, with some exceptions, with increasing IL molecular weight, see Table 3.8 and Figure 3.7. This suggests that a low molecular weight IL should be used if a high selectivity is desired, which is consistent with the finding of Camper et al. [120] and Scovazzo [293], since molar volumes of ILs generally increases with increasing IL molecular weight [9]. Unfortunately, the CO<sub>2</sub> solubility on mole fraction basis is not very high for low molecular weight ILs. In conclusion, there is a trade-off between solubility, which increases with IL molecular weight, and selectivity, which decreases with increasing IL molecular weight. However, the poor CO<sub>2</sub>/CH<sub>4</sub> selectivity for higher molecular weight ILs is not a surprise, since the molecular weight of the ILs is mainly increased by adding alkyl-groups. The obvious consequence of this is that the CH<sub>4</sub> solubility increases as the number or length of the nonpolar alkyl-chains increases.

Table 3.8: Effect of IL molecular weight on the ideal  ${\rm CO_2/CH_4}$  selectivity at 313.15 K.

		~	
Name IL	Molecular weight	Selectivity	Reference
(Abbreviation)	(g/mol)	$(CO_2/CH_4)$	10010101100
[emim][dep]	264.26	10.8	this work
[thtdp][phos]	773.27	14.0	this work
[thtdp][dca]	549.90	5.3	this work
[amim][dca]	189.22	21.8	this work
[bmpyrr][dca]	208.30	16.7	this work
[cprop][dca]	318.46	11.1	this work
$[cprop][Tf_2N]$	532.56	6.8	this work
$[bmpip][Tf_2N]$	436.43	8.8	this work
$[\text{tes}][\text{Tf}_2N]$	399.39	10.4	this work
$[toa][Tf_2N]$	648.85	7.0	this work
$[hmpy][Tf_2N]$	458.43	10.8	[150]
$[\mathrm{thtdp}][\mathrm{Tf_2N}]$	764.00	6.2	[153]
$[bmim][Tf_2N]$	419.36	18.5	[153]
$[hmim][Tf_2N]$	447.42	8.1	[122, 123, 153]
[emim][dca]	177.21	21.0	[122, 123]
$[emim][CF_3SO_3]$	260.23	17.3	[122, 123]
$[emim][Tf_2N]$	391.31	11.2	[122, 123]
$[mmim][MeSO_4]$	208.24	17.6	[122, 123]
$[emim][BF_4]$	197.97	20.0	[122, 123]
$[bmim][BF_4]$	226.02	14.9	[157]
$[bmim][PF_6]$	284.18	12.2	[157]
$[bmim][MeSO_4]$	250.32	14.1	[363]
[emim][FAP]	556.17	9.7	[364]

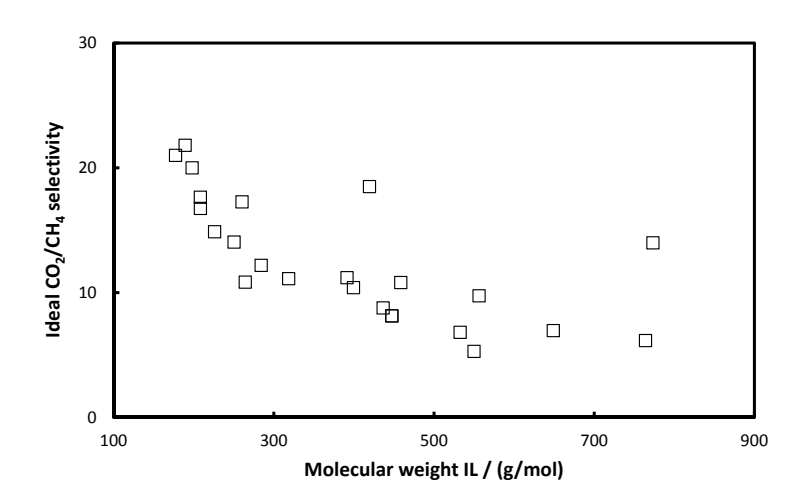


Figure 3.7: Effect of IL molecular weight on the ideal CO<sub>2</sub>/CH<sub>4</sub> selectivity at 313.15 K

So far we have considered the ideal CO<sub>2</sub>/CH<sub>4</sub> selectivities, but in the real natural gas sweetening process, which operates at high pressures, nonidealities are likely to occur. Consequently, the real selectivities will probably differ from the ideal selectivities. Since measurements of mixed-gas solubilities are more difficult, almost no CO<sub>2</sub>-CH<sub>4</sub>-IL mixture data can be found in the literature. Hert et al. [168] reported the solubility of the binary gas mixture CO<sub>2</sub>-CH<sub>4</sub> in the IL [hmim][Tf<sub>2</sub>N] and concluded that the solubility of the sparingly soluble CH<sub>4</sub> is enhanced in the presence of CO<sub>2</sub>. This indicates that in a real process, which typically contains many gaseous components in the feed, interaction and competition between different solutes may influence the dissolution process. In the following chapter, we will provide solubility data and a thorough discussion of CO<sub>2</sub>-CH<sub>4</sub> mixtures in several ILs. We will also show that the data reported by Hert et al. is most likely wrong, which accentuates the difficulty of measuring mixed-gas solubilities.

3.5 Conclusions 93

#### 3.5 Conclusions

The solubility of CO<sub>2</sub> and CH<sub>4</sub> has been measured in the following ionic liquids: [emim][dep], [thtdp][phos], [thtdp][dca], [amim][dca], [bmpyrr][dca], [cprop][dca], [cprop][Tf<sub>2</sub>N], [bmpip][Tf<sub>2</sub>N], [tes][Tf<sub>2</sub>N] and [toa][Tf<sub>2</sub>N]. The solubility data has been reduced by calculating the Henry constants of CO<sub>2</sub> and CH<sub>4</sub> in all the ILs, from which the ideal CO<sub>2</sub>/CH<sub>4</sub> selectivities are obtained. The ideal CO<sub>2</sub>/CH<sub>4</sub> selectivities of the investigated ILs are in the range of the conventional solvents like Selexol, Purisol, Rectisol, Fluor solvent, and Sulfolane. The ideal CO<sub>2</sub>/CH<sub>4</sub> selectivity decreases with increasing temperature and increasing IL molecular weight. Therefore, a low molecular weight IL should be used if a high selectivity is desired. Furthermore, the experimental data has been modeled accurately with the Peng-Robinson equation of state in combination with van der Waals mixingrules.

# Chapter 4

# CO<sub>2</sub>/CH<sub>4</sub> Solubility in Ionic Liquids: Real Selectivity

This chapter is based on the paper: M. Ramdin, A. Amplianitis, T. W. de Loos and T. J. H. Vlugt. Solubility of  $CO_2/CH_4$  gas mixtures in ionic liquids. Fluid Phase Equilib., 375 (2014) 134-142.

#### 4.1 Introduction

As explained in Chapter 3, natural gas is usually contaminated with several impurities like the acid gases carbon dioxide (CO<sub>2</sub>) and hydrogen sulfide (H<sub>2</sub>S), which should be removed at the well to avoid technological problems during transportation and liquefaction of the gas [11]. In Chapter 3, we focused on the application potential of ionic liquids for CO<sub>2</sub> removal from natural gas [345]. Ideal CO<sub>2</sub>/CH<sub>4</sub> selectivities, defined as the ratio of the Henry constant of CH<sub>4</sub> over that of CO<sub>2</sub>, were calculated for 10 different ILs using pure component solubility data. In practice, the real CO<sub>2</sub>/CH<sub>4</sub> selectivity (i.e., the selectivity of CO<sub>2</sub> in the presence of CH<sub>4</sub> in the ternary mixture CO<sub>2</sub>-CH<sub>4</sub>-IL) may differ from the ideal selectivity due to solute-solute interactions as both gases are simultaneously being dissolved in the IL.

The evaluation of real selectivities requires mixed-gas solubility data, which are extremely scarce in the literature [345]. Hert et al. [168] investigated the ternary system CO<sub>2</sub>+CH<sub>4</sub>+[hmim][Tf<sub>2</sub>N] and they reported a substantial enhancement of CH<sub>4</sub> solubility in the presence of CO<sub>2</sub> compared to the binary system at the same conditions. In this case, it is obvious that the ideal CO<sub>2</sub>/CH<sub>4</sub> selectivity will differ from the real selectivity. Petermann et al. [365] studied the system CO<sub>2</sub>-CH<sub>4</sub>-[emim][EtSO<sub>4</sub>] and their experimental data show a slight enhancement (deterioration) of the CH<sub>4</sub> (CO<sub>2</sub>) solubility relative to the pure component solubilities. These two studies are to the best of our knowledge the only literature dealing with the ternary CO<sub>2</sub>-CH<sub>4</sub>-IL system.

The aim of the present study is to investigate the effect of the presence of one gas  $(CO_2)$  on the other  $(CH_4)$  as both are simultaneously being dissolved in a single IL. More specifically, the solubility of gas-mixtures containing carbon dioxide (CO<sub>2</sub>) and methane (CH<sub>4</sub>) has been measured in the following ILs: 1-butyl-3-methylimidazolium bis(trifluoromethylsulfonyl)imide [bmim][Tf<sub>2</sub>N], 1-ethyl-3-methylimidazolium diethylphosphate [emim][dep], trihexyltetradecylphosphonium dicyanamide [thtdp][dca], and trihexyltetradecylphosphonium bis(2,4,4-trimethylpentyl)phosphinate [thtdp][phos]. The ILs were selected based either on their relatively low price ([emim][dep]), good CO<sub>2</sub> solubility ([thtdp][dca] and [thtdp][phos]) or as a reference ([bmim]- $[Tf_2N]$ ). The experiments involve bubble-point measurements in the temperature range 303.15 - 363.15 K and at pressures up to 14 MPa using a visual synthetic method. The effect of gas composition on the bubble-point pressure has been studied systematically by using three different gas-mixtures with a composition of 25 mole % CO<sub>2</sub> - 75 mole % CH<sub>4</sub>, 50 mole % CO<sub>2</sub> - 50 mole % CH<sub>4</sub> and 75 mole % CO<sub>2</sub> - 25 mole % CH<sub>4</sub>. Real CO<sub>2</sub>/CH<sub>4</sub> selectivities (i.e., the selectivity of CO<sub>2</sub> in the presence of CH<sub>4</sub>) were calculated using the Peng-Robinson equation of state in combination with van der Waals mixing rules. A comparison between ideal and real CO<sub>2</sub>/CH<sub>4</sub> selectivities in the investigated ILs are presented. The results show that the real selectivity does not differ significantly from the ideal selectivity (i.e., the ratio of the pure gas Henry constants) regardless of the gas phase composition.

4.2 Experiments 97

#### 4.2 Experiments

Three different gas cylinders containing CO<sub>2</sub>-CH<sub>4</sub> mixtures with a fixed composition (in mole % CO<sub>2</sub>-mole % CH<sub>4</sub>) of  $25.1 \pm 0.5$ - $74.9 \pm 0.5$ , 50.2 $\pm 1.0-49.8 \pm 1.0$  and  $74.7 \pm 0.5-25.3 \pm 0.5$ , henceforth referred as 25-75, 50-50 and 75-25 mixtures, were purchased from the Linde Group. The ILs 1-butyl-3-methylimidazolium bis(trifluoromethylsulfonyl)imide, 1-ethyl-3-methylimidazolium diethylphosphate, trihexyltetradecylphosphonium dicyanamide, and trihexyltetradecylphosphonium bis(2,4,4-trimethylpentyl)phosphinate were purchased from Sigma-Aldrich. The gas-mixtures were used as received, while the ILs were dried for several days in vacuo at 80 °C. After drying, the water content of the ILs was measured using a Karl-Fischer titrator and the results are provided in Table 3.1. The same experimental procedure, as outlined in Chapter 3, was used to measure bubble-point pressures of CO<sub>2</sub>-CH<sub>4</sub> mixtures in ILs. A detailed explanation of the Cailletet method can be found elsewhere [338]. The exact amount of gas used in the experiments was calculated through the virial equation of state, where the second virial cross-coefficients required for the CO<sub>2</sub>-CH<sub>4</sub> mixtures were obtained by the Tsonopoulos method [366]. The binary interaction parameter,  $k_{ij}$ , was obtained by fitting the calculated virial cross-coefficients to the experimental data of Mallu et al. [367]. It is important to note that the Cailletet apparatus operates according to the visual synthetic method and that sampling of the phases is not possible.

We recall that the aim of the present work is to investigate the effect of the presence of one gas (e.g., CO<sub>2</sub>) on the solubility of the other gas (e.g., CH<sub>4</sub>) when both are simultaneously being dissolved in a single IL. In other words, the objective is to obtain real CO<sub>2</sub>/CH<sub>4</sub> selectivities from the VLE data. This is a very challenging task without sampling the composition of the phases, since a synthetic method was used. Therefore, the VLE experiments have to be designed systematically and the adopted approach is illustrated in Figure 4.1. The ternary diagram is only shown for the CO<sub>2</sub>-CH<sub>4</sub>-[thtdp][dca] system, but similar diagrams can be constructed for the other three systems. Note that the diagram is drawn for bubble-point conditions, hence the liquid-phase composition of all the components is known.

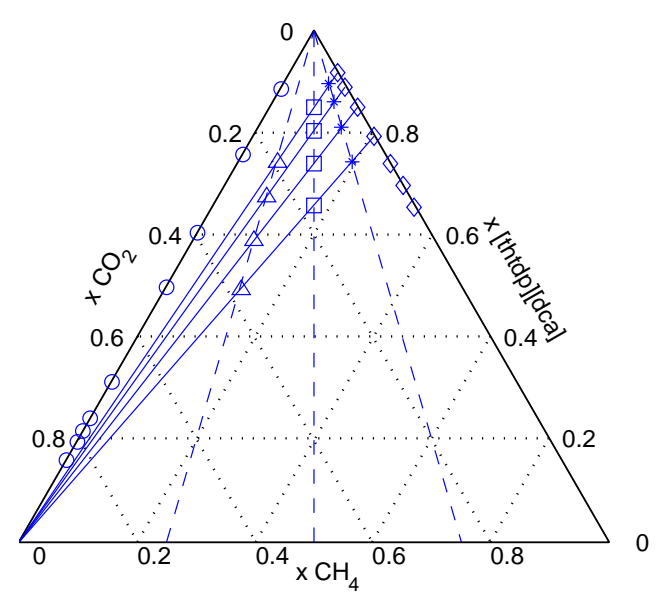


Figure 4.1: Experimental design of the ternary system  $CO_2 + CH_4 + [thtdp][dca]$ . Binary data are located on the edges of the triangle:  $CO_2 + [thtdp][dca]$  (circles) and  $CH_4 + [thtdp][dca]$  (diamonds). Ternary mixture prepared with ( $CO_2$ - $CH_4$ ) gas mixture: 25-75 (triangles), 50-50 (squares) and 75-25 (stars). Solid lines are lines of constant  $CH_4/IL$  ratio and dashed lines are lines of constant  $CO_2/CH_4$  ratio.

The points on the edges of the triangular diagram correspond to the data of the binary systems  $\rm CO_2+IL$  (circles) and  $\rm CH_4+IL$  (diamonds). The ternary mixtures containing  $\rm CO_2$ ,  $\rm CH_4$  and  $\rm IL$  were prepared using three different (i.e., 25-75, 50-50 and 75-25) gas mixtures. Consequently, the prepared mixtures will always lie on a line of constant  $\rm CO_2/CH_4$  ratio (dashed lines). Furthermore, the molar ratio of  $\rm CH_4/IL$  in the ternary mixtures are kept the same as the molar  $\rm CH_4/IL$  ratio in the corresponding binary mixtures (solid lines). This implies that the ternary mixture in fact resemble a pseudo-binary system. So, all the prepared ternary mixtures (triangles, squares and stars) will coincide with the point of intersection of two lines, one of constant  $\rm CH_4/IL$  ratio and the other of constant  $\rm CO_2/CH_4$  ratio.

The importance of this approach will become apparent while elucidating the results.

## 4.3 Thermodynamic Modeling

The experimental data has been modeled using the Peng-Robinson (PR) equation of state (EoS) [340]. The details of the PR EoS have been outlined in the previous chapter. As mentioned before, the critical parameters of ILs are not experimentally available, because most of the ILs start to decompose before attaining the critical point. Therefore, group-contribution methods [341], molecular simulations [206, 342] or suitable correlations [208] have been devised to overcome this problem. The absence of measurable critical properties of ILs makes the application of PR EoS for IL systems vulnerable, but it has successfully been applied by many authors using estimated properties [118, 368]. In this work, the modified Lydersen-Joback-Reid group-contribution method developed by Valderrama et al. [341] is applied to obtain the critical properties of the ILs. The critical parameters and acentric factors used in the modeling are listed in Table 3.2. Subsequently, the PR EoS is applied to predict bubble-point pressures of the binary gas mixture in the ternary system using temperature dependent binary interaction parameters listed in Table 4.1. The binary interaction parameters of the gas-IL systems have been fitted to binary VLE data from our previous work [345]. Thus for each gas-IL (CO<sub>2</sub>-IL and CH<sub>4</sub>-IL) system two binary interaction parameters  $(k_{ij}=k_{ji} \text{ and } l_{ij}=l_{ji})$  were fitted to binary VLE ( $CO_2$ -IL and  $CH_4$ -IL) data. A total of five (two for each gas-IL pair and one for the CO<sub>2</sub>-CH<sub>4</sub> system) binary interaction parameters were used to predict the bubble-point pressure of the ternary system. The binary interaction parameter  $(k_{ij})$  for the  $CO_2/CH_4$  system is according to Kordas et al. [369] temperature independent for the studied temperature range. Note that the  $l_{ij}$  parameter for the  $CO_2/CH_4$  interaction was set to zero. The ternary CO<sub>2</sub>-CH<sub>4</sub>-[thtdp][phos] system is not modeled, because the Valderrama-method yields an unrealistic (i.e., negative) value for the acentric factor of [thtdp][phos]. Recently, Valderrama et al. [372] have extended

Pair	Interaction parameter
$CO_2$ - $CH_4$ <sup>a</sup>	$k_{ij} = 0.1$
${\rm CO_2\text{-}[bmim][Tf_2N]}^b$	$k_{ij} = -5.0833 \times 10^{-6} (T/K)^2 + 2.9980 \times 10^{-3} (T/K) - 0.4967$ $l_{ij} = 1.3297 \times 10^{-5} (T/K)^2 - 9.5584 \times 10^{-3} (T/K) + 2.0321$
$\text{CO}_2$ -[emim][dep] $^c$	$k_{ij} = -1.9642 \times 10^{-6} (T/K)^2 + 1.9598 \times 10^{-3} (T/K) - 0.3809$ $l_{ij} = 2.6595 \times 10^{-5} (T/K)^2 - 1.9986 \times 10^{-2} (T/K) + 3.9723$
${\rm CO_2\text{-}[thtdp][dca]^{\it c}}$	$k_{ij} = -1.9404 \times 10^{-6} (T/K)^2 + 6.8258 \times 10^{-4} (T/K) - 0.0597$ $l_{ij} = -1.9357 \times 10^{-5} (T/K)^2 + 1.1749 \times 10^{-2} (T/K) - 1.0569$
$\mathrm{CH_{4} ext{-}[bmim][Tf_{2}N]}^{b}$	$k_{ij} = -2.8452 \times 10^{-6} (T/\text{K})^2 + 1.3568 \times 10^{-3} (T/\text{K}) - 0.0704$ $l_{ij} = 1.5404 \times 10^{-5} (T/\text{K})^2 - 9.1784 \times 10^{-3} (T/\text{K}) + 1.2921$
$ ext{CH}_4 ext{-}[ ext{emim}][ ext{dep}]^c$	$k_{ij} = 3.2619 \times 10^{-6} (T/K)^2 - 1.4419 \times 10^{-3} (T/K) + 0.3826$ $l_{ij} = -9.5619 \times 10^{-5} (T/K)^2 + 6.4610 \times 10^{-2} (T/K) - 10.9227$
$CH_4$ -[thtdp][dca] <sup>c</sup> a From Kordas et al.	$k_{ij} = -6.4524 \times 10^{-6} (T/K)^2 + 3.7542 \times 10^{-3} (T/K) - 0.4708$ $l_{ij} = 2.3035 \times 10^{-5} (T/K)^2 - 1.5637 \times 10^{-2} (T/K) + 2.9260$ [369]. <sup>b</sup> Fitted to VLE data Baeissi <i>et al.</i> [370, 371].

Table 4.1: Binary interaction parameters used in the PR EoS modeling.

their group contribution method to correctly predict the critical properties of ILs with a high molecular weight.

#### 4.4 Results and Discussion

The experimental data of the systems  $CO_2 + CH_4 + [bmim][Tf_2N]$ ,  $CO_2 + CH_4 + [emim][dep]$ ,  $CO_2 + CH_4 + [thtdp][dca]$  and  $CO_2 + CH_4 + [thtdp][phos]$  are listed in Tables 4.2 to 4.5, respectively. The bubble-point isopleths of the ternary systems are shown in Figures 4.2 to 4.13. Note that for every gas mixture (i.e., 25-75, or 50-50 or 75-25) at least three ternary mixtures with a constant  $CH_4/IL$  ratio have been investigated. The solubility behavior of the binary gas mixture in the ILs is not much different from the behavior of the single gas solubilities. For a fixed composition, the

<sup>&</sup>lt;sup>a</sup> From Kordas et al. [369]. <sup>b</sup> Fitted to VLE data Raeissi et al. [370, 371].

<sup>&</sup>lt;sup>c</sup> Fitted to VLE data Ramdin et al. [345, 346].

Table 4.2: Bubble point data of the system  $CO_2$  (1) +  $CH_4$  (2) +  $[bmim][Tf_2N]$  (3), where  $x_1$  is the mole fraction of  $CO_2$ ,  $x_2$  is the mole fraction of  $CH_4$ , p the bubble-point pressure, T the temperature and u(i) the standard uncertainties.

$x_1$	$x_2$	T / K	p / MPa	$x_1$	$x_2$	T / K	p / MPa	$x_1$	$x_2$	T / K	p / MPa	
	25-75 mixture											
0.014	$0.040^{b}$	303.25	1.872	0.037	$0.110^{c}$	303.43	6.045	0.053	$0.158^{d}$	303.23	10.053	
0.014	0.040	313.22	1.972	0.037	0.110	313.43	6.326	0.053	0.158	313.25	10.468	
0.014	0.040	323.19	2.062	0.037	0.110	323.40	6.606	0.053	0.158	323.19	10.854	
0.014	0.040	333.19	2.147	0.037	0.110	333.19	6.846	0.053	0.158	333.21	11.199	
0.014	0.040	343.19	2.227	0.037	0.110	343.38	7.086	0.053	0.158	343.19	11.544	
0.014	0.040	353.25	2.292	0.037	0.110	353.32	7.316	0.053	0.158	353.20	11.835	
0.014	0.040	363.22	2.362	0.037	0.110	363.34	7.517	0.053	0.158	363.30	12.105	
					50-50	) mixture						
0.040	$0.039^{b}$	303.25	1.981	0.103	$0.102^{c}$	303.53	6.230	0.144	$0.143^{d}$	303.19	10.349	
0.040	0.039	313.20	2.086	0.103	0.102	313.41	6.570	0.144	0.143	313.17	10.915	
0.040	0.039	323.18	2.191	0.103	0.102	323.32	6.881	0.144	0.143	323.18	11.430	
0.040	0.039	333.18	2.306	0.103	0.102	333.33	7.231	0.144	0.143	333.19	11.946	
0.040	0.039	343.20	2.407	0.103	0.102	343.30	7.551	0.144	0.143	343.20	12.406	
0.040	0.039	353.22	2.512	0.103	0.102	353.29	7.831	0.144	0.143	353.19	12.866	
0.040	0.039	363.20	2.602	0.103	0.102	363.19	8.112					
					75-25	i mixture						
0.108	$0.037^{b}$	303.21	2.237	0.189	$0.064^{e}$	303.25	4.500	0.252	$0.085^{d}$	303.26	6.860	
0.108	0.037	313.22	2.407	0.189	0.064	313.20	4.856	0.252	0.085	313.20	7.401	
0.108	0.037	323.21	2.582	0.189	0.064	333.22	5.581	0.252	0.085	323.23	7.942	
0.108	0.037	333.24	2.758	0.189	0.064	323.26	5.221	0.252	0.085	333.24	8.527	
0.108	0.037	343.21	2.933	0.189	0.064	343.22	5.941	0.252	0.085	343.20	9.067	
0.108	0.037	353.23	3.108	0.189	0.064	353.22	6.307	0.252	0.085	353.26	9.612	
0.108	0.037	363.27	3.288	0.189	0.064	363.27	6.672	0.252	0.085	363.28	10.147	

 $u(x_i) = 0.004, u(T) = 0.01 \text{ K} \text{ and } u(p) = 0.005 \text{ MPa}$ 

solubility increases with pressure and decreases with increasing temperature. Figures 4.2 to 4.10 also show the PR EoS modeling results using only binary interaction parameters. The predicted bubble-point pressures are in good agreement with the experiments for low pressures (< 50 bar) and low CH<sub>4</sub>/IL ratios. As the CH<sub>4</sub>/IL ratio and the pressure increases the PR EoS modeling results start to deviate from the experimental data, which is likely due to three-body interactions in the ILs. The three-body interactions are more likely to occur at higher gas concentrations (i.e., higher CH<sub>4</sub>/IL ratios) and at higher pressures. The modeling results for the CO<sub>2</sub>-CH<sub>4</sub>-[emim][dep] system are in good agreement with the experimental data for all the investigated CH<sub>4</sub>/IL ratios, but this is mainly due to the relatively low molar

 $<sup>^{</sup>b}(x_{2}/x_{3}) = 0.043, \ ^{c}(x_{2}/x_{3}) = 0.129, \ ^{d}(x_{2}/x_{3}) = 0.201, \ ^{e}(x_{2}/x_{3}) = 0.086$ 

Table 4.3: Bubble point data of the system  $CO_2$  (1) +  $CH_4$  (2) + [emim][dep] (3), where  $x_1$  is the mole fraction of  $CO_2$ ,  $x_2$  is the mole fraction of  $CH_4$ , p the bubble-point pressure, T the temperature and u(i) the standard uncertainties.

$\overline{x_1}$	$x_2$	T / K	p / MPa	$x_1$	$x_2$	T / K	p / MPa	$x_1$	$x_2$	T / K	p / MPa
25-75 mixture											
0.007	$0.020^{b}$	303.42	1.733	0.011	$0.032^{c}$	303.40	2.892	0.016	$0.046^{d}$	303.43	4.455
0.007	0.020	313.38	1.813	0.011	0.032	313.38	3.042	0.016	0.046	313.41	4.620
0.007	0.020	323.34	1.893	0.011	0.032	323.42	3.142	0.016	0.046	323.40	4.795
0.007	0.020	333.35	1.964	0.011	0.032	333.38	3.263	0.016	0.046	333.43	4.975
0.007	0.020	343.32	2.034	0.011	0.032	343.36	3.363	0.016	0.046	343.50	5.130
0.007	0.020	353.31	2.084	0.011	0.032	353.37	3.463	0.016	0.046	353.53	5.280
0.007	0.020	363.32	2.144	0.011	0.032	363.35	3.563	0.016	0.046	363.53	5.415
					50-50	) mixture					
0.020	$0.020^{b}$	303.25	1.793	0.032	$0.031^{c}$	303.20	2.997	0.045	$0.045^{d}$	303.43	4.554
0.020	0.020	313.18	1.903	0.032	0.031	313.20	3.152	0.045	0.045	313.39	4.785
0.020	0.020	323.17	2.003	0.032	0.031	323.18	3.312	0.045	0.045	323.37	5.055
0.020	0.020	333.16	2.094	0.032	0.031	333.18	3.468	0.045	0.045	333.37	5.266
0.020	0.020	343.19	2.169	0.032	0.031	343.24	3.608	0.045	0.045	343.35	5.486
0.020	0.020	353.21	2.249	0.032	0.031	353.21	3.743	0.045	0.045	353.30	5.686
0.020	0.020	363.22	2.329	0.032	0.031	363.25	3.878	0.045	0.045	363.34	5.886
					75-25	i mixture					
0.056	$0.019^{b}$	303.44	2.024	0.087	$0.030^{c}$	303.40	3.358	0.122	$0.041^{d}$	303.20	5.164
0.056	0.019	313.44	2.194	0.087	0.030	313.40	3.623	0.122	0.041	313.21	5.539
0.056	0.019	323.35	2.355	0.087	0.030	323.37	3.893	0.122	0.041	323.21	5.980
0.056	0.019	333.45	2.515	0.087	0.030	333.38	4.159	0.122	0.041	333.23	6.395
0.056	0.019	343.43	2.675	0.087	0.030	353.35	4.699	0.122	0.041	343.25	6.820
0.056	0.019	353.40	2.835	0.087	0.030	343.36	4.424	0.122	0.041	353.20	7.246
				0.087	0.030	363.36	4.964				

 $<sup>^{</sup>a}u(x_{i}) = 0.004, u(T) = 0.01 \text{ K} \text{ and } u(p) = 0.005 \text{ MPa}$ 

fraction of the dissolved gases. Moreover, the deviation between the modeling and the experiments increases for increasing  $\rm CO_2$  concentrations in the gas phase (e.g., 75-25 mixture) at a fixed  $\rm CH_4/IL$  ratio. At these conditions the predicted bubble-point pressures are higher than the experimental data, which suggests that  $\rm CO_2$  is lowering the pressure required for dissolving a fixed amount of  $\rm CH_4$ . The three-body interactions between  $\rm CO_2$ ,  $\rm CH_4$  and  $\rm IL$  are not accounted for in the modeling, which leads to an overestimation of the bubble-point pressures. Note that the 25-75 mixture, which is mostly relevant for the natural gas sweetening process (e.g., natural gas typically contains up to 10%  $\rm CO_2$ ), is adequately modeled by the PR EoS even at high pressures and high  $\rm CH_4/IL$  ratios.

 $<sup>^{</sup>b}(x_{2}/x_{3}) = 0.020, \ ^{c}(x_{2}/x_{3}) = 0.033, \ ^{d}(x_{2}/x_{3}) = 0.049$ 

Table 4.4: Bubble point data of the system  $CO_2$  (1) +  $CH_4$  (2) + [thtdp][dca] (3), where  $x_1$  is the mole fraction of  $CO_2$ ,  $x_2$  is the mole fraction of  $CH_4$ , p the bubble-point pressure, T the temperature and u(i) the standard uncertainties.

	$x_2$	T / K	p / MPa	$x_1$	$x_2$	T / K	p / MPa			
25-75 mixture										
0.026	$0.077^{b}$	302.16	1.517	0.035	$0.104^{c}$	303.23	2.198			
0.026	0.077	312.26	1.602	0.035	0.104	313.23	2.313			
0.026	0.077	322.49	1.682	0.035	0.104	323.27	2.439			
0.026	0.077	332.48	1.767	0.035	0.104	333.24	2.533			
0.026	0.077	342.26	1.842	0.035	0.104	343.27	2.628			
0.026	0.077	352.36	1.903	0.035	0.104	353.58	2.728			
0.026	0.077	362.52	1.972	0.035	0.104	363.40	2.818			
0.047	$0.141^{d}$	303.39	3.139	0.064	$0.192^{e}$	303.60	4.731			
0.047	0.141	312.63	3.302	0.064	0.192	313.95	4.996			
0.047	0.141	322.73	3.488	0.064	0.192	323.19	5.211			
0.047	0.141	332.58	3.643	0.064	0.192	333.18	5.421			
0.047	0.141	342.67	3.803	0.064	0.192	343.24	5.636			
0.047	0.141	352.74	3.918							
0.047	0.141	362.69	4.034							
			50-50 1	mixture						
0.074	$0.073^{b}$	302.52	1.670	0.098	$0.097^{c}$	302.86	2.397			
0.074	0.073	312.86	1.785	0.098	0.097	312.37	2.567			
0.074	0.073	322.45	1.886	0.098	0.097	322.40	2.728			
0.074	0.073	332.45	2.001	0.098	0.097	332.47	2.878			
0.074	0.073	342.54	2.111	0.098	0.097	342.44	3.023			
0.074	0.073	352.49	2.211	0.098	0.097	352.55	3.163			
0.074	0.073	362.55	2.311	0.098	0.097	362.45	3.293			
0.130	$0.129^{d}$	303.26	3.463	0.172	$0.170^{e}$	322.39	5.824			
0.130	0.129	313.25	3.698	0.172	0.170	332.45	6.154			
0.130	0.129	323.24	3.934	0.172	0.170	342.46	6.464			
0.130	0.129	333.22	4.139	0.172	0.170	352.51	6.770			
0.130	0.129	343.28	4.354	0.172	0.170	362.50	7.050			
			75-25 1	mixture						
0.190	$0.064^{b}$	303.63	2.174	0.241	$0.082^{c}$	303.21	3.029			
0.190	0.064	312.58	2.354	0.241	0.082	313.16	3.299			
0.190	0.064	322.58	2.573	0.241	0.082	323.13	3.585			
0.190	0.064	332.59	2.769	0.241	0.082	333.23	3.860			
0.190	0.064	342.58	2.960	0.241	0.082	343.20	4.145			
0.190	0.064	352.61	3.145	0.241	0.082	353.40	4.420			
0.190	0.064	362.74	3.325	0.241	0.082	363.53	4.685			
0.304	$0.103^{d}$	302.57	4.309	0.377	$0.128^{e}$	302.57	6.402			
0.304	0.103	312.44	4.709	0.377	0.128	312.44	7.007			
0.304	0.103	322.56	5.139	0.377	0.128	322.56	7.662			
0.304	0.103	332.55	5.530	0.377	0.128	332.55	8.283			
0.304	0.103	342.56	5.925	0.377	0.128	342.56	8.893			
0.304	0.103	352.60	6.330	0.377	0.128	352.60	9.483			
0.304	0.103	362.67	6.715	0.377	0.128	362.67	10.064			

 $<sup>^{</sup>a}u(x_{i}) = 0.004, u(T) = 0.01 \text{ K} \text{ and } u(p) = 0.005 \text{ MPa}$ 

 $b(x_2/x_3) = 0.086, c(x_2/x_3) = 0.121, d(x_2/x_3) = 0.174, e(x_2/x_3) = 0.258$ 

Table 4.5: Bubble point data of the system  $CO_2$  (1) +  $CH_4$  (2) + [thtdp][phos] (3), where  $x_1$  is the mole fraction of  $CO_2$ ,  $x_2$  is the mole fraction of  $CH_4$ , p the bubble-point pressure, T the temperature and u(i) the standard uncertainties.

	m-	T / K	p / MPa	œ.	<i>m</i> -	T / K	p / MPa
$\underline{}$	$x_2$	1 / K		$\frac{x_1}{\text{mixture}}$	$x_2$	1 / K	p / MPa
0.035	$0.103^{b}$	302.44	1.051	0.061	$0.183^{c}$	304.01	2.176
0.035	0.103	312.63	1.113	0.061	0.183	312.58	2.176
						322.64	2.200
0.035	0.103	322.63	1.176	0.061	0.183		
0.035	0.103	332.66	1.237	0.061	0.183	332.61	2.527
0.035	0.103	342.64	1.297	0.061	0.183	342.62	2.647
0.035	0.103	352.75	1.362	0.061	0.183	352.70	2.777
0.035	0.103	362.81	1.414	0.061	0.183	362.72	2.897
0.086	$0.255^{d}$	303.29	3.483	0.099	$0.295^{e}$	303.16	4.427
0.086	0.255	313.18	3.698	0.099	0.295	313.17	4.688
0.086	0.255	323.21	3.923	0.099	0.295	323.23	4.999
0.086	0.255	333.22	4.103	0.099	0.295	333.28	5.259
0.086	0.255	343.20	4.298	0.099	0.295	343.30	5.463
0.086	0.255	353.19	4.483	0.099	0.295	353.16	5.703
0.086	0.255	363.29	4.678	0.099	0.295	363.26	5.944
			50-50	mixture			
0.097	$0.096^{b}$	303.25	1.083	0.164	$0.163^{c}$	303.27	2.357
0.097	0.096	313.25	1.158	0.164	0.163	313.37	2.503
0.097	0.096	323.23	1.242	0.164	0.163	322.23	2.678
0.097	0.096	333.20	1.322	0.164	0.163	332.24	2.843
0.097	0.096	343.15	1.412	0.164	0.163	342.60	3.048
0.097	0.096	353.23	1.508	0.164	0.163	352.70	3.224
0.097	0.096	363.12	1.608	0.164	0.163	362.76	3.409
0.220	$0.218^{d}$	303.26	3.914	0.248	$0.246^{e}$	303.252	4.921
0.220	0.218	313.25	4.159	0.248	0.246	313.236	5.261
0.220	0.218	323.24	4.424	0.248	0.246	323.233	5.606
0.220	0.218	333.22	4.669	0.248	0.246	333.259	5.912
0.220	0.218	343.28	4.915	0.248	0.246	343.344	6.228
0.220	0.218	353.32	5.184	0.248	0.246	353.309	6.583
0.220	0.218	363.29	5.474	0.248	0.246	363.259	6.943
				mixture			
0.240	$0.081^{b}$	303.19	1.492	0.365	$0.124^{c}$	303.32	3.278
0.240	0.081	313.08	1.632	0.365	0.124	313.19	3.583
0.240	0.081	323.31	1.777	0.365	0.124	323.26	3.948
0.240	0.081	332.52	1.917	0.365	0.124	333.19	4.203
0.240	0.081	342.08	2.074	0.365	0.124	343.17	4.563
0.240	0.081	351.97	2.239	0.365	0.124	353.15	4.854
0.240	0.081	362.74	2.443	0.365	0.124	363.16	5.194
0.240 $0.452$	0.081 $0.153^d$	303.31	5.305	0.505	0.124	505.10	0.194
0.452 $0.452$	0.153	312.54	5.780				
0.452 $0.452$	0.153	322.81	6.370				
0.452	0.153	332.57	6.831				
0.452	0.153	342.71	7.396				
0.452	0.153	352.86	7.886				
0.452	0.153	362.97	8.442		0.005.3.61		

 $u(x_i) = 0.004, u(T) = 0.01 \text{ K} \text{ and } u(p) = 0.005 \text{ MPa}$ 

 $b(x_2/x_3) = 0.120, c(x_2/x_3) = 0.242, d(x_2/x_3) = 0.387, e(x_2/x_3) = 0.488$ 

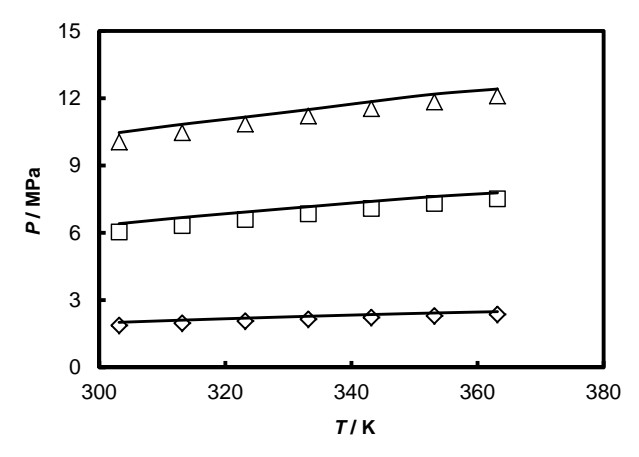


Figure 4.2: Bubble-point isopleths of the system  $CO_2$ - $CH_4$ -[bmim][Tf<sub>2</sub>N] for different  $CH_4$ /IL molar ratios: 0.043 (diamonds), 0.129 (squares) and 0.201 (triangles). Ternary mixtures prepared using the 25-75  $CO_2$ - $CH_4$  gas mixture. The lines are PR EoS modeling results.

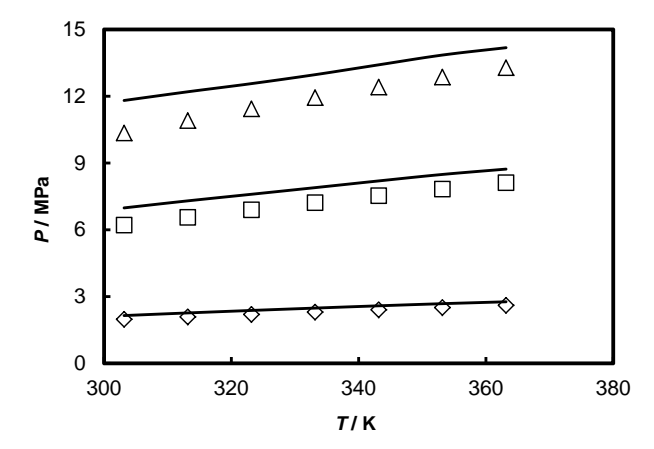


Figure 4.3: Bubble-point isopleths of the system  $CO_2$ -CH<sub>4</sub>-[bmim][Tf<sub>2</sub>N] for different CH<sub>4</sub>/IL molar ratios: 0.043 (diamonds), 0.129 (squares) and 0.201 (triangles). Ternary mixtures prepared using the 50-50  $CO_2$ -CH<sub>4</sub> gas mixture. The lines are PR EoS modeling results.

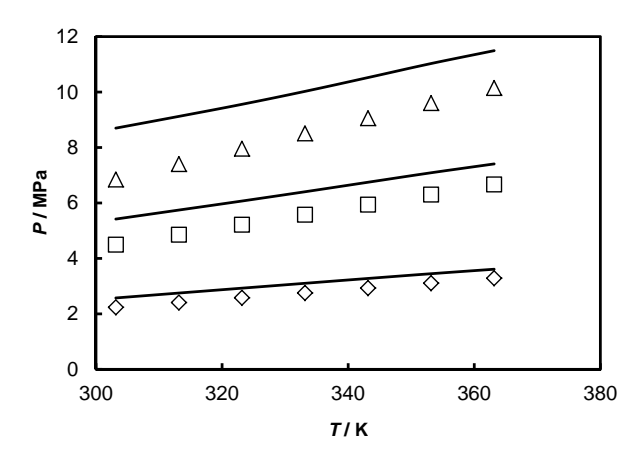


Figure 4.4: Bubble-point isopleths of the system  $CO_2$ - $CH_4$ -[bmim][Tf<sub>2</sub>N] for different  $CH_4$ /IL molar ratios: 0.043 (diamonds), 0.086 (squares) and 0.129 (triangles). Ternary mixtures prepared using the 75-25  $CO_2$ - $CH_4$  gas mixture. The lines are PR EoS modeling results.

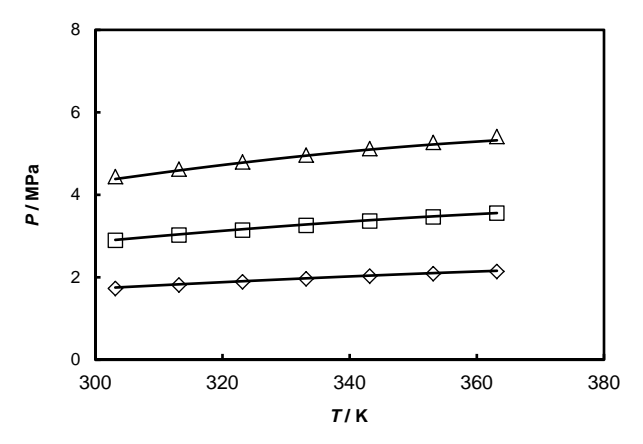


Figure 4.5: Bubble-point isopleths of the system  $CO_2$ - $CH_4$ -[emim][dep] for different  $CH_4/IL$  molar ratios: 0.020 (diamonds), 0.033 (squares) and 0.049 (triangles). Ternary mixtures prepared using the 25-75  $CO_2$ - $CH_4$  gas mixture. The lines are PR EoS modeling results.

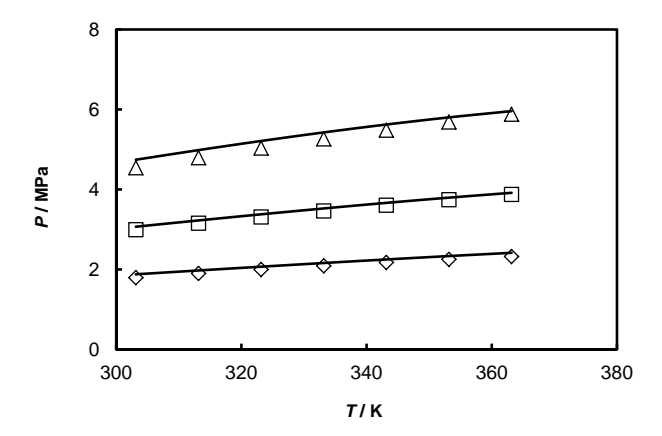


Figure 4.6: Bubble-point isopleths of the system  $CO_2$ - $CH_4$ -[emim][dep] for different  $CH_4/IL$  molar ratios: 0.020 (diamonds), 0.033 (squares) and 0.049 (triangles). Ternary mixtures prepared using the 50-50  $CO_2$ - $CH_4$  gas mixture. The lines are PR EoS modeling results.

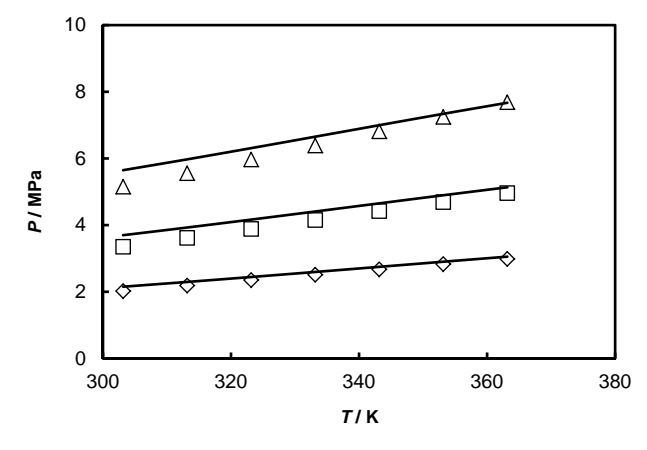


Figure 4.7: Bubble-point isopleths of the system  $CO_2$ - $CH_4$ -[emim][dep] for different  $CH_4/IL$  molar ratios: 0.020 (diamonds), 0.033 (squares) and 0.049 (triangles). Ternary mixtures prepared using the 75-25  $CO_2$ - $CH_4$  gas mixture. The lines are PR EoS modeling results.

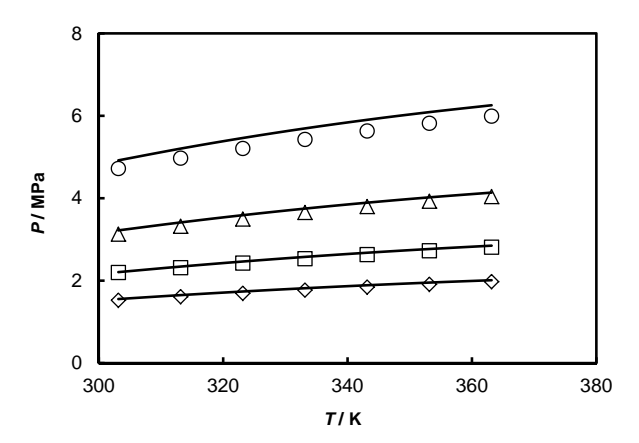


Figure 4.8: Bubble-point isopleths of the system  $CO_2$ -CH<sub>4</sub>-[thtdp][dca] for different CH<sub>4</sub>/IL molar ratios: 0.086 (diamonds), 0.121 (squares), 0.174 (triangles) and 0.258 (circles). Ternary mixtures prepared using the 25-75  $CO_2$ -CH<sub>4</sub> gas mixture. The lines are PR EoS modeling results.

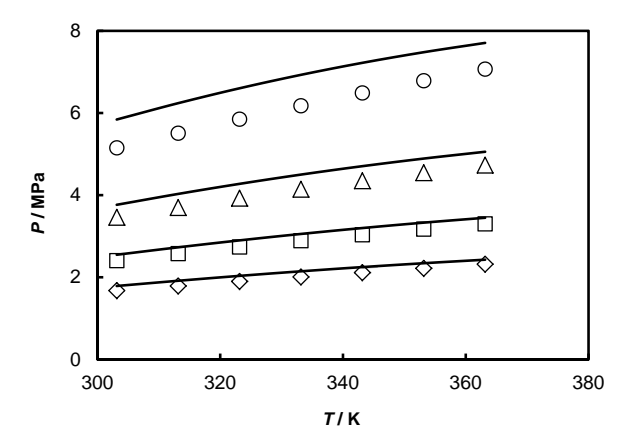


Figure 4.9: Bubble-point isopleths of the system  $CO_2$ -CH<sub>4</sub>-[thtdp][dca] for different CH<sub>4</sub>/IL molar ratios: 0.086 (diamonds), 0.121 (squares), 0.174 (triangles) and 0.258 (circles). Ternary mixtures prepared using the 50-50  $CO_2$ -CH<sub>4</sub> gas mixture. The lines are PR EoS modeling results.

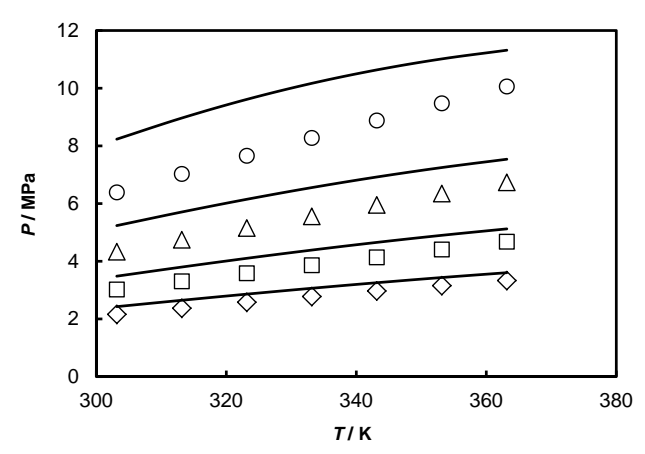


Figure 4.10: Bubble-point isopleths of the system  $CO_2$ -CH $_4$ -[thtdp][dca] for different CH $_4$ /IL molar ratios: 0.086 (diamonds), 0.121 (squares), 0.174 (triangles) and 0.258 (circles). Ternary mixtures prepared using the 75-25  $CO_2$ -CH $_4$  gas mixture. The lines are PR EoS modeling results.

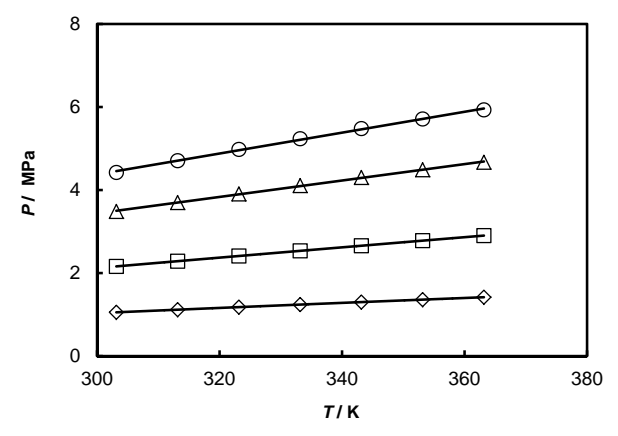


Figure 4.11: Bubble-point isopleths of the system  $CO_2$ -CH<sub>4</sub>-[thtdp][phos] for different CH<sub>4</sub>/IL molar ratios: 0.120 (diamonds), 0.242 (squares), 0.387 (triangles) and 0.488 (circles). Ternary mixtures prepared using the 25-75  $CO_2$ -CH<sub>4</sub> gas mixture. The lines are polynomial fits to guide the eye.

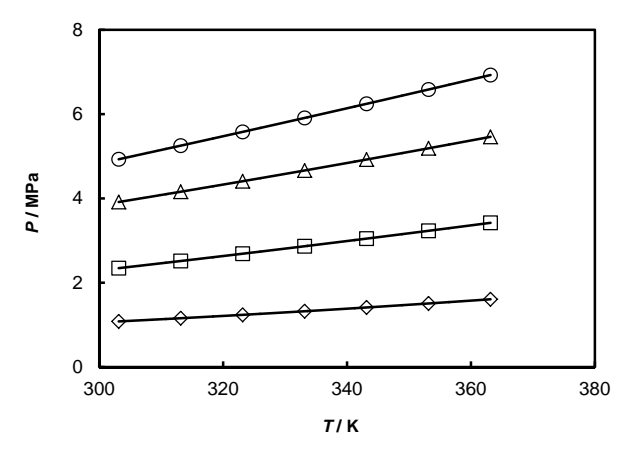


Figure 4.12: Bubble-point isopleths of the system  $CO_2$ - $CH_4$ -[thtdp][phos] for different  $CH_4/IL$  molar ratios: 0.120 (diamonds), 0.242 (squares), 0.387 (triangles) and 0.488 (circles). Ternary mixtures prepared using the 50-50  $CO_2$ - $CH_4$  gas mixture. The lines are polynomial fits to guide the eye.

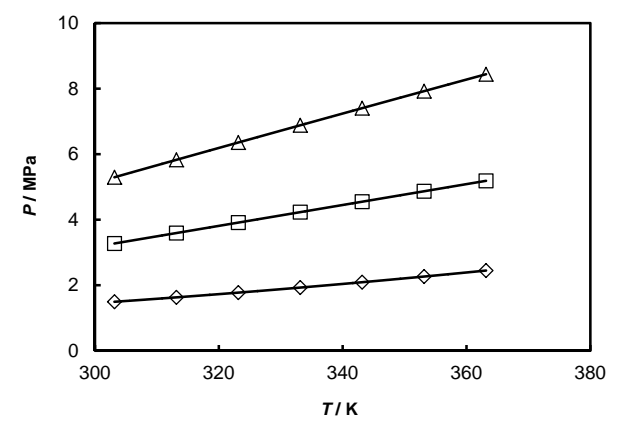


Figure 4.13: Bubble-point isopleths of the system  $CO_2$ - $CH_4$ -[thtdp][phos] for different  $CH_4/IL$  molar ratios: 0.120 (diamonds), 0.242 (squares) and 0.387 (triangles). Ternary mixtures prepared using the 75-25  $CO_2$ - $CH_4$  gas mixture. The lines are polynomial fits to guide the eye.

The modeling results for the ternary systems with a 50-50 or 75-25 gas mixture, which is typical for low quality/uneconomical natural gas reservoirs, are acceptable for low  $\mathrm{CH_4/IL}$  ratios and for moderate pressures, but for high  $\mathrm{CH_4/IL}$  ratios the deviation can be as high as 25 %. However, we are mainly concerned with the selectivities rather than solubilities. As mentioned earlier, it is not possible to obtain real selectivities directly from the reported VLE data, since a synthetic method was used for the experiments. Sampling and subsequent analysis of the phases is inevitable if one wish to obtain real selectivities directly from VLE experiments [373, 374]. However, real selectivities can also be obtained, though indirectly, using an EoS. Here, the PR EoS has been applied to obtain the real  $\mathrm{CO_2/CH_4}$  selectivity,  $S_{\mathrm{CO_2/CH_4}}^{\mathrm{R}}$ , defined as:

$$S_{\text{CO}_2/\text{CH}_4}^{\text{R}} = \left(\frac{y_{\text{CH}_4}/x_{\text{CH}_4}}{y_{\text{CO}_2}/x_{\text{CO}_2}}\right)_{p,T}$$
 (4.1)

where  $y_i$  and  $x_i$  denote the gas-phase and liquid-phase composition of the corresponding components, respectively. The liquid-phase composition at bubble-point conditions is known from the experiments, while the gas-phase composition is obtained from the PR EoS. The calculated (real) selectivities in  $[bmim][Tf_2N]$ , [emim][dep] and [thtdp][dca] are compared in Figures 4.14 to 4.16 with the ideal selectivities from the literature [345]. The ideal selectivities ( $S_{\text{CO}_2/\text{CH}_4}^{\text{I}}$ ) were calculated as the ratio of the Henry constant of CH<sub>4</sub> over that of CO<sub>2</sub>, see Equation (3.7). We note that this definition of the ideal selectivity does not account for nonidealities, while Equation (4.1)for the real selectivity does consider these effects. The real  $CO_2/CH_4$ selectivity in [bmim][Tf<sub>2</sub>N] and [emim][dep] is approximately the same as the ideal selectivity, whereas the real selectivity in [thtdp][dca] is slightly lower than the ideal selectivity. The real selectivities are not influenced by the gas phase composition as it can be seen in Figures 4.14 to 4.16. It is surprising to observe ideal selectivities even for mole fractions of IL as high as 0.7. The reason for this is likely due to the structure/cavities of the ILs. Both solutes are hosted in well defined cavities of the ILs without having the opportunity to interact with each other at low/moderate pressures. This

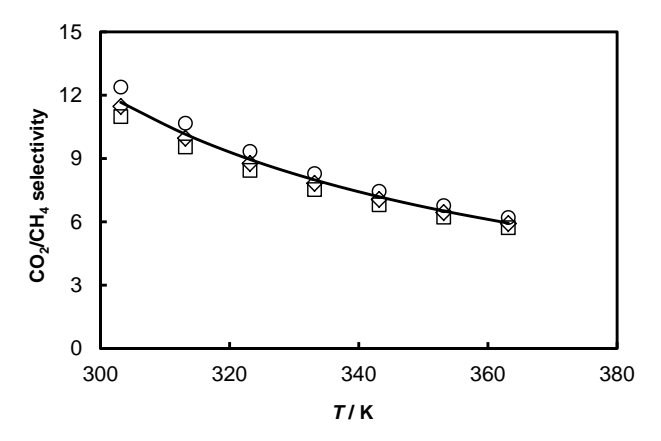


Figure 4.14: Comparison of the ideal and real  $CO_2/CH_4$  selectivity in [bmim][Tf<sub>2</sub>N]: ideal selectivity (line) and real selectivity; 25-75 mixture (squares), 50-50 mixture (diamonds) and 75-25 mixture (circles).

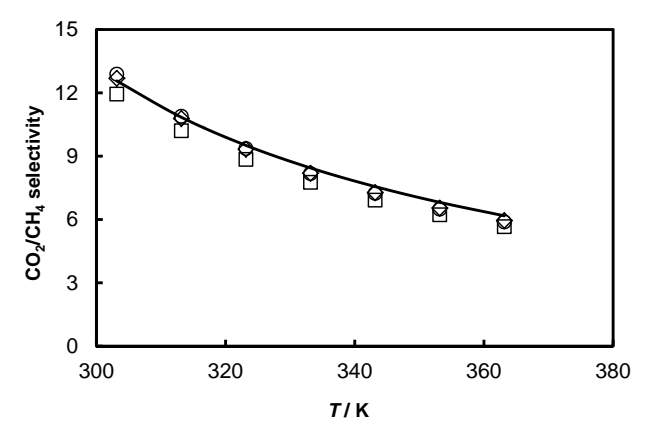


Figure 4.15: Comparison of the ideal and real  $CO_2/CH_4$  selectivity in [emim][dep]: ideal selectivity (line) and real selectivity; 25-75 mixture (squares), 50-50 mixture (diamonds) and 75-25 mixture (circles).

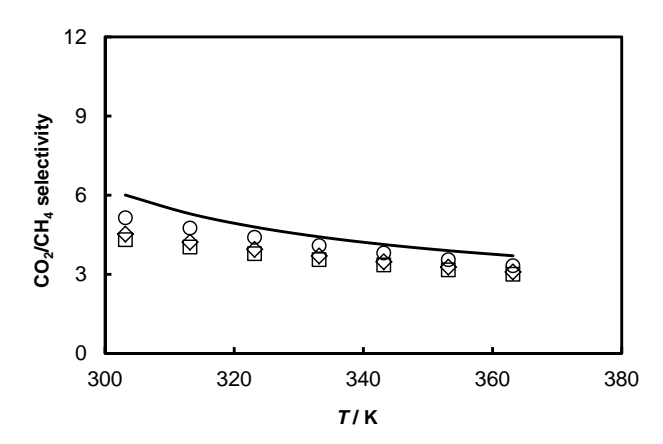


Figure 4.16: Comparison of the ideal and real  $CO_2/CH_4$  selectivity in [thtdp][dca]: ideal selectivity (line) and real selectivity; 25-75 mixture (squares), 50-50 mixture (diamonds) and 75-25 mixture (circles).

explanation is merely a hypothesis, which will be tested in the future using molecular simulations. Recently, molecular simulations have been used to analyse the IL structure in terms of size, shape, and electrostatic potential of the cavities (i.e., free volume) and their effect on gas solubility/selectivity [99, 149, 375–377]. These studies clearly indicate a strong free volume contribution driving gas solubilities in ILs, but more reasearch is required to reveal the solubility mechanism especially for gas mixtures.

The  $\rm CO_2/\rm CH_4$  selectivities in the investigated ILs are comparable with those of conventional solvents like Selexol, Purisol and Rectisol [345]. However, the price/performance ratio of traditional solvents like Selexol and Purisol is better than of ILs considering their low volumetric capacity, high viscosity and cost [9, 378]. In conclusion, the real  $\rm CO_2/\rm CH_4$  selectivity in the investigated ILs is, under the studied conditions, more or less equal to the ideal selectivity regardless of the gas phase composition. In the natural gas sweetening process, which typically contains up to 10%  $\rm CO_2$  in the feed, ideal  $\rm CO_2/\rm CH_4$  selectivity can be expected even at the high operating pressure of the process.

#### 4.5 Conclusions

The solubility of the binary gas mixtures containing carbon dioxide (CO<sub>2</sub>) and methane  $(CH_4)$  has been measured in the following ionic liquids (ILs): 1-butyl-3-methylimidazolium bis(trifluoromethylsulfonyl)imide, 1-ethyl-3methylimidazolium diethylphosphate, trihexyltetradecylphosphonium dicyanamide and trihexyltetradecylphosphonium bis(2,4,4-trimethylpentyl)phosphinate. The experiments involved bubble-point measurements for a temperature range of 303.15 - 363.15 K and for pressures up to 14 MPa using a synthetic method. The influence of the gas composition on the bubble-point pressure was investigated by using three gas mixtures containing 25 mole %  $CO_2$ -75 mole %  $CH_4$ , 50 mole %  $CO_2$ -50 mole %  $CH_4$  and 75 mole % CO<sub>2</sub>-25 mole % CH<sub>4</sub>. The Peng-Robinson (PR) equation of state (EoS) in combination with van der Waals mixing rules was apllied to predict the ternary vapor-liquid equilibrium data and to calculate the real CO<sub>2</sub>/CH<sub>4</sub> selectivities. The real selectivity (i.e., the selectivity of CO<sub>2</sub> in the presence of CH<sub>4</sub> in the ternary mixture CO<sub>2</sub>-CH<sub>4</sub>-IL) does not differ significantly from the ideal selectivity (i.e., the ratio of the pure gas Henry constants) regardless of the gas phase composition. Therefore, in the natural gas sweetening process, which typically contains up to 10% CO<sub>2</sub> in the feed, ideal CO<sub>2</sub>/CH<sub>4</sub> selectivity can be expected even at the high operating pressure of the process.

# Chapter 5

# Solubility of Natural Gas Species from Monte Carlo Simulations

This chapter is based on the paper: M. Ramdin, Q. Chen, S. P. Balaji, J. M. Vicent-Luna, A. Torres-Knoop, D. Dubbeldam, S. Calero, T. W. de Loos and T. J. H. Vlugt. Solubilities of CO<sub>2</sub>, CH<sub>4</sub>, C<sub>2</sub>H<sub>6</sub>, and SO<sub>2</sub> in ionic liquids and Selexol from Monte Carlo simulations. J. Comput. Sci. (2015) (in press).

## 5.1 Introduction

In the previous chapters, CO<sub>2</sub>/CH<sub>4</sub> solubilities and selectivities in ILs were calculated assuming that only CO<sub>2</sub> and CH<sub>4</sub> are present in the feed. However, natural gas typically contains a large number of components (e.g., CO<sub>2</sub>, CH<sub>4</sub>, H<sub>2</sub>S, N<sub>2</sub> and higher alkanes) [9] and the calculation of the selectivity requires solubility data of all the major components participating in the mixture. It is, therefore, practically impossible to experimentally determine the solubility of all these natural gas constituents and their mixtures

for a large number of solvents. Furthermore, the number of theoretically possible ILs is extremely large and predictive tools like equation of states and molecular simulations are essential for selecting a proper IL.

In this chapter, Monte Carlo simulations are used to compute the solubility of natural gas components in ILs and Selexol, which is a mixture of poly(ethylene glycol) dimethyl ethers (PEGDME,  $CH_3O[CH_2CH_2O]_nCH_3$ , where n is typically between 3 and 11) [354]. Simulations of gas solubilities in Selexol are performed, because despite its wide application, gas solubility data in Selexol is scarcely reported in the literature and often limited to Henry constants. The recently developed Continuous Fractional Component Monte Carlo (CFCMC) method [379, 380] is used in the osmotic ensemble to calculate the solubility of the pure gases carbon dioxide ( $CO_2$ ), methane ( $CH_4$ ), ethane ( $C_2H_6$ ), and sulfur dioxide ( $CO_2$ ) in the ILs 1-alkyl-3-methylimidazolium bis(trifluoromethylsulfonyl)imide ( $C_1$ mim)[ $C_2$ mim][ $C_2$ mim] and Selexol ( $CH_3O[CH_2CH_2O]_nCH_3$ ,  $CH_3$ 0 at 313.15 K and several pressures. The solubility of the gases obtained from the MC simulations are compared with available experimental data.

#### 5.2 Simulation Details

Phase equilibria calculations using Monte Carlo simulations rely on insertions and deletions of molecules to and from a system [381]. Standard Monte Carlo methods are inefficient due to the low insertion and deletion probabilities especially for systems with a high density [382]. Therefore, advanced biasing/sampling methods have been devised (e.g., Configurational-bias Monte Carlo (CBMC) and gradual insertions) that can (partially) overcome this problem [383–385]. An example of such a method is the Continuous Fractional Component Monte Carlo (CFCMC) scheme developed by Shi and Maginn [379, 380]. In this approach, the ensemble is expanded with a "fractional" molecule, which is coupled to the system through a parameter  $\lambda$ . The  $\lambda$ -parameter is confined on the interval [0, 1] and is used to gradually increase or decrease the strength of the interactions between the fractional

molecule and the surrounding "whole" molecules in the system. In this way, the system can rearrange as the fractional molecule is slowly inflated, which decreases the probability for atomic overlaps. The Lennard-Jones (LJ) and Coulombic interactions between the fractional molecule and the surrounding molecules are scaled such that the conventional intermolecular potentials are recovered for  $\lambda = 1$  and no interactions in the limit as  $\lambda \to 0$ . The CFCMC scheme performs  $\lambda$ -moves in addition to the standard MC moves like translation, rotation and volume change [7, 386]. A  $\lambda$  change will result in the following three possibilities. (1)  $\lambda$  stays between 0 and 1, 0 <  $\lambda$  < 1, the number of absorbed molecules, atomic positions and intramolecular energies remain unaltered. (2)  $\lambda$  exceeds 1,  $\lambda = 1 + \epsilon$  with  $0 < \epsilon < 1$ , which results in a transformation of the current fractional molecule into a "whole" molecule and a new fractional molecule with  $\lambda = \epsilon$  is randomly added to the system. (3)  $\lambda$  drops below 0,  $\lambda = -\epsilon$ , which implies that the current fractional molecule is deleted and a new fractional molecule with  $\lambda = 1 - \epsilon$  is randomly added to the system. The Wang-Landau (WL) sampling scheme is used to bias the  $\lambda$  moves, which is necessary to prevent the system from being stuck in a certain  $\lambda$  state [387]. The CFCMC scheme is more efficient than conventional MC and CBMC methods in particular for systems with a high density [388]. Details of the CFCMC method can be found in the original papers by Shi and Maginn [124, 172, 379, 380, 389], the excellent review by Dubbeldam et al. [383] and the recent publication by Torres-Knoop et al. [388]. A classical force field including bond-stretching, bond-bending, torsions, Lennard-Jones (LJ) and electrostatic interactions was used for the solvent molecules. The force field parameters of the ILs were taken from Maginn et al. [380, 390, 391]. The TraPPE united-atom (TraPPE-UA) models were used for CO<sub>2</sub>, CH<sub>4</sub>, C<sub>2</sub>H<sub>6</sub>, SO<sub>2</sub> and Selexol [392– 395]. The solute molecules were considered rigid in the simulations. The Lorentz-Berthelot combining rules were used for the LJ interactions between dissimilar atoms [396]. Long-range electrostatic interactions were taken into account by the Ewald method using a relative precision of  $10^{-5}$  [385]. The LJ interactions were truncated and shifted at 12 Å and no tail corrections were used. The internal degrees of freedom of the solvent molecules were sampled using the CBMC scheme [385, 397–399]. The MC simulations were

executed in the osmotic ensemble, which means that the temperature (T), the hydrostatic pressure (P), the fugacity of the solute (f), and the number of solvent molecules (N) were all fixed. In this ensemble, the volume of the system and the number of solute molecules will change as a response to the imposed hydrostatic pressure and gas fugacity. A schematic representation of the osmotic ensemble is shown in Figure 5.1. Note that the Gibbs phase rule is not violated by disallowing IL molecules in the gas phase, because the number of equilibrium conditions and the number of intensive variables are both reduced by one [400]. Furthermore, the assumption that only solutes without solvent molecules are present in the gas phase is reasonable, since ILs and Selexol have a negligible vapor pressure [202]. The fugacity of the gas is related to the pressure of the gas, which exactly equals the hydrostatic pressure of the liquid. The Peng-Robinson (PR) equation of state (EoS) was used to compute the fugacity of the gases as a function of the pressure [340]. The CFCMC simulations were performed at 313.15 K and pressures up to 12 MPa using the molecular simulation software RASPA [401]. The following number of solvent molecules, 50, 50, 70, 75, and 70, were used in the simulations for  $[C_4 \text{mim}][Tf_2N]$ ,  $C_6 \text{mim}[Tf_2N]$ , [emim][dep],  $CH_3O[CH_2CH_2O]_4CH_3$  and  $CH_3O[CH_2CH_2O]_6CH_3$ , respectively. The rationale behind choosing these specific numbers of molecules is to keep the simulation box always larger than twice the cutoff distance, to dissolve at least one (integer) solute molecule, and to avoid excessive computations that are required for larger systems. To save computational time, the MC simulations were preceded by a molecular dynamics (MD) simulation, where the liquid structure was equilibrated for 10 ns in the isobaric-isothermal (NPT) ensemble. The equilibrated ensemble of the MD run was then used to initiate the MC simulations. The CFCMC simulations in the osmotic ensemble were started with an equilibration run of  $10^5$  MC cycles followed by a production run of 0.5 to 2 million cycles. The actual number of simulation cycles were governed by the convergence characteristics of the systems. The IL systems typically required 0.5 to 1 million cycles, while the Selexol systems were run for 1 to 2 million cycles. Note that in RASPA the number of MC steps in a cycle is defined as the total current number of molecules in the system. Once we verified that the system has

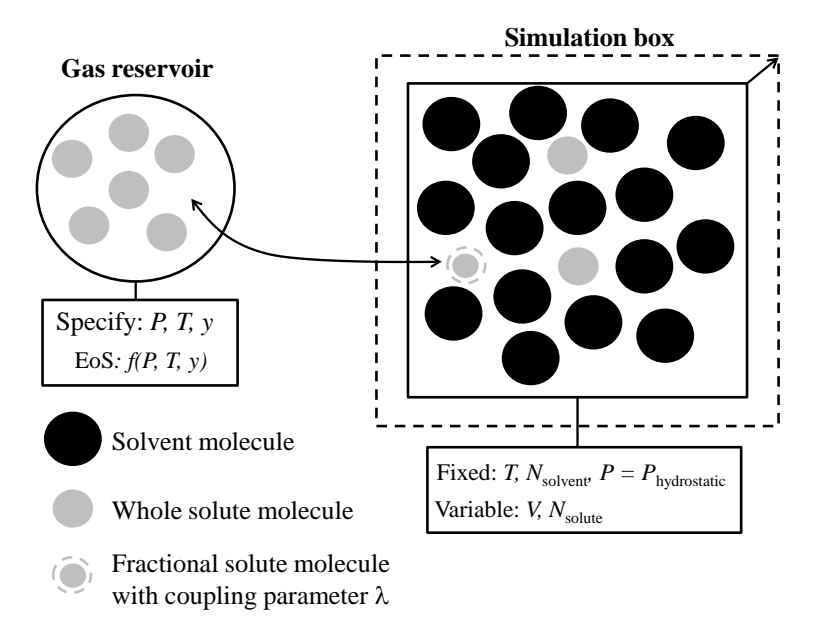


Figure 5.1: A schematic representation of the osmotic ensemble using the CFCMC method. The pressure (P), the temperature (T), and the composition (y) of the gas phase are specified and the fugacity of the gases (f) is calculated from the PR EoS. The number of solvent molecules  $(N_{\rm solvent})$  and the temperature of the simulation box (T) are fixed, while the number of solute molecules  $(N_{\rm solute})$  and the volume (V) fluctuate. The pressure of the gas (P) is equal to the hydrostatic pressure of the liquid  $(P_{\rm hydrostatic})$ . In the CFCMC method, solute molecules are inserted gradually utilizing a parameter  $\lambda$  as explained in the text.

attained its equilibrium state, the solubility data is obtained from block averages and the uncertainty is calculated from the standard deviation.

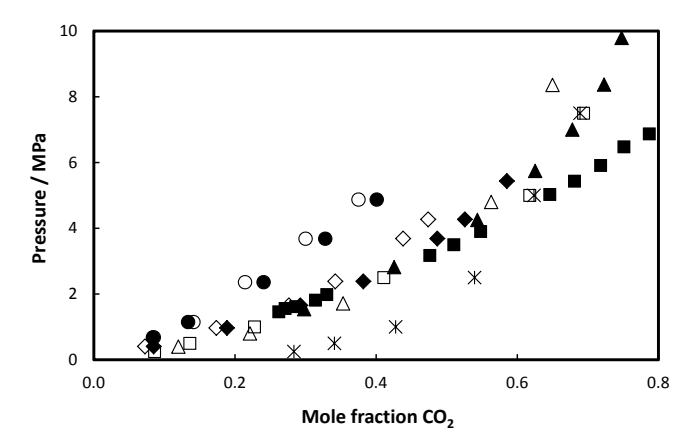


Figure 5.2: Solubility of  $CO_2$  at 313.15 K in ILs and Selexol from experiments (closed symbols) and Monte Carlo simulations (open symbols). [hmim][Tf<sub>2</sub>N], triangles; [bmim][Tf<sub>2</sub>N], diamonds; [emim][dep], circles;  $CH_3O[CH_2CH_2O]_4CH_3$ , squares; and only MC data for  $CH_3O[CH_2CH_2O]_6CH_3$ , stars. Experimental data taken from Refs [97, 345, 370, 402].

#### 5.3 Results and Discussion

Monte Carlo simulations in the osmotic ensemble were used to compute the solubility of the pure gases  $CO_2$ ,  $CH_4$ ,  $C_2H_6$ , and  $SO_2$  in the ILs ( $[C_n mim][Tf_2N]$ , n=4, 6), [emim][dep], and poly(ethylene glycol) dimethyl ethers (PEGDME,  $CH_3O[CH_2CH_2O]_nCH_3$ , n=4, 6), which are the principle ingredients of Selexol. The Selexol solvent is a mixture of PEGDME with n ranging from 3 to 11 [354]. Unfortunately, the exact composition of Selexol is rarely reported in the experimental literature, which makes a direct comparison with the simulations cumbersome. The solubility of the gases in the solvents has been computed at 313.15 K and pressures corresponding to the conditions of the natural gas sweetening process. In Figure 5.2, the solubility of  $CO_2$  obtained from the simulations is compared with experimental absorption data. For the system  $CO_2$ - $CH_3O[CH_2CH_2O]_6CH_3$  only MC data is shown in Figure 5.2, since experimental data of this system is lacking in the literature. Clearly, the  $CO_2$  solubility in the ILs is lower than the

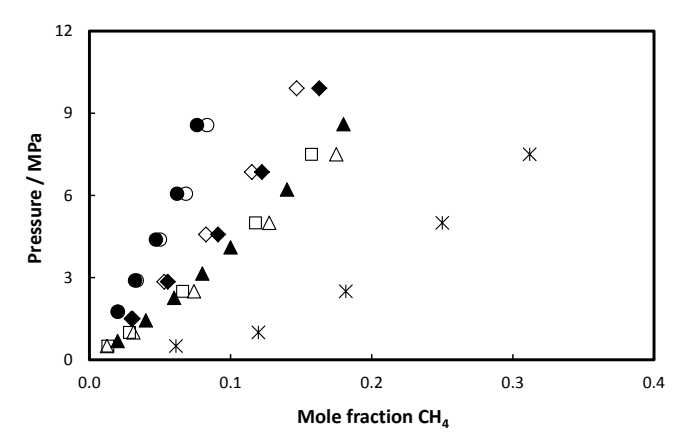


Figure 5.3: Solubility of CH $_4$  at 313.15 K in ILs and Selexol from experiments (closed symbols) and Monte Carlo simulations (open symbols). [hmim][Tf $_2$ N], triangles; [bmim][Tf $_2$ N], diamonds; [emim][dep], circles; CH $_3$ O[CH $_2$ CH $_2$ O] $_4$ CH $_3$ , squares; and only MC data for CH $_3$ O[CH $_2$ CH $_2$ O] $_6$ CH $_3$ , stars. Experimental data taken from Refs [345, 371, 403].

PEGDME solvents. Furthermore, the CO<sub>2</sub> solubility data obtained from the MC simulations are in quantitative agreement with the experimental results. In Figure 5.3, the solubility of CH<sub>4</sub> in all the investigated solvents is compared with experiments. Solvents that exhibit a high CO<sub>2</sub> solubility also have a high CH<sub>4</sub> solubility. The MC data are in excellent agreement with the experimental data at low pressures, but the deviation increases at higher pressures. High pressure VLE data for the system CH<sub>4</sub>-PEGDME is not available in the literature. However, the Henry constant of CH<sub>4</sub> (i.e., the limiting slope of the fugacity vs. the mole fraction  $(x_{\text{CH}_4})$  curve as  $x_{\text{CH}_4}$  $\rightarrow$  0) in CH<sub>3</sub>O[CH<sub>2</sub>CH<sub>2</sub>O]<sub>4</sub>CH<sub>3</sub> at 313.15 K obtained from the simulations is 37.9 MPa, which is in close agreement with the experimental value of 38.2 MPa [353]. Figure 5.3 also shows that  $CH_3O[CH_2CH_2O]_6CH_3$  has a high affinity for CH<sub>4</sub>, which will cause product losses in the natural gas sweetening process. In Figure 5.4, the solubility of C<sub>2</sub>H<sub>6</sub> obtained from the MC simulations is compared with the experimental data. No experimental data have been reported for the PEGDME systems, but the simulation

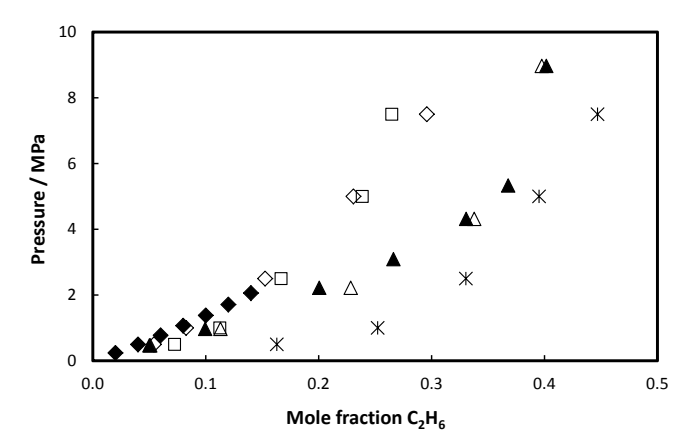


Figure 5.4: Solubility of  $C_2H_6$  at 313.15 K in ILs and Selexol from experiments (closed symbols) and Monte Carlo simulations (open symbols). [hmim][Tf<sub>2</sub>N], triangles; [bmim][Tf<sub>2</sub>N], diamonds;  $CH_3O[CH_2CH_2O]_4CH_3$ , squares; and only MC data for  $CH_3O[CH_2CH_2O]_6CH_3$ , stars. Experimental data taken from Refs [98, 404].

results show that the PEGDME solvents posses a high C<sub>2</sub>H<sub>6</sub> solubility. The solubility of hydrocarbons is increased as the nonpolar domains of the solvents are increased, which is due to nonpolar-nonpolar interactions [345]. The high hydrocarbon solubility is a major drawback of the Selexol solvents, which will require an additional separation step downstream of the natural gas sweetening process. The solubility of SO<sub>2</sub> is only computed for the solvents [C<sub>6</sub>mim][Tf<sub>2</sub>N] and CH<sub>3</sub>O[CH<sub>2</sub>CH<sub>2</sub>O]<sub>4</sub>CH<sub>3</sub>, see Figure 5.5. The results show that  $SO_2$  has an extremely high solubility in both the solvents, which means that SO<sub>2</sub> can selectively be removed in the presence of CO<sub>2</sub>. A first estimate of the ideal SO<sub>2</sub>/CO<sub>2</sub> selectivity can be obtained from the ratio of the Henry constant of  $CO_2$  over that of  $SO_2$ . Note that a lower Henry constant implies a higher solubility. The Henry constants of  $CO_2$  and  $SO_2$  in  $|C_6 \text{mim}||Tf_2N|$  at 313.15 K are respectively 4.3 MPa and 0.23 MPa, which yields an ideal SO<sub>2</sub>/CO<sub>2</sub> selectivity of 19 [123, 151]. The Henry constants of CO<sub>2</sub> and SO<sub>2</sub> in CH<sub>3</sub>O[CH<sub>2</sub>CH<sub>2</sub>O]<sub>4</sub>CH<sub>3</sub> at 313.15 K are respectively 4.3 MPa and 0.037 MPa, which yields an ideal  $SO_2/CO_2$ 

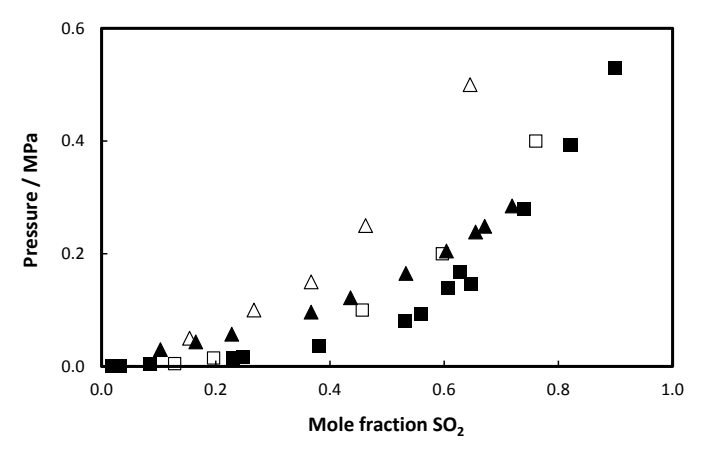


Figure 5.5: Solubility of  $SO_2$  at 313.15 K in ILs and Selexol from experiments (closed symbols) and Monte Carlo simulations (open symbols). [hmim][Tf<sub>2</sub>N], triangles and  $CH_3O[CH_2CH_2O]_4CH_3$ , squares. Experimental data taken from Refs [151, 405].

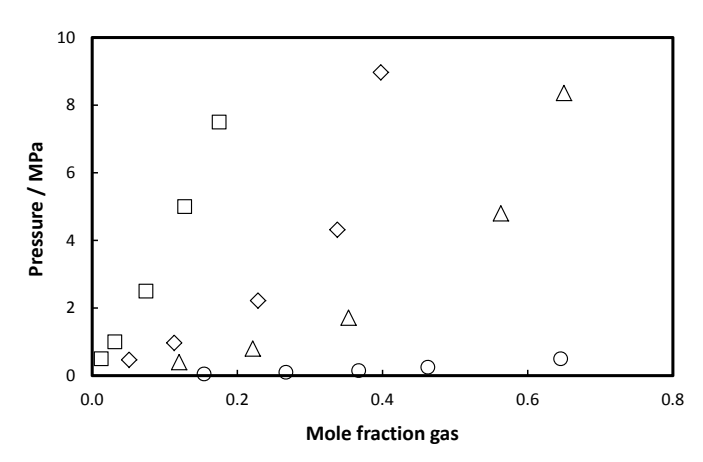


Figure 5.6: Solubility of the gases in  $[C_6 mim][Tf_2N]$  at 313.15 K obtained from MC simulations.  $SO_2$ , circles;  $CO_2$ , triangles;  $C_2H_6$ , diamonds; and  $CH_4$ , squares.

selectivity of 116 [356, 405]. Clearly,  $CH_3O[CH_2CH_2O]_4CH_3$  is more selective towards  $SO_2$  than  $[C_6 mim][Tf_2N]$ . Furthermore, the MC data is in quantitative agreement with the experiments at low  $SO_2$  loadings, but at high loading the deviation is significant. In Figure 5.6, the solubility of the gases in  $[C_6 mim][Tf_2N]$  obtained from the MC simulations are compared. The following solubility trend,  $SO_2 > CO_2 > C_2H_6 > CH_4$ , is observed for all the investigated solvents.

## 5.4 Conclusions

The Continuous Fractional Component Monte Carlo method has been used to compute the solubility of the gases  $CO_2$ ,  $CH_4$ ,  $C_2H_6$ , and  $SO_2$  in the ILs  $([C_n mim][Tf_2N], n = 4, 6), [emim][dep], and poly(ethylene glycol) dimethyl$ ethers (PEGDME,  $CH_3O[CH_2CH_2O]_nCH_3$ , n=4,6). The following gas solubility trend is observed in the experiments and simulations for all the solvents:  $SO_2 > CO_2 > C_2H_6 > CH_4$ . The solubility of  $SO_2$  is substantially higher than that of CO<sub>2</sub>, which indicates that SO<sub>2</sub> can be removed selectively in the presence of  $CO_2$ . However, the PEGDME solvents are roughly a factor 5 more selective towards SO<sub>2</sub> than the ILs. Furthermore, the solubility of CH<sub>4</sub> and C<sub>2</sub>H<sub>6</sub> is higher in PEGDME than in the ILs, which is a wellknown drawback of these Selexol solvents. The price/performance ratio is in favor of the Selexol solvents considering the high cost and viscosity of the investigated ILs. The solubility of the gases obtained from the MC simulations are in quantitative agreement with available experimental data. The results show that molecular simulation is a promising tool to predict gas solubilities in solvents and that it may be used as a screening tool to select ILs for specific applications.

# Chapter 6

# Computing Bubble Points of Mixtures from Molecular Simulations

This chapter is based on the paper: M. Ramdin, S. P. Balaji, J. M. Vicent-Luna, A. Torres-Knoop, Q. Chen, D. Dubbeldam, S. Calero, T. W. de Loos and T. J. H. Vlugt. Computing bubble-points of  $CO_2/CH_4$  gas mixtures in ionic liquids from Monte Carlo Simulations. Fluid Phase Equilib. (2015) (in press).

#### 6.1 Introduction

Industrial processes often involve multicomponent gas mixtures, which have to be separated or purified to obtain the final product [406]. Solubility and selectivity data of the components in the mixture are required to properly design and operate separation processes [9]. The gases dissolved in the solvent may not necessarily form an ideal mixture, since the presence of one gas species may influence the solubility of the other [407]. Therefore, accurate solubility data of gas mixtures are essential to describe this non-ideal

behavior [337]. Recently, we investigated the potential of ionic liquids (ILs) for CO<sub>2</sub> capture from natural gas using experiments and Monte Carlo simulations [7–9, 18, 345, 346, 386]. Bubble-point pressures of carbon dioxide (CO<sub>2</sub>) and methane (CH<sub>4</sub>) mixtures were measured in different ionic liquids using the Cailletet apparatus, which operates according to the visual synthetic method [8]. In this method, known amounts of gases and ionic liquid are introduced in a capillary using mercury as a sealing and pressurizing fluid. The bubble point is measured at a fixed temperature by gradually increasing the pressure until the gas bubble is completely dissolved in the liquid (i.e., the bubble-point pressure) [338]. Note that in the Cailletet setup phase transitions are observed visually and sampling of the phases is not possible. Therefore, the composition of the gas phase at the bubble point is unknown. The aim of this work was to investigate the effect of the presence of CH<sub>4</sub> (CO<sub>2</sub>) on the solubility of CO<sub>2</sub> (CH<sub>4</sub>) as both are simultaneously dissolved in an IL. This effect can be quantified by the so-called real  $CO_2/CH_4$  selectivity as defined in Equation (4.1). The ideal selectivity can be defined in several ways, but for convenience the ratio of Henry constants  $(H_i)$  is used here, see Equation (3.7). The Henry constants,  $H_{ij}$ , of solute i in solvent j are calculated from Equation (3.8). In principle, the real selectivity will differ from the ideal selectivity and the deviation is governed by the degree of non-ideality caused by the simultaneous dissolution of CO<sub>2</sub> and CH<sub>4</sub>. From the data of the Cailletet experiments, it is not possible to calculate the real selectivity  $S_{\text{CO}_2/\text{CH}_4}^{\text{R}}$ , since only the bubble-point pressures of the CO<sub>2</sub>-CH<sub>4</sub> mixtures were measured and the gas phase compositions,  $y_i$ , were unknown. This is, as stated before, because the composition of the phases cannot be sampled. The Peng-Robinson (PR) equation of state (EoS) may be used to calculate the gas phase compositions and therefore one can estimate the real selectivity, see Chapter 4. However, the PR EoS is known to yield less accurate results for the gas phase composition for multicomponent mixtures, even when the liquid phase properties are predicted correctly [408]. We note that bubble-point calculations are extremely important for industrial separation processes [409]. For example, one may want to evaluate the performance of a separation column and hence the quality of the separated product at a certain operating temperature and

6.1 Introduction 127

pressure. This evaluation requires the knowledge of bubble-point pressures of the mixture and the compositions of each phase.

In this study, we aim to compute the gas phase compositions  $(y_i)$  of a CO<sub>2</sub>+CH<sub>4</sub>+IL mixture at a given temperature, liquid phase composition or bubble-point pressure, using molecular simulation. Several molecular simulation techniques (e.g., Gibbs ensemble Monte Carlo, Grand Equilibrium method, COSMO-RS, and fluctuation solution theory) have been used in the 'third industrial fluid properties simulation challenge' to compute bubble-points of HFC/ethanol mixtures [410–416]. Unfortunately, not all (classical) molecular simulation techniques are suitable to compute bubble points of multicomponent mixtures. The Gibbs ensemble Monte Carlo (GEMC) method can be used to compute phase equilibrium at specified temperature, global composition, and volume or pressure. However, standard GEMC simulations are not suitable to directly compute bubble points of multicomponent systems. A suitable ensemble to compute bubble points requires the temperature and liquid phase compositions to be specified, while the pressure and the gas phase compositions need to be calculated. The pseudo bubble point ensemble introduced by Ungerer et al. [417] and the Grand Equilibrium (GE) method proposed by Vrabec and Hasse [418] can be used to compute bubble points of multicomponent mixtures. The method of Ungerer et al. uses a liquid and a vapor box, like in the GEMC method, in which the temperature, the liquid compositions, and the total volume are fixed. The composition of the gas phase and the volume of the phases are allowed to change. The GE method of Vrabec and Hasse is related to the method of Ungerer et al., but avoids direct coupling between the gas phase and the liquid phase. In this method, Taylor expansions of the chemical potentials as a function of pressure in the liquid phase are used to set the chemical potentials of the vapor phase in a pseudo grandcanonical ensemble simulation. The methods of Ungerer et al. [417], and Vrabec and Hasse [418], both require the calculation of the liquid phase chemical potentials using Widom's test particle method or an equivalent method. Here, a different approach is used to compute bubble points of multicomponent mixtures avoiding the computationally demanding chemical potential evaluations. It is important to note that chemical potentials

obtained from Widom's test particle method are usually subjected to large uncertainties [385]. Simulations using the Continuous Fractional Component Monte Carlo (CFCMC) technique in the osmotic ensemble have been used to compute the solubilities of  $\rm CO_2$  and  $\rm CH_4$  gas mixtures in the ILs 1-butyl-3-methylimidazolium bis(trifluoromethylsulfonyl)imide [bmim][Tf<sub>2</sub>N] and 1-ethyl-3-methylimidazolium diethylphosphate [emim][dep]. The composition of the gas is calculated iteratively from the liquid composition by performing two separate simulations in the osmotic ensemble at the same hydrostatic pressure, but for different gas compositions. The composition of the gas that is in equilibrium with the experimental liquid composition is then approximated by a first-order Taylor expansion. The gas phase compositions and  $\rm CO_2/CH_4$  selectivities obtained from the MC simulations are compared with the PR EoS modeling results.

The chapter is organized as follows. In the next section, a theoretical approach is presented to calculate the bubble-point pressure of a (multicomponent) gas-mixture from the knowledge of only pure component solubility data assuming ideal mixing. In a following section, the details of the MC simulations (i.e., ensemble, force field, and simulation parameters) and the method to compute bubble points are outlined. Subsequently, the results for the gas solubilities and selectivities are presented and discussed. In the final section, conclusion are presented regarding the real  $\rm CO_2/CH_4$  selectivities in ILs.

# 6.2 Theory

It is of practical interest to predict the bubble-point pressure of a (multicomponent) gas-mixture from the knowledge of only pure component solubility data, since measuring solubilities of gas mixtures requires an increased experimental effort [419]. Here, we consider the solubility of a (multicomponent) gas-mixture in a single solvent. The equilibrium relations for the solvent and solutes are given by [337]:

$$y_s P \phi_s = x_s \gamma_s P_s^{\text{sat}} \tag{6.1}$$

$$y_i P \phi_i = x_i \gamma_i H_i \tag{6.2}$$

Here, P is the pressure,  $\phi$  the fugacity coefficient, y the gas phase composition, x the liquid phase composition, H the Henry constant,  $P_s^{\rm sat}$  the saturation pressure of the solvent, and  $\gamma$  the activity coefficient. The subscripts s and i denote the solvent and solute, respectively. The pressure, P, can be obtained from Equations (6.1) and (6.2). Since ILs have a negligible vapor pressure [202], Equation (6.1) cancels and after rearranging Equation (6.2) one obtains the bubble-point pressure of a n-solute (i.e., n is the number of components in the gas phase excluding the IL since it is considered non-volatile) system:

$$P = \frac{\sum_{i=1}^{n} x_i \gamma_i H_i}{\sum_{i=1}^{n} y_i \phi_i} \tag{6.3}$$

For a ternary system (e.g.,  $CO_2 + CH_4 + IL$ ) in which the IL is nonvolatile, Equation (6.3) reduces to:

$$P = \frac{x_{\text{CO}_2} \gamma_{\text{CO}_2} H_{\text{CO}_2} + x_{\text{CH}_4} \gamma_{\text{CH}_4} H_{\text{CH}_4}}{y_{\text{CO}_2} \phi_{\text{CO}_2} + y_{\text{CH}_4} \phi_{\text{CH}_4}}$$
(6.4)

For sufficiently low pressures and solubilities (i.e.,  $\phi_{\text{CO}_2} \approx \phi_{\text{CH}_4} \approx 1$  and  $\gamma_{\text{CO}_2} \approx \gamma_{\text{CH}_4} \approx 1$ ), Equation (6.4) reduces to the following well-known equation [337]:

$$P = x_{\text{CO}_2} H_{\text{CO}_2} + x_{\text{CH}_4} H_{\text{CH}_4}$$
 (6.5)

Equation (6.5) allows us to calculate the bubble-point pressure of a binary gas-mixture from the knowledge of pure component Henry constants assuming ideal mixing.

### 6.3 Simulation Details

We recall that the aim is to compute the gas composition  $(y_i)$  of a  $CO_2+CH_4+IL$  mixture at a given temperature (T), liquid composition  $(x_i)$  or bubble-point

pressure (P) using Monte Carlo (MC) simulations. The "or" in the previous sentence denotes a strict constraint, since the number of degrees of freedom for a ternary system containing two phases is three. Therefore, an ensemble with a fixed temperature, liquid composition and pressure would violate the Gibbs phase rule. It turns out that standard ensembles (e.g., Gibbs, osmotic, etc.) commonly used for phase equilibria computations cannot be applied directly to compute bubble-point pressures and compositions of multicomponent mixtures. These ensembles require the specification of the pressure and/or the gas composition, which are apriori unknown and should be computed from the simulations. Several iterative methods have been proposed in the literature to compute bubble-point pressures of multicomponent mixtures using a pseudo-ensemble [417, 418, 420–424]. All of them require the computation of the liquid phase chemical potentials (e.g., using Widom test particle method or an equivalent method [385]), which are typically subjected to large uncertainties for complex dense liquid systems [385]. We have used the following approach to avoid the computationally demanding chemical potential evaluations. We are interested in the change of the solute composition in the liquid phase  $(x_i)$  caused by a change in the gas fugacity  $(f_i(P,T,y_i))$ :

$$\left(\frac{\partial x_i}{\partial y_i}\right)_{T,P,\Sigma} = \frac{(\partial f_i/\partial y_i)_{T,P,\Sigma}}{(\partial f_i/\partial x_i)_{T,P,\Sigma}} \tag{6.6}$$

The differentiation in the left hand side of Equation (6.6) is performed at constant temperature and pressure using the constraints  $\sum_{i=1}^{n} y_i = 1$  and  $\sum_{i=1}^{n} x_i = 1$ , which is indicated by the symbol  $\Sigma$ . Note that in the simulations the IL molecules are considered nonvolatile, hence  $y_{\text{CH}_4} = (1 - y_{\text{CO}_2})$ . The numerator in Equation (6.6),  $(\partial f_i/\partial y_i)$ , can be calculated with an equation of state for the gas phase. The Peng-Robinson (PR) equation of state (EoS) with a binary interaction parameter between CO<sub>2</sub> and CH<sub>4</sub> of 0.1 (i.e.,  $k_{ij} = 0.1$  [369]) is used to calculate the fugacities as a function of pressure and gas composition [340]. We note that one could alternatively compute the gas fugacities from molecular simulations. In this way, the computed fugacities would be fully consistent with the force field used for the gases. However, the computational models for CO<sub>2</sub> and CH<sub>4</sub> are well

established and tuned to reproduce the vapor-liquid properties of the fluids. They reproduce the experimental densities, vapor pressures, and fugacities very well, and therefore explicit fugacity computations using a PR EoS give almost identical results [392, 393]. Therefore, the gas fugacities computed with molecular simulations or the PR EoS will be almost identical. The denominator in Equation (6.6),  $(\partial f_i/\partial x_i)$ , is calculated from two independent simulations in the osmotic ensemble. In this ensemble, the temperature (T), the hydrostatic pressure  $(P_{\text{hydro}})$  which is equal to the pressure of the gas phase (P), the solute fugacities  $(f_i)$ , and the number of solvent molecules (N) are fixed. The volume of the system (V) and the number of solute molecules in the liquid phase will change to satisfy the equilibrium conditions  $f_i^l = f_i^g$ . The fugacity  $(f_i)$  and the hydrostatic pressure are related through the PR EoS for the gas phase. The two simulations in the osmotic ensemble are performed at the same hydrostatic pressure, which is equal to the experimental bubble-point pressure, but at different gas compositions. The difficulty now is to choose the gas compositions at which the two simulations should be performed. Fortunately, the PR EoS can be used to fit the experimental bubble-point pressure of the ternary system CO<sub>2</sub>-CH<sub>4</sub>-IL to obtain an initial guess for the gas composition. The gas compositions for the two simulations are chosen in the vicinity of this initial gas composition. The gas composition that will yield the experimental liquid composition can then be obtained from a first-order Taylor expansion:

$$y_i = y_{i0} + \left(\frac{\partial y_i}{\partial x_i}\right)_{T.P.\Sigma} (x_i - x_{i0})$$
(6.7)

Here,  $y_i$  and  $x_i$  are respectively the gas phase and liquid phase composition of solute i, and  $y_{i0}$  and  $x_{i0}$  denote the reference gas phase and the experimental liquid phase composition of solute i, respectively. In Figure 6.1, the procedure described above is explained graphically. Once the gas phase compositions are known from Equation (6.7), Equation (4.1) can be applied to calculate the real selectivities. The molecular simulation software RASPA [401] was used to perform the molecular simulations. The Continuous Fractional Component Monte Carlo (CFCMC) method in the

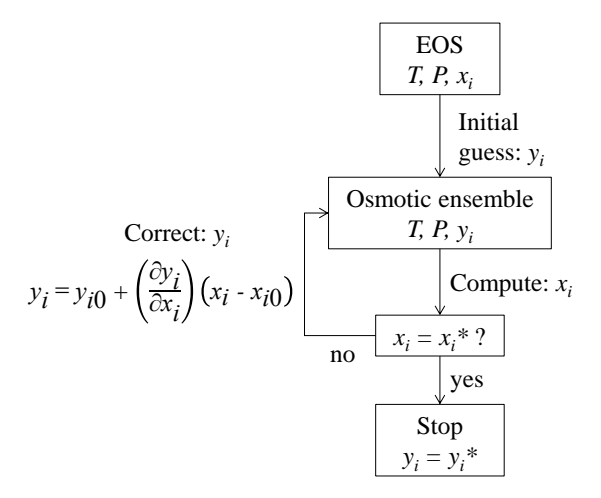


Figure 6.1: Graphical explanation of the procedure used for computing the bubble point of  $\mathrm{CO}_2/\mathrm{CH}_4$  gas mixtures in ILs. The Peng-Robinson (PR) equation of state (EoS) is used to obtain an initial guess for the gas composition,  $y_i$ , by fitting the experimental bubble-point pressure of the  $\mathrm{CO}_2\text{-CH}_4$ -IL system. This initial gas composition is used in the MC simulations in the osmotic ensemble to compute the solubility of the gases  $(x_i)$  in the ILs. In a following step, the computed solubility  $(x_i)$  is compared with the required (experimental) solubility  $(x_i^*)$ . The simulation is stopped once  $x_i \approx x_i^*$  with a tolerance of 0.003, otherwise an additional simulation is performed at constant pressure with a corrected gas composition obtained from Equation (6.7). Using this procedure, one can obtain the gas composition  $(y_i^*)$  that coexist with the experimental liquid composition  $(x_i^*)$ . The PR EoS for the ternary  $\mathrm{CO}_2\text{-CH}_4\text{-IL}$  system is only used to obtain a reasonable initial guess for  $y_i$ , but in principal any value of  $y_i$  can be used in the simulations at an expense of more iterations.

osmotic ensemble was used to compute the solubility of the gases. In this approach, molecules are gradually or fractionally inserted utilizing a coupling parameter  $\lambda$ . The intermolecular (i.e., Lennard-Jones (LJ) and Coulombic) interactions between the "fractional" molecule and the surrounding molecules are scaled with  $\lambda$ . The scaling is such that there is no interaction for  $\lambda=0$ , and for  $\lambda=1$  the conventional LJ and Coulombic interaction potentials are recovered. Slowly inflating the fractional molecule allows the

system to rearrange, which decreases the probability for atomic overlaps and thus increases the efficiency of the simulation [379]. The method has been described in detail by Shi and Maginn [379, 389], and by Dubbeldam et al. [383] and Torres-Knoop et al. [388]. The method has been applied by Shi and Maginn [124, 172, 380] and Ramdin et al. [7, 18, 114, 386] to compute the solubility of several gases in ILs and conventional solvents. An ensemble of 50 and 70 IL molecules was respectively used in the simulations for [bmim][Tf<sub>2</sub>N] and [emim][dep]. These specific numbers of IL ion-pairs were chosen to keep the simulation box always larger than twice the cutoff distance, to dissolve at least one (integer) solute molecule, and to avoid excessively long simulation times that are required for larger systems. A classical force field was used in the simulations for the ILs, which included bond-stretching, bond-bending, torsion, Lennard-Jones and electrostatic interactions. The force field parameters of [bmim][Tf<sub>2</sub>N] and [emim][dep] were taken from Maginn et al. [390, 391]. The TraPPE models were used for CO<sub>2</sub> and CH<sub>4</sub> [392, 393]. The Lennard-Jones (LJ) interactions between different atoms were described by the Lorentz-Berthelot combining rules [385]. The electrostatic interactions were taken into account by the Ewald sum method using a relative precision of  $10^{-5}$  [396]. The LJ interaction was always truncated and shifted at 12 Å and tail corrections were not taken into account. The Configurational-Bias Monte Carlo (CBMC) scheme was used to sample the internal degrees of freedom of the IL molecule [385, 397– 399, 425]. The Wang-Landau sampling scheme was used to bias the  $\lambda$  trial moves, which prevents the system from being stuck in a certain  $\lambda$  state [387]. The CFCMC simulations were started with an equilibration run of 50000 MC cycles, followed by a production run of 0.5 to 1 million cycles. In RASPA, the number of MC steps in a cycle is defined as the total current number of molecules in the system. The simulation is divided into five blocks and the error in the computed properties is obtained from the standard deviation of the block averages. The uncertainty in the solute mole fraction is lower than 0.002, which is lower than the typical uncertainties in experimental data.

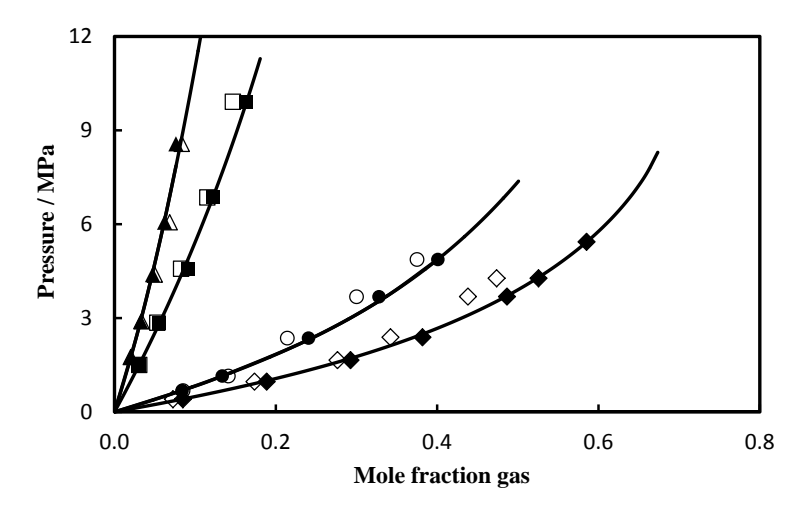


Figure 6.2: Solubility of pure  $CO_2$  and  $CH_4$  in [bmim][Tf<sub>2</sub>N] and [emim][dep] at 313.15 K from experiments (closed symbols) and Monte Carlo simulations (open symbols).  $CO_2$  (diamonds) and  $CH_4$  (squares) in [bmim][Tf<sub>2</sub>N].  $CO_2$  (circles) and  $CH_4$  (triangles) in [emim][dep]. Lines are Peng-Robinson equation of state modeling results [7, 345]. Data taken from Ramdin *et al.* [18, 114].

#### 6.4 Results and Discussion

The CFCMC method in the osmotic ensemble was used to compute the bubble point of CO<sub>2</sub>/CH<sub>4</sub> gas mixtures in [bmim][Tf<sub>2</sub>N] and [emim][dep] at 313.15 K and 333.15 K. In our previous study, the solubility of the pure gases CO<sub>2</sub> and CH<sub>4</sub> in [bmim][Tf<sub>2</sub>N] and [emim][dep] at 313.15 K and 333.15 K was computed from Monte Carlo simulations [7, 114]. The computed isotherms of the pure gases were in quantitative agreement with experimental data measured using the Cailletet technique, see Figure 6.2. Therefore, the MC simulations are expected to yield reasonable results for CO<sub>2</sub>/CH<sub>4</sub> gas mixtures as well. In Table 6.1, the MC simulation results are compared with the experimental data and PR EoS modeling results reported in Ramdin et al. [8]. In the Cailletet experiments, three different gas mixtures

initially containing 25 %  $\rm CO_2$  - 75 %  $\rm CH_4$  (25-75 mixture), 50 %  $\rm CO_2$  - $50 \% \text{ CH}_4 \text{ (50-50 mixture)}, \text{ and } 75 \% \text{ CO}_2 - 25 \% \text{ CH}_4 \text{ (75-25 mixture)}$ were investigated [8]. The given compositions (i.e., 25-75, 50-50, and 75-25) denote only the gas composition at the start of the Cailletet experiment, which changes during the bubble-point measurements due to the operating principle of the Cailletet setup. In our previous experimental study, the gas composition at the bubble point,  $y_{\text{CO}_2}^{\text{PR}}$  in Table 6.1, was estimated from the PR EoS by fitting the experimental bubble-point pressure [8]. In our MC simulations, the composition of the gas phase is obtained iteratively by substitution of Equation (6.6) into Equation (6.7). The method is illustrated in Figure 6.3 at a pressure of 1.97 MPa and 313.15 K, for the first data point in Table 6.1, using three different gas compositions. Similar diagrams can be constructed for the other solutes in a multicomponent system. Note that for the ternary system CO<sub>2</sub>-CH<sub>4</sub>-IL, it is not necessary to draw a diagram for CH<sub>4</sub>, since the gas-phase composition of CH<sub>4</sub> can be obtained from the constraint  $y_{\text{CH}_4} = (1 - y_{\text{CO}_2})$ . In this way, the gas composition can be determined from a given bubble-point pressure and liquid composition. Clearly, the gas composition obtained from the MC simulations  $(y_{\text{CO}_2}^{\text{sim.}})$  and the PR EoS modeling  $(y_{\text{CO}_2}^{\text{PR}})$  are very similar for the 25-75, and 50-50 gas mixture, while a slight deviation is observed for the 75-25 gas mixture. The fit of the bubble-point pressure of the 75-25 gas mixture by the PR EoS was not perfect, see Ramdin et al. [8] for the modeling results. Therefore, the gas composition obtained from the PR EoS is unreliable for the 75-25 gas mixture. Subsequently, the real CO<sub>2</sub>/CH<sub>4</sub> selectivity is calculated from Equation (4.1). The ideal selectivity, which is defined in Equation (3.7) as the ratio of the Henry constants, is also reported in Table 6.1. The real selectivity is approximately the same as the ideal selectivity, which suggests that there is no enhancement of the solubility of one gas due to the presence of the other gas species. In Table 6.1, the bubble-point pressure of the system  $CO_2+CH_4+[bmim][Tf_2N]$  predicted by Equation (6.5) is presented. The predicted bubble-point pressures are in excellent agreement with the experimental data for pressures up to 30 bar. At higher pressures, the predictions are less accurate, which is a consequence of neglecting nonidealities

Table 6.1: Bubble-point compositions of the system  $CO_2 + CH_4 + [bmim][Tf_2N]$  obtained from MC simulations (sim.) and Peng-Robinson (PR) equation of state at a given temperature (T) and bubble-point pressure  $(P^{\mathrm{exp.}})$ .  $P^{\mathrm{pred.}}$  is the bubble-point pressure predicted by Equation (6.5). The gas composition  $(y_i)$ , which is in equilibrium with the experimental liquid composition  $(x_i)$ , is obtained from Equation (6.7). Real and ideal selectivities are obtained from Equation (4.1) and Equation (3.7), respectively. The Henry constants of  $CO_2$  in  $[bmim][Tf_2N]$  at 313.15 K and 333.15 K computed from the MC data are 5.4 MPa and 7.1 MPa, respectively [114]. The Henry constants of  $CH_4$  in  $[bmim][Tf_2N]$  at 313.15 K and 333.15 K computed from the MC data are 50.7 MPa and 53.7 MPa, respectively [114]. The experimental Henry constants of  $CO_2$  ( $CH_4$ ) in  $[bmim][Tf_2N]$  at 313.15 K and 333.15 K are 4.9 MPa (49.3 MPa), and 6.6 MPa (52.4 MPa), respectively [370, 371].

T/K	$x_{\rm CO_2}$	$x_{\mathrm{CH_4}}$	$P^{\exp}$ ./MPa	$P^{\mathrm{pred.}}/\mathrm{MPa}$	$y_{\mathrm{CO}_2}^{\mathrm{PR}}$	$y_{\mathrm{CO}_2}^{\mathrm{sim.}}$	$S_{\mathrm{CO}_2/\mathrm{CH}_4}^{\mathrm{R}}$	$S_{\mathrm{CO}_2/\mathrm{CH}_4}^{\mathrm{I}}$
$313.15^{a}$	0.014	0.04	1.970	2.040	0.034	0.035	9.5	9.4
$313.15^{a}$	0.037	0.11	6.322	5.603	0.036	0.037	8.8	9.4
$313.15^{b}$	0.04	0.039	2.088	2.117	0.092	0.099	9.3	9.4
$313.15^{b}$	0.103	0.102	6.560	5.529	0.097	0.108	8.4	9.4
$313.15^{c}$	0.108	0.037	2.408	2.349	0.217	0.250	8.7	9.4
$313.15^{c}$	0.189	0.064	4.855	4.073	0.221	0.266	8.2	9.4
$333.15^{a}$	0.014	0.04	2.147	2.189	0.043	0.047	7.1	7.6
$333.15^{a}$	0.037	0.11	6.847	6.011	0.044	0.048	6.7	7.6
$333.15^{b}$	0.04	0.039	2.302	2.308	0.114	0.127	7.0	7.6
$333.15^{b}$	0.103	0.102	7.220	6.025	0.119	0.134	6.5	7.6
$333.15^{c}$	0.108	0.037	2.755	2.649	0.263	0.306	6.6	7.6
$333.15^{c}$	0.189	0.064	5.578	4.596	0.269	0.316	6.4	7.6

<sup>&</sup>lt;sup>a</sup> 25-75 gas mixture was used in the Cailletet experiments

in Equation (6.5). As it becomes evident from Equation (6.4), the deviation is caused either by nonidealities in the gas phase (i.e.,  $\phi_i \neq 1$ ) or by nonidealities in the liquid phase (i.e.,  $\gamma_i \neq 1$ ). The deviation is likely caused by non-idealities in the gas phase, since the liquid phase mole fractions of  $CO_2$  and  $CH_4$  are rather low. The concentration of  $CO_2$  in our experiments was kept relatively low in order to dissolve a certain predefined amount of  $CH_4$  in the IL (i.e., the  $CH_4/IL$  molar ratio was fixed), see Ramdin *et al.* [8] for the experimental details. It is, therefore, possible that ideal  $CO_2/CH_4$  selectivities are observed due to the low  $CO_2$  concentrations in the liquid

<sup>&</sup>lt;sup>b</sup> 50-50 gas mixture was used in the Cailletet experiments

<sup>&</sup>lt;sup>c</sup> 75-25 gas mixture was used in the Cailletet experiments

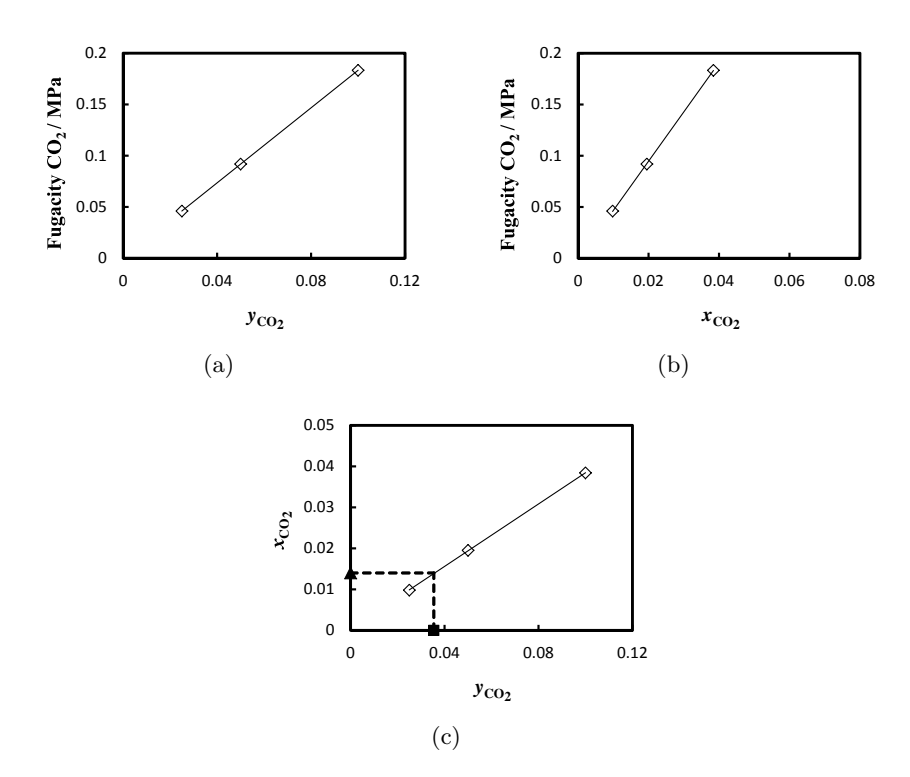


Figure 6.3: (a) Fugacity of  $CO_2$  as a function of  $CO_2$  composition at a constant pressure of 1.970 MPa and 313.15 K calculated with the PR EoS. (b) The solubility of  $CO_2$  in [bmim][Tf<sub>2</sub>N] computed with MC simulations in the osmotic ensemble at  $CO_2$  fugacities corresponding to Figure 6.3(a). (c) Combination of Figures 6.3(a) and 6.3(b) results in a x-y plot (diamonds), which allows the determination of the gas phase composition ( $y_{CO_2}$ , square) at a given liquid composition ( $x_{CO_2}$ , triangle) using Equation (6.7).

phase. We have used MC simulations in the osmotic ensemble to investigate the effect of  $CO_2$  concentration in the liquid phase on the  $CO_2/CH_4$  selectivity, see Table 6.2 and Figure 6.4. The following can be concluded from Tables 6.1 and 6.2 and Figure 6.4: (1) the selectivity decreases with increasing temperature and pressure, (2) the gas composition has only a minor effect on the selectivity, (3) the ideal selectivity is observed for rela-

Table 6.2:  $\mathrm{CO_2/CH_4}$  solubilities and selectivities in [bmim][Tf<sub>2</sub>N] from MC simulations in the osmotic ensemble at a given T, P, and  $y_i$ . The experimental Henry constants of  $\mathrm{CO_2}$  and  $\mathrm{CH_4}$  in [bmim][Tf<sub>2</sub>N] at 313.15 K are 4.9 MPa and 49.3 MPa, respectively [370, 371]. The Henry constants of  $\mathrm{CO_2}$  and  $\mathrm{CH_4}$  in [bmim][Tf<sub>2</sub>N] at 313.15 K computed from the MC data are 5.4 MPa and 50.7 MPa, respectively [18, 114]. The ideal  $\mathrm{CO_2/CH_4}$  selectivities computed from the experiments and MC data as a ratio of the Henry constants are 10.1 and 9.5, respectively.

CD /T.	D /3.5D					αD
T/K	$P/\mathrm{MPa}$	$y_{\rm CO_2}$	$y_{\mathrm{CH_4}}$	$x_{\rm CO_2}$	$x_{\mathrm{CH_4}}$	$S_{\mathrm{CO}_2/\mathrm{CH}_4}^{\mathrm{R}}$
313.15	2.5	0.25	0.75	0.111	0.033	10.0
313.15	5.0	0.25	0.75	0.183	0.056	9.7
313.15	7.5	0.25	0.75	0.230	0.073	9.4
313.15	10.0	0.25	0.75	0.263	0.087	9.1
313.15	2.5	0.50	0.50	0.204	0.020	10.0
313.15	5.0	0.50	0.50	0.317	0.033	9.7
313.15	7.5	0.50	0.50	0.384	0.042	9.2
313.15	10.0	0.50	0.50	0.425	0.050	8.6
313.15	2.5	0.75	0.25	0.284	0.009	10.0
313.15	5.0	0.75	0.25	0.421	0.015	9.5
313.15	7.5	0.75	0.25	0.495	0.019	8.7
313.15	10.0	0.75	0.25	0.534	0.024	7.6

tively low pressures and low CO<sub>2</sub> concentrations in the liquid phase, (4) the real selectivity deviates from the ideal selectivity for relatively high CO<sub>2</sub> concentrations in the liquid phase. Recently, Budhathoki *et al.* [426] used Gibbs ensemble Monte Carlo simulations to compute CO<sub>2</sub>/CH<sub>4</sub> selectivities in [bmim][Tf<sub>2</sub>N]. These authors also observed ideal selectivity for low CO<sub>2</sub> concentrations in the liquid phase, but the selectivity was shown to decrease for relatively high CO<sub>2</sub> concentrations. This is in agreement with our simulation results.

In Table 6.3, the MC results for the system CO<sub>2</sub>-CH<sub>4</sub>-[emim][dep] are presented. Similar conclusions can be drawn for this system, i.e., the real selectivity decreases with increasing temperature and pressure, but the pressure effects are quite small. The real selectivity is approximately the same as the ideal selectivity for low pressures and low solute concentrations in the liquid phase. At higher CO<sub>2</sub> concentrations, the real selectivity starts to deviate from the ideal selectivity. This is not unexpected, because

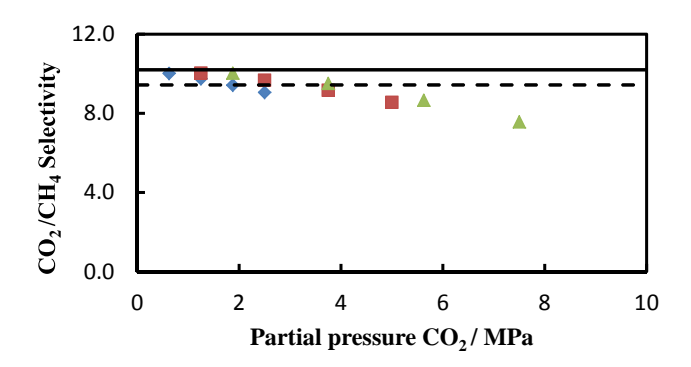


Figure 6.4: Effect of the  $CO_2$  partial pressure on the real  $CO_2/CH_4$  selectivity in [bmim][Tf<sub>2</sub>N] at 313.15 K. 25-75 gas mixture (diamonds), 50-50 gas mixture (squares), and 75-25 gas mixture (triangles). The ideal selectivity computed from MC data (dashed line) and from experiments (solid line) are included.

the definition of the ideal selectivity (Equation (3.7)) does not account for the nonidealities in the mixture. Hert  $et\ al.$  [168] measured the simultaneous solubility of  $\mathrm{CO}_2$  and  $\mathrm{CH}_4$  in the IL 1-hexyl-3-methylimidazolium bis(trifluoromethylsulfonyl)imide [hmim][Tf<sub>2</sub>N]. These authors observed an enhancement of  $\mathrm{CH}_4$  solubility in the presence of  $\mathrm{CO}_2$  by more than 200 %, relative to the pure gas solubility at similar conditions. Nonidealities of this proportion are very unlikely to occur, since the experiments of Hert  $et\ al.$  were performed at relatively low pressures (up to 17 bar) and the liquid phase mole fractions of  $\mathrm{CO}_2$  and  $\mathrm{CH}_4$  were lower than 0.1. Therefore, the data of Hert  $et\ al.$  should be treated with caution until substantiated further [113].

The above outlined method to compute bubble-points at a given temperature and liquid composition deserves some discussion. For example, two simulations were used to evaluate  $(\partial f_i/\partial x_i)$  in Equation (6.6). However, providing a poor initial guess for the gas composition will require more than two independent simulations in order to accurately evaluate Equation (6.7). An educated guess for the gas composition can always be obtained from an

Table 6.3:  $\mathrm{CO_2/CH_4}$  solubilities and selectivities in [emim][dep] from MC simulations in the osmotic ensemble at a given T, P, and  $y_i$ . The Henry constants of  $\mathrm{CO_2}$  in [emim][dep] at 313.15 K and 333.15 K computed from the MC data are 7.7 MPa and 11.7 MPa, respectively [114]. The Henry constants of  $\mathrm{CH_4}$  in [emim][dep] at 313.15 K and 333.15 K computed from the MC data are 81.6 MPa and 103.0 MPa, respectively [114].

T/K	P/MPa	$y_{\rm CO_2}$	$y_{\mathrm{CH}_4}$	$x_{\text{CO}_2}$	$x_{\mathrm{CH}_4}$	$S_{\mathrm{CO}_2/\mathrm{CH}_4}^{\mathrm{R}}$
313.15	2.5	0.25	0.75	0.079	0.021	11.1
313.15	5.0	0.25	0.75	0.123	0.038	9.8
313.15	7.5	0.25	0.75	0.152	0.051	8.9
333.15	2.5	0.25	0.75	0.051	0.018	8.7
333.15	5.0	0.25	0.75	0.091	0.031	8.7
333.15	7.5	0.25	0.75	0.121	0.042	8.6
313.15	2.5	0.5	0.5	0.135	0.014	9.8
313.15	5.0	0.5	0.5	0.203	0.024	8.5
313.15	7.5	0.5	0.5	0.254	0.032	8.0
333.15	2.5	0.5	0.5	0.099	0.011	8.6
333.15	5.0	0.5	0.5	0.169	0.020	8.4
333.15	7.5	0.5	0.5	0.219	0.027	8.2
313.15	2.5	0.75	0.25	0.180	0.007	9.0
313.15	5.0	0.75	0.25	0.295	0.011	8.8
313.15	7.5	0.75	0.25	0.367	0.015	8.2
333.15	2.5	0.75	0.25	0.143	0.006	8.5
333.15	5.0	0.75	0.25	0.237	0.010	8.2
333.15	7.5	0.75	0.25	0.300	0.013	7.7

equation of state provided that the bubble-point pressure of the mixture is known. In practice, bubble-point pressure measurements of multicomponent mixtures are much easier to perform compared to the more elaborate sampling experiments. Typically, the gas composition is then obtained by fitting the bubble-point pressure with a suitable equation of state. Alternatively, Monte Carlo simulations as outlined here can be used to compute gas compositions from a known bubble-point pressure.

6.5 Conclusion 141

## 6.5 Conclusion

Practical processes often require separation of multicomponent mixtures to obtain the final product. Solubility and selectivity data are required to evaluate the separation performance of a process and to design proper separation units. The real selectivity of a solvent for a specific solute in a multicomponent mixture can be obtained by sampling the composition of the phases in an experiment. However, sampling and subsequent analysis of the phases is an elaborate task. Therefore, one often prefers to measure the bubble-point pressure of the multicomponent mixture and apply an equation of state to compute the gas phase compositions required for the selectivity analysis. Here, we outline a method to compute the gas composition from a known bubble-point pressure using Monte Carlo simulations. MC simulations in the osmotic ensemble are used to compute the solubility of  $CO_2$ - $CH_4$  gas mixtures in the ILs [bmim][Tf<sub>2</sub>N] and [emim][dep]. The composition of the gas is derived iteratively from the liquid composition by performing two separate simulations in the osmotic ensemble at the same pressure, but different gas compositions. The composition of the gas that is in equilibrium with the experimental liquid composition is then approximated by a first-order Taylor expansion. The method is applied to compute the gas composition of the ternary system  $CO_2+CH_4+[bmim][Tf_2N]$  using the experimental bubble-point pressure. The gas compositions obtained from the Monte Carlo simulation are compared with gas compositions predicted by the Peng-Robinson equation of state modeling. Both methods yield similar gas compositions. Subsequently, the real CO<sub>2</sub>/CH<sub>4</sub> selectivity in [bmim][Tf<sub>2</sub>N] and [emim][dep] is computed and compared with the ideal selectivity, which is defined as the ratio of the Henry constant of CH<sub>4</sub> over that of  $CO_2$ . The real selectivity is approximately the same as the ideal selectivity for pressures up to 30 bar and for liquid phase solute mole fractions up to 0.3. At higher pressures and higher solute concentrations the real selectivity starts to deviate from the ideal selectivity. The gas composition has only a minor effect on the real selectivity.

## Chapter 7

# Solubility of Pre-combustion Gases from Monte Carlo Simulations

This Chapter is based on the paper: M. Ramdin, S. P. Balaji, J. M. Vicent-Luna, J. J. Gutiérrez-Sevillano, S. Calero, T. W. de Loos and T. J. H. Vlugt. Solubility of the Precombustion Gases  $CO_2$ ,  $CH_4$ , CO,  $H_2$ ,  $N_2$ , and  $H_2S$  in the Ionic Liquid [bmim][Tf<sub>2</sub>N] from Monte Carlo Simulations. J. Phys. Chem. C, 118 (2014) 23599-23604.

## 7.1 Introduction

The previous chapters focused on the application potential of ILs for  $CO_2$  capture in the natural gas sweetening process. In this chapter, the potential of ILs for  $CO_2$  capture in the pre-combustion process is investigated. The pre-combustion process involves a reaction of the fuel with air/oxygen and steam to produce syngas, which is a mixture of carbon monoxide (CO) and hydrogen (H<sub>2</sub>). In the case of natural gas as fuel, the syngas is produced

via the steam-reforming reaction [6]:

$$CH_4 + H_2O \Longrightarrow CO + 3H_2$$
 (R1)

In a next step, the CO is converted according to the water-gas-shift (WGS) reaction to  $CO_2$  and more  $H_2$ :

$$CO + H_2O \Longrightarrow CO_2 + H_2$$
 (R2)

After separating the CO<sub>2</sub> from H<sub>2</sub>, the hydrogen-rich fuel can be used in many applications like gas turbines for electricity production, engines, fuel cells, and chemical synthesis such as ammonia, methanol and Fischer-Tropsch fuels [4]. The advantage of pre-combustion CO<sub>2</sub> capture is the relatively high partial pressure of CO<sub>2</sub> after the WGS reaction allowing for less expensive separation methods including physical absorption/adsorption and membranes [427, 428]. Several existing solvents (e.g., amines, Selexol and Rectisol) and new materials (e.g., zeolites and metal-organic frameworks (MOFs)) have been considered for pre-combustion CO<sub>2</sub> capture [429–432]. The reader is referred to the recent work of Liu et al. [4] for an excellent state-of-the-art review of technologies used for hydrogen/syngas production and purification.

The focus of this chapter is the separation of CO<sub>2</sub> from syngas, either before or after the WGS reaction, using the IL 1-butyl-3-methylimidazolium bis(trifluoromethylsulfonyl)imide [bmim][Tf<sub>2</sub>N]. The equilibrium reactions (R1) and (R2) yield a mixture of reactants and products, which will require a separation step downstream of the process. The relevant separation selectivities are CO<sub>2</sub>/CH<sub>4</sub>, CO<sub>2</sub>/CO, CO<sub>2</sub>/H<sub>2</sub>, CO<sub>2</sub>/N<sub>2</sub> if air instead of pure oxygen is used, and CO<sub>2</sub>/H<sub>2</sub>S if the syngas is not desulfurized prior to CO<sub>2</sub> removal. The selectivity of one gas over the other can be calculated from solubility data of the corresponding gases in the IL. Unfortunately, solubility data of sparingly soluble gases (e.g., H<sub>2</sub>, N<sub>2</sub> and CH<sub>4</sub>) or toxic gases (e.g., CO and H<sub>2</sub>S) are scarcely reported in the literature. An alternative tool for these difficult to conduct experiments is provided by means of molecular simulations. Here, Monte Carlo simulations using a classical force field have been used to predict the solubility of the gases CO<sub>2</sub>, CH<sub>4</sub>, CO, H<sub>2</sub>, N<sub>2</sub>

and H<sub>2</sub>S in the IL [bmim][Tf<sub>2</sub>N] and whenever possible a comparison with experimental data is provided.

## 7.2 Simulation Details

The recently developed Continuous Fractional Component Monte Carlo (CFCMC) method in the osmotic ensemble has been used to compute absorption isotherms of the pre-combustion gases CH<sub>4</sub>, CO<sub>2</sub>, CO, H<sub>2</sub>, N<sub>2</sub>, and H<sub>2</sub>S in the IL [bmim][Tf<sub>2</sub>N] [379, 380]. A brief description of the CFCMC method can be found in Chapter 5 and for more details the reader is referred to the original publication by Shi and Maginn and the recent work by Torres-Knoop *et al.* [379, 383, 388].

A classical force field including bond-stretching, bond-bending, torsion, Lennard-Jones and electrostatic interactions was used for the IL molecules in our simulations. The force field parameters for the IL [bmim][Tf<sub>2</sub>N] have been taken from Liu and Maginn [390]. The molecular models used for the gases contain one or more LJ interaction sites with or without partial charges and/or dipoles. All the gases have been treated as rigid in the simulations. The standard TraPPE model was used for the gases CH<sub>4</sub>, CO<sub>2</sub> and  $N_2$  [392]. The CO model, which includes a dipole moment, has been adopted from Martín-Calvo et al. [433]. For H<sub>2</sub>, the two-center LJ model of Cracknell has been applied [434]. For  $H_2S$ , three different models have been used; the three-site (3S) model of Kamath et al. [435], the four-site (4S) model of Kristóf and Lizi [436], and the five-site (5S) model of Gutiérrez-Sevillano et al. [437]. The Lorentz-Berthelot mixing rules were adopted for the LJ interactions between unlike atoms [396]. The values of all force field parameters are listed in the Supporting Information of Ref. [7]. The Ewald method with a relative precision of  $10^{-5}$  was applied to account for the long range electrostatic interactions. The LJ interactions were truncated and shifted at 12 A and no tail corrections were applied. All the simulations were performed in the osmotic ensemble, see Chapter 5 for more details. The fugacity of the gases was obtained from the Peng-Robinson (PR) equation of state (EoS) [340]. The  $\lambda$  moves were biased using the Wang-Landau

sampling scheme, which enforces the system to visit all the possible  $\lambda$  states and to achieve a flat histogram for  $\lambda$  [387]. The configurational-bias Monte Carlo (CBMC) scheme was used to sample the internal degrees of freedom of the IL molecules [385, 397–399].

The CFCMC simulations were executed at a temperature of 333.15 K using an ensemble of 50 IL molecules. All the MC simulations were performed using the molecular simulation tool RASPA [401]. In order to reduce the simulation time, however, the IL structure was first equilibrated using Molecular Dynamics (MD) simulations in GROMACS [438, 439]. After an energy minimization step, an ensemble of 50 IL molecules were simulated for 2 ns in the NPT ensemble. In a subsequent step, the atomic positions and velocities of the equilibrated ensemble were transferred to RASPA to perform the actual CFCMC simulations. The CFCMC simulations were started with an equilibration run of 50000 MC cycles, where the number of MC steps in a cycle equals the total number of molecules in the simulation box. In this equilibration run, the weights of the various MC moves are adjusted to obtain 50 % acceptance rates. The production runs consisted of 0.5 to 1 million cycles, where the exact number was dictated by the convergence characteristics of the system. The reported data were obtained from block averages, and the standard deviation was used to calculate the uncertainty.

### 7.3 Results and Discussion

## 7.3.1 Solubility

The solubility of CO<sub>2</sub>, CH<sub>4</sub>, CO, H<sub>2</sub>, N<sub>2</sub> and H<sub>2</sub>S in the IL [bmim][Tf<sub>2</sub>N] was obtained from MC simulations in the osmotic ensemble at a temperature of 333.15 K and pressures up to 15 MPa. In Figure 7.1 and Tables 7.1 to 7.4, the solubility of CO<sub>2</sub>, CH<sub>4</sub>, CO and H<sub>2</sub> obtained from the MC simulations is, respectively, compared with the experimental data of Raeissi et al. [370, 371, 440, 441]. The experimental uncertainty is typically 0.003 in the mole fractions, whereas the uncertainty in the simulations is typically lower than 0.002 in the mole fractions (i.e., smaller than the symbol size).

Table 7.1: Solubility of  $CO_2$  (1) in the IL [bmim][Tf<sub>2</sub>N] (2) at a temperature of 333.15 K and different pressures.

$p/\mathrm{MPa}$	$x_1^{\text{exp.}}$	$x_1^{\text{sim.}}$	difference/%
0.569	0.085	0.082	3.3
1.373	0.189	0.182	3.7
2.392	0.293	0.278	4.8
3.469	0.382	0.361	5.3
5.396	0.487	0.462	5.0
6.159	0.526	0.495	5.8
7.908	0.585	0.550	6.1

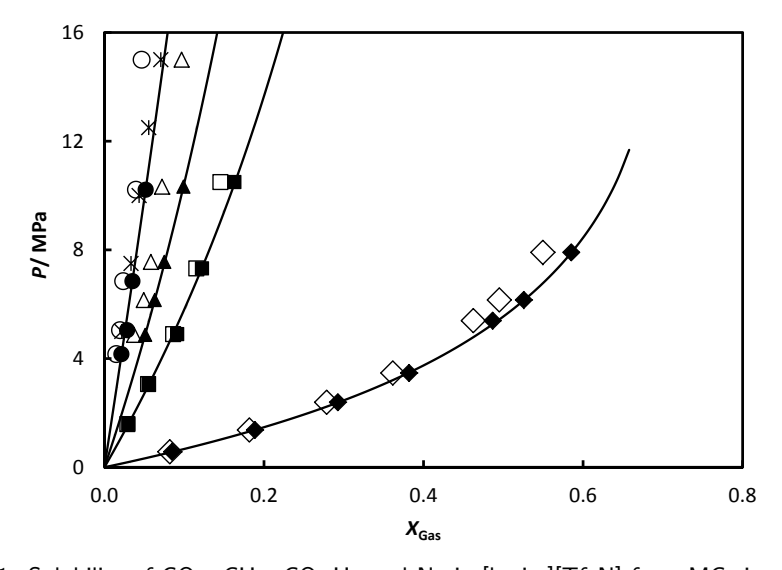


Figure 7.1: Solubility of CO<sub>2</sub>, CH<sub>4</sub>, CO, H<sub>2</sub> and N<sub>2</sub> in [bmim][Tf<sub>2</sub>N] from MC simulations (open symbols) and experiments (filled symbols) at a temperature of 333.15 K. CO<sub>2</sub> experiments (filled diamonds) and MC data (open diamonds); CH<sub>4</sub> experiments (filled squares) and MC data (open squares); CO experiments (filled triangles) and MC data (open triangles); H<sub>2</sub> experiments (filled cricles) and MC data (open circles), and MC data of N<sub>2</sub> (stars). Lines are Peng-Robinson equation of state modeling results [8, 340].

Table 7.2: Solubility of  $CH_4$  (1) in the IL [bmim][Tf<sub>2</sub>N] (2) at a temperature of 333.15 K and different pressures.

$p/\mathrm{MPa}$	$x_1^{\text{exp.}}$	$x_1^{\text{sim.}}$	difference/%
1.591	0.030	0.029	3.8
3.063	0.056	0.055	1.5
4.900	0.091	0.086	5.6
7.320	0.122	0.115	5.9
10.497	0.163	0.145	10.7

Table 7.3: Solubility of CO (1) in the IL [bmim][ $Tf_2N$ ] (2) at a temperature of 333.15 K and different pressures.

$p/\mathrm{MPa}$	$x_1^{\text{exp.}}$	$x_1^{\text{sim.}}$	difference/%
4.871	0.051	0.037	27.1
6.153	0.063	0.049	21.8
7.558	0.075	0.058	22.4
10.326	0.099	0.072	27.1
15.000	-	0.097	-

Table 7.4: Solubility of  $H_2$  (1) in the IL [bmim][Tf<sub>2</sub>N] (2) at a temperature of 333.15 K and different pressures.

$p/\mathrm{MPa}$	$x_1^{\text{exp.}}$	$x_1^{\text{sim.}}$	difference/%
4.167	0.0212	0.015	30.3
5.047	0.0283	0.019	31.3
6.849	0.035	0.023	33.0
10.216	0.0516	0.039	23.7
15.000	-	0.047	-

The uncertainty of the simulations will only be reported if this is higher than the experimental uncertainty. The MC simulations slightly underpredict the solubility of CO and  $H_2$ , but the agreement is excellent for the gases  $CO_2$  and  $CH_4$  even at higher pressures. The simulation results for  $N_2$  solubility in [bmim][Tf<sub>2</sub>N] are reported in Table 7.5 and depicted in Figure 7.1. For the  $N_2$  system no experimental data has been reported, but the predicted solubilities are in between that of  $H_2$  and CO, which is

Table 7.5: Solubility of  $N_2$  (1) in the IL [bmim][Tf<sub>2</sub>N] (2) at a temperature of 333.15 K and different pressures.

$p/\mathrm{MPa}$	$x_1^{\text{sim.}}$
5.00	0.022
7.50	0.033
10.00	0.043
12.50	0.056
15.00	0.071

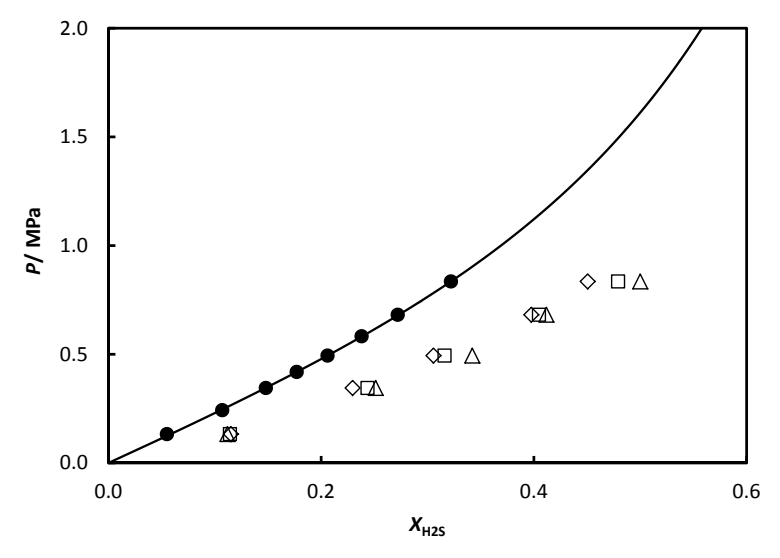


Figure 7.2: Solubility of  $H_2S$  in [bmim][ $Tf_2N$ ] at a temperature of 333.15 K. Experiments (filled circles) and MC data: 3S  $H_2S$  model (open squares), 4S  $H_2S$  model (open diamonds) and 5S  $H_2S$  model (open triangles). Line is Peng-Robinson equation of state modeling result [8, 340].

consistent with the trend observed in other ILs [9, 123, 157, 158]. The H<sub>2</sub>S solubilities obtained from MC simulations using the three different H<sub>2</sub>S models are compared with the experimental data of Jalili *et al.* [442] in Figure 7.2 and Table 7.6. The MC simulations highly overpredict the H<sub>2</sub>S solubility, regardless of the used H<sub>2</sub>S model, compared to the experimental

 $x_1^{\text{sim.}}$  $H_2S$  model difference/% p/MPa $\overline{\mathrm{H}_2\mathrm{S}^a}$ 0.1330.055109.2 0.11555.1 0.3450.1480.23048.3 0.4940.2060.3060.6820.27246.20.3980.8350.3220.45139.9 $H_2S^b$ 0.133 0.0550.114 107.70.2440.3450.14864.60.4940.2060.31653.40.6820.2720.40548.8 0.8350.3220.47948.8 $H_2S^c$ 0.1330.0550.112103.50.3450.1480.25169.80.4940.2060.34266.10.6820.2720.41251.4

0.500

55.3

Table 7.6: Solubility of  $H_2S$  (1) in the IL [bmim][Tf<sub>2</sub>N] (2) at a temperature of 333.15 K and different pressures.

0.835

0.322

data of Jalili et al. The 3S model of Kamath et al. and the 4S model of Kristóf and Lizi are slightly in better agreement with the experimental data than the 5S model of Gutiérrez-Sevillano et al. Differences can be attributed to the used force field, but the simulation results are acceptable considering that none of the interaction parameters used in this study were fitted to the experimental solubility data of [bmim][Tf<sub>2</sub>N]. Moreover, the MC simulations correctly predict the experimental solubility trend, which obeys the following order:  $H_2S > CO_2 > CH_4 > CO > N_2 > H_2$ . These results show that molecular simulation is a promising tool for predicting gas solubilities in complex systems like ionic liquids.

<sup>&</sup>lt;sup>a</sup> Three-site model of Kamath *et al.* [435].

<sup>&</sup>lt;sup>b</sup> Four-site model of Kristóf and Lizi [436].

<sup>&</sup>lt;sup>c</sup> Five-site model of Gutiérrez-Sevillano et al. [437].

solute	$H_{\rm Selexol}^{\rm exp.}/{ m MPa}$	$H_{ m IL}^{ m exp.}/{ m MPa}$	$H_{ m IL}^{ m sim.}/{ m MPa}$	difference/%
$\overline{\mathrm{CO}_2}$	$6.81^{a}$	6.56	7.10	8.2
$\mathrm{CH}_4$	$40.13^{a}$	52.4	53.7	2.5
CO	-	95	125.9	33.0
$\mathrm{H}_2$	$193^{b}$	199	271.7	36.3
$N_2$	$151^{b}$	-	225.7	-
$H_2S$ (3S)	$1.01^{c}$	2.17	1.15	47.0
$H_2S$ (4S)	1.01	2.17	1.16	46.5
$H_2S$ (5S)	1.01	2.17	1.17	46.1

Table 7.7: Henry constants of  $CO_2$ ,  $CH_4$ , CO,  $H_2$ ,  $N_2$ , and  $H_2S$  in Selexol and the IL [bmim][Tf<sub>2</sub>N] at a temperature of 333.15 K.

## 7.3.2 Selectivity

The separation performance of a real process is not governed by the solubility, but the key parameter is the selectivity of a target component with respect to the other components in the mixture [8, 345]. This means that a good solvent for CO<sub>2</sub> capture at pre-combustion conditions should have a high  $CO_2$  solubility, but at the same time a low capacity for the other gases (e.g.  $CH_4$ ). The ideal selectivity can be calculated in many different ways from the pure gas solubility data [345]. Here, the ratio of the Henry constants is used to quantify the ideal selectivity  $(S_{i/i}^{I})$ , where i is the target component and j the undesired component, see Equation (3.7). The Henry constants of the solutes i in the solvent j,  $[bmim][Tf_2N]$ , are calculated from Equation (3.8). The Henry constants derived from the MC data are compared with the experimental data in Table 7.7. The agreement between the MC data and the experiments is excellent for the gases CO<sub>2</sub> and CH<sub>4</sub>. For the other gases the absolute deviation between the predicted and experimental Henry constants can be as high as 40%. However, the sparingly soluble gases (CO,  $H_2$  and  $N_2$ ) are generally difficult to measure and consequently the uncertainty in the experimental Henry constant is

<sup>&</sup>lt;sup>a</sup> Taken from Rayer *et al.* [354, 355].

<sup>&</sup>lt;sup>b</sup> Calculated from Gainar et al. [443].

<sup>&</sup>lt;sup>c</sup> Taken from Xu et al. [263].

separation	$S_{ m Selexol}^{ m exp.}$	$S_{ m IL}^{ m exp.}$	$S_{ m IL}^{ m sim.}$	difference/%
$CO_2/CH_4$	$5.9^{a}$	8.0	7.6	5.3
$CO_2/CO$	-	14.4	17.7	23.0
$CO_2/H_2$	$25^{b}$	30.4	38.3	26.0
$\rm CO_2/N_2$	$20^{b}$	-	31.8	-
$\mathrm{CO_2/H_2S}$	$0.15^{c}$	0.33	0.16	51.0
$CO_2/H_2S$	0.15	0.33	0.16	50.6

0.33

0.16

50.2

Table 7.8: Selectivity of  $CO_2$ ,  $CH_4$ , CO,  $H_2$ ,  $N_2$ , and  $H_2S$  in Selexol and the IL [bmim][Tf<sub>2</sub>N] at a temperature of 333.15 K.

0.15

 $CO_2/H_2S$ 

often large (e.g. in some cases up to 50%) [9]. The relevant selectivities for the pre-combustion process were calculated using Equation (3.7) and are compared with experimental data in Table 7.8. The absolute deviation between the predicted and experimental selectivities are of the same order as for the Henry constants. It is important to note that the high CO<sub>2</sub>/CH<sub>4</sub>, CO<sub>2</sub>/CO, CO<sub>2</sub>/N<sub>2</sub> and CO<sub>2</sub>/H<sub>2</sub> selectivities indicate a great potential of [bmim][Tf<sub>2</sub>N] for CO<sub>2</sub> removal from the pre-combustion process. However, the syngas should be desulfurized before the CO<sub>2</sub> removal step, because CO<sub>2</sub> can not be removed selectively in the presence of H<sub>2</sub>S. A comparison of the Henry constants and the selectivities of the gases in [bmim][Tf<sub>2</sub>N] and the widely used solvent Selexol is provided in Table 7.7 and Table 7.8, respectively. Clearly, the Henry constants and the selectivities in both solvents are very similar, hence considering the price/performance ratio the Selexol solvent outperforms the costly IL [bmim][Tf<sub>2</sub>N].

<sup>&</sup>lt;sup>a</sup> Calculated from Rayer et al. [354, 355].

<sup>&</sup>lt;sup>b</sup> Calculated from Gainar et al. [443].

<sup>&</sup>lt;sup>c</sup> Calculated from Xu et al. [263].

7.4 Conclusions 153

## 7.4 Conclusions

Monte Carlo simulations were used to predict the solubility of the single gases CO<sub>2</sub>, CH<sub>4</sub>, CO, H<sub>2</sub>, N<sub>2</sub> and H<sub>2</sub>S in the ionic liquid (IL) 1-butyl-3-methylimidazolium bis(trifluoromethylsulfonyl)imide [bmim][Tf<sub>2</sub>N]. Simulations in the osmotic ensemble were performed to compute absorption isotherms at a temperature of 333.15 K using the versatile continuous fractional component Monte Carlo (CFCMC) method. The predicted gas solubilities and Henry constants are in good agreement with the experimental data. The MC simulations correctly predict the observed solubility trend, which obeys the following order:  $H_2S > CO_2 > CH_4 > CO > N_2 > H_2$ . The CO<sub>2</sub>/CH<sub>4</sub>, CO<sub>2</sub>/CO, CO<sub>2</sub>/N<sub>2</sub>, CO<sub>2</sub>/H<sub>2</sub> and CO<sub>2</sub>/H<sub>2</sub>S selectivities relevant for the pre-combustion CO<sub>2</sub> capture process were calculated from the ratio of pure gas Henry constants. The results indicate that  $[bmim][Tf_2N]$  can effectively capture CO<sub>2</sub> at pre-combustion conditions, but the syngas should be desulfurized prior to CO<sub>2</sub> removal, because H<sub>2</sub>S is three times more soluble than CO<sub>2</sub>. Moreover, we have shown that molecular simulations can be used to predict gas solubilities in complex systems like ionic liquids.

## Chapter 8

# Monte Carlo Simulations of CO<sub>2</sub> and Monoethanolamine

This chapter is based on the paper: S. P. Balaji, S. Gangarapu, M. Ramdin, A. Torres-Knoop, H. Zuilhof, E. L. V. Goetheer, D. Dubbeldam, and T. J. H. Vlugt. Simulating the reactions of  $CO_2$  in aqueous monoethanolamine solution by Reaction Ensemble Monte Carlo using the Continuous Fractional Component method. J. Chem. Theory. Comput., 11 (2015) 2661-2669.

## 8.1 Introduction

In the previous chapters, we have used Monte Carlo simulations to study the solubility of gases in physical solvents. In this chapter, we develop a method to study the absorption of CO<sub>2</sub> in chemical solvents using molecular simulations. As explained in Chapter 2, CO<sub>2</sub> capture at post-combustion conditions demands a chemical solvent. Typically, the removal of CO<sub>2</sub> from flue gas streams is carried out using liquid amine solvents [33]. Monoethanolamine-containing (MEA) solutions were among the first alkanolamine based solvents used in the capture of CO<sub>2</sub>. This system remains one of the most important solvents in the post combustion CO<sub>2</sub> capture [257]. Some of

the advantages of using MEA solutions for CO<sub>2</sub> capture are the high CO<sub>2</sub> absorption capacity and reaction rates and low cost of solvent [257, 444]. In order to regenerate the solvent back, heat must be supplied [257, 444, 445]. Some of the disadvantages of using MEA solution as solvents include the high energy demand to regenerate the solvent and emissions of MEA solvents as aerosol [446, 447]. MEA solutions are also susceptible to oxidative and thermal degradation [446–448]. The mechanism of CO<sub>2</sub> absorption in MEA solutions is chemical in nature. CO<sub>2</sub> reacts with MEA solution forming stable carbamates [33, 257, 386, 445, 449]. To study the chemisorption of  $CO_2$ in MEA solutions and to reduce the heat required to regenerate the alkanolamine after CO<sub>2</sub> capture, it is necessary to study the chemical reactions that take place in the solution [449]. There are several possible mechanisms explaining how CO<sub>2</sub> reacts with alkanolamines [445, 449–451]. CO<sub>2</sub> reacts through an acid-base buffer mechanism with the alkanolamines to form protonated amines. CO<sub>2</sub> also reacts with some primary and secondary alkanolamines to form carbamates and reacts with tertiary alkanolamines to form bicarbonates [445, 449, 450]. To design a CO<sub>2</sub> amine treating process, it is important to understand the chemical equilibrium as well as the kinetics of the different reactions. There are many studies in the literature about the CO<sub>2</sub>-MEA system [9, 33, 446, 452]. Sartori and Savage obtained the equilibrium constants for carbamate formation [453]. Batt et al. [454] and Maddox et al. [455] qualitatively investigated the reactions occurring in the MEA system. Poplsteinova et al. [456] have studied systems containing MEA and N-methyl-diethanolamine using NMR spectroscopy. Hasse and co-workers [445] have studied the chemical equilibria of CO<sub>2</sub> in aqueous alkanolamines using online NMR spectroscopy. Chemical equilibria and kinetics of CO<sub>2</sub>-alkanolamine solutions are difficult to study experimentally at a molecular level because of the extremely fast reaction rates and the different reaction mechanisms. Molecular simulations play an important role in bridging the gap between our understanding of the reaction phenomena on a molecular level and the experimental observations on a macroscopic scale [385]. The impact of individual reactions and reaction mechanisms on the chemical equilibrium of the system can be studied using molecular simulations. Quantum chemical methods are widely applied to compute

8.1 Introduction 157

stationary points on the potential energy surface like transition states and activation barriers. Time dependent ab-initio methods like Car-Parrinello molecular dynamics [457] can be used to model the reactions directly. These methods scale poorly with system size and are sometimes difficult to apply to liquid phases. A classical based approach developed by Van Duin et al. uses "Reactive" force fields (ReaxFF) that are parameterized to study the chemical reactions of a few systems using classical molecular dynamics simulations [458]. ReaxFF treats the intermolecular interactions between the atoms and molecules through a classical force field which have been parameterized from experimental data or quantum simulations [458]. Another classical based approach called the Reaction Ensemble Monte Carlo (RxMC) for studying chemical reactions in equilibrium ignores transient events like bond breaking and formation (reaction mechanism in general). This approach is ideal to study the equilibrium distributions of the reacting species, since the effect of the intermolecular interactions with the surrounding molecules are taken into account. It is important to realize that equilibrium speciation is determined by thermodynamics of the system, and classical molecular simulations are a suitable tool to study this. The Reaction Ensemble Monte Carlo (RxMC) was developed independently by Johnson et al. [459] and Smith and Triska [460]. An important feature of Reaction Ensemble Monte Carlo (RxMC) is the actual reaction and its transition path is not simulated, but that only the equilibrium configurations of the molecules before and after the reaction are sampled. The forward and backward reactions are sampled using stochastic trial moves. In case of a forward reaction, the reactant molecules are chosen at random and are deleted from the simulation box while the product molecules are inserted randomly according to the stoichiometry of the reaction. This RxMC method requires the input of stoichiometric coefficients of the reactants and products and the ideal gas partition functions of isolated reactant and product molecules along with the intermolecular potential parameters to describe the interactions between the molecules. These ideal gas partition functions of isolated molecules can be obtained from thermophysical tables or quantum mechanical calculations [461–463]. The partition function of ideal gas molecules depend on the volume of the simulation box and this

must be taken into account in the acceptance rules of the RxMC algorithm (see the Supporting Information of Ref. [19] for details). Previous research pertaining to RxMC has focused on small molecules with fixed internal degrees of freedom [459, 460, 464–467]. Lisal and co-workers [468, 469] have developed the Reaction Ensemble Monte Carlo for systems with flexible internal degrees of freedom to study the synthesis of Methyl-tert-butylether (MTBE) from isobutene and methanol. The acceptance rules for the reaction move derived by Lisal and co-workers also include the change in energy due to intramolecular contributions. Intermolecular interactions are counted twice in their derivation of the acceptance rules, which is incorrect [463, 468, 469]. Rosch et al. [463] have derived the correct acceptance rules. Keil et al. [461, 462] have studied propene metathesis reactions within confined environments. These authors have combined the Configurational-Bias Monte Carlo (CBMC) approach with the Reaction Ensemble Monte Carlo for linear alkanes and alkenes. The Configurational-Bias Monte Carlo algorithm is useful for simulating larger molecules as inserting these large molecules in confined systems is extremely difficult. To the best of our knowledge, application of the Reaction Ensemble Monte Carlo for complex molecules and reactions in a dense liquid phase has not been studied. A reaction in the Reaction Ensemble involved the deletion of reactants and the insertion of the reaction products. These so-called "insertions" and "deletions" are accepted in such a way that the correct equilibrium distribution is sampled. The efficiency and accuracy of these simulations depend on the probability of successful insertions and deletions of molecules. At high densities typically encountered in a liquid phase, the probability of successful insertions and deletions is very low due to a large number of overlaps with the existing molecules in the simulation box [379, 385, 388]. To increase the efficiency of the successful insertions and deletions, Maginn et al. [379, 389] have developed the Continuous Fractional Component Monte Carlo (CFCMC) method to insert/delete molecules in a more gradual manner. Torres-Knoop et al. [388] have combined the CBMC with the CFCMC to obtain higher computational efficiencies. Other works have been published proposing methods that try to increase the efficiency of insertion and deletion in dense liquids [470–472]. Rosch et al. have extended the CFCMC

method for the Reaction Ensemble, coupling the CFCMC for inserting the product molecules and deleting the reactant molecules based on their respective stoichiometry [463]. In this work, we use the Reaction Ensemble Monte Carlo using the Continuous Fractional Component (RxMC/CFC) method to study the chemical equilibrium of CO<sub>2</sub> in MEA solution and determine the equilibrium concentrations of the different species in the system. The results are compared to experimental results from literature. We study the effects of different reaction mechanisms on the equilibrium concentrations of the various species. The rest of this paper is organized as follows: Section 2 deals with simulating the reactions of CO<sub>2</sub> in MEA solution along with the derivation of the acceptance rules for the RxMC/CFC algorithm. Section 3 contains the different results and discussions and our findings are summarized in Section 4.

# 8.2 Simulating the reactions of $CO_2$ in MEA solution

The reactions of CO<sub>2</sub> with primary and secondary amine solutions usually takes place through an acid-base buffer mechanism which results in the formation of stable carbamates and bicarbonate followed by the subsequent protonation of the amine [455]. Non-hindered primary and secondary amines react rapidly with CO<sub>2</sub> to form carbamate ions and the addition of water increases the absorption capacity and rate. Tertiary amines react with CO<sub>2</sub> via the bicarbonate pathway to form bicarbonate ion and the ammonium salt of the amine. Since monoethanolamine (HOCH<sub>2</sub>CH<sub>2</sub>NH<sub>2</sub>) is a primary amine, the reactions take place via the carbamate ion pathway [449, 450]:

$$CO_2 + 2H_2O \rightleftharpoons HCO_3^- + H_3O^+$$
 (R1)

$$HCO_3^- + H_2O \rightleftharpoons CO_3^{2-} + H_3O^+$$
 (R2)

$$HOCH_2CH_2NH_2 + H_3O^+ \rightleftharpoons HOCH_2CH_2NH_3^+ + H_2O$$
 (R3)

$$HOCH_2CH_2NH_2 + HCO_3^- \rightleftharpoons HOCH_2CH_2NHCOO^- + H_2O$$
 (R4)

These reactions are generally described in the literature [445, 449, 450, 456]. It is important to note that in the reactions mentioned above, the appearance of H<sub>3</sub>O<sup>+</sup> is to avoid the presence of H<sup>+</sup> in the system, as H<sup>+</sup> does not obey the Born-Oppenheimer approximation for classical simulations [385]. Some other additional reactions have also been described in the literature [445]. MEA is also able to form 2-oxazolidone which is a heterocyclic component [445, 473]. Other amine degradation reaction mechanisms are also possible [473, 474]. In spite of the different possible reaction mechanisms, the aim of all modeling and experimental studies is to obtain the equilibrium concentrations of the different species. In this regard, Reactions R1, R3 and R4 may be combined to result in a simplified Reaction R5 which is given by,

$$CO_2 + 2HOCH_2CH_2NH_2 \rightleftharpoons$$
  
 $HOCH_2CH_2NH_3^+ + HOCH_2CH_2NHCOO^-$  (R5)

## 8.2.1 RxMC/CFC Algorithm

To obtain the equilibrium concentrations of the different species in a reacting mixture, the Reaction Ensemble Monte Carlo (RxMC) [459, 461, 462, 475] is used. The RxMC algorithm samples the reactions directly and bypasses transition states. The RxMC algorithm only requires the stoichiometric coefficients of the reactions as an input and the partition functions of the isolated molecules or ions, along with the force field parameters to compute the intermolecular interactions. Therefore, the RxMC method allows for a systematic study of the effect of the medium (or solvent) on the reaction equilibrium constant. The reaction trial move within the RxMC framework involves choosing the forward or reverse reaction at random. If the forward reaction is chosen, the reactant molecules are deleted and the product molecules are inserted according to their stoichiometries. For dense systems, these insertions and deletions of molecules, if performed in a single step, often lead to overlaps with the surrounding molecules. The probabilities of successful insertions/deletions of the molecules are very low. To circumvent this problem, Maginn et al. [379, 389] have developed the Continuous

Fractional Component Monte Carlo method. Fractional molecules of the reactants and products are introduced into the system. By controlling the interactions of these fractional molecules with the surrounding molecules, the reactants/products are gradually inserted or removed. This is controlled by a pseudocoupling factor,  $\lambda$ . Changes in  $\lambda$  will gradually insert or delete the molecules appropriately. The reaction ensemble is best described by taking the osmotic ensemble as the starting point, since most chemical reactions take place in a system at constant pressure. Let  $N_i$  denote the number of molecules of type i, P the imposed hydrostatic pressure, V the volume and  $\mu_i$  the chemical potential of the species i. For an expanded osmotic ensemble, the partition function for a system of n species can be expressed as [463]

$$\Xi_{\text{biased}}(\mu_{1},..,\mu_{n},p,T) = \beta P \int_{0}^{1} d\lambda \sum_{N_{i}=0}^{\infty} \cdots \sum_{N_{n}=0}^{\infty} \int \exp\left[\beta \sum_{i=1}^{n} N_{i} \mu_{i}\right]$$
$$-\sum_{i=1}^{n} \ln N_{i}! + \sum_{i=1}^{n} N_{i} \ln(\hat{q}_{i}(T)V) - \beta PV$$
$$-\beta U(s^{N},\omega^{N},\lambda)\right] \exp[\eta(\lambda)/k_{B}T]$$
$$\times ds^{N_{1}} d\omega^{N_{1}} \cdots ds^{N_{n}} d\omega^{N_{n}} dV \tag{8.1}$$

where  $s^{N_i}$  are the configurations of the  $N_i$  molecules of type i,  $\omega^{N_i}$  are the orientations and internal configurations of  $N_i$  molecules of type i and  $U(s^N, \omega^N, \lambda)$  is the potential energy of the system.  $\beta = 1/k_B T$ ,  $\hat{q}_i(T)$  is the temperature dependent term in the molecular partition function for the molecule of type i.  $\eta(\lambda)$  are the biasing factors introduced to improve the probabilities of transitions in  $\lambda$ . The reader is referred to the Supporting Information of Ref. [19] for a detailed explanation on the molecular partition functions and partition functions of the osmotic ensemble. From (8.1), it

follows that the probability that the system is in a certain state is

$$p_{\text{biased}} \sim \exp\left[\beta \sum_{i=1}^{n} N_{i} \mu_{i} - \sum_{i=1}^{n} \ln N_{i}! + \sum_{i=1}^{n} N_{i} \ln(\hat{q}_{i}(T)V) - \beta PV - \beta U(s^{N}, \omega^{N}, \lambda)\right] \exp[\eta(\lambda)/k_{B}T]$$
(8.2)

This equation can be used to derive the acceptance rules in our Monte Carlo algorithm.

# Reaction Ensemble Monte Carlo using the Continuous Fractional Component algorithm

Let us consider a reaction involving c species in a system consisting of n molecule types. For the species not involved in the reaction, the stoichiometric coefficient  $\nu_i$  is set to 0 by definition. If a reaction takes place in the forward or reverse direction, there will be a change in the molecules of each component. The state before the reaction takes place is now denoted by old state "o", while the state after the reaction takes place is denoted by new state "n". Since the reaction has taken place, we know how the number of molecules of each component changes:

$$N_{i,n} = N_{i,o} + \nu_i \tag{8.3}$$

The probabilities to exist in states "o" and "n" can be obtained from Eq. (8.2). Substituting Eq. (8.3) in (8.2) for the new state, the expressions for

the probabilities to exist in the old and the new states are,

$$p_{\text{o,biased}} \sim \exp \left[ \beta \sum_{i=1}^{n} N_{i,\text{o}} \mu_{i} - \sum_{i=1}^{n} \ln N_{i,\text{o}}! + \sum_{i=1}^{n} N_{i,\text{o}} \ln(\hat{q}_{i}(T)V_{\text{o}}) \right.$$

$$\left. - \beta P V_{\text{o}} - \beta U_{\text{o}}(s^{N,\text{o}}, \omega^{N,\text{o}}, \lambda_{\text{o}}) \right] \exp[\eta(\lambda_{\text{o}})/k_{B}T] \quad (8.4)$$

$$p_{\text{n,biased}} \sim \exp \left[ \beta \sum_{i=1}^{n} \nu_{i} \mu_{i} + \beta \sum_{i=1}^{n} N_{i,\text{o}} \mu_{i} - \sum_{i=1}^{n} \ln(N_{i,\text{o}} + \nu_{i})! \right.$$

$$\left. + \sum_{i=1}^{n} N_{i,\text{o}} \ln(\hat{q}_{i}(T)V_{\text{n}}) + \sum_{i=1}^{n} \nu_{i} \ln(\hat{q}_{i}(T)V_{\text{n}}) \right.$$

$$\left. - \beta P V_{\text{n}} - \beta U_{\text{n}}(s^{N,\text{n}}, \omega^{N,\text{n}}, \lambda_{\text{n}}) \right] \exp[\eta(\lambda_{\text{n}})/k_{B}T] \quad (8.5)$$

### Acceptance rules in RxMC/CFC

Averages in the Boltzmann ensemble (denoted by  $\langle \cdots \rangle$ ) follow directly from biased averages (denoted by  $\langle \cdots \rangle_{\text{biased}}$ ) according to [396]

$$\langle A \rangle = \frac{\langle A \exp[-\eta(\lambda)] \rangle_{\text{biased}}}{\langle \exp[-\eta(\lambda)] \rangle_{\text{biased}}}$$
 (8.6)

In the Reaction Ensemble Monte Carlo using Continuous Fractional Component method, there are four types of trial moves possible:

- 1. Change the position of a randomly selected molecule (either a regular or a fractional molecule)
- 2. Change the orientation of a randomly selected molecule (either a regular or a fractional molecule)
- 3. Change the volume of the system
- 4. Change the coupling parameter  $\lambda$  of a randomly selected reaction. The reactions are chosen with equal probability. This can be further divided into 3 cases ( $\Delta\lambda$  is the change in  $\lambda$ ):

(a) 
$$0 \le \lambda + \Delta \lambda \le 1$$

(b) 
$$\lambda + \Delta \lambda < 0$$

(c) 
$$\lambda + \Delta \lambda > 1$$

The first two Monte Carlo moves are trivial and have the same acceptance rules as the ones derived previously [385, 396]. For the Volume Change Monte Carlo trial move, random walks are made in  $\ln(V_{\rm n}/V_{\rm ref})$  [385] in which  $V_{\rm ref}$  is an arbitrary reference volume. The probabilities of existing in the old state "o" and the new state "n" are

$$p_{\text{o,biased}} \sim \beta P V_{\text{o}} \exp \left[ \beta \sum_{i=1}^{n} N_{i,\text{o}} \mu_{i} - \sum_{i=1}^{n} \ln N_{i,\text{o}}! + \sum_{i=1}^{n} N_{i,\text{o}} \ln(\hat{q}_{i}(T) V_{\text{o}}) \right.$$
$$\left. - \beta P V_{\text{o}} - \beta U_{\text{o}}(s^{N}, \omega^{N}, \lambda) \right] \exp[\eta(\lambda_{\text{o}})/k_{B}T] \qquad (8.7)$$
$$p_{\text{n,biased}} \sim \beta P V_{\text{n}} \exp \left[ \beta \sum_{i=1}^{n} N_{i,\text{o}} \mu_{i} - \sum_{i=1}^{n} \ln N_{i,\text{o}}! + \sum_{i=1}^{n} N_{i,\text{o}} \ln(\hat{q}_{i}(T) V_{\text{n}}) \right.$$
$$\left. - \beta P V_{\text{n}} - \beta U_{\text{n}}(s^{N}, \omega^{N}, \lambda) \right] \exp[\eta(\lambda_{\text{n}})/k_{B}T] \qquad (8.8)$$

For random walks in  $\ln(V_n/V_{ref})$ ,  $\lambda_o = \lambda_n$  and  $\eta(\lambda_o) = \eta(\lambda_n)$ . The acceptance rule is therefore

$$acc(o \to n) = \min\left(1, \left(\frac{V_{\rm n}}{V_{\rm o}}\right)^{N+1} \exp[-\beta P(V_{\rm n} - V_{\rm o})] \times \exp[-\beta (U_{\rm n}(s^N, \omega^N, \lambda) - U_{\rm o}(s^N, \omega^N, \lambda))]\right)$$
(8.9)

This expression is the same as the acceptance rule derived previously [385]. We now consider the reaction move as a change in  $\lambda$  of the system. For the reaction move,  $V_0 = V_n$ . Looking into more detail at the three different cases when  $\lambda$  is changed, we have: **First case (a)**, where  $0 \le \lambda + \Delta \lambda \le 1$ ,

is the case where there is no addition or deletion of molecules. The old state is denoted by "o" and  $\lambda_{\rm o}$  is the old coupling factor of the reaction. The new state is denoted by "n" and  $\lambda_{\rm n}=\lambda_{\rm o}+\Delta\lambda$ . From Eq. (8.2), we can obtain the probabilities to exist in old and new states. As the number of molecules in the system remain the same for the old and the new configurations, the acceptance rule is

$$acc(o \to n) = \min \left( 1, \exp[-\beta (U_{n}(s^{N}, \omega^{N}, \lambda_{n}) - U_{o}(s^{N}, \omega^{N}, \lambda_{o}))] \times \exp[(\eta(\lambda_{n}) - \eta(\lambda_{o}))/k_{B}T] \right)$$
(8.10)

Second case (b), where  $\lambda + \Delta \lambda > 1$ , is the case of a reverse reaction. The  $\lambda$  of the old fractional reactant and product molecules are set to 1 and 0 respectively. New fractional reactant molecules are inserted into the system with  $\lambda_n = (\lambda_0 + \Delta \lambda) - 1$ . Random product molecules are selected from the system and their  $\lambda$  is set from 1 to  $1-\lambda_n$ . Third case (c), where  $\lambda + \Delta \lambda < 0$ , is when there is a forward reaction. The  $\lambda$  of the old fractional reactant and product molecules are set to 0 and 1 respectively. New fractional product molecules are inserted into the system with  $\lambda_n = (\lambda_0 + \Delta \lambda) - 1$ . Random reactant molecules are selected from the system and their  $\lambda$  is set to  $1-\lambda_n$ . In cases two and three, the reaction has proceeded, either in the forward direction or the backward direction. For a reaction involving n species, equilibrium is achieved when

$$\sum_{i=1}^{n} \nu_i \mu_i = 0 \tag{8.11}$$

Substituting Eq. (8.11) in Eq. (8.5) since the reaction takes place at equilibrium, the expression for the acceptance rule for the forward/reverse

reaction (cases (b) and (c)) is

$$acc(o \to n) = \min \left( 1, \prod_{i=1}^{n} \left( \frac{N_i^{\text{o}!}}{(N_i^{\text{o}} + \nu_i)!} (\hat{q}_i(T)V)^{\nu_i} \right) \right) \\
\times \exp\left[ -\beta (U_{\text{n}}(s^N, \omega^N, \lambda_{\text{n}}) - U_{\text{o}}(s^N, \omega^N, \lambda_{\text{o}})) \right] \\
\times \exp\left[ (\eta(\lambda_{\text{n}}) - \eta(\lambda_{\text{o}}))/k_B T \right] \right) \tag{8.12}$$

The acceptance rule for the RxMC derived above for one reaction can be generalized easily to include many reactions in the same system. It is important to note that in the acceptance rule (Eq. (8.12)), the volume term is included explicitly, since during the simulation the volume of the system changes. It is instructive to consider the case of a reaction in a mixture of ideal gases. In that case, the acceptance rule of Eq. (8.12) reduces to

$$acc(o \to n) = \min\left(1, \prod_{i=1}^{n} \left(\frac{N_i^{\text{o}!}}{(N_i^{\text{o}} + \nu_i)!} (\hat{q}_i(T)V)^{\nu_i}\right)\right)$$
(8.13)

If the total number of molecules does not change during the reaction  $(\sum_{i=0}^{n} \nu_i = 0)$ , it is well known from classical thermodynamics that the equilibrium constant is only a function of the molecular partition functions [476]. From Eq. (8.13), it can also be observed that there will be no dependence on the volume of the system when  $\sum_{i=0}^{n} \nu_i = 0$  as the volume term V cancels out in Eq. (8.13) and the expression reduces to

$$acc(o \to n) = \min\left(1, \prod_{i=1}^{n} \left(\frac{N_i^{\text{o}!}}{(N_i^{\text{o}} + \nu_i)!} (\hat{q}_i(T))^{\nu_i}\right)\right). \tag{8.14}$$

If there is a change in the number of molecules during the reaction  $(\sum_{i=0}^{n} \nu_i \neq 0)$ , the acceptance rule will now depend on the volume of the system, as can be seen from Eq. (8.13). It is important to consider the volume dependent term of the partition function explicitly in the acceptance rules since in many cases, the number of molecules during the reaction changes

 $(\sum_{i=0}^{n} \nu_i \neq 0)$ . It is unclear whether or not this volume term was taken into account correctly in previous studies from literature. Of course, the final results will not be affected if the simulations consider reactions where the number of molecules does not change due to the reaction [461–463].

#### 8.2.2 Simulation Details

Two different sets of reactions are studied to obtain the equilibrium speciations by including: (1) Reactions R1-R4 (2) only Reaction R5. simulations are performed in the Reaction Monte Carlo Ensemble (RxMC) in the constant temperature, constant pressure ensemble. The hydrostatic pressure of the system equals 1 bar. The effect of temperatures on the equilibrium compositions of the mixture is also studied. Different loadings of CO<sub>2</sub> have also been investigated. The initial concentration of MEA in the aqueous MEA solution is 30 weight percent. Boettinger et al [445] measured the speciations at different loadings higher than 0.5 mole CO<sub>2</sub>/mol MEA using online NMR spectroscopy. To achieve high loadings of CO<sub>2</sub> in experiments, the partial pressure of  $CO_2$  ranged from 5 bar to 25 bar. In our simulations, a system with a fixed number of CO<sub>2</sub> molecules is simulated and only the hydrostatic pressure of the system needs to be specified. As the properties of a liquid phase do not depend much on the hydrostatic pressure and the total loading of  $CO_2$  is specified, one can safely assume a hydrostatic pressure of 1 bar. Quantum mechanical simulations using GAUSSIAN 09 [477] are performed to obtain the partition functions  $\hat{q}_i$  of the isolated molecules required for the RxMC/CFC molecular simulations. All molecular species involved in the reaction were optimized with a second order Møller-Plesset perturbation method (MP2) in combination with a 6-311+G(2d,2p) basis set at different temperatures (293 K, 333 K, 353 K). A frequency analysis was performed on the optimized geometries to confirm the true minima on the potential energy surface and to obtain partition functions of all the molecules. All the calculations were performed with GAUSSIAN 09 [477]. Mulliken atomic charges were obtained from population analysis of self-consistent field density matrix. The individual contributions of translational, vibrational, rotational and electronic mo-

tions are considered for the calculation of the partition function for every molecule. [478]. The partition functions were split into a temperature dependent part and a volume dependent part (details are provided in the Supporting Information of Ref. [19]). The values of the computed partition functions of the molecules at different temperatures are listed in the Supporting Information of Ref. [19]. Force fields for the MEA have been taken from the OPLS force field [479]. Intermolecular potential parameters and intramolecular potential parameters for MEACOO<sup>-</sup> and MEAH<sup>+</sup> have also been taken from the OPLS force field. Force field parameters for CO<sub>2</sub> have been taken from the TraPPE force field [392] and for water from the Tip4p water model has been used [480]. The force field parameters for  $H_3O^+$  are taken from Vacha et al. [481] The force field parameters for the HCO<sub>3</sub> and  $\mathrm{CO}_3^{2-}$  have been taken from the OPLS database. Water, MEA, MEA<sup>+</sup>, MEACOO<sup>-</sup>,  $H_3O^+$ ,  $HCO_3^-$  and  $CO_3^{2-}$  are modeled as rigid molecules. The partial charges for HCO<sub>3</sub><sup>-</sup>, CO<sub>3</sub><sup>2-</sup>, MEACOO<sup>-</sup> and MEAH<sup>+</sup> have been computed from quantum mechanical simulations in GAUSSIAN 09 [477]. The force field parameters for all the species are specified in the Supporting Information of Ref. [19]. Electrostatic interactions were handled by the Ewald summation algorithm [482] with a relative precision of  $10^{-5}$ . The cutoff radius was set at 12 Å for the Lennard-Jones interactions.  $\sigma$  and  $\epsilon$  are the Lennard-Jones (LJ) parameters [401]. The Lorentz-Berthelot mixing rules were used to calculate the Lennard-Jones parameters between different atoms ( $\sigma_{ij}$  and  $\epsilon_{ij}$ ). Monte Carlo simulations in the RxMC/CFC ensemble were performed using RASPA, [401] a program for Monte Carlo and Molecular dynamics simulations. Monte Carlo simulations of 1 million cycles were performed for equilibration and production runs of 2 million cycles were performed, where one MC cycle is equal to the total number of molecules in the system. The probabilities of selecting a translation move, a rotation move, a partial reinsertion move and a reaction move were all 0.245. The probability of selecting a volume change move was 0.02. Simulations were performed with 444 water molecules, 56 MEA molecules and the appropriate number of CO<sub>2</sub> molecules depending on the loading. The size of the simulation box varied around 27 Å. By switching off electrostatics and intermolecular van der Waals interactions, the effect of electrostatics and

intermolecular interactions on the reaction equilibrium was studied. At the start of the simulation, fractional molecules were assigned for all reacting species for both reactants and products in the Reactions R1-R4. The net charge of the fractional molecules (both the reactants and products) of all the Reactions R1-R4) is not zero. It is important to note that if we sum Reactions R1, R2, R3, and R4, the total net charge of the reactants equals -1. Similarly, the total net charge of products of the summed reactions also equals -1. To keep the simulation box charge neutral independent of the value of  $\lambda$  for each reaction, two  $H_3O^+$  fractional molecules, one as a reactant and the other as a product in Reaction R2, were added to the simulation box. This ensures that during the reaction the simulation box is always charge neutral. For the RxMC/CFC, the Lennard-Jones parameters as well as the partial charges are scaled with a pseudo coupling factor which is changed during the reaction move. The scaled Lennard-Jones and electrostatic potentials are specified in detail in the Supporting Information of Ref. [19].

## 8.3 Results and Discussion

## 8.3.1 Effect of Electrostatics and intermolecular van der Waals interactions

When there are no intermolecular interactions between molecules, the system behaves as an ideal gas. For an ideal gas system, the equilibrium constant can be written directly in terms of the molecular partition functions of the individual species [483] which can be calculated from quantum simulations. A detailed derivation of this is provided in the Supporting Information of Ref. [19]. To observe the effect of intermolecular interactions, the intermolecular van der Waals interactions and the electrostatics were "switched off" i.e., all the intermolecular Lennard-Jones parameters and electrostatics were set to zero. From the simulations, it was observed that forward reactions did not take place when including (1) reactions R1-R4 and (2) only reaction R5. Equilibrium constants for these ideal gas reactions calculated from quantum simulations are specified in the Supporting

Information of Ref. [19]. The equilibrium constants for the forward reaction are extremely low. Equilibrium concentrations of the species for the ideal gas system can be obtained by solving the non-linear expressions for the equilibrium constants. The analytical solutions yield extremely low concentrations of carbamates and protonated amines. This is consistent with the results obtained from simulations performed when the intermolecular van der Waals interactions and the electrostatic are set to zero. It can be observed from the results of the simulations and analytical solutions that intermolecular interactions are necessary to compute the equilibrium concentrations of the species. Equilibrium speciations cannot be obtained by only performing quantum simulations as the system cannot be treated as an ideal gas. As expected, the solvation of ions in the solution is essential for the different reactions to take place. Classical simulations take into account the intermolecular interactions between the species and this is necessary to compute the equilibrium concentrations of the species. If the reaction occurs in the ideal gas phase, the ions are not solvated and energetically this is very unfavorable.

# 8.3.2 Chemical Equilibrium of reactions R1+R2+R3+R4 and R5

The equilibrium mole fractions of the different species were obtained at different temperatures (293 K, 333 K, 353 K) and at a hydrostatic pressure of 1 bar for different loadings of CO<sub>2</sub> (mol CO<sub>2</sub>/mol MEA) by performing Monte Carlo simulations in the Reaction Ensemble using the Continuous Fractional Component method. In Figures 8.1,8.2 and 8.3, the equilibrium mole fractions of the species MEA, MEAH<sup>+</sup>, MEACOO<sup>-</sup>, CO<sub>2</sub> and HCO<sup>-</sup><sub>3</sub> are compared to experimental data [445, 456]. Poplsteinova et al. [456] and Boettinger et al. [445] measured the equilibrium speciation of CO<sub>2</sub>-MEA-H<sub>2</sub>O system using NMR spectroscopy. Boettinger et al. [445] report the sum of equilibrium concentrations of MEA and MEAH<sup>+</sup>, since it was impossible to distinguish between the protonated and the unprotonated MEA experimentally. In order to obtain the individual equilibrium concentrations of MEA and MEAH<sup>+</sup>, these authors have used a thermodynamic model

(see below). Figure 8.1a shows the speciation of the  $CO_2+MEA$  solution for different loadings of CO<sub>2</sub> (mol CO<sub>2</sub>/mol MEA) at 293 K and 1 bar when the reactions R1-R4 are used. The equilibrium concentration of the different species of CO<sub>2</sub>+MEA solution exhibits the typical behavior of the primary amines. At low loadings until 0.5 mol CO<sub>2</sub>/mol MEA, all CO<sub>2</sub> molecules react with the MEA molecules forming the carbamate and the protonated amine products. The concentrations of the carbamate and the protonated MEA increase as the loading of  $CO_2$  increases until 0.5 mol  $CO_2$ /mol MEA, while the concentration of MEA decreases. At the loading of CO<sub>2</sub> of 0.5 mol CO<sub>2</sub>/mol MEA, all the MEA has now reacted with the CO<sub>2</sub>. Beyond loadings of CO<sub>2</sub> of 0.5 mol CO<sub>2</sub>/mol MEA, the concentrations of the carbamate start to decrease and the concentrations of the protonated MEA increase. Beyond the loadings of CO<sub>2</sub> of 0.5 mol/mol MEA, bicarbonate ions were observed. The simulation results are in excellent agreement with the experimental results of Boettinger et al. [445]. Figure 8.1b shows the equilibrium concentrations of MEA, MEAH<sup>+</sup>, MEACOO<sup>-</sup> and CO<sub>2</sub> for different loadings of CO<sub>2</sub> (mol CO<sub>2</sub>/mol MEA) at 293 K and 1 bar when only the reaction R5 is considered. The results of equilibrium speciations obtained from simulating only reaction R5 follow the same trends for the concentrations of MEA, protonated MEA and the carbamate when we include all reactions R1-R4. Until loadings of 0.5 mol CO<sub>2</sub>/mol MEA, the concentrations of the carbamate and the protonated MEA increase and the concentration of free MEA decreases. Beyond loadings of 0.5 mol CO<sub>2</sub>/mol MEA, typically all the MEA has reacted with the CO<sub>2</sub>. The concentrations of MEA, protonated MEA and MEACOO<sup>-</sup> remain constant, while concentration of unreacted CO<sub>2</sub> increases for loadings higher than 0.5 mol CO<sub>2</sub>/mol MEA. Boettinger et al. [445] also used a thermodynamic model to study the CO<sub>2</sub>-MEA-H<sub>2</sub>O system and obtained the individual equilibrium concentrations of the different species: MEA, MEAH<sup>+</sup>, MEACOO<sup>-</sup>, CO<sub>2</sub>,  $HCO_3^-$ . These authors have developed the model by simultaneously taking into account the chemical reactions and the vapor-liquid equilibria of the  $CO_2$ -MEA- $H_2O$  mixture into consideration. Figure 8.2 compares our simulation results of the individual equilibrium concentrations including MEA and MEA<sup>+</sup> with the results from the thermodynamic model of Boettinger et

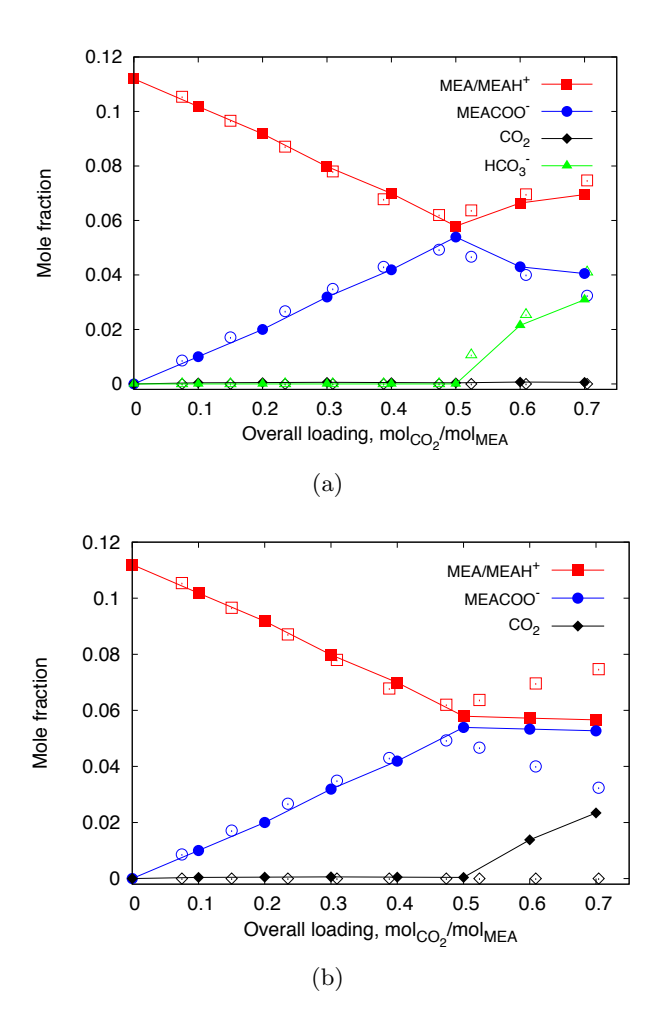


Figure 8.1: The mole fractions of the different species MEA/MEAH $^+$  (squares), MEACOO $^-$  (circles), CO $_2$  (diamonds) and HCO $_3^-$  (triangles) for 30 wt. % aqueous MEA solutions at  $T=293~\rm K$ . The open symbols are results from experiments [445]. The closed symbols are the results obtained from the RxMC/CFC simulations (a) including reactions R1-R4 (b) including only reaction R5. The lines are a guide to the eye.

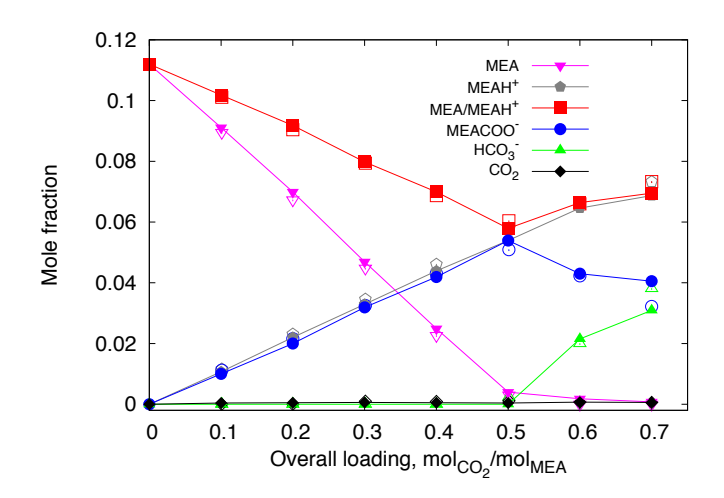


Figure 8.2: The mole fractions of the different species MEA (inverted triangles), MEAH<sup>+</sup> (pentagons), MEA/MEAH<sup>+</sup> (squares), MEACOO<sup>-</sup> (circles), CO<sub>2</sub> (diamonds), HCO<sub>3</sub><sup>-</sup> (triangles) for 30 wt. % aqueous MEA solutions at T=293 K. The open symbols are results from the thermodynamic model combined with experimental data [445]. The closed symbols are results obtained from the RxMC/CFC simulations including reactions R1-R4. The lines are a guide to the eye.

al. We find an excellent agreement with the model. It is important to note that we obtain individual concentrations of all the species in the mixture directly from simulations and we need not use any iterative modeling technique which requires binary interaction parameters, activity coefficients of molecular and ionic species, equilibrium coefficients, etc. as input. Figures 8.3 and 8.4 show the results of the speciations for different temperatures 333 K and 353 K at 1 bar. It can be observed that an increase in temperature does not significantly affect the equilibrium concentrations of the species. For Figure 8.4, there is no experimental data beyond loadings of 0.5 mol  $\rm CO_2/mol~MEA$ . This is again in excellent agreement with the experimental results of Boettinger et al. [445] who also observe that the speciations of the  $\rm CO_2+MEA$  solution are only very weakly temperature dependent.

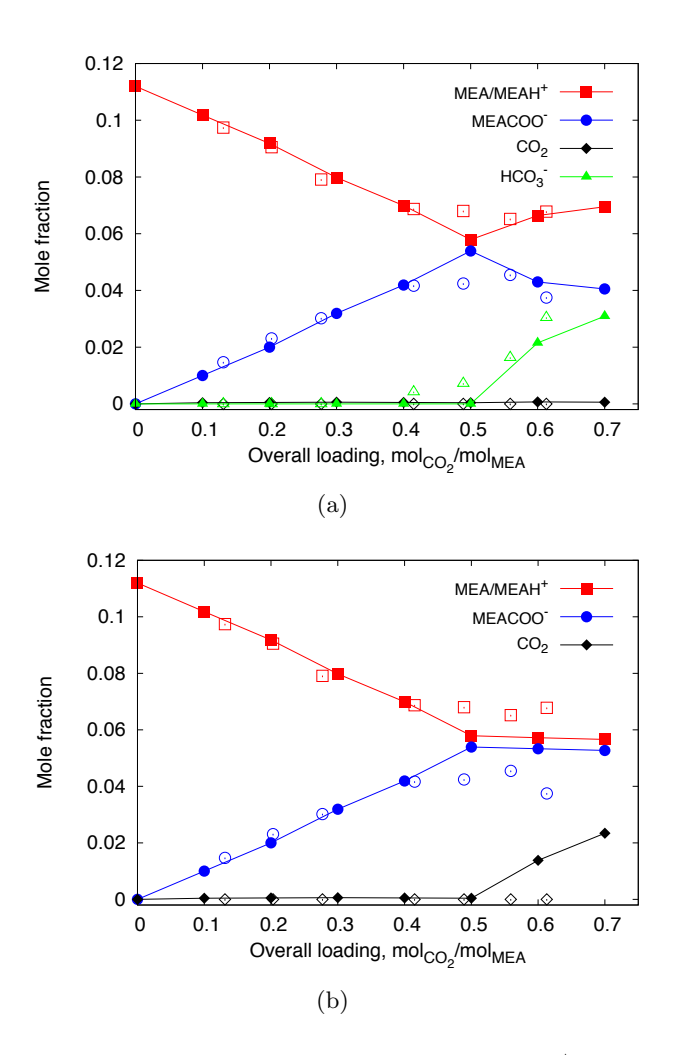


Figure 8.3: The mole fractions of the different species MEA/MEAH $^+$  (squares), MEACOO $^-$  (circles), CO $_2$  (diamonds) and HCO $_3^-$  (triangles) for 30 wt. % aqueous MEA solutions at  $T=333~\rm K$ . The open symbols are results from experiments [445]. The closed symbols are the results obtained from the RxMC/CFC simulations (a) including reactions R1-R4 (b) including only reaction R5. The lines are a guide to the eye.

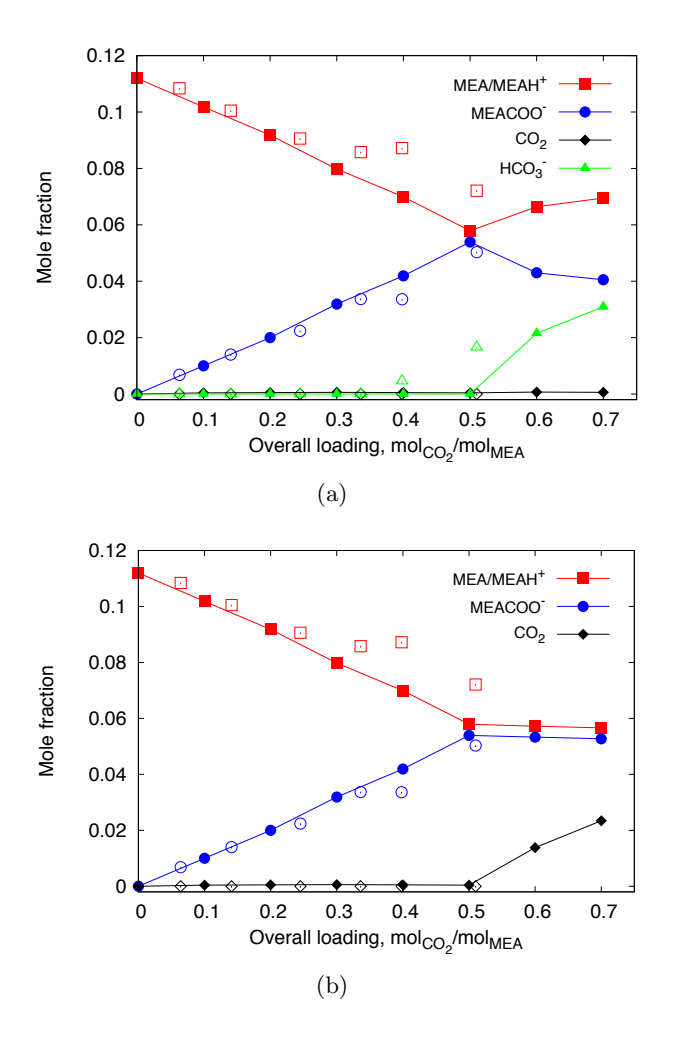


Figure 8.4: The mole fractions of the different species MEA/MEAH $^+$  (squares), MEACOO $^-$  (circles), CO $_2$  (diamonds) and HCO $_3^-$  (triangles) for 30 wt. % aqueous MEA solutions at  $T=353~\rm K$ . The open symbols are results from experiments [445]. The closed symbols are the results obtained from the RxMC/CFC simulations (a) including reactions R1-R4 (b) including only reaction R5. The lines are a guide to the eye.

## 8.4 Conclusions

Monte Carlo simulations in the Reaction Ensemble using a Continuous Fractional Component method provide an excellent description of the equilibrium concentrations of all relevant species in the chemisorption of CO<sub>2</sub> in MEA water solutions. The simulations were performed at different temperatures and the results from simulation are in excellent agreement with the experimental results. Equilibrium concentrations of MEA, MEAH<sup>+</sup>, MEACOO<sup>-</sup>, CO<sub>2</sub> from Reactions R1-R4 and R5 are identical for loadings up to  $0.5 \text{ mol } CO_2/\text{mol } MEA$  and beyond that, they are different. To obtain the accurate results for loadings in excess of 0.5 mol CO<sub>2</sub>/mol MEA, reactions R1-R4 must be included in the simulation. This RxMC/CFC methodology opens up possibilities to investigate the effect of the solvents in the reactions. Chemisorption of CO<sub>2</sub> in different solvents can be studied computationally to obtain the equilibrium concentrations. Only the thermodynamics need to be considered and the different transition states or reaction pathways can be ignored. This method may also investigate the effect of the chemistry of the amines, for example adding different functional groups [449, 451].

# Chapter 9

# CO<sub>2</sub>/CH<sub>4</sub> Solubility: ILs versus Conventional Solvents

This chapter is based on the paper: M. Ramdin, S. P. Balaji, A. Torres-Knoop, D. Dubbeldam, T. W. de Loos and T. J. H. Vlugt. Solubility of Natural Gas Species in Ionic liquids and Commercial Solvents: Experiments and Monte Carlo Simulations. J. Chem. Eng. Data, 60 (2015) 3039-3045.

# 9.1 Introduction

The price/performance ratio of ILs with respect to the traditional solvents is crucial for their potential application as gas sweetening agents. In this chapter, we assess the potential of ILs for CO<sub>2</sub> removal from natural gas. The performance of ILs in terms of CO<sub>2</sub> and CH<sub>4</sub> solubilities/selectivities are compared with respect to the commercial solvents Selexol, Purisol, Rectisol, propylene carbonate, and sulfolane. The principal ingredients in the solvents Selexol, Purisol, and Rectisol are mixtures of poly(ethylene glycol) dimethyl ethers, n-methylpyrrolidone, and methanol, respectively [9, 11]. The solubilities of the gases are compared on mole fraction, molality, and volume basis to eliminate the effect caused by the high molecular weight

of the ILs. The availability of  $\rm CO_2$  and in particular  $\rm CH_4$  solubility data in the conventional solvents is in contrast to the ILs and despite their wide application interest relatively poor. The focus here is mainly on  $\rm CO_2/CH_4$  solubilities and selectivities.

# 9.2 Results and Discussion

#### 9.2.1 $CO_2$ Solubility

The solubilities of CO<sub>2</sub> and CH<sub>4</sub> are compared on mole fraction, molality, and volume (molarity) basis to remove the effect caused by the high molecular weight of ILs. In Chapter 3, we have reported CO<sub>2</sub> and CH<sub>4</sub> solubilities in 10 different ILs composed of several classes of cations and anions [8, 345, 346]. Figure 9.1 shows the mole fraction based solubility of CO<sub>2</sub> in several ILs in comparison with the widely used solvents Selexol, Purisol, Rectisol, propylene carbonate, and sulfolane. Clearly, some of the ILs (e.g., the alkyl-phosphonium-based ILs) have a higher CO<sub>2</sub> capacity on mole fraction basis than the conventional solvents like Selexol, Purisol propylene carbonate, and sulfolane. The solubility of CO<sub>2</sub> seems to be higher in Rectisol than the other solvents, but this is mainly due to the low operating temperature (i.e., around - 25 °C) of the process. However, a careful analysis of the data shows that the solubility increases with an increasing molecular weight of the IL [345]. Therefore, the solubility should be compared on molality or volume basis, which are more practical units from a process point of view. Figure 9.2 shows the same comparison, but now the solubility is expressed in moles per mass solvent or molality. Remarkably, the IL data tend to collapse on a universal solubility curve proposed by Carvalho and Coutinho [125]. The solubility data of CO<sub>2</sub> in conventional solvents do not obey the solubility curve. Clearly, the CO<sub>2</sub> solubility is strongly affected by the high molecular weight of the ILs. As explained in Chapter 3, the dissolution of CO<sub>2</sub> in ILs is a free volume effect, which effectively means that the CO<sub>2</sub> molecules are hosted in the cavities of the IL structure [149, 248]. It is, therefore, also interesting to compare the solubility on a volume basis. A comparison for the CO<sub>2</sub> solubility in ILs and

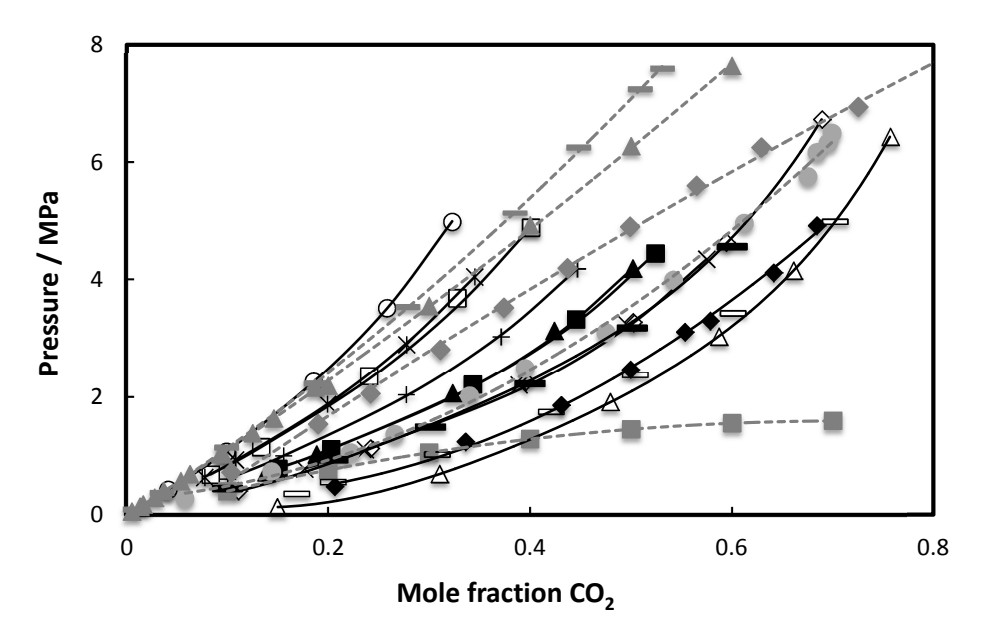


Figure 9.1: Solubility of CO<sub>2</sub> on mole fraction basis in ILs and commercial solvents (gray symbols). All data except for Rectisol are obtained at 313.15 K. The Rectisol process operates at low temperatures, therefore the reported data is at 248.15 K. ILs: trihexyltetradecylphosphonium bis(2,4,4- trimethylpentyl)phosphinate, open triangles; trihexyltetradecylphosphonium dicyanamide, open diamonds; 1-ethyl-3-methylimidazolium diethylphosphate, open squares; 1-allyl-3-methylimidazolium dicyanamide, open circles; 1-butyl-3-methylpyrrolidinium dicyanamide, stars; 1,2,3-tris(diethylamino)cyclopropenylium dicyanamide, pluses; methyltrioctylammonium bis(trifluoromethylsulfonyl)imide, black diamonds; 1-butyl-3-methyl-piperidinium bis(trifluoromethylsulfonyl)imide, black squares; 1,2,3-tris(diethylamino)cyclopropenylium bis(trifluoromethylsulfonyl)imide, crosses; triethylsulfonium bis(trifluoromethylsulfonyl)imide, black triangles; trihexyltetradecylphosphonium bis(trifluoromethylsulfonyl)imide, open rectangles; and 1-ethyl-3-methylimidazolium tris(pentafluoroethyl)trifluorophosphate, black rectangles. Commercial solvents: Selexol (Genosorb 1753), gray circles; propylene carbonate, gray triangles; Rectisol, gray squares; Purisol, gray diamonds; and sulfolane, gray rectangles. Lines are polynomial fits to guide the eye. Data for the ILs can be found in Ramdin et al. [345] and the references cited therein. Data of the commercial solvents can be found in Refs [354, 358, 484–486].

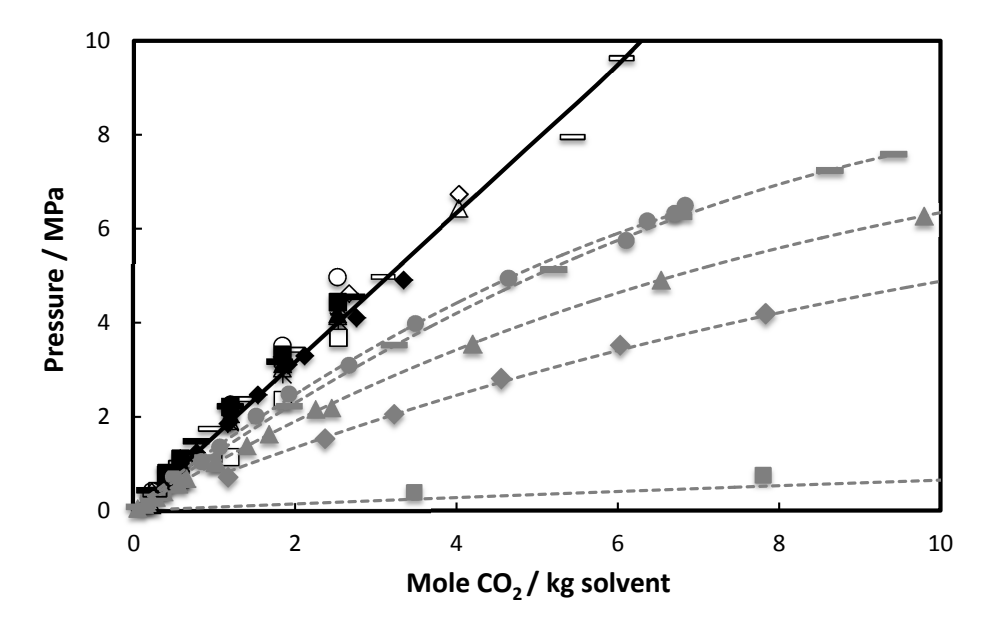


Figure 9.2: Solubility of  $CO_2$  on molality basis in ILs and commercial solvents (gray symbols). Symbols have the same meaning as in Figure 9.1. Solid line is calculated using the correlation of Carvalho and Coutinho [125] at 313.15 K and dashed lines are polynomial fits to guide the eye. All data except for Rectisol, which is at 248.15 K, are obtained at 313.15 K.

in conventional solvents on a molarity (i.e., kilomoles of gas per volume of solvent) basis is provided in Figure 9.3. The difference in solubility between the different ILs on a volume basis is also minimized. Figures 9.2 and 9.3 clearly show that conventional solvents are superior to ILs in terms of mass or volume based solubilities of  $CO_2$ .

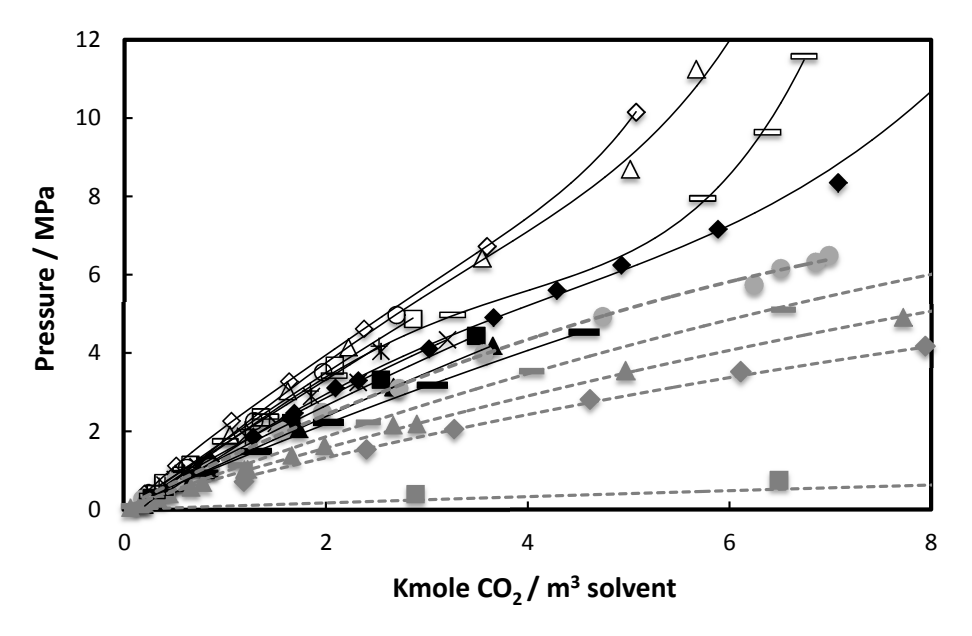


Figure 9.3: Solubility of  $CO_2$  on volume basis in ILs and commercial solvents (gray symbols). Symbols have the same meaning as in Figure 9.1. Lines are polynomial fits to guide the eye. All data except for Rectisol, which is at 248.15 K, are obtained at 313.15 K.

# 9.2.2 CH<sub>4</sub> Solubility

The mole fraction based solubility of  $CH_4$  is shown in Figure 9.4 for several ILs and commercial solvents. The solubility trend for  $CH_4$  is similar to that of  $CO_2$ : the solubility of  $CH_4$  increases also with an increasing IL molecular weight. However, the molality based solubility data of  $CH_4$  do not collapse on a universal curve as in the case of  $CO_2$ , see Figure 9.5. The volume based solubility trend for  $CH_4$  is not much different from the observed solubility trend on molality basis, see Figure 9.6. Furthermore, solubility of  $CH_4$  in conventional solvents are lower than those ILs previously characterized as promising for  $CO_2$  capture. One exception is the 1-ethyl-

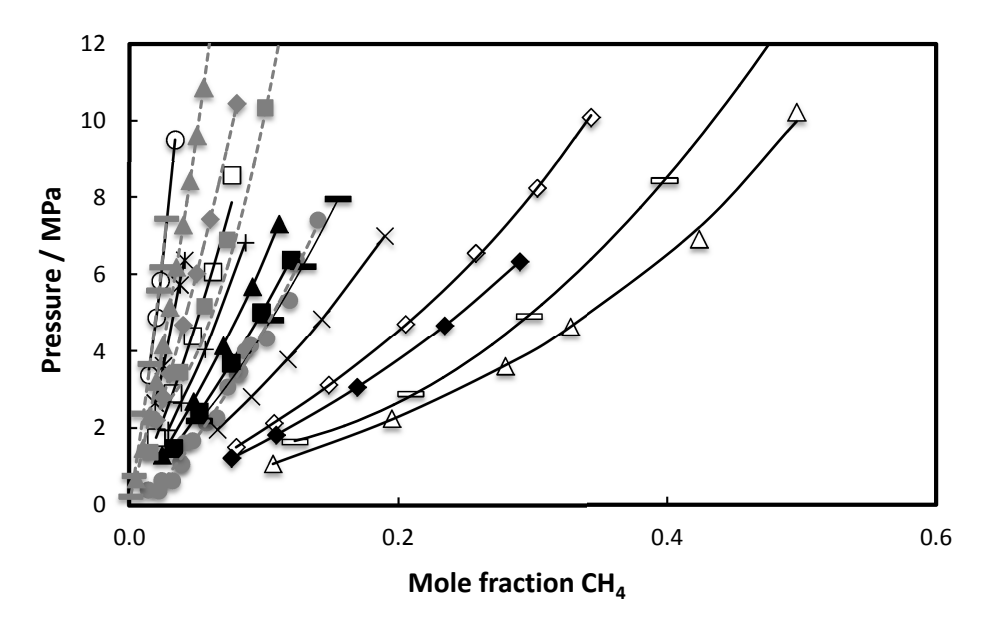


Figure 9.4: Solubility of  $CH_4$  on mole fraction basis in ILs and commercial solvents (gray symbols). Symbols have the same meaning as in Figure 9.1. Lines are polynomial fits to guide the eye. All data except for Rectisol, which is at 248.15 K, are obtained at 313.15 K. Data of commercial solvents can be found in Refs [355, 358, 362, 487, 488].

3-methylimidazolium tris(pentafluoroethyl)trifluorophosphate [emim][FAP] IL, which has a comparable CO<sub>2</sub> and CH<sub>4</sub> solubility as Selexol even on a mass or volume scale. A suitable solvent for natural gas sweetening should not only have a high CO<sub>2</sub> solubility, but at the same time a low CH<sub>4</sub> solubility to avoid valuable product losses.

# 9.2.3 Selectivity

As mentioned earlier, not the solubility, but rather the selectivity is the key parameter for judging the separation performance of an absorption process. In Chapter 3, we showed that the ideal CO<sub>2</sub>/CH<sub>4</sub> selectivity

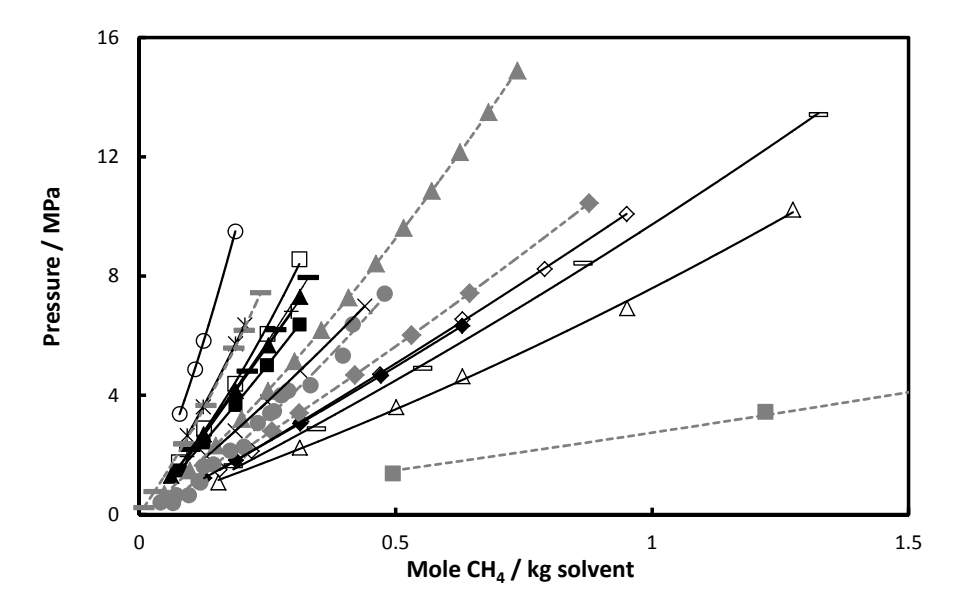


Figure 9.5: Solubility of  $CH_4$  on molality basis in ILs and commercial solvents (gray symbols). Symbols have the same meaning as in Figure 9.1. Lines are polynomial fits to guide the eye. All data except for Rectisol, which is at 248.15 K, are obtained at 313.15 K.

in ILs is comparable to that of commercial solvents like Selexol, Purisol, Rectisol, propylene carbonate, and sulfolane [345]. In Chapters 4 and 6, we showed that the ideal selectivity is approximately the same as the real selectivity. The ideal CO<sub>2</sub>/CH<sub>4</sub> selectivity in ILs and conventional solvents was also shown to decrease dramatically with increasing temperature [345]. Therefore, the process should operate at low temperature to have a high CO<sub>2</sub>/CH<sub>4</sub> selectivity. The viscosity of existing ILs at low temperatures are an order of magnitude higher than that of conventional solvents, which forms a serious barrier for their application in the natural gas process.

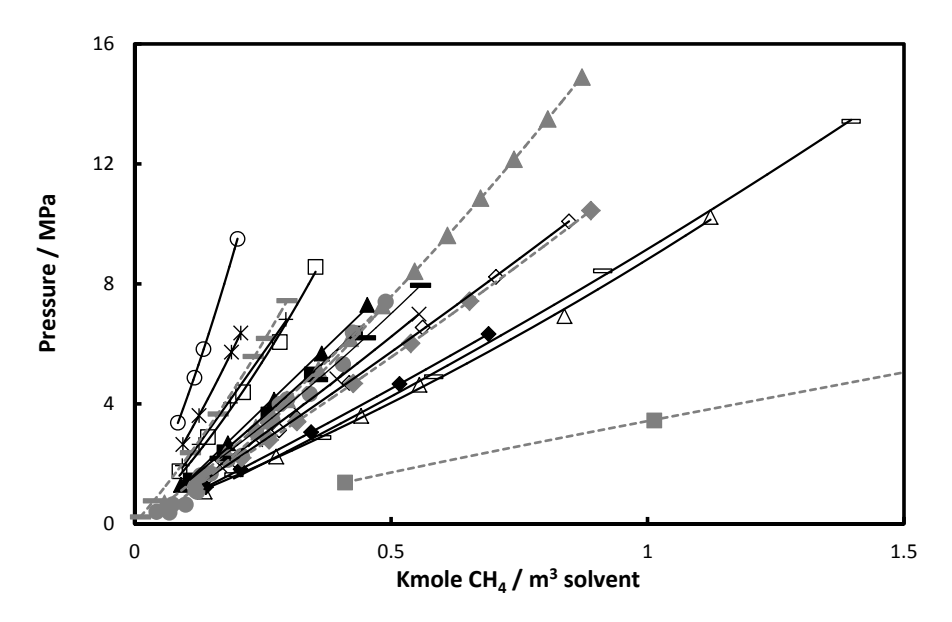


Figure 9.6: Solubility of  $CH_4$  on volume basis in ILs and commercial solvents (gray symbols). Symbols have the same meaning as in Figure 9.1. Lines are polynomial fits to guide the eye. All data except for Rectisol, which is at 248.15 K, are obtained at 313.15 K.

# 9.3 Conclusions

A detailed comparison for the solubility/selectivity of carbon dioxide (CO<sub>2</sub>) and methane (CH<sub>4</sub>) in ionic liquids (ILs) and commercial solvents Selexol, Purisol, Rectisol, propylene carbonate, and sulfolane is presented. The solubilities are compared on mole fraction, molality, and volume basis to avoid the effect caused by the high molecular weight of ILs. Conventional solvents are superior to ILs when CO<sub>2</sub> and CH<sub>4</sub> solubilities are compared on a mass or volume basis. Although the CO<sub>2</sub>/CH<sub>4</sub> selectivity in ILs are similar to that of commercial solvents, the high price and viscosity of ILs may limit their application in the natural gas sweetening process.

## References

[1] WORKING GROUP III OF THE IPCC. IPCC Special Report on Carbon Dioxide Capture and Storage, 2005. https://www.ipcc.ch/publications\_and\_data/\_reports\_carbon\_dioxide.htm.

- [2] IPCC. Climate Change 2007: Synthesis Report, 2007. https://www.ipcc.ch/publications\_and\_data/publications\_ipcc\_fourth\_assessment\_report\_synthesis\_report.htm.
- [3] HASZELDINE, R.S. Carbon Capture and Storage: How Green Can Black Be? *Science*, 325, 2009: 1647–1651.
- [4] Liu, K.; Song, C.; and Subramani, V. Hydrogen and Syngas Production and Purification Technologies. Wiley, Hoboken, 2010.
- [5] FIGUEROA, J.D.; FOUT, T.; PLASYNSKI, S.; MCILVRIED, H.; and SRIVASTAVA, R.D. Advances in CO<sub>2</sub> capture technology-The U.S. Department of Energy's Carbon Sequestration Program. *Int. J. Greenhouse Gas Control*, 2, 2008: 9–20.
- [6] MOULIJN, J.A.; MAKKEE, M.; and VAN DIEPEN, A. Chemical Process Technology. Wiley, Chichester, 2001.
- [7] RAMDIN, M.; BALAJI, S.P.; VICENT-LUNA, J.M.; GUTIÉRREZ-SEVILLANO, J.J.; CALERO, S.; DE LOOS, T.W.; and VLUGT, T.J.H. Solubility of the Precombustion Gases CO<sub>2</sub>, CH<sub>4</sub>, CO, H<sub>2</sub>, N<sub>2</sub>, and H<sub>2</sub>S in the Ionic Liquid [bmim][Tf<sub>2</sub>N] from Monte Carlo Simulations. *J. Phys. Chem. C*, 118, 2014: 23599–23604.
- [8] RAMDIN, M.; AMPLIANITIS, A.; DE LOOS, T.W.; and VLUGT, T.J.H. Solubility of CO<sub>2</sub>/CH<sub>4</sub> gas mixtures in ionic liquids. Fluid Phase Equilib., 375, 2014: 134–142.
- [9] RAMDIN, M.; DE LOOS, T.W.; and VLUGT, T.J.H. State-of-the-Art of CO<sub>2</sub> Capture with Ionic Liquids. *Ind. Eng. Chem. Res.*, 51, 2012: 8149–8177.

- [10] TENNYSON, R.N. and SCHAAF, R.P. Guidelines can help choose proper process for gas-treating plants. *Oil and Gas J.*, 75, 1977: 78–80, 85.
- [11] KOHL, A.L. and Nielsen, R.B. *Gas Purification*. Gulf Publishing Company, Houston, 5th edition, 1997.
- [12] JONES, C.W. CO<sub>2</sub> Capture from Dilute Gases as a Component of Modern Global Carbon Management. Annu. Rev. Chem. Biomol. Eng., 2, 2011: 31–52.
- [13] OLIVIER, J.G.J.; JANSSENS-MAENHOUT, G.; and PETERS, J.A.H.W. *Trends in global CO<sub>2</sub> emissions; 2012 Report*. PBL Netherlands Environmental Assessment Agency, The Hague, The Netherlands, 2012.
- [14] BP. BP Energy Outlook 2035. BP, London, United Kingdom, 2014. http://www.bp.com/en/global/corporate/about-bp/energy-economics/energy-outlook.html.
- [15] D'ALESSANDRO, D.M.; SMIT, B.; and LONG, J.R. Carbon Dioxide Capture: Prospects for New Materials. *Angew. Chem., Int. Ed.*, 49, 2010: 6058–6082.
- [16] Kumar, S.; Cho, J.H.; and Moon, I. Ionic liquid-amine blends and CO<sub>2</sub>BOLs: Prospective solvents for natural gas sweetening and CO<sub>2</sub> capture technology-A review. *Int. J. Greenh. Gas Control*, 20, 2014: 87–116.
- [17] KARADAS, F.; ATILHAN, M.; and APARICIO, S. Review on the Use of Ionic Liquids (ILs) as Alternative Fluids for CO<sub>2</sub> Capture and Natural Gas Sweetening. *Energy Fuels*, 24, 2010: 5817–5828.
- [18] RAMDIN, M.; BALAJI, S.P.; TORRES-KNOOP, A.; DUBBELDAM, D.; DE LOOS, T.W.; and Vlugt, T.J.H. Solubility of Natural Gas Species in Ionic liquids and Commercial Solvents: Experiments and Monte Carlo Simulations. J. Chem. Eng. Data, 60, 2015: 3039–3045.

[19] BALAJI, S.P.; GANGARAPU, S.; RAMDIN, M.; TORRES-KNOOP, A.; ZUILHOF, H.; GOETHEER, E.L.V.; DUBBELDAM, D.; and VLUGT, T.J.H. Simulating the Reactions of CO<sub>2</sub> in Aqueous Monoethanolamine Solution by Reaction Ensemble Monte Carlo Using the Continuous Fractional Component Method. J. Chem. Theory Comput., 11, 2015: 2661–2669.

- [20] INTERNATIONAL ENERGY AGENCY. CO<sub>2</sub> Emissions from Fuel Combustion Highlights 2010. http://www.iea.org/media/training/presentations/statisticsmarch/co2highlights.pdf.
- [21] INTERNATIONAL ENERGY AGENCY. Energy Technology Perspectives 2010. https://www.iea.org/publications/freepublications/publication/etp2010.pdf.
- [22] INTERNATIONAL ENERGY AGENCY. World Energy Outlook 2009. http://www.worldenergyoutlook.org/media/weowebsite/2009/WE02009.pdf.
- [23] MEINSHAUSEN, M.; MEINSHAUSEN, N.; HARE, W.; RAPER, S.C.B.; FRIELER, K.; KNUTTI, R.; FRAME, D.J.; and ALLEN, M.R. Greenhouse-gas emission targets for limiting global warming to 2 °C. *Nature*, 458, 2009: 1158–1162.
- [24] SOLOMON, S. Irreversible climate change due to carbon dioxide emissions. *PNAS*, 106, 2010: 1704–1709.
- [25] MCKINSEY & COMPANY. Pathways to a Low-Carbon Economy. Version 2 of the Global Greenhouse Gas Abatement Cost Curve, 2009. http://www.mckinsey.com/client\_service/sustainability/latest\_thinking/pathways\_to\_a\_low\_carbon\_economy.
- [26] MCKINSEY & COMPANY. Reducing U.S. Greenhouse Gas Emissions: How Much at What Cost?, 2007. http://www.mckinsey.com/client\_service/sustainability/latest\_thinking/reducing\_us\_greenhouse\_gas\_emissions.

- [27] THE MCKINSEY QUARTERLY. A cost curve for greenhouse gas reduction, 2007. http://www.mckinsey.com/insights/sustainability/a\_cost\_curve\_for\_greenhouse\_gas\_reduction.
- [28] MCKINSEY & COMPANY. Carbon Capture & Storage: Assessing the Economics, 2008. http://assets.wwf.ch/downloads/mckinsey2008.pdf.
- [29] MASSACHUSETTS INSTITUTE OF TECHNOLOGY. The Future of Coal, 2007. http://web.mit.edu/coal/The\_Future\_of\_Coal\_Summary\_Report.pdf.
- [30] IEA CLEAN Coal CENTRE. Coal use in the of China. and South economies India Africa. new 2010. http://www.iea-coal.org.uk/documents/ 82270/7433/Coal-use-in-the-new-economies-of-China, -India-and-South-Africa-(CCC/161).
- [31] SOCOLOW, R.H. Can We Bury Global Warming? Sci. Am., July, 2005: 49–55.
- [32] GOUGH, C. State of the art in carbon dioxide capture and storage in the UK: An experts' review. *Int. J. Greenhouse Gas Control*, 2, 2008: 155–168.
- [33] ROCHELLE, G.T. Amine Scrubbing for  $CO_2$  Capture. Science, 325, 2009: 1652-1654.
- [34] VAIDYA, P.D. and KENIG, E.Y. CO<sub>2</sub>-Alkanolamine Reaction Kinetics: A Review of Recent Studies. *Chem. Eng. Technol.*, 30, 2007: 1467–1474.
- [35] DOE-NETL. Carbon Dioxide Capture from Existing Coal-Fired Power Plants, 2007. http://www.netl.doe.gov/ research/energy-analysis/publications/details?pub= a910f7cf-1546-47b2-b6a2-dd4677864c4a.

[36] DOE-NETL. Research and Development Goals for CO<sub>2</sub> Capture Technology, 2011. http://www.netl.doe.gov/File% 20Library/Research/Energy%20Analysis/Publications/DOE-NETL-2009-1366-R-DGoalsforCO2CaptureTech.pdf.

- [37] Tollefson, J. Low cost carbon capture project sparks interest. Nature, 469, 2011: 276–277.
- [38] INVENTYS. CO<sub>2</sub> capture for \$15 per tonne. Carbon Capture J., Jan-Feb, 2011: 6-7.
- [39] HERZOG, H.; MELDON, J.; and HATTON, A. Advanced Post-Combustion CO<sub>2</sub> Capture, 2009. https://mitei.mit.edu/system/files/herzog-meldon-hatton.pdf.
- [40] MACDOWELL, N.; FLORIN, N.; BUCHARD, A.; HALLETT, J.; GALINDO, A.; JACKSON, G.; ADJIMAN, C.S.; WILLIAMS, C.; SHAH, N.; and FENNELL, P. An overview of CO<sub>2</sub> capture technologies. *Energy Environ. Sci.*, 3, 2010: 1645–1669.
- [41] BLANCHARD, L.A.; HANCU, D.; BECKMAN, E.J.; and BRENNECKE, J.F. Green processing using ionic liquids and CO<sub>2</sub>. *Nature*, 399, 1999: 28–29.
- [42] Anthony, J.L.; Maginn, E.J.; and Brennecke, J.F. Solubilities and Thermodynamic Properties of Gases in the Ionic Liquid 1-n-Butyl-3-methylimidazolium Hexafluorophosphate. *J. Phys. Chem. B*, 106, 2002: 7315–7320.
- [43] Freemantle, M. An Introduction to Ionic Liquids. RSC Publishing, London, 2010.
- [44] Freemantle, M. Designer Solvents: Ionic liquids may boost clean technology development. *Chem. Eng. News*, 76, 1998: 32–37.
- [45] SEDDON, K.R. Ionic Liquids for Clean Technology. J. Chem. Tech. Biotechnol., 68, 1997: 351–356.

- [46] Earle, M.J. and Seddon, K.R. Ionic Liquids. Green solvents for the future. *Pure Appl. Chem.*, 72, 2000: 1391–1398.
- [47] Brennecke, J.F. and Maginn, E.J. Ionic Liquids: Innovative Fluids for Chemical Processing. *AIChE J.*, 47, 2001: 2384–2389.
- [48] Berthod, A.; Ruiz-Angel, M.J.; and Carda-Broch, S. Ionic liquids in separation techniques. *J. Chromatogr. A*, 1184, 2008: 6–18.
- [49] Sheldon, R. Catalytic reactions in ionic liquids. *Chem. Commun.*, 23, 2001: 2399–2407.
- [50] Zhao, D.; Wu, M.; Kou, Y.; and Min, E. Ionic liquids: applications in catalysis. *Catalysis Today*, 74, 2002: 157–189.
- [51] Parvulescu, V.I. and Hardacre, C. Catalysis in Ionic Liquids. *Chem. Rev.*, 107, 2007: 2615–2665.
- [52] BUZZEO, M.C.; EVANS, R.G.; and COMPTON, R.G. Non-Haloaluminate Room-Temperature Ionic Liquids in Electrochemistry-A Review. *Chem. Phys. Chem.*, 5, 2004: 1106–1120.
- [53] MACFARLANE, D.R.; FORSYTH, M.; HOWLETT, P.C.; PRINGLE, J.M.; SUN, J.; ANNAT, G.; NEIL, W.; and IZGORODINA, E. Ionic Liquids in Electrochemical Devices and Processes: Managing Interfacial Electrochemistry. Acc. Chem. Res., 40, 2007: 1165–1173.
- [54] BLANCHARD, L.A. and BRENNECKE, J.F. Recovery of Organic Products from Ionic Liquids Using Supercritical Carbon Dioxide. *Ind. Eng. Chem. Res.*, 40, 2001: 287–292.
- [55] HAN, X. and ARMSTRONG, D.W. Ionic liquids in Separations. Acc. Chem. Res., 40, 2007: 1079–1086.
- [56] HUDDLESTON, J.G.; WILLAUER, H.D.; SWATLOSKI, R.P.; VISSER, A.E.; and ROGERS, R.D. Room temperature ionic liquids as novel media for 'clean' liquid-liquid extraction. *Chem. Commun.*, 1998: 1765–1766.

[57] BUZZEO, M.C.; EVANS, R.G.; and COMPTON, R.G. Examination of the Potential of Ionic Liquids for Gas Separations. *Sep. Sci. Technol.*, 40, 2005: 525–541.

- [58] Zhao, H. Innovative Applications of Ionic Liquids as "Green" Engineering Liquids. *Chem. Eng. Commun.*, 193, 2006: 1660–1677.
- [59] Zhu, S.; Wu, Y.; Chen, Q.; Yu, Z.; Wang, C.; Jin, S.; Ding, Y.; and Wu, G. Dissolution of cellulose with ionic liquids and its application: a mini-review. *Green Chem.*, 8, 2006: 325–327.
- [60] ROGERS, R.D. Reflections on ionic liquids. *Nature*, 447, 2007: 917–918.
- [61] WASSERSCHEID, P. and WELTON, T. *Ionic Liquids in Synthesis*, volume 2. Wiley-VCH, Weinheim, 2008.
- [62] ROGERS, R.D. and SEDDON, K. Ionic Liquids-Solvents of the Future? Science, 302, 2003: 792–793.
- [63] SEDDON, K.R. Ionic Liquids: A taste of the future. *Nature*, 2, 2003: 363–365.
- [64] Huang, J. and Rüther, T. Why are Ionic Liquids Attractive for CO<sub>2</sub> Absorption? An Overview. Aust. J. Chem., 62, 2009: 298–308.
- [65] Hasib-ur-Rahman, M.; Siaj, M.; and Larachi, F. Ionic liquids for CO<sub>2</sub> capture-Development and progress. *Chem. Eng. Proc.*, 49, 2010: 313–322.
- [66] Brennecke, J.F. and Gurkan, B.E. Ionic Liquids for CO<sub>2</sub> Capture and Emission Reduction. *J. Phys. Chem. Lett.*, 1, 2010: 3459–3464.
- [67] MAGINN, E.J. What to Do with CO<sub>2</sub>. J. Phys. Chem. Lett., 1, 2010: 3478–3479.
- [68] BARA, J.E.; CAMPER, D.E.; GIN, D.L.; and NOBLE, R.D. Room-Temperature Ionic Liquids and Composite Materials: Platform Technologies for CO<sub>2</sub> Capture. *Acc. Chem. Res.*, 43, 2010: 152–159.

- [69] PLECHKOVA, N.V. and SEDDON, K.R. Applications of ionic liquids in the chemical industry. *Chem. Soc. Rev.*, 37, 2008: 123–150.
- [70] FERON, P.H.M. and HENDRIKS, C.A. CO<sub>2</sub> Capture Process Principles and Costs. *Oil & Gas Sci. Technol.*, 60, 2005: 451–459.
- [71] BIELLO, D. Can Captured Carbon Save Coal? Sci. Am. Earth 3.0, June, 2009: 52–59.
- [72] Bailey, D.W. and Feron, P.H.M. Post-combustion Decarbonisation Processes. Oil & Gas Sci. Technol., 60, 2005: 461–474.
- [73] DOE-NETL. Cost and Performance Baseline for Fossil Energy Plants, Volume 1: Bituminous Coal and Natural Gas to Electricity, 2007. http://www.netl.doe.gov/research/energy-analysis/energy-baseline-studies.
- [74] ROJEY, A.; JAFFRET, C.; CORNOT-GANDOLPHE, S.; DURAND, B.; JULLIAN, S.; and VALAIS, M. Natural Gas Production Processing Transport. Editions Technip, Paris, 1994.
- [75] Eide, L.I. and Bailey, D.W. Precombustion Decarbonisation Processes. Oil & Gas Sci. Technol., 60, 2005: 475–484.
- [76] ANHEDEN, M.; YAN, J.; and DE SMEDT, G. Denitrogenation (or Oxyfuel Concepts). Oil & Gas Sci. Technol., 60, 2005: 485–495.
- [77] DOE-NETL. Cost and Performance Baseline for Fossil Energy Plants, Volume 1: Bituminous Coal and Natural Gas to Electricity, 2010. http://www.netl.doe.gov/research/energy-analysis/energy-baseline-studies.
- [78] DOE-NETL. Coal-Fired Power Plants in the United States: Examination of the Costs of Retrofitting with CO<sub>2</sub> Capture Technology, Revision 3, 2011. http://www.netl.doe.gov/File%20Library/Research/Energy%20Analysis/Publications/GIS\_CCS\_retrofit.pdf.

[79] DOE-NETL. Cost and Performance Baseline for Fossil Energy Plants, Volume 3 Executive Summary: Low Rank Coal and Natural Gas to Electricity, 2011. http://www.netl.doe.gov/research/energy-analysis/energy-baseline-studies.

- [80] DOE-NETL. Cost and Performance Baseline of PC and IGCC Plants for a Range of Carbon Dioxide Capture, 2011. http://www.netl.doe.gov/File%20Library/Research/Energy% 20Analysis/Publications/Gerdes-08022011.pdf.
- [81] DOE-NETL. Cost and Performance Baseline for Fossil Energy Plants, Volume 3a: Low Rank Coal to Electricity: IGCC Cases, 2011. http://www.netl.doe.gov/research/energy-analysis/energy-baseline-studies.
- [82] DOE-NETL. Cost and Performance Baseline for Fossil Energy Plants, Volume 3a: Low Rank Coal to Electricity: Combustion Cases, 2011. http://www.netl.doe.gov/research/energy-analysis/energy-baseline-studies.
- [83] DOE-NETL. Advancing Oxycombustion Technology for Bituminous Coal Power Plants: An R&D Guide, 2012. http://www.netl.doe.gov/File%20Library/Research/Energy%20Analysis/Publications/DOE-NETL-2010-1405FinalReport042012.pdf.
- [84] DOE-NETL. Current and Future Technologies for Power Generation with Post-Combustion Carbon Capture, 2012. http://netl.doe.gov/File%20Library/Research/Energy% 20Analysis/Publications/NETL-DOE-2012-1557.pdf.
- [85] IEA CLEAN COAL CENTRE. Oxyfuel combustion of pulverised coal, 2010. http://www.iea-coal.org.uk/documents/82355/7537/Oxyfuel-combustion-of-pulverised-coal-(CCC/168).
- [86] INTERNATIONAL ENERGY AGENCY. World Energy Outlook 2010. http://www.worldenergyoutlook.org/media/weo2010.pdf.

- [87] Dow CHEMICAL COMPANY. Gas Sweetening, 1998. http://msdssearch.dow.com/PublishedLiteratureDOWCOM/dh\_0039/0901b803800391f8.pdf?filepath=gastreating/pdfs/noreg/170-01395.pdf&fromPage=GetDoc.
- [88] IEA CLEAN COAL CENTRE. Post-combustion carbon capture from coal fired plants solvent scrubbing, 2007. http://www.iea-coal.org.uk/documents/81793/6448/Carbon-capture.
- [89] BLANCHARD, L.A.; Gu, Z.; and BRENNECKE, J.F. High-Pressure Phase Behavior of Ionic Liquid/CO<sub>2</sub> Systems. *J. Phys. Chem. B.*, 105, 2001: 2437–2444.
- [90] NG, H. and ROBINSON, D.B. Equilibrium Phase Properties of the Toluene-Carbon Dioxide System. *J. Chem. Eng. Data*, 23, 1978: 325–327.
- [91] LI, Y.; DILLARD, K.H.; and ROBINSON, R.L. Vapor-Liquid Phase Equilibrium for Carbon Dioxide-n-Hexane at 40, 80, and 120 °C. *J. Chem. Eng. Data*, 26, 1981: 53–55.
- [92] Kroon, M.C.; Shariati, A.; Costantini, M.; van Spronsen, J.; Witkamp, G.; Sheldon, R.A.; and Peters, C.J. High-Pressure Phase Behavior of Systems with Ionic Liquids: Part V. The Binary System Carbon Dioxide + 1-Butyl-3-methylimidazolium Tetrafluoroborate. J. Chem. Eng. Data, 50, 2005: 173–176.
- [93] Shariati, A. and Peters, C.J. High-pressure phase behavior of systems with ionic liquids: II. The binary system carbon dioxide+1-ethyl-3-methylimidazolium hexafluorophosphate. *J. Supercrit. Fluids*, 29, 2004: 43–48.
- [94] CARVALHO, P.J.; ALVAREZ, V.H.; MACHADO, J.J.B.; PAULY, J.; DARIDON, J.; MARRUCHO, I.M.; AZNAR, M.; and COUTINHO, J.A.P. High pressure phase behavior of carbon dioxide in 1-alkyl-3methylimidazolium bis(trifluoromethylsulfonyl)imide ionic liquids. *J. Supercrit. Fluids*, 48, 2009: 99–107.

[95] DANESHVAR, M.; KIM, S.; and GULARI, E. High-Pressure Phase Equilibria of Ploy(ethylene glycol)-Carbon Dioxide Systems. *J. Phys. Chem.*, 94, 1990: 2124–2128.

- [96] KONYNENBURG, P.H.V. and SCOTT, R.L. Critical Lines and Phase Equilibria in Binary Van Der Waals Mixtures. *Phil. Trans. R. Soc.* A, 298, 1980: 495–540.
- [97] AKI, S.N.V.K.; MELLEIN, B.R.; SAURER, E.M.; and BREN-NECKE, J.F. High-Pressure Phase Behavior of Carbon Dioxide with Imidazolium-Based Ionic Liquids. J. Phys. Chem. B, 108, 2004: 20355– 20365.
- [98] Anthony, J.L.; Anderson, J.L.; Maginn, E.J.; and Brennecke, J.F. Anion Effects on Gas Solubility in Ionic Liquids. *J. Phys. Chem.* B, 109, 2005: 6366–6374.
- [99] Cadena, C.; Anthony, J.L.; Shah, J.K.; Morrow, T.I.; Brennecke, J.F.; and Maginn, E.J. Why is CO<sub>2</sub> So Soluble in Imidazolium-Based Ionic Liquids? *J. Am. Chem. Soc.*, 126, 2004: 5300–5308.
- [100] KAZARIAN, S.G.; BRISCOE, B.J.; and WELTON, T. Combining ionic liquids and supercritical fluids: in situ ATR-IR study of CO<sub>2</sub> dissolved in two ionic liquids at high pressures. *Chem. Commun.*, 2000: 2047–2048.
- [101] KANAKUBO, M.; UMECKY, T.; HIEJIMA, Y.; AIZAWA, T.; NANJO, H.; and KAMEDA, Y. Solution Structures of 1-Butyl-3methylimidazolium Hexafluorophosphate Ionic Liquid Saturated with CO<sub>2</sub>: Experimental Evidence of Specific Anion-CO<sub>2</sub> Interaction. J. Phys. Chem. B Lett., 2005: 13847–13850.
- [102] Muldoon, M.J.; Aki, S.N.V.K.; Anderson, J.L.; Dixon, J.K.; and Brennecke, J.F. Improving Carbon Dioxide Solubility in Ionic Liquids. *J. Phys. Chem. B*, 111, 2007: 9001–9009.

- [103] KUMELAN, J.; PEREZ-SALADO KAMPS, A.; TUMA, D.; and MAURER, G. Solubility of CO<sub>2</sub> in the Ionic Liquids [bmim][CH<sub>3</sub>SO<sub>4</sub>] and [bmim][PF<sub>6</sub>]. *J. Chem. Eng. Data*, 51, 2006: 1802–1807.
- [104] Maiti, A. Theoretical Screening of Ionic Liquid Solvents for Carbon Capture. *ChemSusChem*, 2, 2009: 628–631.
- [105] SISTLA, Y.S. and KHANNA, A. Validation and Prediction of the Temperature-Dependent Henry's Constant for CO<sub>2</sub>-Ionic Liquid Systems Using the Conductor-like Screening Model for Realistic Solvation (COSMO-RS). J. Chem. Eng. Data, 56, 2011: 4045–4060.
- [106] Zhang, X.; Liu, Z.; and Wang, W. Screening of Ionic Liquids to Capture  $\rm CO_2$  by COSMO-RS and Experiments. *AIChE J.*, 54, 2008: 2717–2728.
- [107] PALOMAR, J.; GONZALEZ-MIQUEL, M.; POLO, A.; and RODRIGUEZ, F. Understanding the Physical Absorption of CO<sub>2</sub> in Ionic Liquids Using the COSMO-RS Method. *Ind. Eng. Chem. Res.*, 50, 2011: 3452–3463.
- [108] KUMELAN, J.; TUMA, D.; PEREZ-SALADO KAMPS, A.; and MAURER, G. Solubility of the Single Gases Carbon Dioxide and Hydrogen in the Ionic Liquid [bmpy][Tf<sub>2</sub>N]. J. Chem. Eng. Data, 55, 2010: 165–172.
- [109] CARVALHO, P.J.; ALVAREZ, V.H.; MARRUCHO, I.M.; AZNAR, M.; and COUTINHO, J.A.P. High carbon dioxide solubilities in trihexyltetradecylphosphonium-based ionic liquids. *J. Supercrit. Fluids*, 52, 2010: 258–265.
- [110] SCHILDERMAN, A.M.; RAEISSI, S.; and PETERS, C.J. Solubility of carbon dioxide in the ionic liquid 1-ethyl-3-methylimidazolium bis(trifluoromethylsulfonyl)imide. *Fluid Phase Equilib.*, 260, 2007: 19–22.

[111] Almantariotis, D.; Gefflaut, T.; Padua, A.A.H.; Coxam, J.Y.; and Costa Gomes, M.F. Effect of Fluorination and Size of the Alkyl Side-Chain on the Solubility of Carbon Dioxide in 1-Alkyl-3-methylimidazolium Bis(trifluoromethylsulfonyl)amide Ionic Liquids. *J. Phys. Chem. B*, 114, 2010: 3608–3617.

- [112] Shimoyama, Y. and Ito, A. Predictions of cation and anion effects on solubilities, selectivities and permeabilities for CO<sub>2</sub> in ionic liquid using COSMO based activity coefficient model. *Fluid Phase Equilib.*, 297, 2010: 178–182.
- [113] Maginn, E.J. Molecular simulation of ionic liquids: current status and future opportunities. *J. Phys.: Condens. Matter*, 21, 2009: 1–17.
- [114] RAMDIN, M.; CHEN, Q.; BALAJI, S.P.; VICENT-LUNA, J.M.; TORRES-KNOOP, A.; DUBBELDAM, D.; CALERO, S.; DE LOOS, T.W.; and VLUGT, T.J.H. Solubilities of CO<sub>2</sub>, CH<sub>4</sub>, C<sub>2</sub>H<sub>6</sub>, and SO<sub>2</sub> in ionic liquids and Selexol from Monte Carlo simulations. *J. Comput. Sci.*, (in press), 2015.
- [115] KILARU, P.K.; CONDEMARIN, R.A.; and SCOVAZZO, P. Correlations of Low-Pressure Carbon Dioxide and Hydrocarbon Solubilities in Imidazolium-, Phosphonium-, and Ammonium-Based Room-Temperature Ionic Liquids. Part 1. Using Surface Tension. *Ind. Eng. Chem. Res.*, 47, 2008: 900–909.
- [116] BLATH, J.; CHRIST, M.; DEUBLER, N.; HIRTH, T.; and SCHIESTEL, T. Gas solubilities in room temperature ionic liquids-Correlation between RTIL-molar mass and Henry's law constant. *Chem. Eng. J.*, 172, 2011: 167–176.
- [117] CAMPER, D.; SCOVAZZO, P.; KOVAL, C.; and NOBLE, R. Gas Solubilities in Room-Temperature Ionic Liquids. *Ind. Eng. Chem. Res*, 43, 2004: 3049–3054.

- [118] VEGA, L.F.; VILASECA, O.; LLOVELL, F.; and ANDREU, J.S. Modeling ionic liquids and the solubility of gases in them: Recent advances and perspectives. *Fluid Phase Equilib.*, 294, 2010: 15–30.
- [119] CAMPER, D.; KOVAL, C.; and NOBLE, R. Low Pressure Hydrocarbon Solubility in Room Temperature Ionic Liquids Containing Imidazolium Rings Interpreted Using Regular Solution Theory. *Ind. Eng. Chem. Res*, 44, 2005: 1928–1933.
- [120] CAMPER, D.; BARA, J.; KOVAL, C.; and NOBLE, R. Bulk-Fluid Solubility and Membrane Feasibility of Rmim-Based Room-Temperature Ionic Liquids. *Ind. Eng. Chem. Res*, 45, 2006: 6279–6283.
- [121] SCOVAZZO, P.; CAMPER, D.; KIEFT, J.; POSHUSTA, J.; KOVAL, C.; and NOBLE, R. Regular Solution Theory and CO<sub>2</sub> Gas Solubility in Room-Temperature Ionic Liquids. *Ind. Eng. Chem. Res.*, 43, 2004: 6855–6860.
- [122] FINOTELLO, A.; BARA, J.E.; NARAYAN, S.; CAMPER, D.; and NOBLE, R.D. Ideal Gas Solubilities and Solubility Selectivities in a Binary Mixture of Room-Temperature Ionic Liquids. *J. Phys. Chem. B*, 112, 2008: 2335–2339.
- [123] FINOTELLO, A.; BARA, J.E.; CAMPER, D.; and NOBLE, R.D. Room-Temperature Ionic Liquids: Temperature Dependence of Gas Solubility Selectivity. *Ind. Eng. Chem. Res.*, 47, 2008: 3453–3459.
- [124] Shi, W. and Maginn, E.J. Molecular Simulation and Regular Solution Theory Modeling of Pure and Mixed Gas Absorption in the Ionic Liquid 1-n-Hexyl-3-methylimidazolium Bis(Trifluoromethylsulfonyl)amide ([hmim][Tf<sub>2</sub>N]). *J. Phys. Chem. B*, 112, 2008: 16710–1670.
- [125] CARVALHO, P.J. and COUTINHO, J.A.P. On the Nonideality of CO<sub>2</sub> Solutions in Ionic Liquids and Other Low Volatile Solvents. *J. Phys. Chem. Lett.*, 1, 2010: 774–780.

[126] Yim, J.; Song, H.N.; Yoo, K.; and Lim, J.S. Measurement of CO<sub>2</sub> Solubility in Ionic Liquids: [BMP][Tf<sub>2</sub>N] and [BMP][MeSO<sub>4</sub>] by Measuring Bubble-Point Pressure. *J. Chem. Eng. Data*, 56, 2011: 1197–1203.

- [127] Song, H.N.; Lee, B.; and Lim, J.S. Measurement of CO<sub>2</sub> Solubility in Ionic Liquids: [BMP][TfO] and [P14,6,6,6][Tf<sub>2</sub>N] by Measuring Bubble-Point Pressure. *J. Chem. Eng. Data*, 55, 2010: 891–896.
- [128] Galán Sánchez, L.M. Functionalized Ionic Liquids: Absorption Solvents for Carbon Dioxide and Olefin Separation. Ph.D. thesis, Eindhoven University of Technology, 2008.
- [129] REVELLI, A.; MUTELET, F.; and JAUBERT, J. High Carbon Dioxide Solubilities in Imidazolium-Based Ionic Liquids and in Poly(ethylene glycol) Dimethyl Ether. J. Phys. Chem. B, 114, 2010: 12908–12913.
- [130] Carvalho, P.J.; Alvarez, V.H.; Marrucho, I.M.; Aznar, M.; and Coutinho, J.A.P. High pressure phase behavior of carbon dioxide in 1-butyl-3-methylimidazolium bis(trifluoromethylsulfonyl)imide and 1-butyl-3-methylimidazolium dicyanamide ionic liquids. *J. Supercrit. Fluids*, 50, 2009: 105–111.
- [131] COSTANTINI, M.; TOUSSAINT, V.A.; SHARIATI, A.; PETERS, C.J.; and KIKIC, I. High-Pressure Phase Behavior of Systems with Ionic Liquids: Part IV. Binary System Carbon Dioxide + 1-Hexyl-3methylimidazolium Tetrafluoroborate. J. Chem. Eng. Data, 50, 2005: 52–55.
- [132] SHARIATI, A. and PETERS, C.J. High-pressure phase behavior of systems with ionic liquids: III. The binary system carbon dioxide+1hexyl-3-methylimidazolium hexafluorophosphate. J. Supercrit. Fluids, 30, 2004: 139–144.

- [133] Gutkowski, K.I.; Shariati, A.; and Peters, C.J. Highpressure phase behavior of the binary ionic liquid system 1-octyl-3methylimidazolium tetrafluoroborate + carbon dioxide. *J. Supercrit.* Fluids, 39, 2006: 187–191.
- [134] SORIANO, A.N.; DOMA JR, B.T.; and LI, M. Carbon dioxide solubility in some ionic liquids at moderate pressures. *J. Taiwan Inst. Chem. Eng.*, 40, 2009: 387–393.
- [135] Jalili, A.H.; Mehdizadeh, A.; Shokouhi, M.; Sakhaeinia, H.; and Taghikhani, V. Solubility of CO<sub>2</sub> in 1-(2-hydroxyethyl)-3methylimidazolium ionic liquids with different anions. *J. Chem. Ther*modyn., 42, 2010: 787–791.
- [136] MATTEDI, S.; CARVALHO, P.J.; COUTINHO, J.A.P.; ALVAREZ, V.H.; and IGLESIAS, M. High pressure CO<sub>2</sub> solubility in N-methyl-2hydroxyethylammonium protic ionic liquids. *J. Supercrit. Fluids*, 56, 2011: 224–230.
- [137] Crosthwaite, C.P.F.J.M.; Hert, D.G.; Aki, S.N.V.K.; and Brennecke, J.F. Thermophysical Properties of Imidazolium-Based Ionic Liquids. *J. Chem. Eng. Data*, 49, 2004: 954–964.
- [138] Domanska, U. and Krolikowska, M. Density and Viscosity of Binary Mixtures of 1-Butyl-3-methylimidazolium Thiocyanate + 1-Heptanol, 1-Octanol, 1-Nonanol, or 1-Decanol. *J. Chem. Eng. Data*, 55, 2010: 2994–3004.
- [139] Jacquemin, J.; Husson, P.; Padua, A.A.H.; and Majer, V. Density and viscosity of several pure and water-saturated ionic liquids. *Green Chem.*, 8, 2006: 172–180.
- [140] MOKHTARANI, B.; SHARIFI, A.; MORTAHEB, H.R.; MIRZAEI, M.; MAFI, M.; and SADEGHIAN, F. Density and viscosity of pyridinium-based ionic liquids and their binary mixtures with water at several temperatures. *J. Chem. Thermodyn.*, 41, 2009: 323–329.

[141] Tariq, M.; Forte, P.A.S.; Costa Gomes, M.F.; Canongia Lopes, J.N.; and Rebelo, L.P.N. Densities and refractive indices of imidazolium- and phosphonium-based ionic liquids: Effect of temperature, alkyl chain length, and anion. *J. Chem. Thermodyn.*, 41, 2009: 790–798.

- [142] Goncalves, F.A.M.M.; Costa, C.S.M.F.; Ferreira, C.E.; Bernardo, J.C.S.; Johnson, I.; Fonseca, I.M.A.; and Ferreira, A.G.M. Pressure-volume-temperature measurements of phosphonium-based ionic liquids and analysis with simple equations of state. *J. Chem. Thermodyn.*, 43, 2011: 914–929.
- [143] Galan Sanchez, L.; Espel, J.R.; Onink, F.; Meindersma, G.W.; and de Haan, A.B. Density, Viscosity, and Surface Tension of Synthesis Grade Imidazolium, Pyridinium, and Pyrrolidinium Based Room Temperature Ionic Liquids. *J. Chem. Eng. Data*, 54, 2009: 2803–2812.
- [144] Seoane, R.G.; Corderi, S.; Gomez, E.; Calvar, N.; Gonzalez, E.J.; Macedo, E.A.; and Dominguez, A. Temperature Dependence and Structural Influence on the Thermophysical Properties of Eleven Commercial Ionic Liquids. *Ind. Eng. Chem. Res.*, 51, 2012: 2492–2504.
- [145] TAGUCHI, R.; MACHIDA, H.; SATO, Y.; and SMITH, JR, R.L. High-Pressure Densities of 1-Alkyl-3-methylimidazolium Hexafluorophosphates and 1-Alkyl-3-methylimidazolium Tetrafluoroborates at Temperatures from (313 to 473) K and at Pressures up to 200 MPa. *J. Chem. Eng. Data*, 54, 2009: 22–27.
- [146] ESPERANCA, J.M.S.S.; VISAK, Z.P.; PLECHKOVA, N.V.; SEDDON, K.R.; GUEDES, H.J.R.; and REBELO, L.P.N. Density, speed of sound, and derived thermodynamic properties of ionic liquids over an extended pressure range. 4. [c<sub>3</sub>mim][ntf<sub>2</sub>] and [c<sub>5</sub>mim][ntf<sub>2</sub>]. *J. Chem. Eng. Data*, 51, 2006: 2009–2015.

- [147] Zhao, Y.H.; Abraham, M.H.; and Zissimos, A.M. Fast Calculation of van der Waals Volume as a Sum of Atomic and Bond Contributions and Its Application to Drug Compounds. J. Org. Chem., 68, 2003: 7368–7373.
- [148] BONDI, A. van der Waals Volumes and Radii. J. Phys. Chem., 68, 1964: 441–451.
- [149] SHANNON, M.S.; TEDSTONE, J.M.; DANIELSEN, S.P.O.; HINDMAN, M.S.; IRVIN, A.C.; and BARA, J.E. Free Volume as the Basis of Gas Solubility and Selectivity in Imidazolium-Based Ionic Liquids. *Ind. Eng. Chem. Res.*, 51, 2012: 5565–5576.
- [150] ANDERSON, J.L.; DIXON, J.K.; and BRENNECKE, J.F. Solubility of CO<sub>2</sub>, CH<sub>2</sub>, C<sub>2</sub>H<sub>6</sub>, C<sub>2</sub>H<sub>4</sub>, O<sub>2</sub> and N<sub>2</sub> in 1-Hexyl-3-methylpyridinium Bis(trifluoromethylsulfonyl)imide: Comparison to Other Ionic Liquids. Acc. Chem. Res., 40, 2007: 1208–1216.
- [151] ANDERSON, J.L.; DIXON, J.K.; MAGINN, E.J.; and BRENNECKE, J.F. Measurement of SO<sub>2</sub> Solubility in Ionic Liquids. *J. Phys. Chem.* B, 110, 2006: 15059–15062.
- [152] Kumelan, J.; Perez-Salado Kamps, A.; Urukova, I.; Tuma, D.; and Maurer, G. Solubility of oxygen in the ionic liquid [bmim][PF<sub>6</sub>]: Experimental and molecular simulation results. *J. Chem. Thermodyn.*, 37, 2005: 595–602.
- [153] CARVALHO, P.J. and COUTINHO, J.A.P. The polarity effect upon the methane solubility in ionic liquids: a contribution for the design of ionic liquids for enhanced CO<sub>2</sub>/CH<sub>4</sub> and H<sub>2</sub>S/CH<sub>4</sub> selectivities. *Energy Environ. Sci.*, 4, 2011: 4614–4619.
- [154] KUMELAN, J.; PEREZ-SALADO KAMPS, A.; TUMA, D.; and MAURER, G. Solubility of H<sub>2</sub> in the Ionic Liquid [hmim][Tf<sub>2</sub>N]. J. Chem. Eng. Data, 51, 2006: 1364–1367.

[155] KUMELAN, J.; PEREZ-SALADO KAMPS, A.; TUMA, D.; and MAURER, G. Solubility of CO in the ionic liquid [bmim][PF<sub>6</sub>]. Fluid Phase Equilib., 228-229, 2005: 207-211.

- [156] KUMELAN, J.; PEREZ-SALADO KAMPS, A.; TUMA, D.; and MAURER, G. Solubility of the single gases H<sub>2</sub> and CO in the ionic liquid [bmim][CH<sub>3</sub>SO<sub>4</sub>]. Fluid Phase Equilib., 260, 2007: 3–8.
- [157] Jacquemin, J.; Costa Gomes, M.F.; Husson, P.; and Majer, V. Solubility of carbon dioxide, ethane, methane, oxygen, nitrogen, hydrogen, argon, and carbon monoxide in 1-butyl-3-methylimidazolium tetrafluoroborate between temperatures 283 K and 343 K and at pressures close to atmospheric. J. Chem. Thermodyn., 38, 2006: 490–502.
- [158] JACQUEMIN, J.; HUSSON, P.; MAJER, V.; and COSTA GOMES, M.F. Low-pressure solubilities and thermodynamics of solvation of eight gases in 1-butyl-3-methylimidazolium hexafluorophosphate. Fluid Phase Equilib., 240, 2006: 87–95.
- [159] JACQUEMIN, J.; HUSSON, P.; MAJER, V.; and COSTA GOMES, M.F. Influence of the Cation on the Solubility of CO<sub>2</sub> and H<sub>2</sub> in Ionic Liquids Based on the Bis(trifluoromethylsulfonyl)imide Anion. J. Solution Chem., 36, 2007: 967–979.
- [160] YOKOZEKI, A. and SHIFLETT, M.B. Hydrogen purification using room-temperature ionic liquids. *Applied Energy*, 84, 2007: 351–361.
- [161] SHIFLETT, M.B. and YOKOZEKI, A. Separation of CO<sub>2</sub> and H<sub>2</sub>S using room-temperature ionic liquid [bmim][PF<sub>6</sub>]. Fluid Phase Equilib., 294, 2010: 105–113.
- [162] SHIFLETT, M.B.; NIEHAUS, A.M.S.; and YOKOZEKI, A. Separation of CO<sub>2</sub> and H<sub>2</sub>S Using Room-Temperature Ionic Liquid [bmim][MeSO<sub>4</sub>]. *J. Chem. Eng. Data*, 55, 2010: 4785–4793.

- [163] COSTA GOMES, M.F. Low-Pressure Solubility and Thermodynamics of Solvation of Carbon Dioxide, Ethane, and Hydrogen in 1-Hexyl-3methylimidazolium Bis(trifluoromethylsulfonyl)amide between Temperatures of 283 K and 343 K. J. Chem. Eng. Data, 52, 2007: 472–475.
- [164] Weingärtner, H. Understanding Ionic Liquids at the Molecular Level: Facts, Problems, and Controversies. Angew. Chem., Int. Ed., 47, 2008: 654–670.
- [165] BARA, J.E.; GABRIEL, C.J.; LESSMANN, S.; CARLISLE, T.K.; FINOTELLO, A.; ; GIN, D.L.; and NOBLE, R.D. Enhanced CO<sub>2</sub> Separation Selectivity in Oligo(ethylene glycol) Functionalized Room-Temperature Ionic Liquids. *Ind. Eng. Chem. Res.*, 46, 2007: 5380–5386.
- [166] CARLISLE, T.K.; BARA, J.E.; GABRIEL, C.J.; NOBLE, R.D.; and GIN, D.L. Interpretation of CO<sub>2</sub> Solubility and Selectivity in Nitrile-Functionalized Room-Temperature Ionic Liquids Using a Group Contribution Approach. *Ind. Eng. Chem. Res.*, 47, 2008: 7005–7012.
- [167] Mahurin, S.M.; Dai, T.; Yeary, J.S.; Luo, H.; and Dai, S. Benzyl-Functionalized Room Temperature Ionic Liquids for  $CO_2/N_2$  Separation. *Ind. Eng. Chem. Res.*, 50, 2011: 14061–14069.
- [168] HERT, D.G.; ANDERSON, J.L.; AKI, S.N.V.K.; and BRENNECKE, J.F. Enhancement of oxygen and methane solubility in 1-hexyl-3methylimidazolium bis(trifluoromethylsulfonyl) imide using carbon dioxide. Chem. Commun., 2005: 2603–2605.
- [169] SHIFLETT, M.B. and YOKOZEKI, A. Separation of Carbon Dioxide and Sulfur Dioxide Using Room-Temperature Ionic Liquid [bmim][MeSO<sub>4</sub>]. *Energy Fuels*, 24, 2010: 1001–1008.
- [170] YOKOZEKI, A. and SHIFLETT, M.B. Separation of Carbon Dioxide and Sulfur Dioxide Gases Using Room-Temperature Ionic Liquid [hmim][Tf<sub>2</sub>N]. *Energy Fuels*, 23, 2009: 4701–4708.

[171] Kumelan, J.; Tuma, D.; and Maurer, G. Simultaneous solubility of carbon dioxide and hydrogen in the ionic liquid [hmim][Tf<sub>2</sub>N]: Experimental results and correlation. *Fluid Phase Equilib.*, 311, 2011: 9–16.

- [172] Shi, W.; Sorescu, D.C.; Luebke, D.R.; Keller, M.J.; and Wick-Ramanayake, S. Molecular Simulations and Experimental Studies of Solubility and Diffusivity for Pure and Mixed Gases of H<sub>2</sub>, CO<sub>2</sub>, and Ar Absorbed in the Ionic Liquid 1-n-Hexyl-3-methylimidazolium Bis(Trifluoromethylsulfonyl)amide ([hmim][Tf<sub>2</sub>N]). J. Phys. Chem. B, 114, 2010: 6531–6541.
- [173] Kim, Y.S.; Jang, J.; Lim, B.D.; Kang, J.W.; and Lee, C.S. Solubility of mixed gases containing carbon dioxide in ionic liquids: Measurements and predictions. *Fluid Phase Equilib.*, 256, 2007: 70–74.
- [174] Harris, K.R.; Kanakubo, M.; and Woolf, L.A. Temperature and Pressure Dependence of the Viscosity of the Ionic Liquids 1-Methyl-3-octylimidazolium Hexafluorophosphate and 1-Methyl-3-octylimidazolium Tetrafluoroborate. J. Chem. Eng. Data, 51, 2006: 1161–1167.
- [175] Harris, K.R.; Kanakubo, M.; and Woolf, L.A. Temperature and Pressure Dependence of the Viscosity of the Ionic Liquid 1-butyl-3-methylimidazolium Tetrafluoroborate: Viscosity and Density Relationships in Ionic Liquids. J. Chem. Eng. Data, 52, 2007: 2425–2430.
- [176] GARDAS, R.L.; GE, R.; GOODRICH, P.; HARDCARE, C.; HUSSAIN, A.; and ROONEY, D.W. Thermophysical Properties of Amino Acid-Based Ionic Liquids. J. Chem. Eng. Data, 55, 2010: 1505–1515.
- [177] CROSTHWAITE, J.M.; MULDOON, M.J.; DIXON, J.K.; ANDERSON, J.L.; and BRENNECKE, J.F. Phase transition and decomposition temperatures, heat capacities and viscosities of pyridinium ionic liquids. *J. Chem. Thermodyn.*, 37, 2005: 559–568.

- [178] JIN, H.; O' HARE, B.; DONG, J.; ARZHANTSEV, S.; BAKER, G.A.; WISHART, J.F.; BENESI, A.J.; and MARONCELLI, M. Physical Properties of Ionic Liquids Consisting of the 1-Butyl-3-Methylimidazolium Cation with Various Anions and the Bis(trifluoromethylsulfonyl)imide Anion with Various Cations. J. Phys. Chem. B, 112, 2008: 81–92.
- [179] TSUNASHIMA, K. and SUGIYA, M. Physical and electrochemical properties of low-viscosity phosphonium ionic liquids as potential electrolytes. *Electrochemistry Commun.*, 9, 2007: 2353–2358.
- [180] GE, M.; ZHAO, R.; YI, Y.; ZHANG, Q.; and WANG, L. Densities and Viscosities of 1-Butyl-3-methylimidazolium Trifluoromethanesulfonate + H<sub>2</sub>O Binary Mixtures at T=(303.15 to 343.15) K. J. Chem. Eng. Data, 53, 2008: 2408–2411.
- [181] FERNANDEZ, A.; GARCIA, J.; TORRECILLA, J.S.; OLIET, M.; and RODRIGUEZ, F. Volumetric, Transport and Surface Properties of [bmim][MeSO<sub>4</sub>] and [emim][EtSO<sub>4</sub>] Ionic Liquids As a Function of Temperature. J. Chem. Eng. Data, 53, 2008: 1518–1522.
- [182] MORGAN, D.; FERGUSON, L.; and SCOVAZZO, P. Diffusivities of Gases in Room-Temperature Ionic Liquids: Data and Correlations Obtained Using a Lag-Time Technique. *Ind. Eng. Chem. Res.*, 44, 2005: 4815–4823.
- [183] MOGANTY, S.S. and BALTUS, R.E. Diffusivity of Carbon Dioxide in Room-Temperature Ionic Liquids. *Ind. Eng. Chem. Res.*, 49, 2010: 9370–9376.
- [184] AHOSSEINI, A. and SCURTO, A.M. Viscosity of Imidazolium-Based Ionic Liquids at Elevated Pressures: Cation and Anion Effects. *Int.* J. Thermophys., 29, 2008: 1222–1243.
- [185] Andreatta, A.E.; Arce, A.; Rodil, E.; and Soto, A. Physical Properties of Binary and Ternary Mixtures of Ethyl Acetate, Ethanol, and 1-Octyl-3-methyl-imidazolium Bis(trifluoromethylsulfonyl)imide at 298.15 K. J. Chem. Eng. Data, 54, 2009: 1022–1028.

[186] GARDAS, R.L. and COUTINHO, J.A.P. A group contribution method for viscosity estimation of ionic liquids. *Fluid Phase Equilib.*, 266, 2008: 195–201.

- [187] GARDAS, R.L. and COUTINHO, J.A.P. Group Contribution Methods for the Prediction of Thermophysical and Transport Properties of Ionic Liquids. AIChE J., 55, 2009: 1274–1290.
- [188] MAGINN, E.J. Atomistic Simulation of the Thermodynamic and Transport Properties of Ionic Liquids. Acc. Chem. Res., 40, 2007: 1200–1207.
- [189] Davies, G.A.; Ponter, A.B.; and Craine, K. The diffusion of carbon dioxide in organic liquids. *Can. J. Chem. Eng.*, 45, 1967: 372–376.
- [190] HAYDUK, W. and CHENG, S.C. Review of relation between diffusivity and solvent viscosity in dilute liquid solutions. *Chem. Eng. Sci.*, 26, 1971: 635–646.
- [191] McManamey, W.J. and Woollen, J.M. The Diffusivity of Carbon Dioxide in Some Organic Liquids at 25 °C and 50 °C. *AIChE J.*, 19, 1973: 667–669.
- [192] Camper, D.; Becker, C.; Koval, C.; and Noble, R. Diffusion and Solubility Measurements in Room Temperature Ionic Liquids. *Ind. Eng. Chem. Res.*, 45, 2006: 445–450.
- [193] HOU, Y. and BALTUS, R.E. Experimental Measurement of the Solubility and Diffusivity of CO<sub>2</sub> in Room-Temperature Ionic Liquids Using a Transient Thin-Liquid-Film Method. *Ind. Eng. Chem. Res.*, 46, 2007: 8166–8175.
- [194] FERGUSON, L. and SCOVAZZO, P. Solubility, Diffusivity, and Permeability of Gases in Phosphonium-Based Room Temperature Ionic Liquids: Data and Correlations. *Ind. Eng. Chem. Res.*, 46, 2007: 1369–1374.

- [195] CONDEMARIN, R. and SCOVAZZO, P. Gas permeabilities, solubilities, diffusivities, and diffusivity correlations for ammonium-based room temperature ionic liquids with comparison to imidazolium and phosphonium RTIL data. *Chem. Eng. J.*, 147, 2009: 51–57.
- [196] HAYDUK, W. and MALIK, V.K. Density, Viscosity, and Carbon Dioxide Solubility and Diffusivity in Aqueous Ethylene Glycol Solutions. J. Chem. Eng. Data, 16, 1971: 143–146.
- [197] WON, Y.S.; CHUNG, D.K.; and MILLS, A.F. Density, Viscosity, Surface Tension, and Carbon Dioxide Solubility and diffusivity of Methanol, Ethanol, Aqueous Propanol, and Aqueous Ethylene Glycol at 25 °C. J. Chem. Eng. Data, 26, 1981: 141–144.
- [198] DIM, A.; GARDNER, G.R.; PONTER, A.B.; and WOOD, T. Diffusion of Carbon Dioxide into Primary Alcohols and Methyl Cellulose Ether Solutions. J. Chem. Eng. Jap., 4, 1971: 92–95.
- [199] MORROW, T.I. and MAGINN, E.J. Molecular Dynamics Study of the Ionic Liquid 1-n-Butyl-3-methylimidazolium Hexafluorophosphate. J. Phys. Chem. B, 106, 2002: 12807–12813.
- [200] Liu, X.; Vlugt, T.J.H.; and Bardow, A. Maxwell-Stefan Diffusivities in Binary Mixtures of Ionic Liquids with Dimethyl Sulfoxide (DMSO) and H<sub>2</sub>O. *J. Phys. Chem. B*, 115, 2011: 8506–8517.
- [201] ESPERANCA, J.M.S.S.; CANONGIA LOPES, J.N.; TARIQ, M.; SANTOS, L.M.N.B.F.; MAGEE, J.W.; and REBELO, L.P.N. Volatility of Aprotic Ionic Liquids A Review. *J. Chem. Eng. Data*, 55, 2010: 3–12.
- [202] EARLE, M.J.; ESPERANCA, J.M.S.S.; GILEA, M.A.; CANONGIA LOPES, J.N.; REBELO, L.P.N.; MAGEE, J.W.; SEDDON, K.R.; and WIDEGREN, J.A. The distillation and volatility of ionic liquids. *Nature*, 439, 2006: 831–834.

[203] Ludwig, R. and Kragl, U. Do We Understand the Volatility of Ionic Liquids? *Angew. Chem., Int. Ed.*, 46, 2007: 6582–6584.

- [204] Armstrong, J.P.; Hurst, C.; Jones, R.G.; Licence, P.; Lovelock, K.R.J.; Satterley, C.J.; and Villar-Garcia, I.J. Vapourisation of ionic liquids. *Phys. Chem. Chem. Phys.*, 9, 2007: 982–990.
- [205] LEAL, J.P.; ESPERANCA, J.M.S.S.; MINAS DA PIEDADE, M.E.; CANONGIA LOPES, J.N.; REBELO, L.P.N.; and SEDDON, K.R. The Nature of Ionic Liquids in the Gas Phase. *J. Phys. Chem. A*, 111, 2007: 6176–6182.
- [206] RAI, N. and MAGINN, E.J. Vapor-Liquid Coexistence and Critical Behavior of Ionic Liquids via Molecular Simulations. J. Phys. Chem. Lett., 2, 2011: 1439–1443.
- [207] KÖDDERMANN, T.; PASCHEK, D.; and LUDWIG, R. Ionic Liquids: Dissecting the Enthalpies of Vaporization. *ChemPysChem*, 9, 2008: 549–555.
- [208] REBELO, L.O.N.; CANONGIA LOPES, J.N.; ESPERANCA, J.M.S.S.; and FILIPE, E. On the Critical Temperature, Normal Boiling Point, and Vapor Pressure of Ionic Liquids. J. Phys. Chem. B Lett., 109, 2005: 6040–6043.
- [209] Fumino, K.; Wulf, A.; Verevkin, S.P.; Heintz, A.; and Ludwig, R. Estimating Enthalpies of Vaporization of Imidazolium-Based Ionic Liquids from Far-Infrared Measurements. *ChemPysChem*, 11, 2010: 1623–1626.
- [210] Deyko, A.; Lovelock, K.R.J.; Corfield, J.; Taylor, A.W.; Gooden, P.N.; Villar-Garcia, I.J.; Licence, P.; Jones, R.G.; Krasovskiy, V.G.; Chernikova, E.A.; and Kustov, L.M. Measuring and predicting  $\Delta_{\text{vap}}H_{298}$  values of ionic liquids. *PhysChem-ChemPhys*, 11, 2009: 8544–8555.

- [211] VEREVKIN, S.P. Predicting Enthalpy of Vaporization of Ionic Liquids: A Simple Rule for a Complex Property. *Angew. Chem.*, 120, 2008: 5149–5152.
- [212] Zaitsau, D.H.; Kabo, G.J.; Strechan, A.A.; Paulechka, Y.U.; Tschersich, A.; Verevkin, S.P.; and Heintz, A. Experimental Vapor Pressures of 1-Alkyl-3-methylimidazolium Bis(trifluoromethylsulfonyl)imides and a Correlation Scheme for Estimation of Vaporization Enthalpies of Ionic Liquids. *J. Phys. Chem.* A, 110, 2006: 7303–7306.
- [213] ROCHA, M.A.A.; LIMA, C.F.R.A.C.; GOMES, L.R.; SCHRÖDER, B.; COUTINHO, J.A.P.; MARRUCHO, I.M.; ESPERANCA, J.M.S.S.; REBELO, L.P.N.; SHIMIZU, K.; CANONGIA LOPES, J.N.; and SANTOS, L.M.N.B.F. High-Accuracy Vapor Pressure Data of the Extended [C<sub>n</sub>C<sub>1</sub>im][Ntf<sub>2</sub>] Ionic Liquid Series: Trend Changes and Structural Shifts. J. Phys. Chem., 115, 2011: 10919–10926.
- [214] WASSERSCHEID, P. Volatile times for ionic liquids. *Nature*, 439, 2006: 797.
- [215] BATES, E.D.; MAYTON, R.D.; NTAI, I.; and DAVIS, J.H. CO<sub>2</sub> Capture by a Task-Specific Ionic Liquid. *J. Am. Chem. Soc.*, 124, 2002: 926–927.
- [216] DAVIS JR, J.H. Task-Specific Ionic Liquids. *Chem. Lett.*, 33, 2004: 1072–1077.
- [217] GALAN SANCHEZ, L.; MEINDERSMA, G.W.; and DE HAAN, A.B. Solvent Properties of Functionalized Ionic Liquids for  $CO_2$  Absorption. *IChemE*, 85, 2007: 31–39.
- [218] CAMPER, D.; BARA, J.; GIN, D.L.; and NOBLE, R. Room-Temperature Ionic Liquid-Amine Solutions: Tunable Solvents for Efficient and Reversible Capture of CO<sub>2</sub>. Ind. Eng. Chem. Res, 47, 2008: 8496–8498.

[219] Yu, G.; Zhang, S.; Zhou, G.; Liu, X.; and Chen, X. Structure, Interaction and Property of Amino-Functionalized Imidazolium ILs by Molecular Dynamics Simulation and Ab Initio Calculation. Applied Energy, 53, 2007: 3210–3221.

- [220] GUTOWSKI, K.E. and MAGINN, E.J. Amine-Functionalized Task-Specific Ionic Liquids: A Mechanistic Explanation for the Dramatic Increase in Viscosity upon Complexation with CO<sub>2</sub> from Molecular Simulation. J. Am. Chem. Soc., 130, 2008: 14690–14704.
- [221] GURKAN, B.E.; DE LA FUENTE, J.; MINDRUP, E.M.; FICKE, L.E.; GOODRICH, B.F.; PRICE, E.A.; SCHNEIDER, W.F.; and BREN-NECKE, J.F. Equimolar CO<sub>2</sub> Absorption by Anion-Functionalized Ionic Liquids. J. Am. Chem. Soc., 132, 2010: 2116–2117.
- [222] GOODRICH, B.F.; DE LA FUENTE, J.C.; GURKAN, B.E.; ZADIGIAN, D.J.; PRICE, E.A.; HUANG, Y.; and BRENNECKE, J.F. Experimental Measurements of Amine-Functionalized Anion-Tethered Ionic Liquids with Carbon Dioxide. *Ind. Eng. Chem. Res.*, 50, 2011: 111–118.
- [223] D. CHINN AND D. Q. VU AND M. S. DRIVER AND L. C. BOUDREAU. CO<sub>2</sub> removal from gas using ionic liquid absorbents. *United States Patent*, US 7,527,775 B2, May 5, 2009.
- [224] E. J. MAGINN. Design and Evaluation of Ionic Liquids as Novel CO<sub>2</sub> Absorbents, May 31, 2005. http://www.osti.gov/scitech/servlets/purl/859167-Pborns/.
- [225] Shiflett, M.B.; Kasprzak, D.J.; Junk, C.P.; and Yokozeki, A. Phase Behavior of carbon dioxide + [bmim][Ac] mixtures. *J. Chem. Thermodyn.*, 40, 2008: 25–31.
- [226] SHIFLETT, M.B.; DREW, D.W.; CANTINI, R.A.; and YOKOZEKI, A. Carbon Dioxide Capture Using Ionic Liquid 1-Butyl-3methylimidazolium Acetate. *Energy Fuels*, 24, 2010: 5781–5789.

- [227] SHIFLETT, M.B. and YOKOZEKI, A. Phase Behavior of Carbon Dioxide in Ionic Liquids: [emim][Acetate], [emim][Trifluoroacetate], and [emim][Acetate] + [emim][Trifluoroacetate] Mixtures. *J. Chem. Eng. Data*, 54, 2009: 108–114.
- [228] CARVALHO, P.J.; ALVAREZ, V.H.; SCHRODER, B.; GIL, A.M.; MARRUCHO, I.M.; AZNAR, M.; SANTOS, L.M.N.B.F.; and COUTINHO, J.A.P. Specific Solvation Interactions of CO<sub>2</sub> on Acetate and Trifluoroacetate Imidazolium Based Ionic Liquids at High Pressures. *J. Phys. Chem. B*, 113, 2009: 6803–6812.
- [229] Gurau, G.; Rodriguez, H.; Kelley, S.P.; Janiczek, P.; Kalb, R.S.; and Rogers, R.D. Demonstration of Chemisorption of Carbon Dioxide in 1,3-Dialkylimidazolium Acetate Ionic Liquids. *Angew. Chem., Int. Ed.*, 50, 2011: 12024–12026.
- [230] Besnard, M.; Cabaco, M.I.; Chavez, F.V.; Pinaud, N.; Sebastiao, P.J.; Coutinho, J.A.P.; and Danten, Y. On the spontaneous carboxylation of 1-butyl-3-methylimidazolium acetate by carbon dioxide. *Chem. Commun.*, 48, 2012: 1245–1247.
- [231] Gurkan, B.E.; Goodrich, B.F.; Mindrup, E.M.; Ficke, L.E.; Massle, M.; Seo, S.; Senftle, T.P.; Wu, H.; Glaser, M.F.; Shah, J.K.; Maginn, E.J.; Brennecke, J.F.; and Schneider, W.F. Molecular Design of High Capacity, Low Viscosity, Chemically Tunable Ionic Liquids for CO<sub>2</sub> Capture. *J. Phys. Chem. Lett.*, 1, 2010: 3494–3499.
- [232] WANG, C.; Luo, H.; JIANG, D.; LI, H.; and DAI, S. Carbon Dioxide Capture by Superbase-Derived Protic Ionic Liquids. *Angew. Chem.*, *Int. Ed.*, 49, 2010: 5978–5981.
- [233] WANG, C.; MAHURIN, S.M.; LUO, H.; BAKER, G.A.; LI, H.; and DAI, S. Reversible and robust CO<sub>2</sub> capture by equimolar task-specific ionic liquid-superbase mixtures. *Green Chem.*, 12, 2010: 870–874.

[234] WANG, C.; Luo, H.; Luo, X.; Li, H.; and Dai, S. Equimolar CO<sub>2</sub> Capture by imidazolium-based ionic liquids and superbase systems. *Green Chem.*, 12, 2010: 2019–2023.

- [235] WANG, C.; LUO, X.; LUO, H.; JIANG, D.; LI, H.; and DAI, S. Tuning the Basicity of Ionic Liquids for Equimolar CO<sub>2</sub> Capture. Angew. Chem., Int. Ed., 50, 2011: 4918–4922.
- [236] Jessop, P.G.; Heldebrant, D.J.; Li, X.; Eckert, C.A.; and Liotta, C.L. Reversible nonpolar-to-polar solvent. *Nature*, 436, 2005: 1102.
- [237] HART, R.; JESSOP, P.G.; THOMAS, C.A.; ECKERT, C.A.; and LIOTTA, C.L. The Reaction of 1,8-Diazabicyclo[5.4.0]undec-7-ene (DBU) with Carbon Dioxide. *J. Org. Chem.*, 70, 2005: 5335–5338.
- [238] LIU, Y.; JESSOP, P.G.; CUNNINGHAM, M.; ECKERT, C.A.; and LIOTTA, C.L. Switchable Surfactants. *Science*, 313, 2006: 558–560.
- [239] Phan, L.; Chiu, D.; Heldebrant, D.J.; Huttenhower, H.; John, E.; Li, X.; Pollet, P.; Wang, R.; Eckert, C.A.; Liotta, C.L.; and Jessop, P.G. Switchable Solvents Consisting of Amide/Alcohol or Guanidine/Alcohol Mixtures. *Ind. Eng. Chem. Res.*, 47, 2008: 539–545.
- [240] HELDEBRANT, D.J.; YONKER, C.R.; JESSOP, P.G.; and PHAN, L. Organic liquid CO<sub>2</sub> capture agents with high gravimetric CO<sub>2</sub> capacity. *Energy Environ. Sci.*, 1, 2008: 487–493.
- [241] BLASUCCI, V.M.; HART, R.; POLLET, P.; LIOTTA, C.L.; and ECK-ERT, C.A. Reversible ionic liquids designed for facile separations. Fluid Phase Equilib., 294, 2010: 1–6.
- [242] BLASUCCI, V.M.; HART, R.; MESTRE, V.L.; HAHNE, D.J.; BURLAGER, M.; HUTTENHOWER, H.; THIO, B.J.R.; POLLET, P.; LIOTTA, C.L.; and ECKERT, C.A. Single component, reversible ionic liquids for energy applications. *Fuel*, 89, 2010: 1315–1319.

- [243] Jessop, P.G.; Mercer, S.M.; and Heldebrant, D.J. CO<sub>2</sub>-triggered switchable solvents, surfactants, and other materials. *Energy Environ. Sci.*, 2012.
- [244] SHANNON, M.S. and BARA, J.E. Reactive and Reversible Ionic Liquids for CO<sub>2</sub> Capture and Acid Gas Removal. Separation Science and Technology, 47, 2012: 178–188.
- [245] Reddy, S.; Johnson, D.; and Gilmartin, J. Fluor's econamine fg plus<sup>SM</sup> technology for co<sub>2</sub> capture at coal-fired power plants. In *Power Plant Air Pollutant Control "Mega" Symposium*. Air and Waste Management Association, 2008, 1–17.
- [246] Henni, A.; Hromek, J.J.; Tontiwachwuthikul, P.; and Chakma, A. Volumetric Properties and Viscosities for Aqueous Disopropanolamine Solutions from 25 °C to 70 °C. *J. Chem. Eng. Data*, 48, 2003: 1062–1067.
- [247] Bucklin, R.W. and Schendel, R.L. Comparison of Fluor Solvent and Selexol Processes. *Energy Progress*, 4, 1984: 137–142.
- [248] Shannon, M.S.; Tedstone, J.M.; Danielsen, S.P.O.; and Bara, J.E. Evaluation of Alkylimidazoles as Physical Solvents for CO<sub>2</sub>/CH<sub>4</sub> Separation. *Ind. Eng. Chem. Res.*, 51, 2012: 515–522.
- [249] Burr, B. and Lyddon, L. A comparison of physical solvents for acid gas removal. In 87th Annual Convention Proceedings. Gas Processors Association, 2008, 100–113.
- [250] Zhang, S.; Sun, N.; He, X.; Lu, X.; and Zhang, X. Physical Properties of Ionic Liquids: Database and Evaluation. *J. Phys. Chem. Ref. Data*, 35, 2006: 1475–1517.
- [251] FILBURN, T.; HELBLE, J.J.; and WEISS, R.A. Development of Supported Ethanolamines and Modified Ethanolamines for CO<sub>2</sub> Capture. *Ind. Eng. Chem. Res.*, 44, 2005: 1542–1546.

[252] FULEM, M.; RUZICKA, K.; and RUZICKA, M. Recommended vapor pressures for thiophene, sulfolane, and dimethyl sulfoxide. *Fluid Phase Equilib.*, 303, 2011: 205–216.

- [253] HOCHGESAND, G. Rectisol and Purisol. *Ind. Eng. Chem.*, 62, 1970: 37–43.
- [254] ISAACS, E.E.; OTTO, F.D.; and MATHER, A.E. Solubility of Hydrogen Sulfide and Carbon Dioxide in an Aqueous Diisopropanolamine Solution. *J. Chem. Eng. Data*, 22, 1977: 71–73.
- [255] ISAACS, E.E.; OTTO, F.D.; and MATHER, A.E. The Solubility of Mixtures of Carbon Dioxide and Hydrogen Sulphide in an Aqueous DIPA Solution. Can. J. Chem. Eng., 55, 1977: 210–212.
- [256] ISAACS, E.E.; OTTO, F.D.; and MATHER, A.E. Solubility of Hydrogen Sulfide and Carbon Dioxide in a Sulfinol Solution. J. Chem. Eng. Data, 22, 1977: 317–319.
- [257] JOU, F.; MATHER, A.E.; and Otto, F.D. The Solubility of CO<sub>2</sub> in a 30 Mass Percent Monoethanolamine Solution. Can. J. Chem. Eng., 73, 1995: 140–147.
- [258] LEE, J.I.; OTTO, F.D.; and MATHER, A.E. The Solubility of H<sub>2</sub>S and CO<sub>2</sub>, in Aqueous Monoethanolamine Solutions. *Can. J. Chem. Eng.*, 52, 1974: 803–805.
- [259] Mandal, B.P.; Kundu, M.; and Bandyopadhyay, S.S. Density and Viscosity of Aqueous Solutions of (N-Methyldiethanolamine + Monoethanolamine), (N-Methyldiethanolamine + Diethanolamine), (2-Amino-2-methyl-1-propanol + Monoethanolamine), and (2-Amino-2-methyl-1-propanol + Diethanolamine). J. Chem. Eng. Data, 48, 2003: 703–707.

- [260] MURRIETA-GUEVARA, F.; ROMERO-MARTINEZ, A.; and TREJO, A. Solubilities of Carbon Dioxide and Hydrogen Sulfide in Propylene Carbonate, N-methylpyrrolidone and Sulfolane. Fluid Phase Equilib., 44, 1998: 105–115.
- [261] NICHOLS, G.; ORF, J.; REITER, S.M.; CHICKOS, J.; and GOKEL, G.W. The vaporization enthalpies of some crown and polyethers by correlation gas chromatography. *Thermochimica Acta*, 346, 2000: 15–28.
- [262] VEREVKIN, S.P.; TOKTONOV, A.V.; CHERNYAK, Y.; SCHAFFNER, B.; and BORNER, A. Vapour pressure and enthalpy of vaporization of cyclic alkylene carbonates. *Fluid Phase Equilib.*, 268, 2008: 1–6.
- [263] Xu, Y.; Schutte, R.P.; and Hepler, L.G. Solubilities of Carbon Dioxide, Hydrogen Sulfide and Sulfur Dioxide in Physical Solvents. *Can. J. Chem. Enq.*, 70, 1992: 569–573.
- [264] NGUYEN, T.; HILLIARD, M.; and ROCHELLE, G.T. Amine volatility in CO<sub>2</sub> capture. *Int. J. Greenhouse Gas Control*, 4, 2010: 707–715.
- [265] NGUYEN, T.; HILLIARD, M.; and ROCHELLE, G.T. Volatility of aqueous amines in CO<sub>2</sub> capture. *Energy Procedia*, 4, 2011: 1624–1630.
- [266] GOFF, G.S. and ROCHELLE, G.T. Monoethanolamine Degradation: O<sub>2</sub> Mass Transfer Effects under CO<sub>2</sub> Capture Conditions. *Ind. Eng. Chem. Res.*, 43, 2004: 6400–6408.
- [267] Davis, J. and Rochelle, G.T. Thermal degradation of monoethanolamine at stripper conditions. *Energy Procedia*, 1, 2009: 327–333.
- [268] Reddy, S.; Scherffius, J.; Freguia, S.; and Roberts, C. Fluor's econamine fg plus<sup>SM</sup> technology; an enhanced amine-based co<sub>2</sub> capture process. In Second National Conference on Carbon Sequestration. DOE-NETL, 2003, 1–11.

[269] ARENAS, M.F. and REDDY, R.G. Corrosion of steel in ionic liquids. J. Min. Met., 39, 2003: 81–91.

- [270] BARANYAI, J.; DEACON, G.B.; MACFARLANE, D.R.; PRINGLE, J.M.; and Scott, J.L. Thermal Degradation of Ionic Liquids at Elevated Temperatures. *Aust. J. Chem.*, 57, 2004: 145–147.
- [271] Perissi, I.; Bardi, U.; Caporali, S.; and Lavacchi, A. High temperature corrosion properties of ionic liquids. *Corrosion Science*, 48, 2006: 2349–2362.
- [272] Perissi, I.; Caporali, S.; Fossati, A.; and Lavacchi, A. Corrosion Resistance of Metallic Materials in Ionic Liquids. *Advances in Chemistry Research*, 6, 2011: 315–322.
- [273] PISAROVA, L.; GABLER, C.; DORR, N.; PITTENAUER, E.; and ALL-MAIER, G. Thermo-oxidative stability and corrosion properties of ammonium based ionic liquids. *Tribology International*, 46, 2012: 73–83.
- [274] Tolstoguzov, A.B.; Bardi, U.; and Chenakin, S.P. Study of the Corrosion of Metal Alloys Interacting with an Ionic Liquid. *Bulletin of the Russian Academy of Sciences: Physics*, 72, 2008: 605–608.
- [275] UERDINGEN, M.; TREBER, C.; BALSER, M.; SCHMITT, G.; and WERNER, C. Corrosion behaviour of ionic liquids. *Green Chem.*, 7, 2005: 321–325.
- [276] Gabler, C.; Tomastik, C.; Pisarova, L.; Doerr, N.; and Allmaier, G. Corrosion properties of ammonium based ionic liquids evaluated by SEM-EDX, XPS and ICP-OES. *Green Chem.*, 13, 2011: 2869–2877.
- [277] PREDEL, T.; SCHLUCKER, E.; WASSERSCHEID, P.; GERHARD, D.; and Arlt, W. Ionic Liquids as Operating Fluids in High Pressure Applications. *Chem. Eng. Technol.*, 30, 2007: 1475–1480.

- [278] Fraser, K.J. and MacFarlane, D.R. Phosphonium-Based Ionic Liquids: An Overview. *Aust. J. Chem.*, 62, 2009: 309–321.
- [279] SHUKLA, S.K.; MURULANA, L.C.; and EBENSO, E.E. Inhibitive Effect of Imidazolium Based Aprotic Ionic Liquids on Mild Steel Corrosion in Hydrochloric Acid Medium. *Int. J. Electrochem. Sci.*, 6, 2011: 4286–4295.
- [280] SCOVAZZO, P.; KIEFT, J.; FINAN, D.A.; KOVAL, C.; DUBOIS, D.; and NOBLE, R. Gas separations using non-hexafluorophosphate [PF<sub>6</sub>]-anion supported ionic liquid membranes. *J. Membrane Sci.*, 238, 2004: 57–63.
- [281] SCOVAZZO, P.; HAVARD, D.; MCSHEA, M.; MIXON, S.; and MORGAN, D. Long-term, continuous mixed-gas dry fed CO<sub>2</sub>/CH<sub>4</sub> and CO<sub>2</sub>/N<sub>2</sub> separation performance and selectivities for room temperature ionic liquid membranes. *J. Membrane Sci.*, 327, 2009: 41–48.
- [282] SAN ROMAN, M.F.; BRINGAS, E.; IBANEZ, R.; and ORTIZ, I. Liquid membrane technology: fundamentals and review of its applications. J. Chem. Technol. Biotechnol., 85, 2010: 2–10.
- [283] Kocherginsky, N.N.; Yang, Q.; and Seelam, L. Recent advances in supported liquid membrane technology. *Separation and Purification Technology*, 53, 2007: 171–177.
- [284] Noble, R.D. and Gin, D.L. Perspective on ionic liquids and ionic liquid membranes. *J. Membrane Sci.*, 369, 2011: 1–4.
- [285] ILCONICH, J.; MYERS, C.; PENNLINE, H.; and LUEBKE, D. Experimental investigation of the permeability and selectivity of supported ionic liquid membranes for CO<sub>2</sub>/He separation at temperatures up to 125 °C. J. Membrane Sci., 298, 2007: 41–47.

[286] HANIOKA, S.; MARUYAMA, T.; SOTANI, T.; TERAMOTO, M.; MATSUYAMA, H.; NAKASHIMA, K.; HANAKI, M.; KUBOTA, F.; and GOTO, M. CO<sub>2</sub> separation facilitated by task-specific ionic liquids using a supported liquid membrane. *J. Membrane Sci.*, 314, 2008: 1–4.

- [287] MYERS, C.; PENNLINE, H.; LUEBKE, D.; ILCONICH, J.; DIXON, J.K.; MAGINN, E.J.; and BRENNECKE, J.F. High temperature separation of carbon dioxide/hydrogen mixtures using facilitated supported ionic liquid membranes. J. Membrane Sci., 322, 2008: 28–31.
- [288] Yoo, S.; Won, J.; Kang, S.W.; Kang, Y.; and Nagase, S. CO<sub>2</sub> separation membranes using ionic liquids in a Nafion matrix. *J. Membrane Sci.*, 363, 2010: 72–79.
- [289] NEVES, L.A.; CRESPO, J.G.; and COELHOSO, I.M. Gas permeation studies in supported ionic liquid membranes. *J. Membrane Sci.*, 357, 2010: 160–170.
- [290] IARIKOV, D.D.; HACARLIOGLU, P.; and OYAMA, S.T. Supported room temperature ionic liquid membranes for CO<sub>2</sub>/CH<sub>4</sub> separation. *Chem. Eng. J.*, 166, 2011: 401–406.
- [291] BARA, J.E.; CARLISLE, T.K.; GABRIEL, C.J.; CAMPER, D.; FINOTELLO, A.; GIN, D.L.; and NOBLE, R.D. Guide to CO<sub>2</sub> Separations in Imidazolium-Based Room-Temperature Ionic Liquids. *Ind. Eng. Chem. Res.*, 48, 2009: 2739–2751.
- [292] Robeson, L.M. The upper bound revisited. J. Membrane Sci., 320, 2008: 390–400.
- [293] SCOVAZZO, P. Determination of the upper limits, benchmarks, and critical properties for gas separations using stabilized room temperature ionic liquid membranes (SILMs) for the purpose of guiding future research. J. Membrane Sci., 343, 2009: 199–211.

- [294] Stern, S.A. Polymers for gas separations: the next decade. *J. Membrane Sci.*, 94, 1994: 1–65.
- [295] KILARU, P.K. and SCOVAZZO, P. Correlations of Low-Pressure Carbon Dioxide and Hydrocarbon Solubilities in Imidazolium-, Phosphonium-, and Ammonium-Based Room-Temperature Ionic Liquids. Part 2. Using Activation Energy of Viscosity. *Ind. Eng. Chem.* Res., 47, 2008: 910–919.
- [296] BARA, J.E.; GABRIEL, C.J.; CARLISLE, T.K.; CAMPER, D.E.; FINOTELLO, A.; GIN, D.L.; and NOBLE, R.D. Gas separations in fluoroalkyl-functionalized room-temperature ionic liquids using supported liquid membranes. *Chemical Engineering Journal*, 147, 2009: 43–50.
- [297] CSERJESI, P.; NEMESTOTHY, N.; and BELAFI-BAKO, K. Gas separation properties of supported liquid membranes prepared with unconventional ionic liquids. *J. Membrane Sci.*, 349, 2010: 6–11.
- [298] LAZANO, L.J.; GODINEZ, C.; DE LOS RIOS, A.P.; HERNANDEZ-FERNANDEZ, F.J.; SANCHEZ-SEGADO, S.; and ALGUACIL, F.J. Recent advances in supported ionic liquid membrane technology. *J. Membrane Sci.*, 376, 2011: 1–14.
- [299] Anastas, P.T. and Kirchhoff, M.M. Origins, Current Status, and Future Challenges of Green Chemistry. *Acc. Chem. Res.*, 35, 2002: 686–694.
- [300] Sanderson, K. It's not easy being green. Nature, 469, 2011: 19–20.
- [301] SCAMMELLS, P.J.; SCOTT, J.L.; and SINGER, R.D. Ionic Liquids: The Neglected Issues. *Aust. J. Chem.*, 58, 2005: 155–169.
- [302] EUROPEAN COMMISSION. REACH Registration, Evaluation, Authorisation and Restriction of Chemicals. http://ec.europa.eu/enterprise/sectors/chemicals/reach/index\_en.htm.

[303] MATZKE, M.; STOLTE, S.; THIELE, K.; JUFFERNHOLZ, T.; ARNING, J.; RANKE, J.; WELZ-BIERMANN, U.; and JASTORFF, B. The influence of anion species on the toxicity of 1-alkyl-3-methylimidazolium ionic liquids observed in an (eco)toxicological test battery. *Green Chem.*, 9, 2007: 1198–1207.

- [304] Gathergood, N.; Garcia, M.T.; and Scammells, P.J. Biodegradable ionic liquids: Part 1. Concept, preliminary targets and evaluation. *Green Chem.*, 6, 2004: 166–175.
- [305] JOGLEKAR, H.G.; RAHMAN, I.; and KULKARNI, B.D. The Path Ahead for Ionic Liquids. *Chem. Eng. Technol.*, 30, 2007: 819–828.
- [306] BOETHLING, R.S.; SOMMER, E.; and DIFIORE, D. Designing Small Molecules for Biodegradability. *Chem. Rev.*, 107, 2007: 2207–2227.
- [307] Gathergood, N. and Scammells, P.J. Design and Preparation of Room-Temperature Ionic Liquids Containing Biodegradable Side Chains. Aus. J. Chem., 55, 2002: 557–560.
- [308] COLEMAN, D. and GATHERGOOD, N. Biodegradation studies of ionic liquids. *Chem. Soc. Rev.*, 39, 2010: 600–637.
- [309] Garcia, M.T.; Gathergood, N.; and Scammells, P.J. Biodegradable ionic liquids Part II. Effect of the anion and toxicology. *Green Chem*, 7, 2005: 9–14.
- [310] Gathergood, N.; Scammells, P.J.; and Garcia, M.T. Biodegradable ionic liquids Part III. The first readily biodegradable ionic liquids. *Green Chem*, 8, 2006: 156–160.
- [311] MORRISSEY, S.; PEGOT, B.; COLEMAN, D.; GARCIA, M.T.; FER-GUSON, D.; QUILTY, B.; and GATHERGOOD, N. Biodegradable, non-bactericidal oxygen-functionalised imidazolium esters: A step towards 'greener' ionic liquids. *Green, Chem.*, 11, 2009: 475–483.

- [312] Farrell, J.R.H.J.; Garcia, M.T.; Singer, R.D.; and Scam-Mells, P.J. Further investigation of the biodegradability of imidazolium ionic liquids. *Green Chem.*, 11, 2009: 821–829.
- [313] DOCHERTY, K.M.; DIXON, J.K.; and KULPA JR, C.F. Biodegradability of imidazolium and pyridinium ionic liquids by an activated sludge microbial community. *Biodegradation*, 18, 2007: 481–493.
- [314] Zhang, C.; Wang, H.; Malhotra, S.V.; Dodge, C.J.; and Francis, A.J. Biodegradation of pyridinium-based ionic liquids by an axenic culture of soil Corynebacteria. *Green Chem.*, 12, 2010: 851–858.
- [315] HARJANI, J.R.; SINGER, R.D.; GARCIA, M.T.; and SCAMMELLS, P.J. Biodegradable pyridinium ionic liquids: design, synthesis and evaluation. *Green Chem.*, 11, 2009: 83–90.
- [316] FORD, L.; HARJANI, J.R.; ATEFI, F.; GARCIA, M.T.; SINGER, R.D.; and SCAMMELLS, P.J. Further studies on the biodegradation of ionic liquids. *Green Chem.*, 12, 2010: 1783–1789.
- [317] Wells, A.S. and Coombe, V.T. On the Freshwater Ecotoxicity and Biodegradation Properties of Some Common Ionic Liquids. *Org. Process Res. Development*, 10, 2006: 794–798.
- [318] Yu, Y.; Lu, X.; Zhou, Q.; Dong, K.; Yao, H.; and Zhang, S. Biodegradable Naphthenic Acid Ionic Liquids: Synthesis, Characterization, and Quantitative Structure-Biodegradation Relationship. Chem. Eur. J., 14, 2008: 11174–11182.
- [319] PAVLOVICA, S.; ZICMANIS, A.; GZIBOVSKA, E.; KLAVINS, M.; and MEKSS, P. (2-Hydroxyethyl)ammonium Lactates-Highly Biodegradable and Essentially Non-Toxic Ionic Liquids. *Green Sus. Chem.*, 1, 2011: 103–110.
- [320] Atefi, F.; Garcia, M.T.; Singer, R.D.; and Scammells, P.J. Phosphonium ionic liquids: design, synthesis and evaluation of biodegradability. *Green Chem.*, 11, 2009: 1595–1604.

[321] Zhao, D.; Liao, Y.; and Zhang, Z. Toxicity of Ionic Liquids. *Clean*, 35, 2007: 42–48.

- [322] RANKE, J.; STOLTE, S.; STÖRMANN, R.; ARNING, J.; and JASTORFF, B. Design of Sustainable Chemical Products-The Example of Ionic Liquids. Chem. Rev., 107, 2017: 2183–2206.
- [323] Pham, T.P.T.; Cho, C.; and Yun, Y. Environmental fate and toxicity of ionic liquids: A review. *Water Research*, 44, 2010: 352–372.
- [324] Frade, R.F.M. and Afonso, C.A.M. Impact of ionic liquids in environment and humans: An overview. *Hum. Exp. Toxicol.*, May, 2010: 1–17.
- [325] Petkovic, M.; Seddon, K.R.; Rebelo, L.P.N.; and Pereira, C.S. Ionic liquids: a pathway to environmental acceptability. *Chem. Soc. Rev.*, 40, 2011: 1383–1403.
- [326] COULING, D.J.; BERNOT, R.J.; DOCHERTY, K.M.; DIXON, J.K.; and MAGINN, E.J. Assessing the factors responsible for ionic liquid toxicity to aquatic organisms via quantitative structure-property relationship modeling. *Green Chem.*, 8, 2006: 82–90.
- [327] ROMERO, A.; SANTOS, A.; TOJO, J.; and RODRÍGUEZ, A. Toxicity and biodegradability of imidazolium ionic liquids. *J. Hazardous Mat.*, 151, 2008: 268–273.
- [328] Pretti, C.; Chiappe, C.; Pieraccini, D.; Gregori, M.; Abramo, F.; Monni, G.; and Intorre, L. Acute toxicity of ionic liquids to the zebrafish (Danio rerio). *Green Chem.*, 8, 2006: 238–240.
- [329] Papaiconomou, N.; Estager, J.; Traore, Y.; Bauduin, P.; Bas, C.; Legeai, S.; Viboud, S.; and Draye, M. Synthesis, Physicochemical Properties, and Toxicity Data of New Hydrophobic Ionic Liquids Containing Dimethylpyridinium and Trimethylpyridinium Cations. *J. Chem. Eng. Data*, 55, 2010: 1971–1979.

- [330] Salminen, J.; Papaiconomou, N.; Kumar, R.A.; Lee, J.; Kerr, J.; Newman, J.; and Prausnitz, J.M. Physicochemical properties and toxicities of hydrophobic piperidinium and pyrrolidinium ionic liquids. Fluid Phase Equilib., 261, 2007: 421–426.
- [331] STOLTE, S.; MATZKE, M.; ARNING, J.; BÖSCHEN, A.; PITNER, W.; WELZ-BIERMANN, U.; JASTORFF, B.; and RANKE, J. Effects of different head groups and functionalised side chains on the aquatic toxicity of ionic liquids. *Green Chem.*, 9, 2007: 1170–1179.
- [332] Latala, A.; Nedzi, M.; and Stepnowski, P. Toxicity of imidazolium and pyridinium based ionic liquids towards algae. Chlorella vulgaris, Oocystis submarina (green algae) and Cyclotella meneghiniana, Skeletonema marinoi (diatoms). *Green Chem.*, 11, 2009: 580–588.
- [333] Pretti, C.; Chiappe, C.; Brunini, I.B.S.; Monni, G.; and Intorre, L. Acute toxicity of ionic liquids for three freshwater organisms: Pseudokirchneriella subcapitata, Daphnia magna and Danio rerio. *Ecotoxicol. Environ. Saf.*, 72, 2009: 1170–1176.
- [334] Frade, R.F.M.; Rosatella, A.A.; Marques, C.S.; Branco, L.C.; Kulkarni, P.S.; Mateus, N.M.M.; Afonso, C.A.M.; and Duarte, C.M.M. Toxicological evaluation on human colon carcinoma cell line (CaCo-2) of ionic liquids based on imidazolium, guanidinium, ammonium, phosphonium, pyridinium and pyrrolidinium cations. *Green Chem.*, 11, 2009: 1660–1665.
- [335] Lei, Z.; Dai, C.; and Chen, B. Gas Solubility in Ionic Liquids. *Chem. Rev.*, 114, 2014: 1289–1326.
- [336] MORTAZAVI-MANESH, S.; SATYRO, M.A.; and MARRIOTT, R.A. Screening Ionic Liquids as Candidates for Separation of Acid Gases: Solubility of Hydrogen Sulfide, Methane, and Ethane. *AIChE J.*, 59, 2013: 2993–3005.

[337] PRAUSNITZ, J.M.; LICHTENTHALER, R.N.; and GOMES DE AZEVEDO, E. *Molecular Thermodynamics of Fluid-Phase Equilib*ria. Prentice Hall PTR, New Jersey, USA, 3rd edition, 1999.

- [338] DE LOOS, T.W.; VAN DER KOOI, H.J.; and OTT, P.L. Vapor-Liquid Critical Curve of the System Ethane + 2-Methylpropane. *J. Chem. Eng. Data*, 31, 1986: 166–168.
- [339] SIGMA-ALDRICH. MSDS of Ionic Liquids. http://www.sigmaaldrich.com/chemistry/chemistry-products.html? TablePage=16255866.
- [340] Peng, D. and Robinson, D.B. A New Two-Constant Equation of State. *Ind. Eng. Chem. Fundam.*, 15, 1976: 59–64.
- [341] VALDERRAMA, J.O. and ROJAS, R.E. Critical Properties of Ionic Liquids. Revisited. *Ind. Eng. Chem. Res.*, 48, 2009: 6890–6900.
- [342] RAI, N. and MAGINN, E.J. Critical behaviour and vapour-liquid coexistence of 1-alkyl-3-methylimidazolium bis(trifluoromethylsulfonyl)amide ionic liquids via Monte Carlo simulations. *Faraday Discuss.*, 154, 2012: 53–69.
- [343] Martin, A.; Bermejo, M.D.; Mato, F.A.; and Cocero, M.J. Teaching advanced equations of state in applied thermodynamics courses using open source programs. *Educ. Chem. Eng.*, 6, 2011: e114–e121.
- [344] Poling, B.E.; Prausnitz, J.M.; and O'Connell, J.P. *The Properties of Gases and Liquids*. Mc Graw Hill, Singapore, 5th edition, 2007.
- [345] RAMDIN, M.; AMPLIANITIS, A.; BAZHENOV, S.; VOLKOV, A.; VOLKOV, V.; VLUGT, T.J.H.; and DE LOOS, T.W. Solubility of CO<sub>2</sub> and CH<sub>4</sub> in Ionic Liquids: Ideal CO<sub>2</sub>/CH<sub>4</sub> Selectivity. *Ind. Eng. Chem. Res.*, 53, 2014: 15427–15435.

- [346] RAMDIN, M.; ZUZUARREGUI OLASAGASTI, T.; VLUGT, T.J.H.; and DE LOOS, T. High pressure solubility of CO<sub>2</sub> in non-fluorinated phosphonium-based ionic liquids. *J. Supercrit. Fluids*, 82, 2013: 41–49.
- [347] NAM, S.G. and LEE, B. Solubility of carbon dioxide in ammonium-based ionic liquids: Butyltrimethylammonium bis(trifluoromethylsulfonyl)imide and methyltrioctylammonium bis(trifluoromethylsulfonyl)imide. *Korean J. Chem. Eng.*, 30, 2013: 474–481.
- [348] SPAN, R. and WAGNER, W. A New Equation of State for Carbon Dioxide Covering the Fluid Region from the Triple-Point Temperature to 1100 K at Pressures up to 800 MPa . J. Phys. Chem. Ref. Data, 25, 1996: 1509–1596.
- [349] Setzmann, U. and Wagner, W. A New Equation of State and Tables of Thermodynamic Properties for Methane Covering the Range from the Melting Line to 625 K at Pressures up to 1000 MPa. J. Phys. Chem. Ref. Data, 20, 1991: 1061–1155.
- [350] PALGUNADI, J.; KANG, J.E.; NGUYEN, D.Q.; KIM, J.H.; MIN, B.K.; LEE, S.D.; K., H.; and KIM, H.S. Solubility of CO<sub>2</sub> in dialkylimidazolium dialkylphosphate ionic liquids. *Thermochim. Acta*, 494, 2009: 94–98.
- [351] Nonthanasin, T.; Henni, A.; and Saiwan, C. Densities and low pressure solubilities of carbon dioxide in five promising ionic liquids. *RSC Adv.*, 4, 2014: 7566–7578.
- [352] Benson, B.B. and Krause, D. Empirical laws for dilute aqueous solutions of nonpolar gases. *J. Chem. Phys.*, 64, 1976: 689–709.
- [353] Henni, A.; Tontiwachwuthikul, P.; and Chakma, A. Solubility Study of Methane and Ethane in Promising Physical Solvents for Natural Gas Sweetening Operations. *J. Chem. Eng. Data*, 51, 2006: 64–67.

[354] RAYER, A.V.; HENNI, A.; and TONTIWACHWUTHIKUL, P. High Pressure Physical Solubility of Carbon Dioxide (CO<sub>2</sub>) in Mixed Polyethylene Glycol Dimethyl Ethers (Genosorb 1753). *Can. J. Chem. Eng.*, 90, 2012: 576–583.

- [355] RAYER, A.V.; HENNI, A.; and TONTIWACHWUTHIKUL, P. High-Pressure Solubility of Methane (CH<sub>4</sub>) and Ethane (C<sub>2</sub>H<sub>6</sub>) in Mixed Polyethylene Glycol Dimethyl Ethers (Genosorb 1753) and Its Selectivity in Natural Gas Sweetening Operations. *J. Chem. Eng. Data*, 57, 2012: 764–775.
- [356] Henni, A.; Tontiwachwuthikul, P.; and Chakma, A. Solubilities of Carbon Dioxide in Polyethylene Glycol Ethers. *Can. J. Chem. Eng.*, 83, 2005: 358–361.
- [357] MIYANO, Y. and FUJIHARA, I. Henry's constants of carbon dioxide in methanol at 250-500 K. Fluid Phase Equilib., 221, 2004: 57–62.
- [358] JOU, F.Y.; DESHMUKH, R.D.; OTTO, F.D.; and MATHER, A.E. Solubility of H<sub>2</sub>S, CO<sub>2</sub>, CH<sub>4</sub> and C<sub>2</sub>H<sub>6</sub> in Sulfolane at elevated pressures. Fluid Phase Equilib., 56, 1990: 313–324.
- [359] MELZER, W.M.; SCHRODTER, F.; and KNAPP, H. Solubilities of Methane, Propane and Carbon Dioxide in solvent mixtures consisting of water, N,N-Dimethylformamide, and N-methyl-2-pyrrolidone. Fluid Phase Equilib., 49, 1989: 167–186.
- [360] RIVAS, O.R. and PRAUSNITZ, J.M. Sweetening of Sour Natural Gases by Mixed-Solvent Absorption: Solubilities of Ethane, Carbon Dioxide, and Hydrogen Sulfide in Mixtures of Physical and Chemical Solvents. AIChE J., 25, 1979: 975–984.
- [361] SCHNABEL, T.; VRABEC, J.; and HASSE, H. Molecular simulation study of hydrogen bonding mixtures and new molecular models for mono- and dimethylamine. *Fluid Phase Equilib.*, 63, 2008: 144–159.

- [362] Wu, Y.; Carroll, J.J.; and Zhu, W. Sour Gas and Related Technologies. Wiley, Canada, 2012.
- [363] Kumelan, J.; Perez-Salado Kamps, A.; Tuma, D.; and Maurer, G. Solubility of the Single Gases Methane and Xenon in the Ionic Liquid [bmim][CH<sub>3</sub>SO<sub>4</sub>]. *J. Chem. Eng. Data*, 52, 2007: 2319–2324.
- [364] ALTHULUTH, M.; KROON, M.C.; and PETERS, C.J. Solubility of Methane in the Ionic Liquid 1.Ethyl-3-methylimidazolium Tris(pentafluoroethyl)trifluorophosphate. *Ind. Eng. Chem. Res.*, 51, 2012: 16709–16712.
- [365] Petermann, M.; Weissert, T.; Kareth, S.; Lösch, H.W.; and Dreisbach, F. New instrument to measure the selective sorption of gas mixtures under high pressures. *J. Supercrit. Fluids*, 45, 2008: 156–160.
- [366] TSONOPOULOS, C. An Empirical Correlation of Second Virial Coefficients. *AIChE J.*, 20, 1974: 263–272.
- [367] MALLU, B.V. and VISWANATH, D.S. Compression factors and second virial coefficients of  $H_2$ ,  $CH_4$ ,  $\{xCO_2 + (l-x)H_2\}$ , and  $\{xCO_2 + (l-x)CH_4\}$ . J. Chem. Thermodyn., 22, 1990: 997–1006.
- [368] Shariati, A. and Peters, C.J. High-pressure phase behavior of systems with ionic liquids: measurements and modeling of the binary system fluoroform + 1-ethyl-3-methylimidazolium hexafluorophosphate.

  J. of Supercritical Fluids, 25, 2003: 109–117.
- [369] KORDAS, A.; TSOUTSOURAS, K.; STAMATAKI, S.; and TASSIOS, D. A generalized correlation for the interaction coefficients of CO<sub>2</sub>hydrocarbon binary mixtures. Fluid Phase Equilib., 93, 1994: 141– 166.
- [370] RAEISSI, S. and PETERS, C.J. Carbon Dioxide Solubility in the Homologous 1-Alkyl-3-methylimidazolium Bis(trifluoromethylsulfonyl)-imide Family. *J. Chem. Eng. Data*, 54, 2009: 382–386.

[371] Raeissi, S. and Peters, C.J. High pressure phase behaviour of methane in 1-butyl-3-methylimidazolium bis(trifluoromethylsulfonyl)-imide. Fluid Phase Equilib., 294, 2010: 67–71.

- [372] VALDERRAMA, J.O.; FORERO, L.A.; and ROJAS, R.E. Extension of a Group Contribution Method To Estimate the Critical Properties of Ionic Liquids of High Molecular Mass. *Ind. Eng. Chem. Res.*, 54, 2015: 3480–3487.
- [373] DOHRN, R.; FONSECA, J.M.S.; and PEPER, S. Experimental Methods for Phase Equilibria at High Pressures. *Annu. Rev. Chem. Biomol. Eng.*, 3, 2012: 343–367.
- [374] Peper, S. and Dohrn, R. Sampling from fluid mixtures under high pressure: Review, case study and evaluation. *J. Supercrit. Fluids*, 66, 2012: 2–15.
- [375] HUANG, X.; MARGULIS, C.J.; LI, Y.; and BERNE, B.J. Why Is the Partial Molar Volume of CO<sub>2</sub> So Small When Dissolved in a Room Temperature Ionic Liquid? Structure and Dynamics of CO<sub>2</sub> Dissolved in [Bmim<sup>+</sup>][PF<sub>6</sub>]. J. Am. Chem. Soc., 127, 2005: 17842–17851.
- [376] TURNER, C.H.; COOPER, A.; ZHANG, Z.; SHANNON, M.S.; and BARA, J.E. Molecular Simulation of the Thermophysical Properties of N-Functionalized Alkylimidazoles. *J. Phys. Chem. B*, 116, 2012: 6529–6535.
- [377] LIU, H.; ZHANG, Z.; BARA, J.E.; and TURNER, C.H. Electrostatic Potential within the Free Volume Space of Imidazole-Based Solvents: Insights into Gas Absorption Selectivity. *J. Phys. Chem. B*, 118, 2014: 255–264.
- [378] RAMDIN, M.; VLUGT, T.J.H.; and DE LOOS, T.W. Solubility of CO<sub>2</sub> in the Ionic Liquids [TBMN][MeSO<sub>4</sub>] and [TBMP][MeSO<sub>4</sub>]. *J. Chem. Eng. Data*, 57, 2012: 2275–2280.

- [379] Shi, W. and Maginn, E.J. Continuous Fractional Component Monte Carlo: An Adaptive Biasing Method for Open System Atomistic Simulations. J. Chem. Theory Comput., 3, 2007: 1451–1463.
- [380] Shi, W. and Maginn, E.J. Atomistic Simulation of the Absorption of Carbon Dioxide and Water in the Ionic Liquid 1-n-Hexyl-3-methylimidazolium Bis(trifluoromethylsulfonyl)imide ([hmim][Tf<sub>2</sub>N]). J. Phys. Chem. B, 112, 2008: 2045–2055.
- [381] Panagiotopoulos, A.Z. Monte Carlo methods for phase equilibria of fluids. *J. Phys.: Condens. Matter*, 12, 2000: R25–R52.
- [382] DE PABLO, J.J.; YAN, Q.; and ESCOBEDO, F.A. Simulation of Phase Transitions in Fluids. *Annu. Rev. Phys. Chem.*, 50, 1999: 377–411.
- [383] Dubbeldam, D.; Torres-Knoop, A.; and Walton, K.S. On the inner workings of Monte Carlo codes. *Mol. Simul.*, 39, 2013: 1253–1392.
- [384] Consta, S.; Vlugt, T.J.H.; Hoeth, J.W.; Smit, B.; and Frenkel, D. Recoil growth algorithm for chain molecules with continuous interactions. *Mol. Phys.*, 97, 1999: 1243–1254.
- [385] Frenkel, D. and Smit, B. Understanding Molecular Simulation: From Algorithms to Applications. Academic Press, San Diego, USA, 2002.
- [386] Chen, Q.; Balaji, S.P.; Ramdin, M.; Gutiérrez-Sevillano, J.J.; Bardow, A.; Goetheer, E.; and Vlugt, T.J.H. Validation of the CO<sub>2</sub>/N<sub>2</sub>O Analogy Using Molecular Simulation. *Ind. Eng. Chem. Res.*, 53, 2014: 18081–18090.
- [387] WANG, F. and LANDAU, D.P. Efficient, Multiple-Range Random Walk Algorithm to Calculate the Density of States. *Phys. Rev. Lett.*, 86, 2001: 2050–2053.

[388] TORRES-KNOOP, A.; BALAJI, S.P.; VLUGT, T.J.H.; and DUBBEL-DAM, D. A Comparison of Advanced Monte Carlo Methods for Open Systems: CFCMC vs CBMC. *J. Chem. Theory Comput.*, 10, 2014: 942–952.

- [389] SHI, W. and MAGINN, E.J. Improvement in Molecule Exchange Efficiency in Gibbs Ensemble Monte Carlo: Development and Implementation of the Continuous Fractional Component Move. J. Comput. Chem., 29, 2008: 2520–2530.
- [390] Liu, H. and Maginn, E. A molecular dynamics investigation of the structural and dynamic properties of the ionic liquid 1-n-butyl-3-methylimidazolium bis(trifluoromethanesulfonyl)imide. *J. Chem. Phys.*, 135, 2011: 124507.
- [391] TENNEY, C.M.; MASSEL, M.; MAYES, J.M.; SEN, M.; BRENNECKE, J.F.; and MAGINN, E.J. A Computational and Experimental Study of the Heat Transfer Properties of Nine Different Ionic Liquids. *J. Chem. Eng. Data*, 59, 2014: 391–399.
- [392] POTOFF, J.J. and SIEPMANN, J.I. Vapor-Liquid Equilibria of Mixtures Containing Alkanes, Carbon Dioxide, and Nitrogen. *AIChE J.*, 47, 2001: 1676–1682.
- [393] Martin, M.G. and Siepmann, J.I. Transferable potentials for phase equilibria. 1. United-atom description of n-alkanes. *J. Phys. Chem. B*, 102, 1998: 2569–2577.
- [394] STUBBS, J.M.; POTOFF, J.J.; and SIEPMANN, J.I. Transferable potentials for phase equilibria. 6. United-atom description for ethers, glycols, ketones and aldehydes. J. Phys. Chem. B, 108, 2004: 17596– 17605.
- [395] Ketko, M.H.; Kamath, G.; and Potoff, J.J. Development of an Optimized Intermolecular Potential for Sulfur Dioxide. J. Phys. Chem. B, 115, 2011: 4949–4954.

- [396] ALLEN, M.P. and TILDESLEY, D.J. Computer Simulation of Liquids. Oxford University Press, New York, USA, 1987.
- [397] Siepmann, J.I. A method for the direct calculation of chemical potentials for dense chain systems. *Mol. Phys.*, 70, 1990: 1145–1158.
- [398] SIEPMANN, J.I. and FRENKEL, D. Configurational-bias Monte Carlo A new sampling scheme for flexible chains. *Mol. Phys.*, 75, 1992: 59–70.
- [399] VLUGT, T.J.H.; KRISHNA, R.; and SMIT, B. Molecular Simulations of Adsorption Isotherms for Linear and Branched Alkanes and Their Mixtures in Silicalite. J. Phys. Chem. B, 103, 1999: 1102–1118.
- [400] URUKOVA, I.; VORHOLZ, J.; and MAURER, G. Solubility of CO<sub>2</sub>, CO, and H<sub>2</sub> in the Ionic Liquid [bmim][PF<sub>6</sub>] from Monte Carlo Simulations. *J. Phys. Chem. B*, 109, 2005: 12154–12159.
- [401] Dubbeldam, D.; Calero, S.; Ellis, D.E.; and Snurr, R.Q. RASPA: molecular Simulation Software for Adsorption and Diffusion in Flexible Nanoporous Materials. *Mol. Simul.*, in press, 2015: DOI: 10.1080/08927022.2015.1010082.
- [402] Kodama, D.; Kanakubo, M.; Kokubo, M.; Hashimoto, S.; Nanjo, H.; and Kato, M. Density, viscosity, and solubility of carbon dioxide in glymes. *Fluid Phase Equilib.*, 302, 2011: 103–108.
- [403] Kumelan, J.; Perez-Salado Kamps, A.; Tuma, D.; and Maurer, G. Solubility of the Single Gases Methane and Xenon in the Ionic Liquid [hmim][Tf<sub>2</sub>N]. *Ind. Eng. Chem. Res.*, 46, 2007: 8236–8240.
- [404] FLORUSSE, L.J.; RAEISSI, S.; and PETERS, C.J. High-Pressure Phase Behavior of Ethane with 1-Hexyl-3-methylimidazolium Bis(trifluoromethylsulfonyl)imide. *J. Chem. Eng. Data*, 53, 2008: 1283–1285.

[405] SCHMIDT, K.A.G. and MATHER, A.E. Solubility of Sulphur Dioxide in Mixed Polyethylene Glycol Dimethyl Ethers. *Can. J. Chem. Eng.*, 79, 2001: 946–960.

- [406] SEADER, J.D.; HENLEY, E.J.; and ROPER, D.K. Separation Process Principles. Wiley, New York, 3th edition, 2013.
- [407] Jessop, P.G. and Subramaniam, B. Gas-Expanded Liquids. *Chem. Rev.*, 107, 2007: 2666–2694.
- [408] Valderrama, J.O. The State of the Cubic Equations of State. *Ind. Eng. Chem. Res.*, 42, 2003: 1603–1618.
- [409] SMITH, J.M.; NESS, H.C.V.; and ABBOTT, M.M. Introduction to Chemical Engineering Thermodynamics. Mc Graw Hill, New York, 7th edition, 2005.
- [410] Case, F.H.; Brennan, J.; Chaka, A.; Dobbs, K.D.; Friend, D.G.; Frurip, D.; Gordon, P.A.; Moore, J.; Mountain, R.D.; Olson, J.; Ross, R.B.; Schiller, M.; and Shen, V.K. The third industrial fluid properties simulation challenge. *Fluid Phase Equilib.*, 260, 2007: 153–163.
- [411] RAI, N.; RAFFERTY, J.L.; MAITI, A.; and SIEPMANN, J.I. Prediction of the bubble point pressure for the binary mixture of ethanol and 1,1,1,2,3,3,3-heptafluoropropane from Gibbs ensemble Monte Carlo simulations using the TraPPE force field. *Fluid Phase Equilib.*, 260, 2007: 199–211.
- [412] Kelkar, M.S.; Rafferty, J.L.; Maginn, E.J.; and Siepmann, J.I. Prediction of viscosities and vapor-liquid equilibria for five polyhydric alcohols by molecular simulation. *Fluid Phase Equilib.*, 260, 2007: 218–231.
- [413] ECKL, B.; HUANG, Y.; VRABEC, J.; and HASSE, H. Vapor pressure of R227ea + ethanol at 343.13 K by molecular simulation. *Fluid Phase Equilib.*, 260, 2007: 177–182.

- [414] YAZAYDIN, A.O. and MARTIN, M.G. Bubble point pressure estimates from Gibbs ensemble simulations. *Fluid Phase Equilib.*, 260, 2007: 195–198.
- [415] Christensen, S.; Peters, G.H.; Hansen, F.Y.; O'Connell, J.P.; and Abildskov, J. State conditions transferability of vapor-liquid equilibria via fluctuation solution theory with correlation function integrals from molecular dynamics simulation. *Fluid Phase Equilib.*, 260, 2007: 169–176.
- [416] Klamt, A. and Eckert, F. Prediction, fine tuning, and temperature extrapolation of a vapor liquid equilibrium using COSMOtherm. *Fluid Phase Equilib.*, 260, 2007: 183–189.
- [417] Ungerer, P.; Boutin, A.; and Fuchs, A.H. Direct calculation of bubble points by Monte Carlo simulation. *Mol. Phys.*, 97, 1999: 523–539.
- [418] VRABEC, J. and HASSE, H. Grand Equilibrium: vapour-liquid equilibria by a new simulation method. *Mol. Phys.*, 100, 2002: 3375–3383.
- [419] Hendriks, E.; Kontogeorgis, G.M.; Dohrn, R.; de Hemptinne, J.; Economou, I.G.; Zilnik, L.F.; and Vesovic, V. Industrial Requirements for Thermodynamics and Transport Properties. *Ind. Eng. Chem. Res.*, 49, 2010: 11131–11141.
- [420] LOTFI, A.; VRABEC, J.; and FISCHER, J. Vapour liquid equilibria of the Lennard-Jones fluid from the NpT plus test particle method. *Mol. Phys.*, 76, 1992: 1319–1333.
- [421] VRABEC, J. and FISCHER, J. Vapour liquid equilibria of mixtures from the *NpT* plus test particle method. *Mol. Phys.*, 85, 1995: 781–792.
- [422] Boda, D.; Liszi, J.; and Szalai, I. An extension of the NpT plus test particle method for the determination of the vapour-liquid equilibria of pure fluids. *Chem. Phys. Lett.*, 235, 1995: 140–145.

[423] ESCOBEDO, F.A. Novel pseudoensembles for simulation of multicomponent phase equilibria. *J. Chem. Phys.*, 108, 1998: 8761–8772.

- [424] ESCOBEDO, F.A. Tracing coexistence lines in multicomponent fluid mixtures by molecular simulation. *J. Chem. Phys.*, 110, 1999: 11999–12010.
- [425] VLUGT, T.J.H.; MARTIN, M.G.; SMIT, B.; SIEPMANN, J.I.; and KRISHNA, R. Improving the efficiency of the configurational-bias Monte Carlo algorithm. Mol. Phys., 94, 1998: 727–733.
- [426] BUDHATHOKI, S.; SHAH, J.K.; and MAGINN, E.J. Molecular Simulation Study of the Solubility, Diffusivity and Permselectivity of Pure and Binary Mixtures of CO<sub>2</sub> and CH<sub>4</sub> in the Ionic Liquid 1-n-Butyl-3-methylimidazolium bis(trifluoromethylsulfonyl)imide. *Ind. Eng. Chem. Res.*, 54, 2015: 8821–8828.
- [427] NUGENT, P.; BELMABKHOUT, Y.; BURD, S.D.; CAIRNS, A.J.; LUEBKE, R.; FORREST, K.; PHAM, T.; MA, S.; SPACE, B.; WOJTAS, L.; and *et al.* Porous materials with optimal adsorption thermodynamics and kinetics for CO<sub>2</sub> separation. *Nature*, 495, 2013: 80–84.
- [428] Scholes, C.A.; Smith, K.H.; Kentish, S.E.; and Stevens, G.W. CO<sub>2</sub> capture from pre-combustion processes-Strategies for membrane gas separation. *Int. J. Greenh. Gas Control*, 4, 2010: 739–755.
- [429] VORA, S.; BRICKETT, L.; INDRIKANTI, P.; MUNSON, R.; MURPHY, J.; RIFE, T.; STROCK, J.; and ZAREMSKY, C. DOE/NETL Advanced Carbon Dioxide Capture R&D Program: Technology Update. Technical report, U.S. Department of Energy/National Energy Technology Laboratory, Pittsburgh, PA, 2013. http://www.netl.doe.gov/File%20Library/Research/Coal/carbon% 20capture/handbook/C02-Capture-Tech-Update-2013.pdf.

- [430] Sumida, K.; Rogow, D.L.; Mason, J.A.; McDonald, T.M.; Bloch, E.D.; Herm, Z.R.; Bae, T.; and Long, J.R. Carbon Dioxide Capture in Metal-Organic Frameworks. *Chem. Rev.*, 112, 2012: 724–781.
- [431] HERM, Z.R.; SWISHER, J.A.; SMIT, B.; KRISHNA, R.; and LONG, J.R. Metal-Organic Frameworks as Adsorbents for Hydrogen Purification and Precombustion Carbon Dioxide Capture. J. Am. Chem. Soc., 133, 2011: 5664–5667.
- [432] SMIT, B.; REIMER, J.A.; OLDENBURG, C.M.; and BOURG, I.C. Introduction to Carbon Capture and Sequestration. Imperial College Press, London, UK, 2014.
- [433] Martín-Calvo, A.; Lahoz-Martín, F.D.; and Calero, S. Understanding Carbon Monoxide Capture Using Metal-Organic Frameworks. J. Phys. Chem. C, 116, 2012: 6655–6663.
- [434] Cracknell, R.F. Molecular simulation of hydrogen adsorption in graphitic nanofibres. *Phys. Chem. Chem. Phys.*, 3, 2001: 2091–2097.
- [435] KAMATH, G.; LUBNA, N.; and POTOFF, J.J. Effect of partial charge parametrization on the fluid phase behavior of hydrogen sulfide. *J. Chem. Phys.*, 123, 2005: 124505.
- [436] Kristóf, T. and Liszi, J. Effective Intermolecular Potential for Fluid Hydrogen Sulfide. J. Phys. Chem. B, 101, 1997: 5480–5483.
- [437] GUTIÉRREZ-SEVILLANO, J.J.; MARTÍN-CALVO, A.; DUBBELDAM, D.; CALERO, S.; and HAMAD, S. Adsorption of hydrogen sulphide on Metal-Organic Frameworks. *RSC Adv.*, 3, 2013: 14737–14749.
- [438] HESS, B.; KUTZNER, C.; VAN DER SPOEL, D.; and LINDAHL, E. GROMACS 4: Algorithms for Highly Efficient, Load-Balanced, and Scalable Molecular Simulation. *J. Chem. Theory Comput.*, 4, 2008: 435–447.

[439] PRONK, S.; PÁLL, S.; SCHULZ, R.; LARSSON, P.; BJELKMAR, P.; APOSTOLOV, R.; SHIRTS, M.R.; SMITH, J.C.; KASSON, P.M.; VAN DER SPOEL, D.; and et al. GROMACS 4.5: a high-throughput and highly parallel open source molecular simulation toolkit. Bioinformatics, 29, 2013: 845–854.

- [440] RAEISSI, S.; FLORUSSE, L.J.; and PETERS, C.J. Purification of Flue Gas by Ionic Liquids: Carbon Monoxide Capture in [bmim][Tf<sub>2</sub>N]. *AIChE J.*, 59, 2013: 3886–3891.
- [441] RAEISSI, S. and PETERS, C.J. Understanding Temperature Dependency of Hydrogen Solubility in Ionic Liquids, Including Experimental Data in [bmim][Tf<sub>2</sub>N]. *AIChE J.*, 58, 2012: 3553–3559.
- [442] Jalili, A.H.; Rahmati-Rostami, M.; Ghotbi, C.; Hosseini-Jenab, M.; and Ahmadi, A.N. Solubility of H<sub>2</sub>S in Ionic Liquids [bmim][PF<sub>6</sub>], [bmim][BF<sub>4</sub>], and [bmim][Tf<sub>2</sub>N]. *J. Chem. Eng. Data*, 54, 2009: 1844–1849.
- [443] Gainar, I. and Anitescu, G. The solubility of CO<sub>2</sub>, N<sub>2</sub> and H<sub>2</sub> in a mixture of dimethylether polyethylene glycols at high pressures. Fluid Phase Equilib., 109, 1995: 281–289.
- [444] ABU-ZAHRA, M.R.M.; SCHNEIDERS, L.H.J.; NIEDERER, J.P.M.; FERON, P.H.M.; and VERSTEEG, G.F. CO<sub>2</sub> capture from power plants Part I. A parametric study of the technical performance based on monoethanolamine. *Int. J. Greenh. Gas Cont.*, 1, 2007: 37–46.
- [445] BOETTINGER, W.; MAIWALD, M.; and HASSE, H. Online NMR spectroscopic study of species distribution in MEA-H<sub>2</sub>O-CO<sub>2</sub> and DEA-H<sub>2</sub>O-CO<sub>2</sub>. Fluid Phase Equilib., 263, 2008: 131–143.
- [446] KHAKHARIA, P.; BRACHERT, L.; MERTENS, J.; HUIZINGA, A.; SCHALLERT, B.; SCHABER, K.; VLUGT, T.J.H.; and GOETHEER, E. Investigation of aerosol based emission of MEA due to sulphuric acidaerosol and soot in a Post Combustion CO<sub>2</sub> Capture process. *Int.* J. Greenh. Gas Control, 19, 2013: 138–144.

- [447] Khakharia, P.; Kvamsdal, H.M.; da Silva, E.F.; Vlugt, T.J.H.; and Goetheer, E.L.V. Field study of a Brownian Demister Unit to reduce aerosol based emission from a Post Combustion CO<sub>2</sub> Capture plant. *Int. J. Greenh. Gas Cont.*, 28, 2014: 57–64.
- [448] Khakharia, P.; Huizinga, A.; Jurado Lopez, C.; Sanchez Sanchez, C.; de Miguel Mercader, F.; Vlugt, T.J.H.; and Goetheer, E. Acid Wash Scrubbing as a Countermeasure for Ammonia Emissions from a Postcombustion CO<sub>2</sub> Capture Plant. *Ind. Eng. Chem. Res.*, 53, 2014: 13195–13204.
- [449] GANGARAPU, S.; MARCELIS, A.T.M.; and ZUILHOF, H. Improving the Capture of CO<sub>2</sub> by Substituted Monoethanolamines: Electronic Effects of Fluorine and Methyl Substituents. *ChemPhysChem*, 13, 2012: 3973–3980.
- [450] Danckwerts, P.V. The Reaction of CO<sub>2</sub> with Ethanolamines. *Chem. Eng. Sci.*, 34, 1979: 443–446.
- [451] GANGARAPU, S.; MARCELIS, A.T.M.; and ZUILHOF, H. Carbamate Stabilities of Sterically Hindered Amines from Quantum Chemical Methods: Relevance for CO<sub>2</sub> Capture. *ChemPhysChem*, 14, 2013: 3936–3943.
- [452] Manzolini, G.; Fernandez, E.S.; Rezvani, S.; Macchi, E.; Goetheer, E.L.V.; and Vlugt, T.J.H. Economic assessment of amine based CO<sub>2</sub> capture technologies in power plants based on European Benchmarking Task Force methodology. *Appl. Energy*, 138, 2014: 546–558.
- [453] SARTORI, G. and SAVAGE, G.W. Sterically Hindered Amines for CO<sub>2</sub> Removal from Gases. *Ind. Eng. Chem. Res.*, 22, 1983: 239–249.
- [454] Batt, W.T.; Maddox, R.N.; Mains, G.J.; Rahman, M.; and Vaz, R.N. Chemical and Engineering Fundamentals of Ethanolamine Sweetening. 1980 Gas Conditioning Conference, 1980.

[455] Maddox, R.N.; Mains, G.J.; and Rahman, M. Reactions of carbon dioxide and hydrogen sulfide with some alkanolamines. *Ind. Eng. Chem. Res.*, 26, 1987: 27–31.

- [456] JAKOBSEN, J.P.; KRANE, J.; and SVENDSEN, H.F. Liquid-Phase Composition Determination in CO<sub>2</sub>-H<sub>2</sub>O-Alkanolamine Systems: An NMR Study. *Ind. Eng. Chem. Res.*, 44, 2005: 9894–9903.
- [457] CAR, R. and PARINELLO, M. Unified Approach for Molecular Dynamics and Density-Functional Theory. Phys. Rev. Lett., 55, 1985: 2471–2474.
- [458] VAN DUIN, A.C.; DASGUPTA, S.; LORANT, F.; and III, W.A.G. ReaxFF: A Reactive Force Field for Hydrocarbons. J. Phys. Chem. A, 105, 2001: 9396–9409.
- [459] JOHNSON, J.K.; PANAGIOTOPOULOS, A.Z.; and Gubbins, K.E. Reactive canonical Monte Carlo A new simulation technique for reacting or associating fluids. *Mol. Phys.*, 81, 1994: 717–733.
- [460] SMITH, W.R. and TRISKA, B. The reaction ensemble method for the computer simulation of chemical and phase equilibria. 1. Theory and basic examples. J. Chem. Phys., 100, 1994: 3019–3027.
- [461] Hansen, N.; Jakobtorweihen, S.; and Keil, F.J. Reactive Monte Carlo and grand-canonical Monte Carlo simulations of the propene metathesis reaction system. *J. Chem. Phys*, 122, 2005: 1–11.
- [462] Jakobtorweihen, S.; Hansen, N.; and Keil, F.J. Combining reactive and configurational-bias Monte Carlo: Confinement influence on the propene metathesis reaction system in various zeolites. *J. Chem. Phys.*, 125, 2006: 1–9.
- [463] ROSCH, T.W. and MAGINN, E.J. Reaction Ensemble Monte Carlo Simulation of Complex Molecular Systems. J. Chem. Theory Comput., 7, 2011: 269–279.

- [464] Turner, C.H.; Johnson, J.K.; and Gubbins, K.E. Effect of confinement on chemical reaction equilibria: The reactions  $2NO-\xi N_2O_2$  and  $N_2+3H_2-\xi 2NH_3$  in carbon micropores. *J. Chem. Phys.*, 114, 2001: 1851–1859.
- [465] Carrero-Mantilla, J. and Llano-Restrepo, M. Vapor-phase chemical equilibrium for the hydrogenation of benzene to cyclohexane from reaction-ensemble molecular simulation. *Fluid Phase Equilib.*, 219, 2004: 181–193.
- [466] LISAL, M.; NEZBEDA, I.; and SMITH, W.R. The reaction ensemble method for the computer simulation of chemical and phase equilibria. II. The Br<sub>2</sub>+Cl<sub>2</sub>+BrCl system. J. Chem. Phys., 110, 1999: 8597–8604.
- [467] LISAL, M.; BRENNAN, J.K.; and SMITH, W.R. Chemical reaction equilibrium in nanoporous materials: NO dimerization reaction in carbon slit nanopores. *J. Chem. Phys.*, 124, 2006: 064712.
- [468] LISAL, M.; SMITH, W.R.; and NEZBEDA, I. Molecular simulation of multicomponent reaction and phase equilibria in MTBE ternary system. AIChE J., 46, 2000: 866–875.
- [469] LISAL, M.; SMITH, W.R.; and NEZBEDA, I. Accurate computer simulation of phase equilibrium for complex fluid mixtures. Application to binaries involving isobutene, methanol, methyl tert-butyl ether, and n-butane. J. Phys. Chem. B, 103, 1999: 10496–10505.
- [470] BALAJI, S.P.; SCHNELL, S.K.; McGarrity, E.S.; and Vlugt, T.J.H. A direct method for calculating thermodynamic factors for liquid mixtures using the Permuted Widom test particle insertion method. *Mol. Phys.*, 111, 2013: 285–294.
- [471] BALAJI, S.P.; SCHNELL, S.K.; and VLUGT, T.J.H. Calculating thermodynamic factors of ternary and multicomponent mixtures using the Permuted Widom test particle insertion method. *Theor. Chem. Acc.*, 132, 2013: 1–8.

[472] SCHNELL, S.K.; ENGLEBIENNE, P.; SIMON, J.M.; KRUGER, P.; BALAJI, S.P.; KJELSTRUP, S.; BEDEAUX, D.; BARDOW, A.; and VLUGT, T.J.H. How to apply the Kirkwood-Buff theory to individual species in salt solutions. *Chem. Phys. Lett.*, 582, 2013: 154–157.

- [473] POLDERMAN, L.D.; DILLON, C.P.; and STEELE, A.B. Degradation of monoethanolamine in natural gas treating service. *Oil Gas J.*, 53, 1955: 180–183.
- [474] STRAZISAR, B.R.; ANDERSON, R.R.; and WHITE, C.M. Degradation Pathways for Monoethanolamine in a CO<sub>2</sub> Capture Facility. *Energy Fuels*, 17, 2003: 1034–1039.
- [475] TURNER, C.H.; BRENNAN, J.K.; LISAL, M.; SMITH, W.R.; JOHNSON, J.K.; and GUBBINS, K.E. Simulation of chemical reaction equilibria by the reaction ensemble Monte Carlo method: a review. *Mol. Simul.*, 34, 2008: 119–146.
- [476] MAYER, J.E. and MAYER, M.G. Statistical Mechanics. Wiley, New York, 1963.

- [477] Frisch, M.J.; Trucks, G.W.; Schlegel, H.B.; Scuseria, G.E.; ROBB, M.A.; CHEESEMAN, J.R.; SCALMANI, G.; BARONE, V.; MEN-NUCCI, B.; PETERSSON, G.A.; NAKATSUJI, H.; CARICATO, M.; LI, X.; Hratchian, H.P.; Izmaylov, A.F.; Bloino, J.; Zheng, G.; Sonnenberg, J.L.; Hada, M.; Ehara, M.; Toyota, K.; Fukuda, R.; HASEGAWA, J.; ISHIDA, M.; NAKAJIMA, T.; HONDA, Y.; KITAO, O.; NAKAI, H.; VREVEN, T.; MONTGOMERY, JR., J.A.; PERALTA, J.E.; OGLIARO, F.; BEARPARK, M.; HEYD, J.J.; BROTHERS, E.; KUDIN, K.N.; STAROVEROV, V.N.; KOBAYASHI, R.; NORMAND, J.; RAGHAVACHARI, K.; RENDELL, A.; BURANT, J.C.; IYENGAR, S.S.; Tomasi, J.; Cossi, M.; Rega, N.; Millam, J.M.; Klene, M.; KNOX, J.E.; CROSS, J.B.; BAKKEN, V.; ADAMO, C.; JARAMILLO, J.; Gomperts, R.; Stratmann, R.E.; Yazyev, O.; Austin, A.J.; CAMMI, R.; POMELLI, C.; OCHTERSKI, J.W.; MARTIN, R.L.; Mo-ROKUMA, K.; ZAKRZEWSKI, V.G.; VOTH, G.A.; SALVADOR, P.; Dannenberg, J.J.; Dapprich, S.; Daniels, A.D.; Farkas, .; Foresman, J.B.; Ortiz, J.V.; Cioslowski, J.; and Fox, D.J. Gaussian 09 Revision D.01. Gaussian Inc. Wallingford CT 2009.
- [478] OCHTERSKI, J.W. Thermochemistry in gaussian, 2000. http://www.gaussian.com/g\_whitepap/thermo/thermo.pdf.
- [479] RIZZO, R.C. and JORGENSEN, W.L. OPLS All-Atom Model for Amines: Resolution of the Amine Hydration Problem. *J. Am. Chem. Soc*, 121, 1999: 4827–4836.
- [480] JORGENSEN, W.L.; CHANDRASEKHAR, J.; MADURA, J.D.; IMPEY, R.W.; and KLEIN, M.L. Comparison of Simple Potential Functions for Simulating Liquid Water. J. Chem. Phys., 79, 1983: 926–935.
- [481] VACHA, R.; BUCH, V.; MILET, A.; DEVLIND, J.P.; and JUNGWIRTH, P. Autoionization at the surface of neat water: is the top layer pH neutral, basic, or acidic? *Phys. Chem. Chem. Phys.*, 9, 2007: 4736– 4747.

REFERENCES 243

[482] EWALD, P.P. Die Berechnung optischer und elektrostatischer gitterpotentiale. Ann. Phys., 64, 1921: 253–287.

- [483] HILL, T.L. An Introduction to Statistical Thermodynamics. Dover: New York (Reprint), 1987.
- [484] MANTOR, P.D.; ABIB, JR., O.; SONG, K.Y.; and KOBAYASHI, R. Solubility of Carbon Dioxide in Propylene Carbonate at Elevated Pressures and Higher than Ambient Temperatures. J. Chem. Eng. Data, 27, 1982: 243–245.
- [485] WEBER, W.; ZECK, S.; and KNAPP, H. Gas solubilities in liquid solvents at high pressures: Apparatus and results for binary and ternary systems of N<sub>2</sub>, CO<sub>2</sub>, and CH<sub>3</sub>OH. *Fluid. Phase Equilib.*, 18, 1984: 253–278.
- [486] LAZZARONI, M.J.; BUSH, D.; BROWN, J.S.; and ECKERT, C.A. High-Pressure Vapor-Liquid Equilibria of Some Carbon Dioxide + Organic Binary Systems. *J. Chem. Eng. Data*, 50, 2005: 60–65.
- [487] CLEVER, H.L. and YOUNG, C.L. Solubility data series: Methane, volume 27-28. Pergamon Press, Headington Hill Hall, England, 1987.
- [488] Hong, J.H.; Malone, P.V.; Jett, M.D.; and Kobayashi, R. The measurement and interpretation of the fluid-phase equilibria of a normal fluid in a hydrogen bonding solvent: The methane-methanol system. *Fluid Phase Equilib.*, 38, 1987: 83–96.

### Summary

Carbon dioxide (CO<sub>2</sub>) is considered the main greenhouse gas, and is inevitably produced in large quantities by fossil-fuel based industries. Therefore, it is essential to limit CO<sub>2</sub> emissions into the atmosphere. One of the tools to achieve this goal is carbon dioxide capture and storage (CCS). However, due to the extremely large scale of the problem, the capture part of the CCS process turns out to be very challenging in terms of energy efficiency and cost. The currently used amine-based solvents for CO<sub>2</sub> capture, at post-combustion conditions, have several drawbacks including their volatility, corrosivity, and high regeneration cost. CO<sub>2</sub> is captured by a chemical reaction with the amines, which requires a huge amount of heat to release the CO<sub>2</sub> from the solvent. This is the main motivation for research on energy efficient processes and the search for environment friendly materials for CO<sub>2</sub> capture. An alternative for the post-combustion process is the pre-combustion process, which is associated with the integrated gasification combined cycle (IGCC). In this process, a fuel is gasified to produce syngas, which is subsequently shifted in a water-gas-shift reactor to produce a mixture containing predominantly hydrogen (H<sub>2</sub>) and CO<sub>2</sub>. After removing  $CO_2$ , the hydrogen can be used in several applications. The pre-combustion process operates at high pressures, which allows the use of physical sorbents for  $CO_2$  removal.

 $\mathrm{CO}_2$  capture is not only relevant from an environmental perspective, but it has a major application in the natural gas sweetening process. Natural gas is typically contaminated with several impurities including the sour gases  $\mathrm{CO}_2$  and hydrogen sulfide (H<sub>2</sub>S). These sour gases need to be

246 Summary

removed to avoid technological problems during transportation and to meet customer specifications. CO<sub>2</sub> is typically removed in an absorber-stripper configuration utilizing a physical solvent, a chemical solvent, or a mixture of both solvent types (hybrid solvent) depending on the type and concentration of the impurities. Despite the inherent high pressure of the sweetening process, which is favorable for physical absorption purposes, the majority of the units in the field utilize chemical solvents (e.g., monoethanolamine (MEA)). The use of physical solvents (e.g., Purisol, Rectisol, Selexol, etc.) is not uncommon in the natural gas industry and is in fact preferred over chemical solvents at high acid gas partial pressures.

In this thesis, we investigate the potential of ionic liquids (ILs), which are salts with melting points lower than 100 °C, for CO<sub>2</sub> capture at precombustion and natural gas sweetening conditions. ILs exhibit very interesting properties like a very low vapor pressure, a high thermal and chemical stability, a high tunability, a low flammability, and a relatively high acid gas capacities. These properties of ILs can be used to overcome some of the problems associated with the conventional solvents. Only physical ILs are considered here, which are suitable for the high pressure pre-combustion and the natural gas sweetening process. Experiments have been used to measure the solubility of natural gas components in many different kinds of ILs. In addition, molecular simulations have been used to predict the solubility of gases in ILs at pre-combustion and natural gas sweetening conditions. A detailed comparison of the performance of ILs in terms of gas solubilities and selectivities with respect to conventional solvents is provided.

In Chapter 2, a detailed overview of the recent achievements and difficulties that has been encountered in finding a suitable ionic liquid for CO<sub>2</sub> capture from flue-gas streams is presented. A major part of this review focuses on experimental data of CO<sub>2</sub> solubility, selectivity and diffusivity in different ionic liquids. The effect of anions, cations and functional groups on the CO<sub>2</sub> solubility, biodegradability and toxicity of the ionic liquids are highlighted. Recent developments on task-specific ionic liquids and supported ionic liquid membranes are also discussed. Scarcely available results of molecular simulations, which is a valuable tool in designing and evaluating ionic liquids, are also reviewed.

In Chapter 3, the potential of ILs for natural gas sweetening was investigated. A synthetic method has been used to measure the solubility of  $\rm CO_2$  and  $\rm CH_4$  in many different kinds of ILs. The solubility data has been reduced by calculating the Henry constants of  $\rm CO_2$  and  $\rm CH_4$  in all the ILs, from which the ideal  $\rm CO_2/\rm CH_4$  selectivities are obtained (i.e., from the ratio of the Henry constants). The ideal  $\rm CO_2/\rm CH_4$  selectivities of the investigated ILs are compared with that of the conventional solvents like Selexol, Purisol, Rectisol, Fluor Solvent, and sulfolane. The ideal  $\rm CO_2/\rm CH_4$  selectivities in ILs are similar to that of the conventional solvents. The ideal  $\rm CO_2/\rm CH_4$  selectivity decreases with increasing temperature and increasing IL molecular weight. Therefore, a low molecular weight IL should be used if a high selectivity is desired.

In Chapter 4, the solubility of  $\rm CO_2/\rm CH_4$  gas mixtures in ILs has been measured experimentally. The aim was to investigate the effect of the presence of one gas (e.g.,  $\rm CO_2$ ) on the solubility of the other gas (e.g.,  $\rm CH_4$ ) when both are simultaneously being dissolved in a single IL. In other words, the objective was to obtain real  $\rm CO_2/\rm CH_4$  selectivities from the VLE data. It was not possible to directly obtain the  $\rm CO_2/\rm CH_4$  selectivities from the VLE data, since only bubble-point pressures of the mixtures were measured. Sampling of the phases was not possible in the experiments and thus the compositions of the phases required for calculating the real selectivity were unknown. The Peng-Robinson (PR) equation of state (EoS) was used to calculate the gas phase compositions. Under the investigated conditions, the real  $\rm CO_2/\rm CH_4$  selectivities were approximately the same as the ideal  $\rm CO_2/\rm CH_4$  selectivities.

In Chapter 5, the Continuous Fractional Component Monte Carlo method (CFCMC) in the osmotic ensemble have been used to predict the solubility of the natural gas components  $CO_2$ ,  $CH_4$ ,  $C_2H_6$ , and  $SO_2$  in ILs, and Selexol, which is a mixture of poly(ethylene glycol) dimethyl ethers (PEGDME). The following gas solubility trend is observed in the experiments and simulations for all the solvents:  $SO_2 > CO_2 > C_2H_6 > CH_4$ . The solubility of  $SO_2$  is substantially higher than that of  $CO_2$ , which indicates that  $SO_2$  can be removed selectively in the presence of  $CO_2$ . However, the PEGDME solvents are more selective towards  $SO_2$  than the ILs. Furthermore, the

248 Summary

solubility of  $CH_4$  and  $C_2H_6$  are higher in PEGDME than in the ILs, which is a well-known drawback of these Selexol solvents. Overall, the solubility data obtained from the MC simulations were in very good agreement with available experimental data.

In Chapter 6, CFCMC simulations in the osmotic ensemble were used to compute the bubble-points of CO<sub>2</sub>/CH<sub>4</sub> gas mixtures in ILs. Standard ensembles (e.g., Gibbs, osmotic, etc.) commonly used for phase equilibria calculations cannot be applied directly to compute bubble-point pressures. These ensembles require the specification of the pressure and/or the gas composition, which are apriori unknown and should be computed from the simulations. A method is outlined where the composition of the gas is derived iteratively from the liquid composition by performing two separate simulations in the osmotic ensemble at the same pressure, but different gas compositions. The composition of the gas that is in equilibrium with the experimental liquid composition is then approximated by a first-order Taylor expansion. The effect of temperature, pressure, and gas phase composition on the real CO<sub>2</sub>/CH<sub>4</sub> selectivity was investigated. The computed real selectivities were compared with the experimentally obtained real and ideal selectivities. The real CO<sub>2</sub>/CH<sub>4</sub> selectivity decreases with increasing temperature and pressure, while the gas phase composition has a minor effect. The real selectivity was only marginally different from the ideal selectivity, which was defined as the ratio of the Henry constants.

In Chapter 7, the potential of ILs for  $\mathrm{CO}_2$  capture at pre-combustion conditions was investigated. Monte Carlo simulations were used to compute the solubility of the pure gases  $\mathrm{CO}_2$ ,  $\mathrm{CH}_4$ ,  $\mathrm{CO}$ ,  $\mathrm{H}_2$ ,  $\mathrm{N}_2$  and  $\mathrm{H}_2\mathrm{S}$  in the IL [bmim][Tf<sub>2</sub>N]. Simulations in the osmotic ensemble were performed to compute absorption isotherms at a temperature of 333.15 K using the versatile Continuous Fractional Component Monte Carlo (CFCMC) method. The predicted gas solubilities and Henry constants were in good agreement with the experimental data. The Monte Carlo simulations correctly predict the observed solubility trend, which obeys the following order:  $\mathrm{H}_2\mathrm{S} > \mathrm{CO}_2$  >  $\mathrm{CH}_4 > \mathrm{CO} > \mathrm{N}_2 > \mathrm{H}_2$ . Relevant separation selectivities for the precombustion process were calculated from the pure gas Henry constants and a comparison with experimental data was provided. The results indicated

that  $[bmim][Tf_2N]$  can effectively capture  $CO_2$  at pre-combustion conditions, but the syngas should be desulfurized prior to  $CO_2$  removal, because  $H_2S$  was three times more soluble than  $CO_2$ .

In Chapter 8, a novel Monte Carlo method in the Reaction Ensemble using the Continuous Fractional Component technique (RxMC/CFC) has been developed to study the reactions of  $\rm CO_2$  with aqueous monoethanolamine (MEA). The RxMC/CFC method was used to compute the equilibrium speciation of all relevant species formed during the chemisorption process of  $\rm CO_2$  with aqueous MEA solutions. The computed equilibrium speciation results were in excellent agreement with available experimental data. The RxMC/CFC method can be used to screen and design chemical solvents for  $\rm CO_2$  capture.

In Chapter 9, the performance of ILs in terms of CO<sub>2</sub>/CH<sub>4</sub> solubilities and selectivities are compared with respect to the commercial solvents Selexol, Purisol, Rectisol, propylene carbonate, and sulfolane. The solubilities of the gases were compared on mole fraction, molality, and volume basis to demonstrate the effect caused by the high molecular weight of the ILs. The results indicate that conventional solvents are superior to ILs when CO<sub>2</sub> and CH<sub>4</sub> solubilities are compared on a mass or volume basis. Although the CO<sub>2</sub>/CH<sub>4</sub> selectivity in ILs are similar to that of commercial solvents, the high price and viscosity of ILs may limit their application in the pre-combustion and natural gas sweetening process.

# Samenvatting

Koolstofdioxide (CO<sub>2</sub>) is het belangrijkste broeikasgas dat in grote hoeveelheden wordt geproduceerd door de industrie. Het is daarom noodzakelijk om CO<sub>2</sub> emissies te beperken. Een methode om dit te bereiken is door middel van koolstofdioxide opvang en opslag (CCS). Door de extreem grote schaal van het probleem is het CCS proces echter zeer uitdagend in termen van energie efficiëntie en kosten. De momenteel gebruikte amines voor CO<sub>2</sub> opvang bij post-combustion condities hebben meerdere nadelen, zoals een hoge volatiliteit, corrosiviteit en regeneratie kosten. CO<sub>2</sub> wordt opgevangen door middel van een chemische reactie met de amines. Een grote hoeveelheid energie is vereist om de gebonden  $CO_2$  weer los te krijgen. Dit is de voornaamste reden voor onderzoek naar energie-efficiënte processen en milieuvriendelijke materialen voor CO<sub>2</sub> opvang. Een alternatief voor het post-combustion proces is het pre-combustion proces welke geassocieerd wordt met een zogenaamde "integrated gasification combined cycle". In dit proces wordt synthese gas geproduceerd door een brandstof te vergassen. Vervolgens wordt het synthese gas in een water-gas-shift reactor geconverteerd naar een mengsel van overwegend waterstof (H<sub>2</sub>) en CO<sub>2</sub>. Na het verwijderen van CO<sub>2</sub> kan waterstof voor verschillende doeleinden gebruikt worden. Fysische oplosmiddelen kunnen gebruikt worden voor CO<sub>2</sub> opvang, omdat het pre-combustion proces bij hoge drukken opereert.

 $CO_2$  opvang is niet alleen interessant vanuit een milieuoogpunt, maar het heeft ook een belangrijke toepassing in het zuiveringsproces van aardgas. Aardgas is doorgaans verontreinigd met verschillende onzuiverheden waaronder  $CO_2$  en waterstofsulfide ( $H_2S$ ). Deze gassen moeten verwijderd worden 252 Samenvatting

om technologische problemen tijdens gastransport te voorkomen en om aan de specificatie van de klant te kunnen voldoen.  $CO_2$  wordt, afhankelijk van het type en concentratie van de onzuiverheden, in een absorber-stripper configuratie door middel van een fysisch oplosmiddel, een chemische oplosmiddel, of combinatie van beide typen verwijderd. In de praktijk worden vaak chemische oplosmiddelen zoals monoethanolamine (MEA) gebruikt voor  $CO_2$  opvang bij atomsferische druk, terwijl de hoge druk van het zuiveringsproces gunstig is voor  $CO_2$  absorptie door middel van fysische oplosmiddelen. Het gebruik van fysische oplosmiddelen zoals Purisol, Rectisol, Selexol en dergelijke is gebruikelijk in de aardgas industrie. Fysische oplosmiddelen worden geprefereerd boven chemische oplosmiddelen indien de partiële drukken van de zwavelhoudende componenten en  $CO_2$  hoog zijn.

In dit proefschrift wordt de potentie van ionic liquids (ILs) voor CO<sub>2</sub> opvang bij pre-combustion en aardgas zuivering condities onderzocht. ILs zijn zouten met een smeltpunt lager dan 100 °C en hebben interessante eigenschappen zoals een verwaarloosbare dampspanning, een hoge thermische en chemische stabiliteit, een hoge mate van afstembaarheid, een lage ontvlambaarheid, en een relatief hoge capaciteit voor zure gassen. Deze eigenschappen van ILs kunnen gebruikt worden om de nadelen van conventionele oplosmiddelen te vermijden. We concentreren voornamelijk op fysische oplosmiddelen welke geschikt zijn voor het hoge druk pre-combustion proces en het aardgas zuiveringproces. Experimenten zijn gebruikt om de oplosbaarheden van componenten in aardgas in verschillende ILs te meten. Daarnaast zijn moleculaire simulaties gebruikt om de oplosbaarheden van gassen in ILs te voorspellen. We vergelijken gas oplosbaarheden en selectiviteiten in ILs en conventionele oplosmiddelen.

In Hoofdstuk 2 presenteren we een gedetailleerd overzicht van recente onderzoek over het vinden van een geschikte IL voor CO<sub>2</sub> opvang. Een groot deel van dit hoofdstuk concentreert zich op experimentele data van CO<sub>2</sub> oplosbaarheid, selectiviteit, en diffusie in verschillende ILs. Het effect van anionen, cationen, en functionele groepen op de oplosbaarheid van CO<sub>2</sub>, de biologische afbreekbaarheid en toxiciteit van ILs worden besproken. Recente ontwikkelingen op het gebied van 'task-specific' ILs en 'supported IL membranes' worden ook besproken. Resultaten van moleculaire simulaties,

welke een waardevol instrument is voor het ontwerpen en evalueren van ILs, worden kort besproken.

In Hoofdstuk 3 is de potentie van ILs voor aardgas zuivering onderzocht. Een synthetische methode is gebruikt om de oplosbaarheden van  $\mathrm{CO}_2$  en  $\mathrm{CH}_4$  in verschillende ILs te meten. De Henry coëfficiënten van  $\mathrm{CO}_2$  en  $\mathrm{CH}_4$  in alle onderzochte ILs zijn gemeten en daaruit zijn ideale  $\mathrm{CO}_2/\mathrm{CH}_4$  selectiviteiten bepaald. De ideale  $\mathrm{CO}_2/\mathrm{CH}_4$  selectiviteiten in ILs zijn vergeleken met die van conventionele oplosmiddelen zoals Selexol, Purisol, Rectisol, Fluor Solvent, en sulfolane. De ideale  $\mathrm{CO}_2/\mathrm{CH}_4$  selectiviteiten in ILs zijn vergelijkbaar met die van de conventionele oplosmiddelen. De ideale  $\mathrm{CO}_2/\mathrm{CH}_4$  selectiviteit neemt af bij toenemende temperatuur en IL moleculair gewicht. Een IL met een laag moleculair gewicht moet gebruikt worden als een hoge  $\mathrm{CO}_2/\mathrm{CH}_4$  selectiviteit gewenst is.

In Hoofdstuk 4 presenteren we experimentele data betreffende oplosbaarheden van  $CO_2/CH_4$  gasmengsels in ILs. Het doel was om het effect van de aanwezigheid van één gas op de oplosbaarheid van een ander gas te onderzoeken. In andere woorden, we waren geïnteresseerd in het verkrijgen van de werkelijke  $CO_2/CH_4$  selectiviteit. Het was niet mogelijk om direct  $CO_2/CH_4$  selectiviteiten uit de VLE data te bepalen, omdat alleen bubbelpunten van de mengsels konden worden gemeten. De samenstelling van de gas- en vloeistof fase bij evenwicht is vereist voor het bepalen van de echte  $CO_2/CH_4$  selectiviteit, maar het bemonsteren van de fasen is helaas niet mogelijk in de experimenten. De Peng-Robinson (PR) equation of state (EoS) is gebruikt om de samenstelling van het gas te bepalen. De echte  $CO_2/CH_4$  selectiviteit blijkt ongeveer hetzelfde te zijn als de ideale  $CO_2/CH_4$ .

In Hoofdstuk 5 hebben we de Continuous Fractional Component Monte Carlo (CFCMC) methode in het osmotische ensemble gebruikt om de oplosbaarheden van aardgas componenten  $CO_2$ ,  $CH_4$ ,  $C_2H_6$ , en  $SO_2$  in ILs en Selexol te voorspellen. De experimentele en simulatie resultaten voor de oplosbaarheid van de gassen laat de volgende trend zien:  $SO_2 > CO_2 > C_2H_6 > CH_4$ . Het is dus mogelijk om  $SO_2$  in aanwezigheid van  $CO_2$  selectief te verwijderen, omdat  $SO_2$  een veel hogere oplosbaarheid heeft dan  $CO_2$ . De resultaten laten ook zien dat Selexol selectiever is voor  $SO_2$  dan de ILs. Het

254 Samenvatting

nadeel van Selexol ten opzichte van de ILs is dat de oplosbaarheid van  $\mathrm{CH}_4$  en  $\mathrm{C}_2\mathrm{H}_6$  ook hoger zijn. In het algemeen zijn de oplosbaarheden verkregen uit Monte Carlo simulaties in goede overeenkomst met de experimentele data.

In Hoofdstuk 6 hebben we de CFCMC methode in de osmotische ensemble gebruikt om bubbelpunten van CO<sub>2</sub>/CH<sub>4</sub> gasmengsels in ILs uit te rekenen. De ensembles die standaard gebruikt worden om fase-evenwichten te voorspellen (b.v., Gibbs, osmotisch, enz.) kunnen niet direct toegepast worden. Deze ensembles vereisen de specificatie van de druk en/of de gassamenstelling welke bij voorbaat onbekend zijn en in de simulaties uitgerekend moeten worden. We presenteren een nieuwe methode waarbij de gassamenstelling iteratief aan de hand van de vloeistofsamenstelling kan worden bepaald. Hiervoor zijn twee simulaties in het osmotische ensemble nodig bij dezelfde druk, maar bij verschillende samenstellingen van de gasfase. De samenstelling van het gas dat in evenwicht is met de experimentele vloeistofsamenstelling wordt gevonden met een eerste-orde Taylor expansie. Het effect van temperatuur, druk, en gassamenstelling op de echte CO<sub>2</sub>/CH<sub>4</sub> selectiviteit is onderzocht. De echte selectiviteiten verkregen uit de simulaties zijn vergeleken met de experimentele selectiviteiten. De echte CO<sub>2</sub>/CH<sub>4</sub> selectiviteit neemt af bij toenemende temperatuur en druk, terwijl de gassamenstelling een gering effect heeft. De ideale selectiviteit, gedefinieerd als de ratio van de Henry constanten, is bij benadering gelijk aan de echte selectiviteit.

In Hoofdstuk 7 onderzoeken we de potentie van ILs voor  $CO_2$  opvang bij pre-combustion condities. Monte Carlo simulaties in het osmotische ensemble bij een temperatuur van 333.15 K zijn gebruikt om de oplosbaarheden van de volgende gassen in de IL [bmim][Tf<sub>2</sub>N] uit te rekenen:  $CO_2$ ,  $CH_4$ , CO,  $H_2$ ,  $N_2$ , en  $H_2S$ . De voorspelde gas oplosbaarheden en Henry coëfficiënten zijn in goede overeenstemming met de experimentele data. De Monte Carlo simulaties voorspellen de volgende trend voor de oplosbaarheden (welke in overeenstemming is met experimenten):  $H_2S > CO_2 > CH_4 > CO > N_2 > H_2$ . De Henry coëfficiënten zijn gebruikt om relevante selectiviteiten voor het pre-combustion proces te bepalen. De resultaten tonen aan dat [bmim][Tf<sub>2</sub>N] potentieel gebruikt kan voor  $CO_2$  opvang bij pre-combustion

condities. Echter, het synthese gas dient eerst ontzwaveld te worden, omdat  $H_2S$  drie keer beter oplost dan  $CO_2$ .

In Hoofdstuk 8 hebben we een nieuwe Monte Carlo methode in het 'Reaction Ensemble' ontwikkeld die gebruikt maakt van de CFCMC techniek (RxMC/CFC). Deze techniek is toegepast om de reacties tussen CO<sub>2</sub> en MEA in een waterige oplossing te bestuderen. De RxMC/CFC methode is gebruikt om de 'equilibrium speciation' van de relevante componenten die gevormd worden tijdens het chemisorptie proces van CO<sub>2</sub> met MEA te bestuderen. De uitgerekende 'speciation' resultaten zijn in excellente overeenstemming met beschikbare experimentele data. De RxMC/CFC methode kan gebruikt worden om nieuwe chemische oplosmiddelen voor CO<sub>2</sub> opvang te ontwikkelen.

In Hoofdstuk 9 vergelijken we de CO<sub>2</sub>/CH<sub>4</sub> oplosbaarheden en selectiviteiten in ILs en de commerciële oplosmiddelen Selexol, Purisol, Rectisol, propylene carbonate, en sulfolane. De oplosbaarheden van de gassen zijn op massa basis, volume basis, en mol basis vergeleken om het effect van de hoge moleculaire massa van ILs te demonstreren. De resultaten tonen aan dat conventionele oplosmiddelen zoals Selexol, Purisol en Rectisol superieur zijn ten opzichte van bestaande ionic liquids in termen van gasoplosbaarheid en prijs. De CO<sub>2</sub>/CH<sub>4</sub> selectiviteiten in ILs zijn vergelijkbaar met die van de commerciële oplosmiddelen, maar de hoge prijs en viscositeit van ILs zal de toepassing ervan in de industrie beperken.

#### Curriculum Vitae

Mahinder Ramdin was born on the 31<sup>th</sup> of December 1985 in Nickerie, Suriname. At an age of 16 he moved with his family to the Netherlands. He obtained his B.Sc degree in Chemical Engineering in 2008 from the Hogeschool Rotterdam. Subsequently, he started a M.Sc. program at Delft University of Technology and obtained his M.Sc. degree in Chemical Engineering in 2010. At the end of 2010, he started a Ph.D. project in the Engineering Thermodynamics group headed by Prof.dr.ir. Thijs Vlugt at Delft University of Technology. During the project, which concentrated on CO<sub>2</sub> capture with ionic liquids, he was supervised by Prof.dr.ir. Thijs Vlugt and Dr.ir. Theo de Loos. He spent a vast majority of the time in the Thermolab to obtain high pressure solubility data of several gases in many different ionic liquids. In the last stage of his Ph.D. project, he performed Monte Carlo simulations to compute gas solubilities in physical solvents including ionic liquids. The experimental and simulation results are presented in this dissertation.

# Publications by the Author

- M. Ramdin, T. W. DE LOOS AND T. J. H. VLUGT; State-of-the-Art of CO<sub>2</sub> Capture with Ionic Liquids. *Ind. Eng. Chem. Res.*, 51 (2012) 8149-8177.
- 2. M. Ramdin, T. J. H. VLUGT AND T. W. DE LOOS; Solubility of CO<sub>2</sub> in the Ionic Liquids [TBMN][MeSO<sub>4</sub>] and [TBMP][MeSO<sub>4</sub>]. *J. Chem. Enq. Data*, 57 (2012) 2275-2280.
- 3. M. Ramdin, T. Zuzuarregui Olasagasti, T. J. H. Vlugt and T. W. de Loos; High pressure solubility of CO<sub>2</sub> in non-fluorinated phosphonium-based ionic liquids. *J. Supercrit. Fluids*, 82 (2013) 41-49
- 4. S. Bazhenov, M. Ramdin, A. Volkov, V. Volkov, T. J. H. Vlugt and T. W. de Loos; CO<sub>2</sub> Solubility in Biodegradable Hydroxylammonium-Based Ionic Liquids. *J. Chem. Eng. Data*, 59 (2014) 702-708.
- 5. M. Ramdin, A. Amplianitis, S. Bazhenov, A. Volkov, V. Volkov, T. J. H. Vlugt and T. W. de Loos; Solubility of  $CO_2$  and  $CH_4$  in Ionic Liquids: Ideal  $CO_2/CH_4$  Selectivity. *Ind. Eng. Chem. Res.*, 53 (2014) 15427-15435.
- M. Ramdin, A. Amplianitis, T. W. de Loos and T. J. H. Vlugt; Solubility of CO<sub>2</sub>/CH<sub>4</sub> gas mixtures in ionic liquids. Fluid Phase Equilib., 375 (2014) 134-142.

- 7. M. Ramdin, S. P. Balaji, J. M. Vicent-Luna, J. J. Gutiérrez-Sevillano, S. Calero, T. W. de Loos and T. J. H. Vlugt; Solubility of the Precombustion Gases CO<sub>2</sub>, CH<sub>4</sub>, CO, H<sub>2</sub>, N<sub>2</sub>, and H<sub>2</sub>S in the Ionic Liquid [bmim][Tf<sub>2</sub>N] from Monte Carlo Simulations. *J. Phys. Chem. C*, 118 (2014) 23599-23604.
- 8. Q. Chen, S. P. Balaji, **M. Ramdin**, J. J. Gutiérrez-Sevillano, A. Bardow, E. Goetheer and T. J. H. Vlugt; Validation of the CO<sub>2</sub>/N<sub>2</sub>O Analogy Using Molecular Simulation. *Ind. Eng. Chem. Res.*, 53 (2014) 18081-18090.
- 9. S. P. BALAJI, S. GANGARAPU, M. Ramdin, A. TORRES-KNOOP, H. ZUILHOF, E. L. V. GOETHEER, D. DUBBELDAM AND T. J. H. VLUGT; Simulating the Reactions of CO<sub>2</sub> in Aqueous Monoethanolamine Solution by Reaction Ensemble Monte Carlo Using the Continuous Fractional Component Method. J. Chem. Theory. Comput., 11 (2015) 2661-2669.
- 10. M. Ramdin, Q. Chen, S. P. Balaji, J. M. Vicent-Luna, A. Torres-Knoop, D. Dubbeldam, S. Calero, T. W. de Loos and T. J. H. Vlugt; Solubilities of CO<sub>2</sub>, CH<sub>4</sub>, C<sub>2</sub>H<sub>6</sub>, and SO<sub>2</sub> in ionic liquids and Selexol from Monte Carlo simulations. *J. Comput. Sci.*, (2015) (in press).
- M. Ramdin, S. P. Balaji, A. Torres-Knoop, D. Dubbeldam, T. W. De Loos and T. J. H. Vlugt; Solubility of Natural Gas Species in Ionic liquids and Commercial Solvents: Experiments and Monte Carlo Simulations. J. Chem. Eng. Data, 60 (2015) 3039-3045.
- 12. M. Ramdin, S. P. Balaji, J. M. Vicent-Luna, A. Torres-Knoop, D. Dubbeldam, S. Calero, T. W. de Loos and T. J. H. Vlugt; Computing bubble-points of CO<sub>2</sub>/CH<sub>4</sub> gas mixtures in ionic liquids from Monte Carlo simulations. *Fluid Phase Equilib.*, (2015) (in press).

### Acknowledgements

It is impossible to perform a PhD without the help of others. I am grateful to all the people that have supported me to accomplish this difficult task. More specifically, I thank my promotor Prof.dr.ir. Thijs Vlugt for providing me a PhD position and for his excellent guidance from the beginning of the project. Thijs, I admire your knowledge on molecular simulation techniques and thermodynamics in general. You always motivated me to write papers and your extremely fast comments have helped me to write many of them. Thanks for giving me, an experimentalist, the opportunity to learn molecular simulations.

I gratefully thank my copromotor Dr.ir. Theo de Loos for his daily supervision and guidance of the experimental part of the work. Theo, I admire your experimental and theoretical understanding of phase equilibria of complex systems. It was a pleasure to discuss the phase diagrams with you and to repeat the wrong experiments until we had an "error-free" curve. I think this critical attitude is very important to produce high quality data, which is suitable for publication.

I thank Ir. Eugene Straver for his advise and help with the experiments. Eugene, you are the most loyal and hard working person I have ever seen. I enjoyed drinking beer with you and to discuss the clumsiness of my students. I also thank you on behalf of my Master students for all the help and support in the thermolab.

262 Acknowledgements

Thanks to my coauthors, Sofia, David, Vladimir, Alexey, Ariana, Jose Manuel, Juan Jose, and Stepan for reading and correcting my manuscripts.

Thanks to my Master students Teresa and Aris for performing the time consuming experiments with the Cailletet equipment.

Special thanks go to Sayee, Dennis, Mariette, and Sondre. Sayee, many thanks for your friendship and for teaching me molecular simulations. Dennis, thank you for the coffee breaks and for dropping me at home after an outing. Mariette, thanks for all the help in the thermolab and for explaining me the difficult phase diagrams. Sondre, thanks for solving all my computer related problems.

Thanks to all my roommates and colleagues from P&E. In random order I thank Christian, Sander, Somnath, Norbert, Guido, Fatemeh, Jurriaan, David, Antonella, Julia, Fan, Thijs vW, Bernardo, Hongxia, Ali, Sayed, Meng, Tim, Dion, Karsten, Pablo, Erin, Frank, Juanjo, Xin, Martijn, Alexandr, Marloes, Rohit, Weiwei, Lalit, Hassan, Uttiya, Samir, Milos, Vincent, Nikos, Valentina, Michel vdB, Carlos, Brian, Wim, and Li-Chiang for the nice time and useful discussions.

Thanks to Mamoun, Mayte, Somayeh and Samaneh for fruitful discussions in the thermolab.

Thanks to all the people at the workshop and the supporting staff, Judith, Ilona, Leslie, Helma, Rob vdB for their kind services.

I thank my mother and sister for their support and unconditional love.

Special thanks to my parents-in-law for their love and encouragement.

Finally, I thank my wife for her support and patience, especially when I had to work in the nights or in the weekends.